THE CHARACTERISATION OF WHITE-ETCHING LAYERS FORMED ON ENGINEERING STEELS.

A Thesis submitted for the degree of Doctor of Philosophy

by

Robert Bulpett.

Experimental Techniques Centre, Brunel University

October 1991.

ABSTRACT.

Metal surfaces, and particularly steels, may be modified by processes which include; plastic-deformation, chemical changes and heating. These layers are often characterised by high hardness and a pronounced resistance to chemical etching. This latter characteristic giving rise to the generically descriptive term "White Layer", which is often applied to such features.

Processes which may result in the formation of "White Layer" can be broadly separated into three groups; thermal, chemical and mechanical. In practice, "White Layers" observed on materials removed from service environments have generally experienced a combination of these processes.

In this work white-etching layers formed on engineering steels have been characterised, using a variety of electron beam and X-ray analytical techniques, to establish the chemical nature and structural properties of "white layer" material. Specimens drawn from such diverse service applications as; high-pressure tank gun barrels, digger-teeth from gravel extraction plant and adiabatically-sheared armour steel have been compared with samples produced in the laboratory by conventional pin-on-disc wear testing apparatus, specialised machining techniques and laser surface-hardening heat-treatment.

The presence of a hard white-etching layer on each of the samples was first established using metallographic examination by light microscopy and microhardness testing to confirm the etch-resistance and high hardness of the white-layer. The chemical composition of the white-etching layer was then compared with the bulk steel composition using scanning electron microscopy and conventional microprobe analysis ($Z > 11$), and no significant differences were observed. Light element microprobe analysis and SIMS showed an increase in H, C, N, O in the white-etching layers formed within gun barrels, and on abusively turned steel. The levels detected were not considered to be significant in terms of white-layer formation but may well have an influence on strain aging and embrittlement phenomena. A technique for the preparation of cross-sectional thin foils was developed which allowed the structure of the white-etching layers to be compared with the underlying matrix by TEM and electron diffraction.

The results of this study showed clear similarities between white-etching layers formed by wear and abusive machining and those formed by adiabatic shear. From these results it is concluded that " white layer " is a fine grain martensite which forms on steel as a result of thermo-mechanical transformation.

ACKNOWLEDGEMENTS.

The author wishes to acknowledge the assistance and support of the following organisations and individuals who helped in the pursuance of this work :

Dr. B.J.Griffiths and Dr. D.C.Furze of the Department of Manufacturing and Engineering Systems, Brunel University for their assistance with the supply of specimens of abusively machined steel and help with the preparation of laser heat-treated surfaces.

Dr. W.Steen of Imperial College who made available facilities for laser-heat-treatment of steel specimens.

Dr. D.F.Allsop of the Royal Military College of Science, Cranfield who supplied a section of RARDEN gun barrel for examination and Mr.J.Winn of RARDE Fort Halstead who provided sections removed from a Chieftain tank gun barrel.

Dr. J.Greenbank of RARDE Chertsey for the provision of sections of armour steel exhibiting adiabatic shear bands and Dr.T.S.Eyre of Materials Technology, Brunel who supplied sections of a worn digger tooth, and worn surfaces from a pin-on-disc wear rig.

My thanks are also due to the above named for helpful discussion on the various methods of white-layer generation and to other colleagues at Brunel University for advice on methods of sample preparation and analysis

including Dr. S. Biswas for assistance with SIMS analysis and Dr J.K.Critchley and Dr.D.Gawne for advice on nickel plating formulae.

I am also grateful for the assistance given to me by the staff of the Experimental Techniques Centre during the course of this work, in particular that of Mrs.B.Reed and Dr, A.J.Reynolds, and the guidance and advice provided by Dr.T.S.Eyre and Professor B.R.Ralph of the Department of Materials Technology who supervised this research.

Finally I am most appreciative of the encouragement and support given to me throughout this endeavour by my wife, children, parents and family.

CONTENTS

CHAPTER 1. GENERAL INTRODUCTION

Historically, the occurrence of "white-layer" as an identifiable constituent, is traceable to the early 1900's with perhaps the first published work being that of Stead (1912) who observed unusually hard layers on the surface of used steel wire ropes. Subsequently, layers having similar properties; of high hardness and a degree of resistance to chemical etching, were identified on other engineering components removed from service, and on the surface of steels following certain machining operations.

The term "white-layer" derives from the comparative resistance of this material to chemical etching used to reveal the metallographic structure of the underlying metal matrix. Examination of such a layer under incident illumination using a light microscope, shows an apparently structureless, highly reflective "white" phase.

A more definitive descriptive term which is commonly applied to this material is that of a "transformed-layer", although it is by no means certain that all "white-etching" layers are the product of a crystallographic transformation, such as that of austenite to martensite.

The conditions under which such layers may be formed has been studied extensively, and the succeeding literature survey will consider some of the many publications and reviews which comprehensively detail the occurrence of "white-layers". This includes; layers produced on engineering steels during forming and machining operations, those resulting from frictional

couples, and white-layers formed as a consequence of wear and plastic deformation experienced during service and under laboratory test conditions.

White-etching bands may be observed within the bulk of steel components as a result of an "adiabatic-shear" mechanism experienced during forging operations, or more commonly, following explosive deformation or ballistic impact. This type of band is generally considered to be associated with a distinct crystallographic transformation.

A further class of "white-layers" are those identified on the internal bore of gun barrels following firing, which have similar properties of high hardness and increased resistance to chemical etching, when compared to the matrix material, as layers produced during machining or mechanical service operations.

Whilst all these types of "white-layer" have a generic similarity based on their resistance to chemical etching and high hardness, white-layers produced by different processes can be distinguished in terms of their similarity or dissimilarity to the bulk material in terms of chemical composition, metallurgical structure and the basic processes underlying their formation.

The properties of "white-layers" are such that their occurrence on the surface of components is generally undesirable, leading to premature failure in service or difficulty in machining operations. However, more recently it has been demonstrated that "white-layers" produced

under controlled machining conditions, have certain advantages in terms of improved wear resistance, over other forms of surface hardening treatment.

It is apparent that it would be advantageous to develop a better understanding of the nature of "white-layers" and also the conditions under which they may be formed, so as to either prevent, or facilitate their generation.

This study seeks to correlate the observed properties of "white-layers" drawn from a variety of sources, and identified as such by their properties of etching-resistance and high hardness, with chemical and structural information obtained by electron microprobe analysis, secondary ion mass spectrometry and scanning and transmission electron microscopy.

CHAPTER 2.

2.1. Introduction.

In reviewing the large body of literature relating to the formation , observation, nature and properties of "white-layers", it is useful to discriminate between sources of such layers with reference to their mode of generation; making a distinction between those layers produced in service, those formed during a machining process and those generated in the laboratory.

Consideration of the basic processes leading to their formation provides another means of classifying the published literature, and allows comparison with micro-structures formed in engineering steels by conventional heat-treatments.

2.2 Observation and identification of "white-layers".

2.2.1. Layers produced in service applications.

Perhaps the earliest recorded observation of a "white-layer" is that by Stead (1912), who observed hardened surface layers, which resisted etching in nital and picral, on the surface of steel wire ropes after use. He attributed their formation to transitory frictional heating, followed by rapid cooling due to the quenching effect of the colder sub-layers. The resultant material was identified as martensite although the structure of the surface layer was apparently featureless. Trent (1941) also investigated failed wire ropes removed from colliery winding gear and noted the presence of white-etching layer

on the wire surface and deduced that this layer, being brittle, was the source of cracks which then propagated through the underlying material, causing the wire to fail. He calculated that the temperature had risen to 1150°C at the surface, and following a series of tests involving cutting and striking the wire, which also produced white-layers, concluded that they were composed of an extremely fine-grained martensite, produced by rapid heating and cooling.

Pre-stressed concrete reinforcing wires examined by Steininger and Krzeminski (1962), (1965), were found to have developed white-etching layers both during drawing, and in service. These layers were identified as containing martensite by microhardness tests and X-ray diffraction studies. They did not however find evidence of conventional martensitic structure by metallographic examination. Schottky and Hiltenkamp (1936), found evidence of hardened layers which had formed on the surface of leaf springs, and also on a turbine shaft which had failed in service. Chemical analysis indicated that the surface layers had a higher nitrogen content than the bulk material, and it was concluded that hardening was due to a combination of nitriding and cold working.

Studies on the running surface of railway rails by Clayton (1976), showed that white-layers had formed and subsequently cracked and spalled away from the surface. Further work by Harrison (1979), demonstrated that the white-layers formed at the crests of corrugations on rails

had a hardness of between 900-1300 HV, and could be softened by tempering at 250°C. The white-layer was identified as martensite, formed by a combination of frictional heating and rapid cooling.

White-layers were also observed on the surfaces of components removed from engines and bearing assemblies; Kuritsyna (1956) used X-ray diffraction techniques to study the white-layers formed on the surface of grey cast iron rings after running in. He found that the white-layer contained a fine distribution of carbides in a ferritic matrix and believed that the white phase, which was softened at 900°C, was formed in the presence of active-carbon from decomposed lubricant. He went on to propose that white-layer was formed by the plastic deformation of martensite.

The scuffing of piston rings was studied by Rogers (1969) under lubricated conditions, and by Wilson and Eyre (1969) under dry sliding conditions. In each case, white-layers were produced having a range of hardness values. Rogers (1969) attributed formation of the hardest of these to the generation of a Fe-C-N compound, and noted that the various phases tempered at different temperatures.

Etching-resistant features have also been observed at or close to the surfaces of rolling element bearings by several workers; their formation was attributed by Styri (1951), to the influence of inclusions acting as stress raisers, to localised plastic deformation by Gentile (1965), to high contact stresses with localised high temperature flashes by Scott (1967) and to a combination

of simultaneous high contact pressures and shear stresses by Schlicht (1973).

That a hardened surface was formed on the inner bore of gun barrels during firing, has been known for many years; Fay (1917) attributing formation primarily to cold working and Howe (1918), to austenitisation during firing, with subsequent rapid cooling. Wheeler (1922) and De Sveschnikoff (1925), both considered that the propellant gases had an appreciable effect on the structure of the layer formed, and demonstrated changes in the chemical composition of the layer by the analysis of filings. Lester (1929), found evidence to support the nitriding theory and observed a lack of tempering at 400°C and similarities with the X-ray diffraction patterns of nitrided steels. Snair and Wood (1939), considered that the process within the gun barrel was a complex one in which very high temperatures and pressures, in combination with combustion products, resulted in chemical and structural changes. More recently, work on white-layer formation in high pressure tank gun barrels, carried out by Amos and Sheward (1983), demonstrated that such white-layers were formed by interaction between the gun steel and hot propellant gases. The resultant hard layer was shown to contain increased levels of carbon and nitrogen.

White-layers or more properly "white-bands", may also arise in service applications, due to the occurrence of intense localised shear within the bulk of a component.

McIntire and Manning (1958), commented upon the safety aspect of chips of "untempered martensite" which formed on hammer heads. It was concluded that the chips occurred as a result of fracture along lines of martensite, which had formed following localised heating. It seems clear that their observations related to "adiabatic shear" bands, formed as a result of intense localised shear. Glenn and Leslie (1971), observed several such shear bands in impacted steel armour plate, which appeared in metallographic sections as white-streaks. Electron diffraction studies indicated that the white-streaks had a bcc structure, and it was concluded that they were formed by a martensitic transformation in heavily deformed austenite. More recently, Derep (1987), made a detailed study by electron diffraction, of adiabatic shear bands in armour steel, and reported that the centre of the band contained delta ferrite, martensite and austenite. Formation of the band being attributed to rapid heating and cooling under high pressure and stress.

2.2.2. Layers produced by Machining Processes.

The phenomenon of surface hardening in steels as a result of a machining or forming process has been recognised for a considerable period. It was reported by Murdock (1932), that the useful life of a punching tool could be considerably extended by grinding to final dimensions using a wheel filled with beeswax. This method of hardening was found to be preferable to conventional

heat-treatment, in which small components became distorted on quenching.

The effect of grinding, on the surface properties of steels has been the subject of extensive study, with reviews by; Tarasov (1946), Torrance (1978) and Griffiths (1985), providing a comprehensive view of this field of work. Reports of interest include the observation by Tarasov (1946), that abusive grinding can produce conditions under which continuous non-etching layers may be produced on steels. These layers were identified as "white-martensite" produced by re-hardening of isolated regions or "spots". Further work by Tarasov and Lundberg (1949), on high speed steels, demonstrated the presence of a transition zone between the hardened martensitic layer and the matrix. This zone was thought to be tempered martensite.

White-etching layers were also observed on ground surfaces by Torrance (1978), who agreed with the general body of opinion; that such layers appeared white because their structure, refined by intense plastic shear, was too fine to be resolved by optical microscopy. El Heliaby and Rowe (1981) formed thick, hardened layers on steel by abusive grinding, which they identified as being martensitic by metallographic examination. In contrast, recent work by Blunt (1989), on white-layers produced by centreless grinding, concluded that such layers were formed by a process of intense plastic deformation and that no transformation occurred.

White-etching layers produced by reaming, were

studied by Turley (1975), who used electron microscopy to demonstrate that plastic deformation had resulted in a fine sub-grain structure. He did not consider that the layers were martensitic and used electron diffraction to establish that the structure was bcc.

Turning experiments by Watson and Murphy (1979), in which duplex white-layers were formed, showed that machining conditions influenced the nature of the layers. Dao and Shockey (1979) examined machining chips produced by lathe-cutting and identified white-etching bands, generated by the shearing mechanism involved in chip formation.

Griffiths (1985), carried out a series of tests on deep hole drilling of steel in which non uniform white-layers were produced with high hardness. It was demonstrated that the pressures and temperatures reached during drilling, would be sufficient to allow transformation to austenite with subsequent quenching to martensite.

During punching and blanking operations, conditions of highly localised and rapid deformation may exist causing adiabatic shear bands to be formed. Zener and Holloman (1944), studied such bands and described them as having a tetragonal martensite structure. Manion and Stock (1970), carried out tempering experiments on adiabatic shear bands produced by punching, and found the white-etching material to be resistant to tempering. They concluded from this that the layers were not necessarily

martensite. Wingrove (1971) also carried out tempering experiments and showed by electron diffraction that the structure was martensitic, but contained a high dislocation density.

Surface-hardening by laser treatment is a well established technique in which rapid heating and cooling permits the generation of martensite on the surface of steel. Stahli (1981), used a high frequency laser to surface harden steel and considered that white-layers similar to those produced in machining or wear processes could not be generated purely by thermal treatment. Steen (1978) (1985), commented that laser treatment could produce martensite structures on a much finer scale than conventional heat-treatment.

2.2.3. Layers produced in laboratory tests.

It is difficult to make a clear distinction between layers produced in laboratory tests and those formed under controlled machining or forming operations. As a result, several of the processes leading to the formation of hardened or etch-resistant surface layers, referred to in section 2.2.2. could as readily be classified as "laboratory experiments". The distinction that has been applied here is that if the process in question is intended as a machining or forming operation, such as for example controlled grinding or laser-hardening, then the work is not considered to be a "laboratory test" for the purpose of this survey.

White-layers have been produced, and their formation

studied, by many workers using various wear testing procedures; Eyre and Baxter (1972), reviewed the formation of white-layers at rubbing surfaces, and compared the results of friction and wear experiments in their own laboratories, with previously published work. They found a general agreement that "white-layers" were formed by a fine dispersion of second phase particles, pinning a fine crystalline structure. Among other work discussed, they cited research by Welsh (1957), which demonstrated that the carbon content of the steel did not appear to have any effect on the formation or hardness of white-layers. This observation does not however appear to be compatible with the findings of Grozin and Iankovich (1962), who found that white-layers having different structures, and presumably therefore different hardness, could be formed in different steels by the same basic process.

Perry (1976), in studies on the dry sliding wear of grey cast iron against 817M40 alloy steel, showed that the white-layer formed on the cast iron produced a polycrystalline electron diffraction pattern, indicating that the predominant phase in the white-layer was austenite. Scanning Auger microscopy of the layer showed an increase of up to 50% in carbon content in comparison to the bulk material.

In his thesis, Rowntree (1982) reported the results of studies on the formation of phase transformed material during the unlubricated rubbing of plain carbon steels. He demonstrated that white-layers could form under multiple

or single rub conditions, as a result of high flash temperatures. Comparative studies of phase-transformed layers with conventionally produced martensite structures, showed that the white-layer was essentially a fine grained martensite.

The phenomenon of surface-hardening resulting from the rubbing of metal components, is not restricted only to steels or other ferrous alloys. Furuichi and Nakamura (1984) carried out a series of tests with copper, stainless steel and pure iron, in which repeated frictional contact caused the formation of hard, plastically-deformed layers on each of the materials tested. Electron microscopy revealed that these layers were composed of material having a very fine grain structure.

Experiments were carried out by Quirke (1987) using a modified abrasive wear testing rig to assess the resistance of a range of alloy steels to abrasion by soils during tillage operations. He showed that white-layers could be produced in a variety of forms; some being duplex whilst others were separated from the matrix by a sub-layer of softer material. In some cases, white-layers were found in regions where the underlying material showed no evidence of strain.

Metallographic examination of scuffed surfaces produced during wear tests utilising a four ball machine, reported by Leng and Davies, (1989) revealed a featureless white-layer, both on and below the surface. They concluded that the layers were similar to adiabatic shear bands and

had been produced by microscopic friction welding.

2.3. Properties of White Layers.

White-layers may be distinguished by virtue of observable differences in their physical and chemical properties, from those of the bulk material within which or upon which they are formed. The high hardness of white-layers is well documented, but differences in fatigue strength, wear resistance and corrosion resistance have also been noted.

2.3.1. Hardness and Tempering Behaviour.

Many workers have reported values of hardness for white-layers which are substantially greater than that of the underlying bulk material, and generally well in excess of the hardness attainable in that material by conventional heat-treatment. Furthermore, the tempering behaviour of the layers was found to differ markedly from that of bulk martensite, requiring much higher temperatures to initiate observable changes. Kuznetsov et al, (1963) studied the hardness and structural changes accompanying the tempering of a hard transformation product formed on the surface of worn mild steel. They found that the high hardness was retained up to tempering temperatures of 800°C, and considered that the layer, which was formed under lubricated conditions, was partially graphitised cementite. Rogers (1969), also carried out tempering studies of white-layers formed on

cast iron diesel engine cylinder liners and piston rings as a result of sliding wear. He noted the formation of two distinct types of white-etching layer, which he designated W1 and W2 respectively. He found that the W1 material, which appeared as a 13μm thick layer with values of hardness above 1300 HV, was resistant to tempering up to 720°C, at which point the hardness fell abruptly to that of the bulk material. (Figure 2.1).

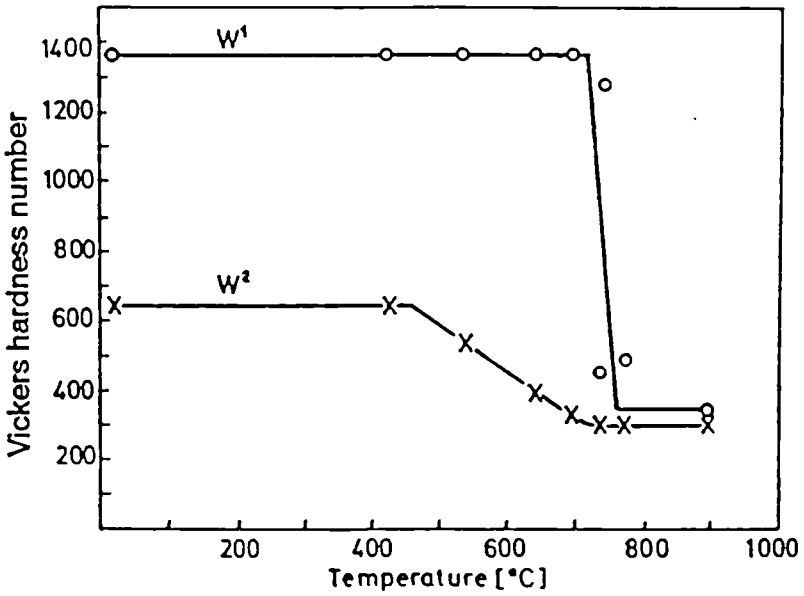

Figure 2.1. Annealing behaviour of W1 and W2 phases.
(After Rogers 1969)

The W2 etching-resistant layer was less than 2μm thick, had a lower initial hardness of 655 HV and began to soften at 460°C, attaining bulk hardness levels at 750°C. He concluded that W1 was a distinct phase, possibly containing relatively high levels of carbon and nitrogen, and formed by transformation at the high flash temperatures reached during scuffing. In contrast, the W2 phase was thought to be associated with regions of high plastic deformation.

Eyre and Baxter (1972) measured surface hardness on worn 0.24% C steel at levels of over 1100 HV, and compared these values with the hardness of a 0.24% C steel martensite structure obtained by conventional heat-treatment, of approximately 500 HV. Examination of untempered and tempered white-layers on 3.0% Cr, 0.3% C steel by electron microscopy, showed coarsening of dispersed particles in the white-layer following tempering for 1 hour at 700°C. Perry (1976), recorded a series of micrographs taken in a photo-emission electron microscope, of a scuffed Armco-iron specimen from a pin-on-disc wear experiment. The micrographs, which were taken over a range of temperatures from room temperature up to 850°C, show structural changes in the untransformed material, with the onset of grain growth at 600°C. At this temperature no change in the structure of the white-layer was evident. At 850°C, the white-layer was completely transformed to austenite, as evidenced by the presence of recrystallisation twins.

In some machining processes, conditions occur in which the formation of a transformed-layer is rapidly followed by complete or partial tempering of that layer due to heat generated by the machining process. Griffiths (1985) carried out a series of deep drilling experiments with the facility of a "quick stop" mechanism. Cross-sections prepared through the work piece showed a region of white-etching material beneath the burnished surface, which had a hardness of 1200 HV. The material adjacent to this layer exhibited a deformed structure to the same depth as the

transformed layer, but the hardness in this area was reduced to 800 HV. The conclusion was drawn that the transitory white-layer, formed by the burnishing process, was rapidly transformed to a polycrystalline structure by the residual heat in the work piece.

Quirke (1987) referred to a dark-etching layer which often appeared directly below the white-layer formed on the surface of wear test specimens of tillage tools. He found that the hardness of this layer was lower than that of the bulk material, having a value of 600HV compared with 950HV for the white layer and 700HV for the underlying matrix. This suggests that the dark-etching layer was a region of tempered material, but it is not clear whether this was tempered white-layer or tempered bulk martensite.

The tempering behaviour of white-etching adiabatic shear bands was studied by Manion and Stock (1970) who observed two distinct types of white layer on discs punched from 0.6% C steel. One of the layers was found to temper at 300°C and become black-etching, whilst the other remained etch-resistant until tempered at 575°C for 30 minutes. The shear bands identified as "white-streaks" in impacted steel armour plate by Glenn and Leslie (1971), were found to be considerably harder than the matrix, with values of 1025 HV compared to bulk values of 777 HV. A transition zone between the white-streak and the matrix was somewhat softer at 728 HV.

In contrast, the surface-hardened layers produced by

laser-treatment, whilst having higher hardness than martensite produced by conventional heat-treatment, with values of 946HV quoted by Stahli (1981) for 1% C steel, show clear evidence of a fine grain martensitic structure and only limited resistance to etching, and do not therefore appear to be white-layers as such.

2.3.2. Corrosion Resistance and Fatigue Strength.

That the white-layers formed in steel exhibit greater corrosion resistance than the untransformed matrix material, is self evident from the popular, generically descriptive term, applied to these layers or bands as being "white", or alternatively "non-etching". This feature or property is generally used to detect and identify such layers in the first instance, prior to confirmatory measurement of hardness values.

There is an apparent conflict with respect to the effect of white-layer on stress-corrosion and corrosion-fatigue. Karpenko et al (1965) cited by Babei et al (1971), states that; " the continuous white-layers formed during the mechanical working of steel, effectively increase resistance to corrosion-cracking ". Contradictory results were reported by Field et al (1970), cited by Griffiths (1985); " white-layers at machined surfaces were found to have a detrimental effect on stress-corrosion cracking". This inconsistency is probably related to the effect of localised, accelerated corrosion at "breaks" or discontinuities in a corrosion resistant surface layer.

Similarly, although Karpenko et al (1965) reported an increase in the fatigue strength of steel exhibiting a continuous white-layer at the surface, Field *et al (1970)* found that white-layer reduced fatigue strength by up to 35%. This apparent disparity is again most probably attributable to the nature of the white-layers on the test samples in terms of their thickness and continuity.

2.3.3. Wear Resistance.

Tests carried out by Babei, Golubets et al (1971) and Golubets, Dyadchenko and Babei (1971) on low alloy steels, showed that white-layers produced by turning or ultrasonic mechanical means, increased the wear resistance of friction pairs. The improvement was most noticeable on those specimens having a normalised matrix, with little improvement being noted for material in the martensitic condition. Griffiths and Furze (1986) produced continuous white-layers on the surface of 817M40 steel bars by turning, and tested the wear-resistance of these layers by the block-on-ring method. Results showed a marked increase in the wear resistance of the material and an advantageous, gradual transition, between the turned white-layer and the bulk material. More recently, work by Tomlinson et al, (1988) on the running-in-wear of white-layer formed on 817M40 steel by centreless grinding, showed that the white-layer provided a wear-resistant surface. The degree of wear resistance being proportional to the thickness of the white-layer. It was concluded that

white-layers could be produced in such a way as to control the initial running-in properties of components.

2.4. Basic Processes of White-Layer Formation.

Widely differing views on the underlying mechanisms of white-layer formation in various systems, have been presented by recognised authorities, based on the perceived circumstances of each process. Although recognising that in most instances, a combination of contributory factors may exist where white-layer formation occurs, an attempt has been made to classify the published literature in terms of basic processes.

2.4.1. Plastic Deformation.

Turley, Doyle and Samuels (1974), considered that the white-etching layer observed at the surface of abrasively-machined steel was a plastically-deformed fragmented layer. In their opinion, although recognising that white layers could form as a result of surface heating, to temperatures above the transformation temperature, they did not consider that the majority of white-layers formed by machining processes were of this type. They cited electron diffraction results published by Wilman and colleagues ; Argawala and Wilman, (1955), Scott and Wilman, (1958), Goddard, Harker and Wilman, (1962) and Stroud and Wilman, (1965), together with transmission electron microscopy studies, Turley (1971), and Turley and Samuels (1972), which showed the white-layers to have a very fine sub-grain structure consistent with an

extensively deformed material. Torrance and Cameron (1974), used transmission electron microscopy to study white-layers formed at the surface of scuffed 535A99 steel. They observed that white-layers, formed at high and low running speeds, had similar properties of high hardness and fine grain structure. Frictional heating was implicated at high running speeds, with the matrix beneath the white-layer being tempered to a hardness of 400HV. In contrast the matrix underlying the low speed white-layer showed no loss of initial hardness, and transformation was attributed to a high degree of plastic shear under compressive stress. This mechanism of white-layer formation is also implicated in the report by Torrance (1978) of a metallurgical examination of worn surfaces produced by plunge-grinding in which formation of a white-etching zone some 5μm below the worn surface was attributed to a localised accumulation of plastic strain. This postulate was supported by a simple contact geometry approximation for the grinding process which predicted that maximum shear stress would occur below the surface.

A further example of white-layer generation in circumstances where heating by friction was not thought to be significant, was reported by Newcomb and Stobbs (1984), who used TEM to study rail head material. They observed that the white-etching phase was a heavily deformed martensite, which contained no retained austenite or carbides. They calculated that temperatures at the surface of the steel could not have exceeded 400°C, and that the

local pressures would not have been sufficient to appreciably reduce the austenite transformation temperature. They suggested an alternative explanation for the absence of carbides in the white-layer based on the dissolution of carbide at high dislocation densities.

In his thesis, Blunt (1989) observed that the white-layer thickness was directly related to the size of the plastic zone, produced in the grinding operation. He concluded that the white-layers produced by centreless-grinding were not a transformation product (as transformation temperatures were not attained), but a region of intense plastic deformation. In contrast, Leng and Davies (1989) accredited the formation of a fine-grained untempered martensite layer at the scuffed surface of a specimen tested on a four ball machine, to the generation of high temperatures by gross plastic deformation.

2.4.2. Adiabatic Shear.

During certain high speed metal forming and ballistic-impact processes, strain localisation phenomena may occur in which "adiabatic shear" bands are generated within the bulk of the material. Their formation is generally attributed to a plastic instability, arising from thermal softening during adiabatic or quasi-adiabatic plastic-deformation. In steels, these bands appear as white-etching areas, having a high hardness and a fine-grained structure. The similarity between these bands and

the white-etching layers produced at the surface of worn components suggests that there may be some common feature in their generation. Zener and Holloman (1944) produced highly localised shear in a steel plate by punching at a very high strain rate of some 2000 s^{-1}. A cross-section of the plate, revealed a white-band, assumed by the authors to be martensitic. They estimated that the material in the white-band had suffered a shear-strain of nearly 100, whereas a strain of 5 would be sufficient to raise the temperature by 1000°C. Thornton and Heiser (1971) examined adiabatic shear zones produced in low alloy steel by explosive loading. Strain rates of up to $10^8 s^{-1}$ generated white-etching bands, with hardness values of 790HV in comparison to matrix values of 480 HV. X-Ray diffraction measurements gave a lattice parameter for the shear band consistent with martensite. White-etching bands may also be generated by ballistic impact, as demonstrated by Glenn and Leslie (1971) who formed white-etching bands with hardness values of 1025 HV, in steel armour plate.

The possible role of adiabatic shear in metal cutting was discussed by Black (1979), who demonstrated that a cyclic build up and annihilation of dislocations could result in catastrophic shear at the tool tip region. Dao and Shockey (1979) studied the formation of white-bands generated on machining chips, and using an infrared microscope focussed on the forming chip, measured a temperature rise of 180°C. From this result they were able to estimate the temperature at the shear band as being 500°C. Rogers (1979) and Timothy (1987), have reviewed the

extensive literature available relating to adiabatic shear phenomena in different systems. It is notable that the reported properties and structures of the shear bands considered, appear indistinguishable from those of white-layer produced in many machining operations or wear processes.

2.4.3. Rapid Heating and Cooling.

It would appear that one of the unifying factors of many of the white-layer forming mechanisms proposed, is the combination of high local temperatures, sufficient to cause austenitisation, and the rapid cooling necessary for the subsequent transition to martensite. In some instances it has been assumed that because a layer or band observed in steel has high hardness, that the structure must be untempered martensite. This assumption may be supported by the occurrence of a region of adjoining tempered material suggesting that high, localised temperatures have been achieved. This observation is not restricted to processes where frictional heating is clearly contributory, as for example, in the wear or rubbing of rail heads, Torrance and Cameron (1974), but has also been observed under adiabatic shear conditions, as in for example the report by McIntire and Manning (1958), in which an impact hardened surface, formed on a hammer head, was found to overlay a region of tempered martensite having a lower hardness than the bulk material. Similar observations were

reported by Wrazej (1945), who investigated the hardened layer formed on the outer surface of a shell case when fired from a gun. He demonstrated that the pearlitic steel had partially transformed, with areas of ferrite persisting at the surface, indicating that the Ac3 point had not been reached. Areas of pearlite however, had transformed to martensite showing that not only had the Ac1 point been reached but that subsequent quenching must have been rapid.(The relative positions of Ac1 and Ac3 are shown in the iron-carbon phase diagram, figure 2.2).

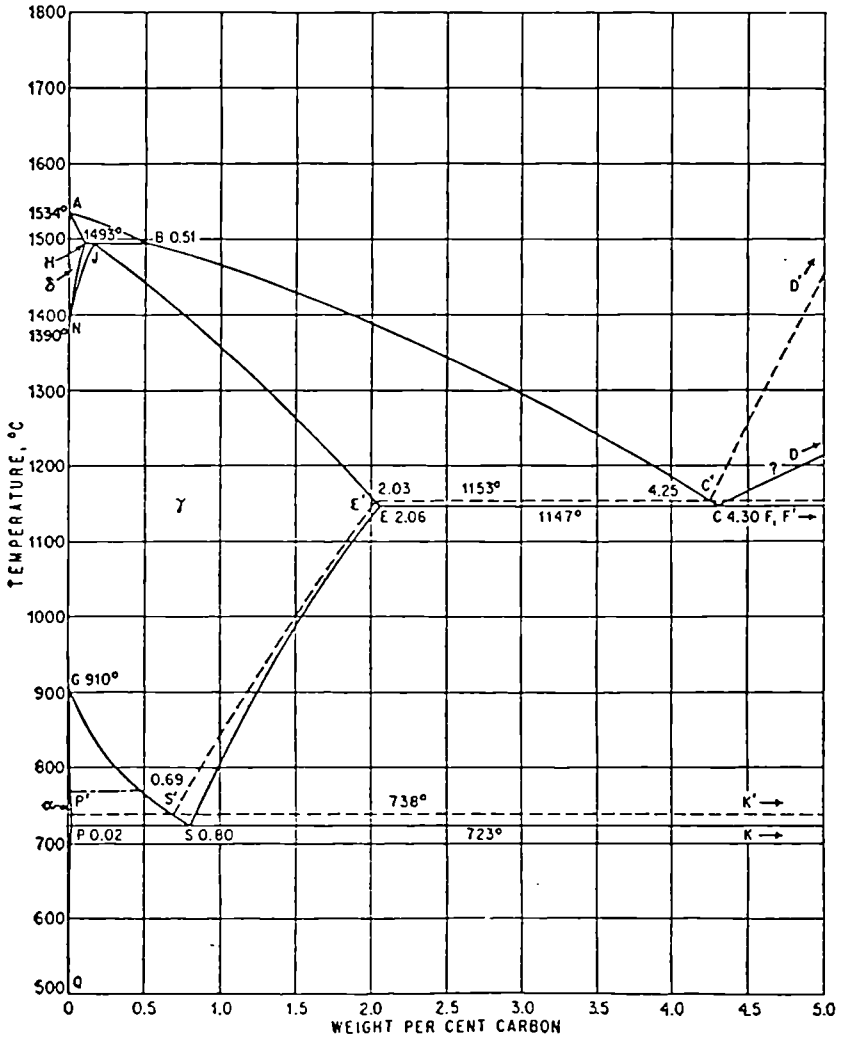

Figure 2.2. The iron - carbon phase diagram. (After Hansen 1958).

Archard (1959) produced a simplified graphical model for the estimation of "flash temperatures" attained at the surface of solids during rubbing or frictional contact. (Figure 2.3). In tests on a 0.52% C steel with a pin-on-ring machine, he found that transition to a lower rate of wear, generally taken as evidence of a martensitic transformation, occurred under conditions for which his graphical model predicted a rise in temperature sufficient to allow austenitic transformation. In order that the rise in temperature due to frictional effects be restricted to a thin surface layer in metals, the speed of sliding, must according to this model necessarily be greater than $10^5 ms^{-1}$.

It is clear that this postulate leads to the notion that those layers formed by low speed abrasion at light applied loads, as reported by Argawala and Wilman (1955) and Samuels (1967) must have a different basis of formation than those produced where frictional heating effects are significant.

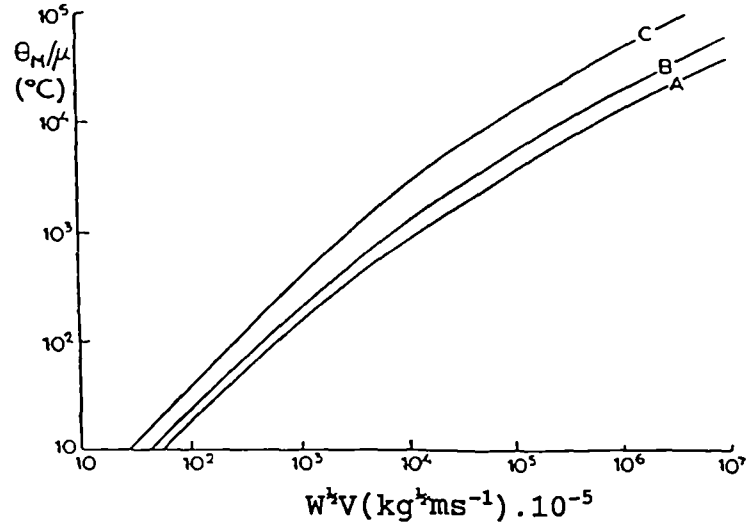

Fig 2.3. Maximum attainable flash temperatures for sliding contacts of steel. A 150 HV, B 250 HV, C 850 HV (From Archard 1959)

Welsh (1964) conducted a series of pin-on-ring wear tests on steel samples at various loads and showed that the surface hardness of a 0.12% C steel pin increased initially from 400 HV at low loads, to over 700 HV at the onset of the transition from severe wear to mild wear. This increase was attributed to strain-hardening at low loads and the transformation to austenite and subsequent quenching to martensite at higher loadings. The harder surface layers resulting in a pronounced reduction in wear rate. Measurements of temperatures by a thermocouple inserted 3mm below the rubbing surface, showed values of over 200°C for the pin, implying that considerably higher temperatures would have been attained at the pin surface. Whilst these results were obtained at sliding speeds an order of magnitude lower than the minimum considered necessary by Archard (1959) for transformation temperatures to be attained, the work provides considerable support for the proposal that white-layers may be formed as a result of frictional heating effects.

More recently, Rowntree (1982) studied the metallurgical transformations consequent on the rubbing of steels using a crossed-cylinders machine. He demonstrated that phase transformed material having high hardness and a martensitic structure could be produced as the result of a single rub. He used the simplification proposed by Archard (1959) for estimation of the flash temperature attained under the experimental conditions employed, and found that temperatures of 1100°C were required for austenite transformation . Although conditions were

severe, he did not consider that the effects of plastic deformation, shear strain or pressure, had a marked influence on the surface phase transformations observed.

The instantaneous surface and sub-surface temperature reached during the grinding of 817M40 steel was calculated by Jain et al (1986), who produced complex surface layers exhibiting; a soft white-layer due to decarburisation, a region of rehardened material and a tempered zone. Under particularly abusive conditions they observed a surface layer with a hardness of 800 HV, but their temperature calculations for these conditions showed a rise to 6900°C at the surface, falling to 1000°C at 80μm depth. Much in excess of the temperature required for transformation to austenite, yet thick hardened layers were not observed.

It is difficult to envisage a white-layer forming process involving mechanical working of surface layers, which could be described as wholly or primarily dependent upon surface frictional heating effects, without considering the plastic deformation experienced by the surface. Likewise many of the proponents of white-layer formation by plastic-deformation, appear to completely discount the heat evolved during deformation, although it is generally accepted that over 85% of the energy required to plastically deform material is converted into heat .

The controversy may be partially resolved by considering surface layers hardened by short-duration localised heating, followed by rapid self-quenching, as in the case of laser-treated steels. These layers, whilst

harder than conventionally heat-treated bulk specimens, are not structureless when etched, and do not exhibit the high values of hardness observed in white-layer produced by thermo-mechanical deformation. Even where pulse laser treatment of very short duration was employed by Stahli (1981), and surface temperatures of the melting point of iron carbide (1320°C) were attained, the structures produced at the surface and in the sub-surface layers of a low alloy steel, were clearly mixtures of retained austenite and martensite. From the foregoing it would appear that the apparently structureless white-layer observed on the surface of various steel components, following wear or abusive machining, require a degree of plastic deformation to allow their formation to proceed.

2.4.4. Chemical Interactions.

One of the characteristic properties of white-layer is that of very high hardness (sometimes as much as 1300 HV), when compared to the properties of the bulk material. Various explanations for this phenomenon have been put forward; including high local strain, small grain size and transformation to martensite. In many instances the hardness exceeds that attainable in the bulk for a particular carbon content and it has been proposed by many workers that reaction between the component surface and the local environment permits a localised change in chemical composition.

The hardness of iron-carbon martensite increases to a limiting value of approximately 1000 HV at a carbon

content of some 1.2 wt% , see figure 2.4, from Petty (1970). Similarly the presence of interstitial nitrogen in the iron lattice permits the formation of a nitrogen-austenite phase, which on quenching transforms to a nitrogen-martensite.(Hume-Rothery.1966).

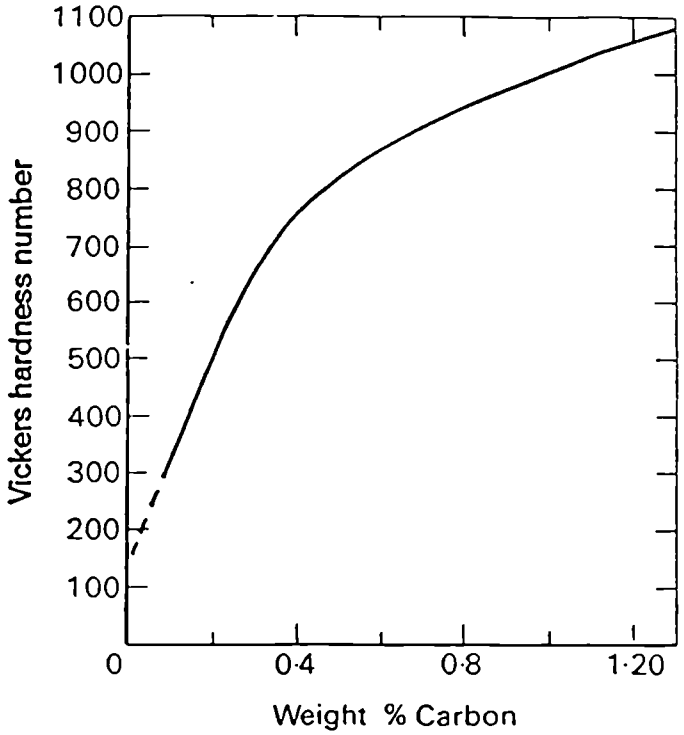

Figure 2.4. The hardness of iron - carbon martensite. (Petty: Martensite fundamentals and technology. 1970)

Theories of white-layer formation have been proposed in which reaction with the local chemical environment is considered to have changed the chemical composition of the surface with respect to the bulk, thus allowing for example, the generation of a higher carbon or nitrogen martensite at the component surface.

Possible interactions with the local environment which may be considered in more detail include:

1) The take up of nitrogen by reaction with atmospheric nitrogen containing compounds.

2) Reaction with carbon present at the sample surface, for example as hydrocarbon or contained in the lubricant.

3) Interaction with atmospheric oxygen to form oxide particles which become incorporated into an amorphous hard layer.

2.4.4.1 The effect of nitrogen.

That nitrogen from the atmosphère could combine with a steel to form a nitrided layer or possibly a nitrogen martensite under conditions of wear or rubbing was considered a possibility by Welsh (1957). It was also considered by Farrell (1969), that conditions for diffusion of nitrogen into the steel matrix were met during the process of rubbing contact between steel components in atmosphere, with the partial pressure of nitrogen at contacting asperities rising to values of over 4,000 atmospheres. This estimate was based on the premise that contact pressures at asperities are of the order of the yield point for the material involved and that nitrogen atoms occluded onto the sample surface could therefore pass into solution in the matrix.

A consideration of the equilibrium constant for nitrogen in the local atmosphere and that in solution, and taking into account the effect of temperature, showed that a pressure of some 10 atmospheres was required to dissolve 0.29wt% of nitrogen in 0.25wt% carbon steel. The combination of both carbon and nitrogen allowing a martensitic product to form having an equivalent carbon

content of 0.5wt%. The hardness of this phase as predicted by Burwell and Strang (1952), being 700 HV, a value not inconsistent with those measured by Farrell (1969). An objection to this theory was raised by Torrance and Cameron (1974) who considered that whilst high stresses were generated in metals during rubbing contact, that this would reduce the solubility of gas in the metal rather than increase it. They quoted work by Paranjpe et al, (1950) which showed that at 600°C the α phase of the metastable Fe-N system contains 0.1 wt% nitrogen, whilst at this temperature, iron will only dissolve 0.001 wt% nitrogen under standard atmospheric pressure. This would imply that a partial pressure of nitrogen gas of 10,000 atmospheres would be necessary to form this phase, with still higher pressures being required to form the precursor to the nitrogen martensite phase. They also referred to the results of analyses of frictionally hardened layers by Schottky and Hiltenkamp (1936), which showed some absorption of nitrogen but no more than would be expected from the stable equilibrium diagram.

Rogers (1969), considered that nitrogen could be a constituent of white-layer in view of the tempering properties of this material and the difficulty in correlating measured X-ray diffraction results with reference values for known Fe-C compounds. Whilst many workers have postulated that the absorption of nitrogen into the surface layers of steel could be a contributory factor in the generation of white-layer during the rubbing

of metals, there is little evidence in the form of chemical analyses or structural information to support this view. Indeed those analyses reported, show only low levels of nitrogen, insufficient to initiate any recognised change of phase within steel.

The mechanism of white-layer formation on the internal bore of a gun barrel as a result of firing, is quite different to that of rubbing contact, and it is reasonable to expect that the high temperatures and pressures experienced in the presence of gaseous propellant residuals would increase the likelihood of a surface chemical change. Snair and Wood (1939) observed a 50μm thick white-layer in the bores of machine gun barrels, and concluded that the layers consisted of nitrides in solution, rather than a martensitic structure. Many subsequent investigations of layers formed in gun barrels have been published and an unclassified Ministry of Defence report by Amos and Sheward (1983), considered specifically the mechanism of duplex white-layer formation, both in a high pressure tank gun barrel and by laser and plasma arc simulation within a pseudo propellant atmosphere. Structural analysis by X-ray diffraction techniques of gun barrel samples indicated that the outer, harder white-layer contained ϵ-iron nitride or carbo-nitride, with a cph structure consistent with a 6 wt% nitrogen + carbon content. Sophisticated analyses by EPMA, Auger spectroscopy, SIMS and nuclear microprobe analysis gave somewhat conflicting results, with measurements of nitrogen content varying between 3.5

wt% by Auger analysis and zero detection by SIMS.

A similar analysis of the surface of steel specimens by exposed to plasma arc in a controlled atmosphere, showed that white-layers could not be produced in the presence of nitrogen alone, and that carbon was a necessary constituent of the local environment for white-layer formation.

2.4.4.2 The effect of carbon.

The hardness of quenched steel increases rapidly with carbon content, as shown in the figure 2.4, to a value in excess of 1000HV for carbon levels above 1.2 wt%. In practice, plain carbon steels containing more than 0.5 wt% C, become extremely brittle and are prone to quench cracking at the high cooling rates required to form the martensitic structure. Alloying elements such as manganese, nickel or chromium are added to increase hardenability by reducing the critical cooling rate necessary to form martensite.

Several authors have considered that the high hardness of white-layers formed by frictional heating, or by the reaction with combustion products, may be attributed to the diffusion of carbon into the surface of the steel, with the subsequent formation of a high carbon martensite. Welsh (1957) , observed that a hard surface formed more quickly on steels with higher carbon contents under dry rubbing conditions, but also noted that low carbon steels produced a layer almost as hard after a

longer rubbing time. He generated similar hard phases by sparking mild steel surfaces under oil and in air, and concluded that the steel had absorbed nitrogen from the air and carbon from the oil. White-layers having a range of hardness from 1000 HV to 1300 HV, were produced by Kuznetsov et al, (1963) in a series of friction tests on mild steel, with oil lubrication. As the layers were resistant to nital etch but became dark when etched in alkaline sodium picrate, and as they disintegrated into graphite and pearlite on heating to 850°C, the authors concluded that the layers were carbidic. They observed that carbon must have been taken up from the oil, as the steel did not contain sufficient carbon for graphite or pearlite to form with conventional heat treatment.

Rogers (1970) studied white layers on scuffed cast iron cylinder liners and noted that their tempering characteristics were similar to those of Fe_3C. He suggested that they were formed by reaction of oil with the liner. An attempt was made by Torrance (1974), to establish the relative carbon content of white-layer on a scuffed steel peg, with a view to determining whether carbon was absorbed from the lubricant. A metallographic comparison of the scuffed surface with the matrix, following vacuum heat treatment for 25 hours at 700°C, showed no significant difference in the volume of carbides,indicating that no take up of carbon was necessary for white-layer formation.

In contrast, the white-layer observed on sections of gun barrels and steel samples exposed to plasma arc in a

simulated propellant residue atmosphere, Amos and Sheward (1983) showed clear evidence of an increase in the carbon content when compared to the matrix composition

2.4.4.3 The effect of oxygen.

The majority of processes leading to the formation of white-layers at the surface of steel components would allow exposure of the material to oxygen in the atmosphere. The range of diffusion of oxygen into steel is however limited to the first few atomic layers, even under high pressures, as oxidation occurs very readily, within the first few atomic layers. It is unlikely therefore that oxygen directly influences the formation of white-layer.

Oxides formed during the wear process do however influence the rate of wear, and thus indirectly, the rate of formation of white-layer. Tests carried out in vacuo by Kawamoto and Okabayashi (1971) showed that the initial wear rate was higher in vacuum and that the white-layer generated was considerably thicker. This suggests that surface oxidation reduces the extent of plastic deformation within the underlying material and prevents the formation of a thick white-layer. Eyre and Baxter (1972) considered that the striated appearance of oxide particles entrapped within white-layers was indicative of a fragmentation mechanism, in which intensive plastic deformation caused the surface oxide film to be broken up and mixed into the white-layer. They tested this supposition by tempering the transformation product at

800°C, and noted that the steel immediately below the white-layer became decarburised, indicating the presence of oxygen.

2.4.4.4. Summary of Chemical Interactions.

It is apparent from the work by Welsh (1957) using inert atmosphere, that of Kawamoto and Okabayishi (1971) in vacuo and Griffiths (1985) in deep drilling operations, that the presence of oxygen or nitrogen is not necessary for the formation of white-layer on steel, during rubbing or machining operations. Equally however, there is clear evidence that these elements are incorporated into some types of white-layer, thereby affecting both their formation and their physical and chemical properties.

2.5.1. The Structure of White-Layer.

The goal of identifying unambiguously, the "true" structure of white-layer has exercised many workers who have sought to explain the properties of high hardness and etch-resistance. This task has been complicated by attempts to demonstrate that all white-etching layers, however formed, had the same basic structure. The review by Grozin and Iankovich (1962), addressed this difficulty by considering that as many as seven different types of white-layer structure could be formed on steel and cast iron surfaces, these being : 1) austenitic, 2) austenitic-martensitic, saturated with nitrogen and carbon, 3) ferritic-martensitic, 4) austenitic-martensitic, with

tempered martensite, 5) ferritic-cementite, 6) carbidic (chromium carbides), 7) layers of precipitated noncarburizing elements.

The authors further considered that the various types of white-layer were formed by rapidly developing thermal processes, chemical thermal processes, or a combination of these two, with the added complication of plastic deformation and other physical metallurgical factors. To these two basic forming mechanisms, Turley (1975), added as a distinct process, the production of white-layers by intense plastic deformation alone.

General reviews by Scott et al (1975) and Griffiths (1986), detail the structural characterisation of white layers produced under a wide variety of conditions whilst Timothy (1987), has critically reviewed the special case of white-bands formed within bulk material under conditions of adiabatic shear.

Much of the published work describes white-layer as being martensitic without reference to crystallographic structural characterisation. Observation of the etching or tempering behaviour of the unknown material being used to enable phase identification. Whilst this information is undoubtedly of value, unguarded use of such an imprecise structural classification of the layers leads to confusion and should be avoided where possible.

The considerable practical difficulties experienced in the preparation and presentation of samples of white-layer for X-ray and electron diffraction structural

studies, have led to a paucity of reliable crystallographic information. A convenient method of examining the limited data available is to group the results in terms of the primary formation mechanism :

1) Plastic deformation at high temperatures;
2) Plastic deformation at low temperatures;
3) Chemically induced structural changes.
4) Adiabatic shear processes

(The process of adiabatic shear may be considered as a special case of plastic deformation at high temperatures, but both the volume of literature on shear band phenomena and the absence of any surface interaction makes this process more readily reviewed as a separate section.)

2.5.2. The structure of white-layers formed by high temperature plastic deformation.

The pin-on-disc wear test is an example of a system where the combination of plastic deformation and high temperatures may lead to the formation of white-layer. Perry and Eyre (1977) described the preparation of thin foils through the wear surface of cast iron pins exhibiting white-layers, using ion beam thinning techniques. The subsequent examination in a high voltage transmission electron microscope revealed the surface layer to be microcrystalline, having a grain size which varied between 0.05μm and 0.25μm. The ring pattern obtained by selected area electron diffraction (SAD),

confirmed the microcrystallinity of the product, which was not identified. Rowntree, (1982) compared X-ray diffraction patterns obtained from light abrasion of an unworn surface, with material from single and multiple rubbed tracks. The unworn material was found to contain ferrite and iron carbide whilst those from the worn tracks exhibited line broadening and limited evidence of martensite. Transmission electron microscopy showed evidence of a bct structure, which together with other evidence was taken to show that a fine grained martensitic transformation product was formed as the result of a single rub, in which temperatures in excess of 1100°C were reached at the sample surface.

2.5.3. The structure of white-layers formed by low temperature plastic deformation.

Turning to those authors who regarded that white-layers could also be formed primarily by plastic deformation, the work of Argawala and Wilman (1955) and Turley, Doyle and Samuels (1974) demonstrated that crystallographic changes may be induced in surface layers by hand abrasion, under conditions in which any temperature rise would be small.

Turley (1975) produced evidence of a fine grain structure product on the surface of reamed holes, and compared these with white-etching layers produced by abrasion and abusive grinding. Transmission electron microscopy was used to show that both the reamed and

abraded surfaces exhibited a fine grain bcc structure produced by intense plastic deformation. The loss of carbides within the white-layer was attributed to dissolution under highly localised stress. The abusively ground material however exhibited a martensitic white-layer, formed by rapid heating and cooling and modified by plastic deformation. Newcomb and Stobbs (1984) also proposed that the local dissolution of carbides at high dislocation densities, rather than high temperatures, was responsible for the loss of carbides in the white-layers formed on railway lines. The formation of the white-layer was attributed to a deformation mechanism and the structure, as observed by TEM, found to be a heavily deformed ferrous martensite.

2.5.4. Chemically induced structural changes.

Chemical changes induced in the surface layers of steel during for example; machining or wear processes, interaction with combustion products, and laser or plasma arc heat-treatment, may lead to the development of associated microstructural changes. Grozin and Iankovich (1962), referred to cementitic-ferritic white-etching layers formed on cast iron piston rings due to gas leakage, and an austenitic-martensitic layer developed on steel exposed to gunpowder gases. Rogers (1969) indexed X-ray diffraction data acquired from scrapings removed from the surface of scuffed cast iron piston rings, to give a good fit with a calculated tetragonal unit cell, with a = 0.55nm, and c = 0.46nm. He did not identify

the material but believed that it was an Fe-C-N compound of high carbon content.

A more obvious source of white-etching layers having a different chemical composition to the bulk, are those generated within gun barrels. Amos and Sheward (1983) used X-ray diffraction analysis to characterise the structure of white-etching layers formed in high pressure tank gun barrels, and simulated white-layers formed by a pulsed laser beam. They found the gun barrel white-layer to consist of some 70% of a cph structure identified as ϵ phase carbo-nitride, and 30% α-ferrite. The simulated white-layer, whilst appearing similar to gun barrel white-layer, was found to consist of α-ferrite and a complex nitrogen containing spinel.

2.5.5. The structure of Adiabatic shear bands.

The reviews by Rogers (1979) and Timothy (1987), cover the mechanisms of formation, and attempts at structural characterisation, of a wide range of shear-band phenomena.

White-etching bands produced in steel under conditions of adiabatic shear were examined by Wingrove (1955), using TEM techniques. He compared SAD results from the white-etching area with X-ray diffraction data for martensite in the same steel. Finding correspondence between the lattice spacings he concluded that the white-etching band was martensite, with a high density of dislocations. Subsequent work on shear-bands produced by

explosive loading by Thornton and Heiser (1971), confirmed that the white-etching zones were a fine-grain, heavily deformed martensite with a bct structure.

Glenn and Leslie (1971) also found the white-etching bands produced in armour steel by ballistic impact, to be a fine-grained martensitic product, but interpreted electron diffraction data to indicate that the structure was bcc. More recently Derep (1987,) also used TEM to study shear bands in armour steel and found the structure to be composed of small equiaxed grains of ferrite, containing martensite laths. He considered that the presence of ferrite and the fact that the carbides were dissolved, indicated that the material had partially melted to produce delta ferrite. The variety of structures proposed for the transformed adiabatic shear bands in steel reflects the difficulty of obtaining accurate measurements to establish for example; the degree of tetragonality. This parallels the situation with respect to the structural characterisation of white-layers produced by other mechanisms.

2.6 Conventional steel microstructures.

This thesis is concerned with the characterisation of white-etching layers, formed on the surface of low alloy steels of different composition, under various laboratory or service conditions. Very high hardness is a characteristic of these white-etching layers, and it is generally accepted that those layers formed under

conditions where temperatures have exceeded the austenite transformation temperature, such as frictional rubbing and adiabatic shear, are a fine grain martensite product. It is therefore of value to consider briefly some of the details of the transformations involved, the factors which may influence those transformations and the properties of the martensite product.

Pure iron crystallises with a body centre cubic structure (bcc), at temperatures below 911°C and transforms above this temperature to a face centre cubic (fcc) or "austenitic" structure. The fcc structure has the property of being able to dissolve considerably more carbon than the bcc structure and many of the properties of steels are based on the various structures formed when the material is cooled through the austenite transformation temperature. *(figure 2.1.)*. *Rapidly cooled* steels are much harder than slowly cooled steels of the same carbon content. In particular, those which are quenched from the austenite phase achieve very high values of hardness, due to the formation of martensite.

Steels containing interstitial carbon or nitrogen, at levels of more than approximately 3 at%, form acicular martensite, a metastable phase which forms from the parent austenite when the material is cooled at a rate exceeding a critical value which suppresses the formation of pearlite. The martensite unit cell is body centred tetragonal (bct) with the carbon atoms lying in the 0,0,½ and ½,½,0, octahedral interstices, distorting the

structure from bcc. The axial ratio of the lattice constants "a" and "c", vary with the carbon content as shown in the figure 2.5. The curves of "a" and "c" can be extrapolated linearly to the "a" parameter of carbon-free alpha iron, and this is taken to indicate that acicular martensite is tetragonal, even with very low concentrations of carbon. Bell(1970). Work by Bibby and Parr (1964) demonstrated that at cooling rates in excess of 35 k°C s^{-1}, a martensitic structure was formed in iron containing less than 0.0017 wt% C.

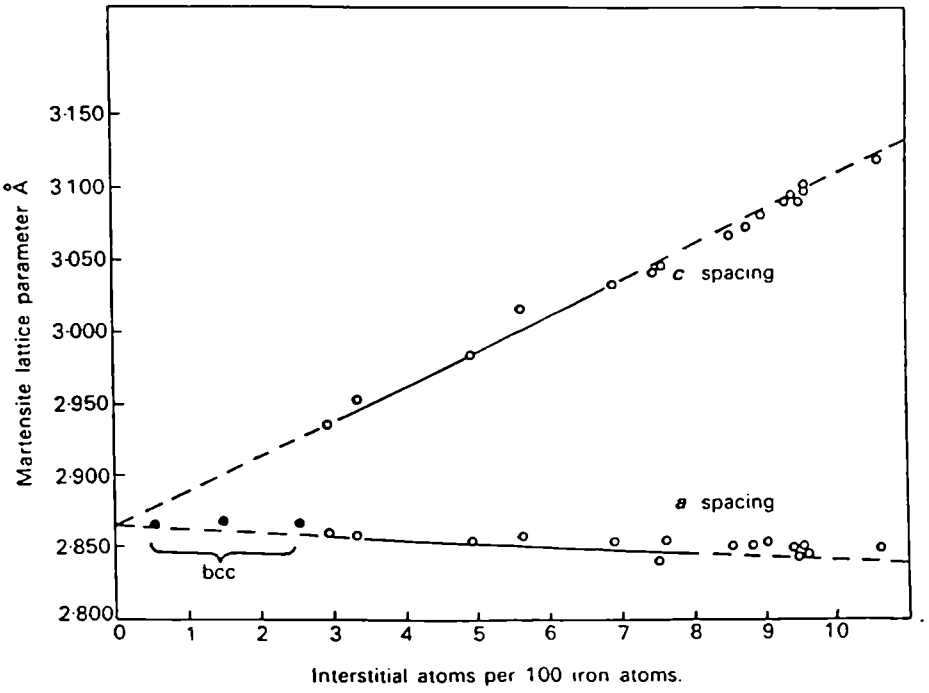

Figure. 2.5. Variation of martensite lattice parameter with carbon content. (After Petty 1970).

The structure takes the form of lenticular plates embedded in retained austenite with an internally twinned sub-structure. The transformation from austenite to martensite is diffusionless which implies that the parent and product phases have the same chemical composition.

For interstitial contents between 3 at % and 8 at%, the relationship between the bct martensite phase and the parent austenite is associated with the $\{225\}_\gamma$ habit plane and described by the Kurdjumov-Sachs orientation relationship, (taken from Martensite, Fundamentals and Technology, ed E.R Petty, (1970):

$$\{111\}_\gamma \parallel \{011\}_\alpha \text{ with } \langle 011\rangle_\gamma \parallel \langle 111\rangle_\alpha$$

At higher interstitial contents the orientation is related to the $\{259\}_\gamma$ habit and is described by the Greninger - Troiano relationship:

$$\{111\}_\gamma \parallel \{011\}_\alpha \text{ but with } \langle 112\rangle_\gamma \parallel \langle 011\rangle_\alpha.$$

For interstitial element contents of less than approximately 3 at% , (0.6 wt% C), austenite transforms to "massive" martensite on rapid cooling. The structure is a single phase disordered bcc containing no retained austenite, generated by a shear transformation associated with the $\{111\}_\gamma$ habit plane. The microstructure consists of parallel bundles of ferrite plates or lathes typically several micrometers long, with a range of widths from 0.3μm to 2 μm .

The martensite reaction begins following undercooling at a temperature known as the M_S point, which varies with alloy composition and is also influenced by prior heat treatment conditions. The transformation is athermal and requires continuous cooling. Due to stresses developed in the parent material, the reaction does not go to

completion; the volume of austenite retained in carbon steel being a function of the carbon content.

Martensite may be induced at higher temperatures than M_S by deformation; the process of ausforming requires heavy deformation of the austenite phase with potential strength increases of up to 50%. It should be noted that the micro-structure of strain induced martensite is not necessarily the same as that of a spontaneously formed martensite in the same material.(Bowles and Barrett 1953).

The interstitial solid solution martensite formed in carbon steels can have a five fold increase in hardness over the annealed material, with the attainable hardness being related to the carbon content as shown in the figure 2.4, in which hardness values over 1000 HV are indicated for steel containing 1.2 wt% carbon. Nitrogen may also form an interstitial solid solution in steel to produce a nitrogen martensite *having similar properties to the* carbon martensite. In addition to the effect of interstitial solution hardening, other factors have been considered to influence the hardness of martensite, Garwood, (1970) as follows:

1) Solution hardening by substitutional elements;
2) Cluster or precipitation hardening;
3) The effect of austenite grain size;
4) Strengthening by sub structure;
5) Microplastic deformation and rapid work hardening.

The above factors are not necessarily additive and in some cases would act in opposition, for example

precipitation could reduce the effect of both interstitial and substitutional hardening processes.

The accepted relationship between the carbon content and the hardness of steel may well be modified by such factors and this may explain the apparent discrepancy between the hardness of martensitic white layers and the hardness of conventional martensite formed in the bulk material of the same composition. In particular, the effect of plastic deformation and the observed small grain size of the white layer material should be considered.

The Hall-Petch relationship can be used to predict the effect of grain refinement on the strength of carbon steel,(Petch 1953).

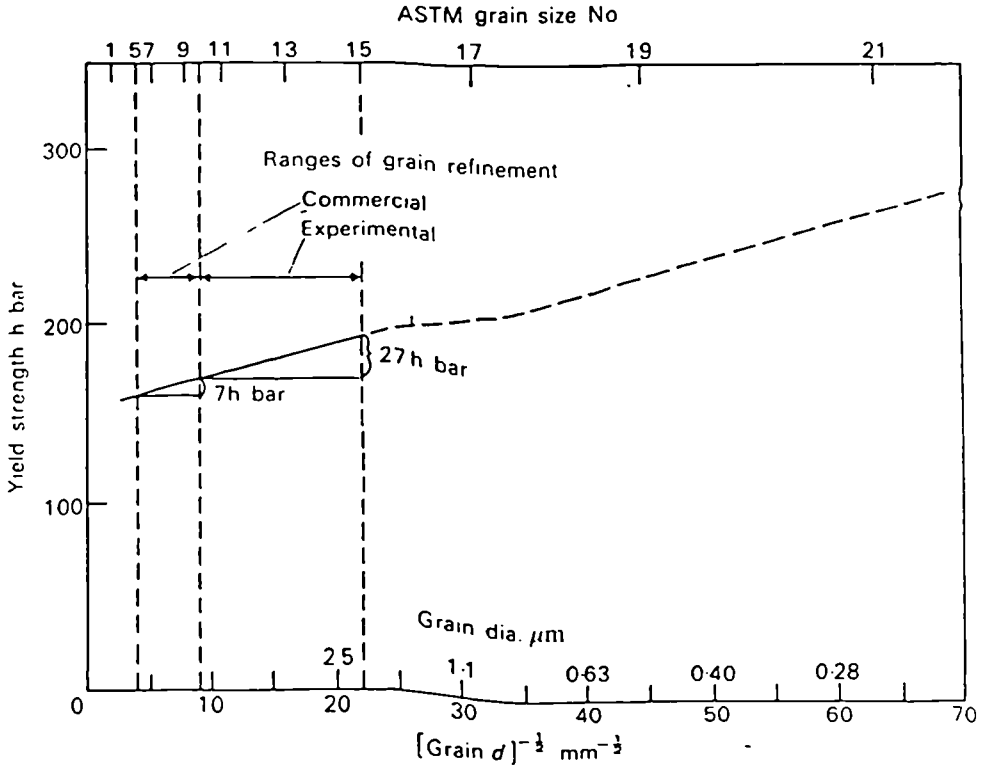

Figure 2.6. The strength of 0.5% C steel as a function of grain size. (After Grange. 1966)

Commercial and experimental grain refinement of 0.5 wt% C steel has been shown to increase the yield strength by a significant factor, (figure 2.6). Extrapolation to grain sizes of the order of 0.25μm would imply an increase in hardness from approximately 500HV to 840 HV, but this relationship is reputably unreliable at the small grain sizes observed in white-layers. (Rowntree, 1982).

2.7 Summary.

It is apparent from the available literature that white-etching layers may be generated by a number of different processes. It is also clear that no unique white-layer structure or composition has been identified, and that the process of generation as well as the nature of the bulk material is influential. The effect of environment is perhaps minimal under most machining and wear situations but it would be surprising if the white-etching layers observed on gun barrels for example, did not reflect the nature of the propellant gases used, and it is to be expected therefore, that in certain cases, white-etching layers will be generated having a different chemical composition to the bulk material.

2.8 Aims and objectives.

This project has been designed to clarify some of the aforementioned uncertainties as to the composition and structure of "white-layer".

A comparison will be made between white-etching layers

formed on steel by processes representative of; high temperature thermo-mechanical deformation, low temperature thermo-mechanical deformation, short-duration laser-heat-treatment, surface-chemical reaction under conditions of high pressure and temperature, and adiabatic shear.

An initial identification of the presence of a white-etching layer will be made by conventional metallographic techniques of light microscopy and hardness testing.

Following this initial survey, a series of chemical and micro-structural analyses will be made using microprobe analysis, secondary ion mass spectrometry and electron microscopy.

From this data, it is anticipated that a distinction will be made between the various types of white-etching layer formed by the processes previously described. This information will facilitate an understanding of the nature, and methods of formation of these layers.

Finally, it is intended that a clear distinction will be made between surface deposits which may be described as white-etching layers, and the "white-layer" observed on steel subjected to wear, abusive machining or adiabatic shear.

CHAPTER 3.

Materials and Experimental Techniques.

3.1. Introduction.

The extensive volume of literature relating to the occurrence, observation and characterisation of white-etching material at the metal surface, and in the special case of adiabatic shear, within the bulk, testifies to the widespread manifestation and significance of this phenomenon. Whilst the nature of such layers have been studied in detail by various workers who have considered specific systems, the controversy over the "true structure" of white-layer continues with little agreement over the underlying mechanism of generation.

In order to resolve some of the uncertainties regarding the nature of white-layer, this work centres on the study of a number of steel samples exhibiting different forms of white-etching layers. In the following sub-sections, the stages of the investigation are described:

First the differing nature and origins of the specimens, obtained from various sources and representative of some of the primary modes of white-layer generation, are presented.

Second, to provide a sound basis for comparison, the conventional metallographic techniques of light microscopy and microhardness testing were employed to establish the

presence of white-layer. The application and limitations of these techniques are briefly considered.

Finally, the techniques of electron microscopy, X-ray microprobe analysis and secondary ion mass spectrometry were used to provide micro-structural and chemical analysis of the various white-layers. The specialist sample preparation methods required, the principal of the techniques as applied to this work, and their particular advantages and disadvantages are described.

3.2. Sources of Material.

The various sources of material and different types of white-layer examined in this work, are detailed in the following section, classified in terms of the primary processes involved in their production. The nominal composition of the base or starting material of each white-layer generating system is indicated in the table (figure 3.1).

3.2.1. Laser Treated Samples.

3.2.1.1. Introduction and general procedures.

A 2kW BOC CO_2 gas laser was used to heat-treat the surfaces of specimens manufactured from 080M40, 817M40 steels and Armco iron, with a view to establishing the effect of laser heat-treatment on the resistance to wear.

The laser was operated at a nominal power output of 2.2kW, but measurement of the continuous on line beam output power on the day, showed an output of between 1.3kW

Nominal Material Composition Wt%								
Specimen	C	Si	V	Cr	Mn	Ni	Cu	Mo
Armco Iron	0.03	---	---	---	---	0.15	0.2	----
080M40 Steel	0.4	---	---	---	0.9	---	---	---
817M40 and RARDEN gun steel	0.4	---	---	1.2	0.6	1.5	---	0.3
Chieftain gun steel	0.4	0.2	0.2	1.0	0.5	3.0	---	0.5
Armour Steel	0.3	---	---	1.6	0.7	0.7	---	0.4

Figure 3.1. Composition of materials examined. (In this table and generally throughout the text, the terms 817M40 and 080M40 refer to steels to BS 970: 1970/72).

Laser heat-treatment conditions.			
Track No.	Traverse speed mms^{-1}	Depth of HAZ. in μm	Width of HAZ in mm
1	25	600	3.5
2	50	350	2.8
3	75	200	2.3
4	100	120	1.2
5	125	110	1.1
6	150	90	1.0

Figure 3.2. The relationship between the extent of the laser heat-affected zone and the sample traverse rate.

and 1.5kW with the "off-line" output set to 1.8kW. Full output power was not attained due to difficulties associated with power stabilisation.

Alignment of the optical path of the laser was accomplished by using a low power He/Ne laser to adjust the focussing objective lens and sample working distance. The beam energy distribution of the CO_2 laser, was determined by the operating mode, (in this instance a "mixed mode") and varied between a Gaussian and a "doughnut" distribution. By adjusting the distance of the work piece from the focal point of the system final objective lens, the laser spot size on the sample could be continuously varied as required. For these experiments it was determined that a spot size of 5mm could be achieved at a working distance of 28mm, whilst an effective spot size of 6mm was attained at a working distance of 34mm.

Samples were coated with a thin layer of matte black material to assist in the absorption of the laser power and to prevent a build up of contaminants at the working interface, a high pressure jet of argon "shroud" gas was directed at the work piece.

Controlled surface hardening was accomplished by traversing the sample surface beneath the laser beam, either as a single track, or as overlapping tracks to produce a relatively uniformly hardened surface.

3.2.1.2 817M40 Steel.

Ten discs 100mm in diameter turned from hardened and

tempered 817M40 steel in preparation for pin-on-disc wear testing, were supplied for laser-hardening treatment.

To establish the depth of the hardening treatment an initial experiment was conducted at various rates of sample traverse over a 100mm distance, to give a range of sample treatments in terms of the depth and width of the hardened track. (Figure 3.2).

From this preliminary experiment, it was determined that a traverse speed of $75mms^{-1}$, produced a hardened white-etching track, some 250μm thick by 2.5mm wide. A number of discs were then treated to produce a hardened surface for wear testing. The initial test specimen was retained for characterisation of the heat-treated tracks, by the methods described in subsequent sections.

3.2.1.3. 080M40 Steel.

Samples of 080M40 steel, prepared in the form of plates for reciprocating wear test specimens, were laser surface-hardened under similar conditions to the 817M40 disc specimens, following an initial experiment to determine the depth of the laser heat-treated zone. The depth of the white-etching layer formed by laser treatment was found to be 250μm for a traverse speed of $75mms^{-1}$.

3.2.1.4. Armco Iron.

Samples of Armco iron, previously machined into the form of rectangular plates for reciprocating wear tests, were surface-hardened using an on-line laser power of 1.5kW, in a similar fashion to the previous treatment

detailed for steel specimens. A range of traverse speeds at a fixed beam diameter of 6mm produced a set of 10 tracks exhibiting a range of treatment depths from 10μm to 600μm.

3.2.2. Abusively Turned 817M40 Steel.

Several small sections removed from discs of abusively-turned 817M40 steel, prepared for wear-testing and exhibiting a thin layer of white-etching material, were supplied by Brunel University . The hardness of the white-layers was stated to be in the region of 1100HV, in comparison to a matrix value of 350HV. Full details of the machining conditions under which white-layer was generated using carbide tools with artificial wear lands, are described by Griffiths and Furze (1986).

3.2.3. 817M40 Steel Wear pins.

A number of steel pins 5mm in diameter, conforming in composition to the 817M40 specification, which had been rubbed against steel discs (also manufactured from 817M40 steel) on a pin-on-disc wear testing rig, were provided for examination. The pins, which had been austenitised at 835°C and oil quenched to produce a martensitic structure, had been subsequently tempered at 200°C prior to wear testing in normal laboratory atmosphere, under conditions of load and running speed conducive to the generation of white-layer. See figure 3.3.

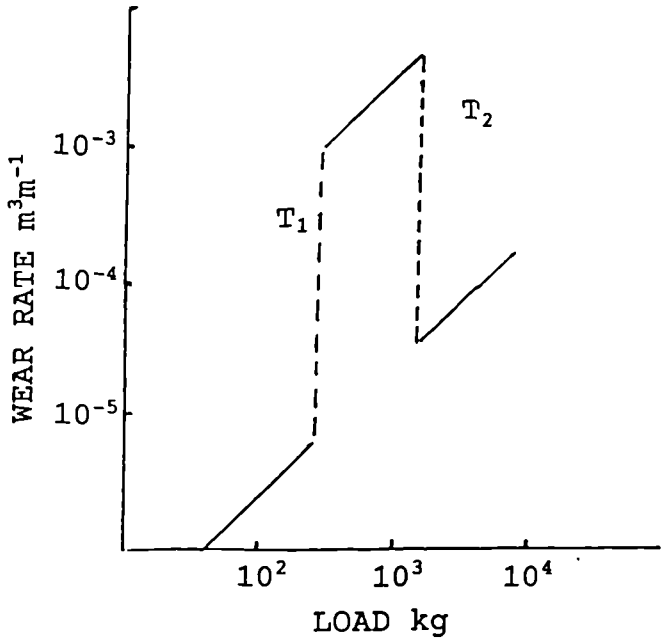

Figure 3.3. Surface hardness changes associated with the transitions from mild wear to severe wear (T1) and severe wear to mild wear (T2) under differing loads and a constant sliding speed of $1ms^{-1}$ (From Welsh, 1964).

3.2.4. Gravel Digger Tooth.

A section of a heavily worn digger-tooth, previously used for gravel extraction, was supplied for examination and analysis. Full details of the service history, material specification, chemical composition and heat-treatment condition were not made available.

3.2.5. Chieftain Gun Barrel.

A set of four mounted sections prepared from the commencement-of-rifling section, close to the breech of Chieftain tank gun barrels and exhibiting white-etching surface layers, were supplied by RARDE Fort Halstead for comparative analysis.

Details of the temperature rise, nature of the propellant charge and the number of rounds fired, were not

made available, but the base composition of the material (a low alloy medium carbon steel, close to 826M31) was indicated. (Figure 3.1).

3.2.6. RARDEN Gun Barrel.

A sample taken from a 30mm RARDEN barrel manufactured from steel close in composition to 817M40 specification, in the form of a barrel section some 50mm long, was supplied by the Royal Military College of Science. The specimen was taken from a position 25mm from the commencement-of-rifling, this being the position where most wear is usually measured. Information supplied, revealed that the barrel had fired 3750 rounds with various propellant charges.

Surface temperature measurement by means of a thermocouple situated in the rifling grooves, indicated that a rapid rise in surface temperature to almost 1000°C was measured 1 ms after firing. The temperature then dropped to 500°C above ambient, 8 ms after firing. (Figure 3.4). It was reported that the pressure curve was similar in appearance to the temperature curve, with a peak pressure of 4000 bar at each firing.

3.2.7. Adiabatic shear specimen.

To allow a comparative analysis of adiabatic shear bands with surface white-layers, a sample of low alloy steel with a hardness of 570 HV, exhibiting white-etching shear bands, was supplied by RARDE Chertsey for evaluation. The sample, which took the form of a section

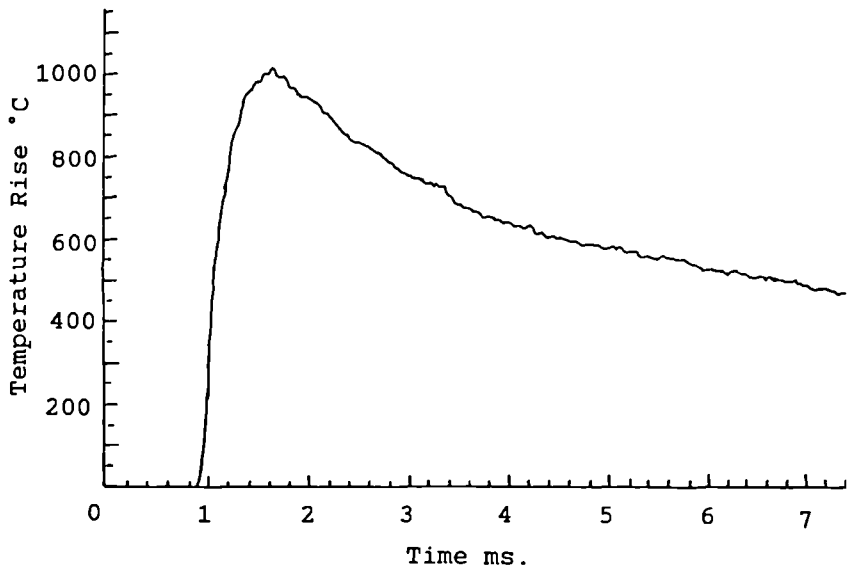

Figure 3.4. RARDEN gun barrel. Bore surface temperatures as a function of time after firing a round.

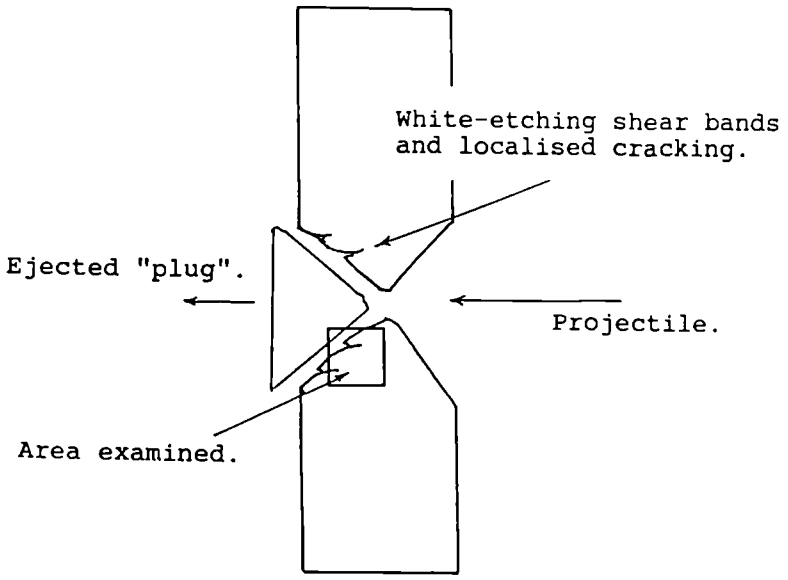

Figure 3.5. Schematic of the effect of ballistic impact on Armour steel, showing the location from which samples were removed for examination.

of steel plate, had been subjected to an impact with a high energy chemical round and had experienced strain rates in excess of $10^5 s^{-1}$, resulting in the ejection of a "plug" of material from the plate. The specimen supplied, represented a section through the steel plate adjacent to the impact area from which a "plug" of material had been ejected. (Figure 3.5.).

3.3. Specification and Nominal Composition of Materials.

The nominal bulk compositions of the materials examined in this work and a summary of their characteristics and properties have been obtained with reference to the appropriate British Standards, information provided by the suppliers and the source book on Metallic Materials compiled by Ross, (1968).

3.3.1. Armco Iron.

Iron is a relatively soft ductile material which cannot be hardened by thermal treatment and will accept a great deal of cold work without the necessity for interstage annealing.

Armco iron contains a very low level of carbon at 0.03 wt% and low levels of nickel and copper. See figure 3.1, in which the nominal compositions are compared .

3.3.2. Plain Carbon Steel. To BS 970.080M40.

These steels are hardenable by thermal treatment and cold work, with the degree of hardenability being proportional to the carbon content.

The material will not accept a great deal of cold work without intermediate annealing, ideally at temperatures between 880-900°C followed by slow cooling. A sub-critical anneal at 650-670°C will normally suffice except where severe cold work is to be followed by further cold work.

3.3.3. Low to Medium Carbon Alloy Steels.

The majority of the samples examined were formed from steels in this general classification, containing a carbon content of between 0.25 - 0.65 wt%, with two or more alloying elements, which ensure a high strength when fully tempered.

Both the RARDEN 30 mm gun barrel and the section of steel plate subjected to high velocity shear under adiabatic conditions, were manufactured from alloy steel with a composition close to 817M40 specification.

The precise specification of the Chieftain tank gun barrel steel was not known, but the indicated composition as shown in figure 3.1, classifies this material as a medium carbon alloy steel similar to 826M31.

In general, these steels are hardened by heating to 780-900°C followed by oil or air quenching, and are then tempered to the desired final hardness. The various alloy

additions affect the formation of carbides and strength of the ferrite matrix. Specific heat-treatments are required to attain the most suitable structure for each steel.

3.4 Experimental Procedures (1)
Metallographic examination.

3.4.1. Introduction.

Metallographic examination using incident reflected light microscopy was combined with microhardness testing, to identify white-layers in terms of etching resistance and hardness, relative to the bulk material.

3.4.2 Light Microscopy

One of the primary techniques employed in the identification of white-layers, from the earliest observations of such features, for example, Stead (1912), through to the present, has been the examination by light microscopy, of metallographically prepared specimens. The high resistance to chemical etching of the white-layer, relative to that of the more conventional steel microstructures, allows rapid visual detection of this material for subsequent testing and analysis.

The various steel samples examined in this study were prepared using the standard methods of metallographic preparation as described by Samuels (1967) and examined by incident reflected bright field and Nomarski differential interference contrast (DIC), which allowed small differences in surface relief to be revealed.

The technique of chemical etching, which is dependent

upon differential dissolution of different phases or crystals within the metal matrix, was utilised to render the various microstructural features visible for examination. Many etchant formulations have been developed for use with carbon steels to assist in the identification of the various phases and structures developed during processing, forming and heat treatment. These etchants are catalogued in a number of publications, e.g, Modin and Modin (1973). For this work, the standard etchant employed to reveal the matrix microstructure and indicate the presence of white-layer was a 5% solution of nitric acid in methyl alcohol, (Nital).

3.4.3. Hardness Testing

The hardness of a metal, defined as the resistance to penetration, gives an indication of its deformation behaviour. Most hardness testing instruments rely upon the accurate measurement of the diameter of an indentation formed on the surface of the metal, by forcing an indenter into the metal under a known and controlled load. The hardness may also be related to the yield or tensile strength of the metal, since during the indentation, the material around the impression is plastically-deformed. In this work a Vickers diamond pyramid indenter fitted to a Leitz Miniload hardness tester was used to obtain microhardness results in Vickers hardness number, (HV).

Where results are compared with those obtained by other workers using different hardness testing apparatus,

a conversion has been made to HV values, with reference to standard tables eg,(Robb 1987). It should be noted that a direct comparison could contain a considerable degree of error, as different hardness testing instruments make use of different loads and different shaped indenters.

Calibration of the hardness indenter was checked with reference to a standard block with a quoted hardness of 591 HV. It was found that for a series of ten readings, that measurements with a 100g load underestimated hardness by 4% whilst the 25g load overestimated the test block hardness by 9%.

3.5. Experimental Procedures (2)

Analytical Techniques.

Scanning electron microscopy of the specimen surfaces and metallographically prepared cross-sections, together with semi-quantitative microprobe analysis were used to characterise the various white-layers. A microstructural study of selected areas was effected by transmission electron microscopy and electron diffraction analysis.

To establish the distribution of low atomic number elements in the surface layers, a light element wavelength dispersive X-ray spectrometer system was utilised, these results were then compared with those obtained by the more recently developed technique of secondary ion mass spectrometry.

Specific advantages and disadvantages of each technique,

and details of specimen preparation are discussed more fully in the following sub-sections.

3.5.1. Scanning Electron Microscopy.

The Scanning Electron Microscope (SEM), is an invaluable tool for the examination of materials and possesses several advantages over the light microscope including; increased resolution, improved depth of field and a wide range of image contrast techniques based on electron interactions.

In this work, both a Cambridge S250 and a JEOL 840A SEM were used to study the surface morphology of the worn, machined and surface treated samples, to establish a comparison between the surface texture and the underlying metal microstructure.

A number of interactions may occur when a beam of energetic electrons strikes the surface of the specimen. (Figure 3.6). Those of most relevance to imaging in this work are outlined as follows:

1) Secondary electrons; generated by interaction between the incident electron beam and the sample, these electrons have an escape depth limited to a few tens of nm due to their low energy of between 5eV and 100eV. This imaging mode offers the highest resolution, limited by the aberrations of the electron lens system and stability of the microscope to 5nm, allowing examination at magnifications well in excess of those attainable by light microscopy.

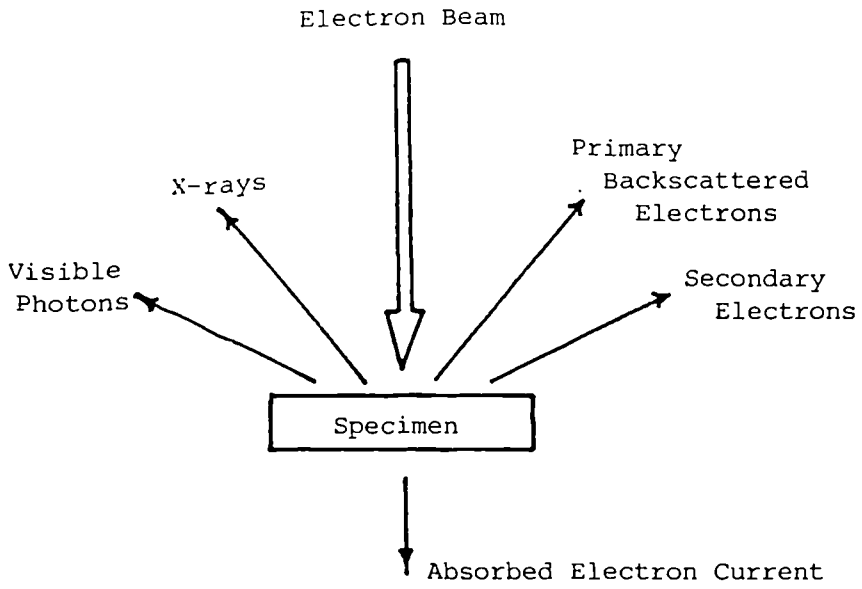

Figure 3.6. Electron beam - specimen interactions.

2) Backscattered electrons; *electrons may be* backscattered from the sample surface with little loss of energy. The efficiency of backscattering is proportional to the average atomic number of the specimen, thus local variations in composition may be detected and used to produce atomic number contrast images. Backscattered electrons leave the sample with well defined trajectories, and a very strong topographic contrast image will result if a directional electron detector is used.

The resolution of this signal is considerably lower than that of the secondary electron image, due to the greater escape depth of the high energy electrons and the volume of scattering within the sample, which could extend over 1μm from the position of the electron probe.

3.5.2. Electron Microprobe Analysis.

3.5.2.1. Introduction.

To assess the usefulness and limitations of microprobe analysis with respect to this work, it is helpful to briefly consider the physical principles underlying the technique:

High energy electrons incident upon a solid sample may interact inelastically with sample atoms, causing core shell ionisation. The subsequent rearrangement of electrons within the atom may result in the emission of an X-ray having a characteristic wavelength or energy.

The X-ray spectrum generated by the interaction between a beam of high energy electrons and a solid, consists of a series of sharp characteristic lines, superimposed on a background of continuous radiation. A qualitative analysis may be achieved by measurement of emitted X-ray wavelengths, as in the wavelength-dispersive X-ray spectrometer (WDX), or by measurement of the X-ray energy, as in the solid state, energy-dispersive X-ray detector system, (EDX).

Whilst the EDX system has many advantages in terms of; signal collection efficiency, speed of analysis and ease of operation, the spectral resolution is poor compared to that of the WDX spectrometer. More significantly, the sensitivity to low energy, long wavelength X-radiation is limited, and analysis of low atomic number elements

($Z < 11$) is difficult.

The JEOL 840A scanning electron microscope used in this work is fitted with two fully focussing, WDX spectrometers, each equipped with two different types of crystals, enabling analysis of elements from boron to uranium. The spectrometers are aligned vertically with respect to the electron optical column and are of the linear type, with curved and ground diffracting crystals of the "Johansson" type. (Reed, 1975). For light element analysis, stearate and thallium hydrogen phthalate, (TAP) crystals were used to diffract the long wavelength, low energy X-rays into a gas-flow proportional counter, operated with a mixture of argon and methane. This type of spectrometer has the advantage of high spectral resolution and good sensitivity to low atomic number elements, but suffers from the disadvantage of low detection efficiency, and for most analyses a high incident beam current is required.

To enable analysis of specific features identified by SEM and light microscopical examination, a set of metallographic cross sections through; surface treated, machined, and worn steel samples, were prepared in conductive phenolic resin mounts. To facilitate quantification of data acquired from these specimens, a length of high purity copper wire was incorporated into each mount to act as a reference standard for EDX analysis.

Data was acquired from features of interest identified

on the samples and stored on disc, together with a spectrum recorded from the standard copper incorporated into the mount, to allow standardisation of data recorded on different dates.

3.5.2.2. Quantitative Analysis

A quantitative analysis was obtained from the ratios of measured intensities of characteristic X-radiation using a LINK SYSTEMS ZAF4 quantification routine based on Castaing's approximation;

$$I_A/I_{STD} = C_A$$

where IA is the intensity of characteristic radiation generated within the sample, Istd is the intensity generated within a pure standard, and CA is the concentration of the element A in the sample.

In bulk specimens, most X-rays are generated within a small volume below the surface and corrections must be applied to the simple ratio to take account of the "matrix" effects. (Reed 1975).

The so-called ZAF corrections may be applied in an iterative manner very conveniently by computer to modify Castaing's expression :

$$C_A = I_A/I_{STD} \cdot k_Z, k_A, k_F.$$

where k_Z is the atomic number correction, k_A the absorption factor and k_F the fluorescence factor. The significance of these factors to bulk analysis may be considered as follows;

1) The atomic number correction, kZ : The ionisation efficiency, electron stopping power and the electron backscatter coefficient, vary for different atomic number materials and accelerating voltages. This correction is small unless there are large differences between the average atomic number of the specimen and that of the standard. This correction would be most pronounced for low atomic number elements in the steel matrix.

2) The absorption factor, kA : The generated X-ray is attenuated by the matrix, the degree of attenuation being dependent on the average mass absorption coefficient and the X-ray path length. In principle, this correction can be minimised by suitable selection of sample tilt and accelerating voltage, in practice a minimum excitation energy of 20 keV was required to efficiently excite characteristic radiation, and a sample tilt of 35° was found to be most appropriate for the instrument used.

3) The fluorescence factor, kF: X-rays generated in the sample matrix, may have sufficient energy to excite further radiation from other elements present in the matrix. These "fluoresced" X-rays, will lead to an overestimate of that particular element in the analysis. The correction is usually small unless $\Delta Z = 2$ as in Fe/Cr alloys where the Cr signal is enhanced.

To minimise cumulative errors, counts from both specimen and standards were taken under the same conditions of sample tilt , working distance and accelerating voltage. Data was acquired for counting

periods of 100s, this being sufficient to reduce statistical errors for the smaller peaks to less than 2 standard deviations, as required by the ZAF 4 quantitative routine. Following normalisation or estimation of light element content by difference, the results are quoted to one decimal place.

3.5.2.3. Wavelength Dispersive Techniques.

Semi-quantitative light-element analysis was undertaken using the wavelength crystal spectrometers fitted to the JEOL 840A SEM. The low atomic number elements of particular interest in this study i.e; carbon, nitrogen and oxygen were detected using the stearate and TAP diffracting crystals and the gas-flow proportional counter previously described.

Electron microprobe analysis of light elements is complicated by a combination of experimental and fundamental difficulties. The latter includes the much reduced ionisation cross section for X-ray emission for low atomic number materials described by Reed (1975), and the somewhat compensatory increase in emission due to the higher overvoltage ratio under standard analytical conditions. Operating at high voltages however, whilst maintaining relatively high count rates, also increases the depth of electron beam penetration, particularly in low average atomic number matrices. This in turn increases the probability of absorption of the generated X-ray and creates further problems for data quantification. (Goldstein and Colby, 1975). A further difficulty is

presented by the overlapping of L or M spectra from heavier elements. A particular problem in steel analysis being the overlapping of the Lα line for titanium, (a common alloy addition), with the Kα line for nitrogen, which with a wavelength of 31.6nm is inseparable from the Ti Lα at 31.4nm.

Experimental difficulties encountered, included the degradation in spatial resolution of the electron beam when working at the high electron beam currents necessary for WDX analysis, this problem being particularly severe at low values of accelerating voltage. For example, under the operating conditions chosen for light element analysis, a beam diameter of some 5μm was measured on the sample surface, for an incident beam current of $3x10^{-8}$A, at 5keV.

A further problem was presented by the carbon containing contaminant layer, which was found to develop on the sample surface, as a result of polymerisation under the electron beam of organic material originating from the vacuum pump oils. To reduce this effect it was found beneficial to allow the sample chamber to evacuate over a prolonged period prior to commencing microprobe analysis. The effect of this carbon contaminant was to generate a background carbon signal which effectively masked small variations in the carbon content of the samples. In an attempt to establish the true carbon distribution, a qualitative analysis was carried out with a moving sample to reduce the effect of contamination, pending

modification to the instrument by addition of a liquid nitrogen cooled diffusion pump baffle to improve the pumping speed and reduce backstreaming of pump oil.

It was found in practice, that the effect of the contaminant layer could be reduced in the "spot" analysis mode necessary for analysis of discrete features, by selecting an accelerating voltage of 10keV. The increase in penetration effectively allowing analysis of material underlying the contaminant layer.

3.5.2.4. Calibration Curves.

Quantification models developed for ZAF corrections are not generally applicable to light element analysis where large absorption corrections are required and mass absorption coefficients for long X-ray wavelengths are not well known,(Goldstein and Colby, 1975). An alternative technique which can provide reliable data is to use standards whose composition is close to that of the material being analysed. An example being the analysis of carbon in iron and nickel containing steels, where calibration curves for carbon levels from zero to 1.3 wt% have been published by Fisher and Farningham (1972). (Figure 3.7).

In this work, a series of carbon containing steel samples, homogenised by heat-treatment, were used to generate a calibration curve for carbon contents of between 0.12 and 1.22 wt% . Data was acquired from standards and specimens with a beam energy of 10 keV, for

counting periods of 100s at the C Kα peak position, with a beam current of $2x10^{-8}$ A, as measured between counts with a Faraday cup. Correction for beam current drift during the counting period was made by simultaneously monitoring a suitable fraction of the continuum background (between 3 - 3.5 keV), using the EDX detector .

In practice, calibration was established for each set of experiments to compensate for minor day-to-day changes in counting efficiency, due for example, to changes in counter gas temperature and flow rate. The average of these calibration curves is shown in figure 3.8, in which the straight line is derived by linear regression analysis of the five highest points. The deviation from this fit at low carbon contents is attributed to system carbon contamination, at a base level of between 0.2 - 0.3 wt%.

The relative error for this calibration technique for a 0.34 wt% carbon standard, assuming counts lie within 3 sd of the mean, is 15%. This implies that changes in carbon content of 0.05wt% may determined.

3.6. Transmission Electron Microscopy.

3.6.1. Introduction.

Transmission electron microscopy (TEM) provides a means of directly examining the micro-structure of materials, provided that they can be prepared as electron-transparent thin foils. In this work, specimens prepared from different forms of white-etching layer were examined in the JEOL 100CX TEM and the JEOL 2000FX TEM at accelerating voltages of 100kV and 200kV

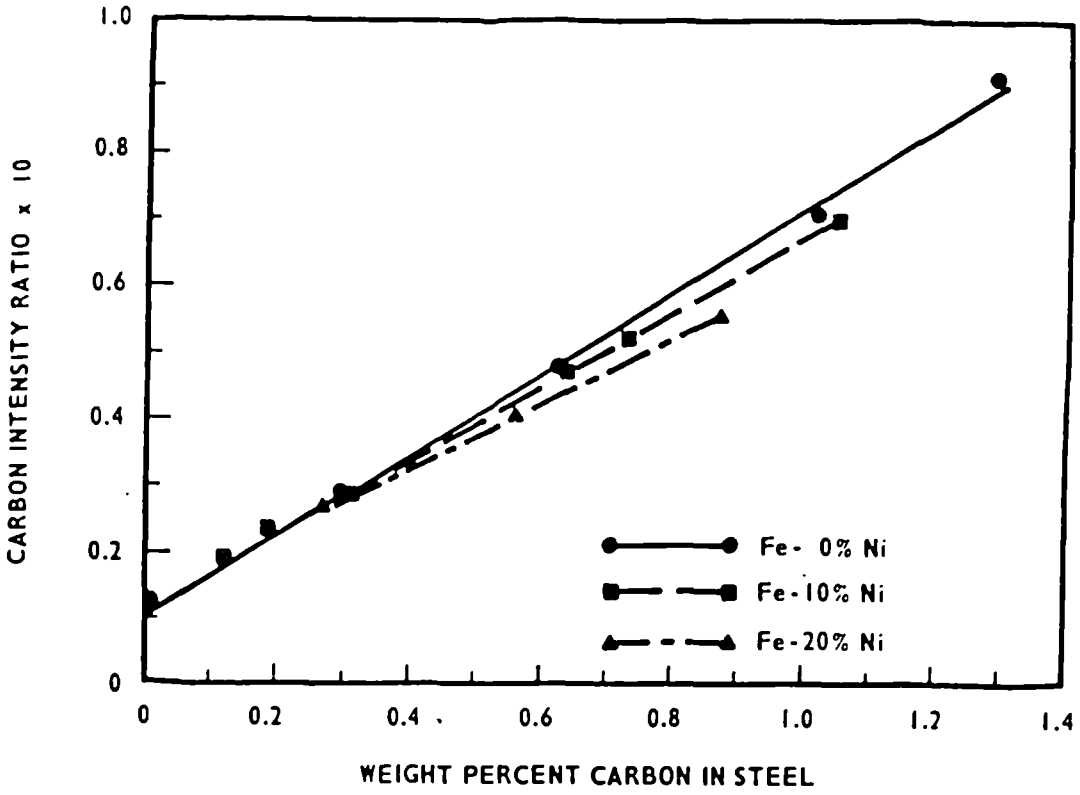

Figure 3.7. Calibration curve for carbon in steels. (From Fisher and Farningham 1972)

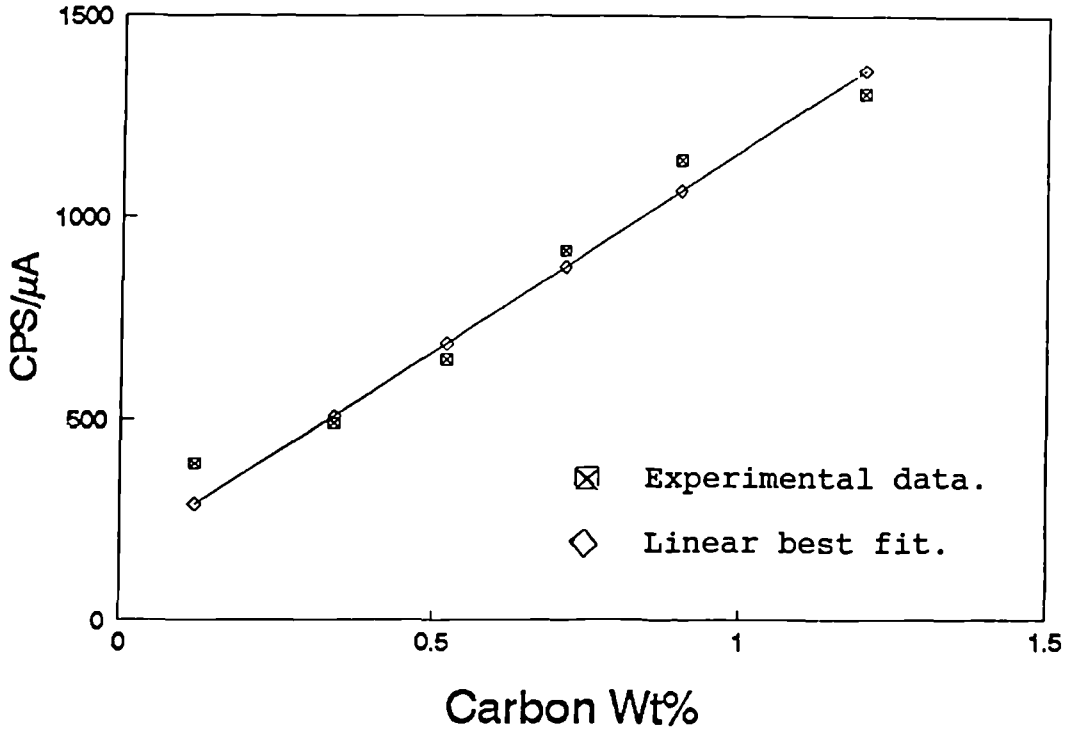

Figure 3.8. Calibration curve obtained from steels with carbon contents from 0.12 - 1.2 Wt%.

respectively. The higher voltage affording greater electron penetration and higher resolution. Both of these instruments were equipped with an EDX detector and scan coils, permitting operation as a high resolution SEM and as a scanning transmission electron microscope, (STEM).

3.6.2. Specimen Preparation.

Specimens suitable for transmission electron microscopy should , in addition to being sufficiently thin to be transparent to electrons, possess a number of desirable features, Goodhew, (1985), and as follows should be :

i) representative of the bulk material;
ii) thin and parallel sided;
iii) largely flat, although some buckled areas can be helpful in location of zone axes in crystalline foils;
iv) undamaged by preparation;
v) able to be handled; not fragile;
vi) stable against oxidation or other degradation;
vii) free from surface segregation;
viii) clean;
ix) electrically and thermally conductive;
x) non-magnetic.

The last of these being a particular problem when examining ferromagnetic thin foils in microscopes with strongly excited objective lenses.

In developing techniques suitable for the preparation of

thin foils containing white-layer, reference has been made to the extensive literature available detailing preparation techniques, and in particular the specialist publications by Kay,(1965) and Goodhew,(1985).

3.6.3. Thin Foil Preparation.

The techniques of electrochemical thinning and ion-beam thinning were applied to the preparation of thin foil specimens from regions containing white-etching layers at the surface of the various steel samples examined.

It was found to be necessary to plate surfaces with nickel, prior to metallographical preparation and mechanical sectioning of the specimen. First to preserve the white-layer, which on some samples was extremely thin, and secondly to present the area of interest close to the centre of the 3mm diameter foil finally produced.

Various electroless and electroplate nickel plating techniques and solutions were used in an attempt to produce the desired thick ($\approx$ 1mm), adherent and ductile layer required. The most satisfactory procedure involved the application of a thin coating of nickel, using a solution of "Wood's nickel", applied in an ultrasonic bath to provide a "flash". This was then electroplated using a plating solution formulated on the "Watt's bath " to produce a thick layer of ductile, stress free nickel up to 1mm thick. Details of the nickel plating process are included in the Appendix to this thesis.

Following metallographic preparation of the plated

specimen to reveal areas of interest, sections were cut from the sample using a low speed, low deformation diamond saw. Additional mechanical thinning was achieved by mounting the section onto a steel block using double-sided adhesive tape, and hand grinding on 600 and 1200 grit silicon carbide papers, before diamond polishing to a 1μm finish. Following polishing of one side, the sample was removed from the steel block and remounted to allow preparation of the reverse. Great care was taken when removing the sample from the double sided tape to avoid introducing strain into the foil.

At this stage the polished disc was lightly etched in 5% Nital and inspected by light microscopy, to confirm that white-layer was present and to assess the adherence of the nickel plated layer. The various steps in this complex preparation procedure are shown in figure 3.9.

Electrochemical thinning was carried out using a Tenupol two jet unit, with the Struers electrolyte A8, following the general guidelines in the Struers handbook, and with reference to recommendations made by, Brammar, (1965) and Goodhew, (1985).

It was found that satisfactory foils could be produced from 3mm discs of material some 50μm thick, with thinning times of approximately 30 s, using electrolyte cooled to 5° C by adding liquid nitrogen to the electrolyte prior to thinning. The foils were washed in analar grade methanol following thinning, and examined immediately to avoid the development of oxide films on the sample surface. Where samples were preserved for further examination they were

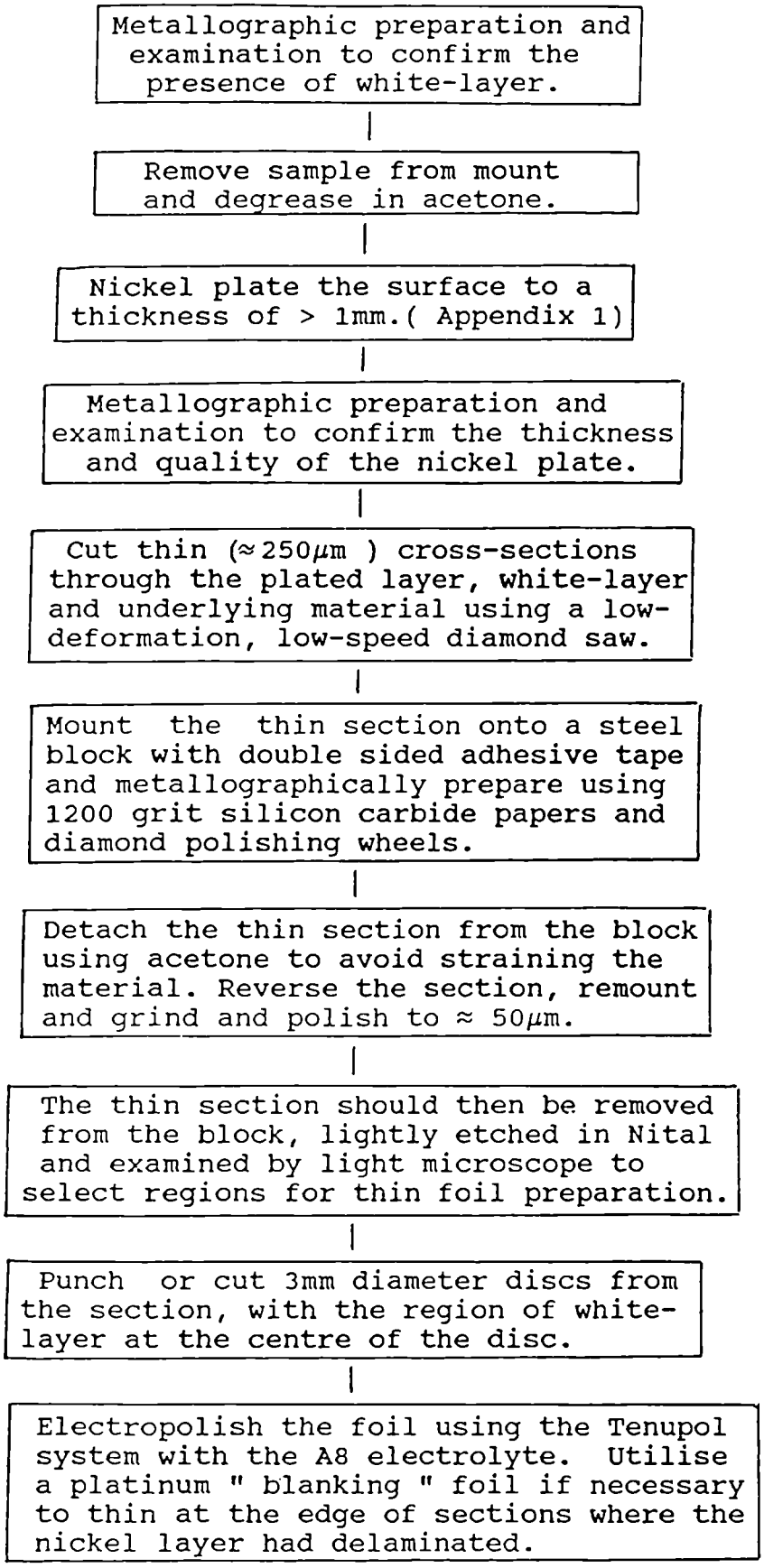

Figure 3.9. Thin foil preparation procedure.

stored in glass jars containing analar grade methanol.

It was extremely difficult to prepare 3mm discs for electro-chemical thinning from the polished 50μm thick material, without causing the nickel layer to break away. In order not to waste the resulting half-disk, a most effective method of thinning close to the straight edge of the half disc was developed. This utilised a small sheet of platinum foil, carefully perforated to produce a 250μm semi-circular hole. By carefully aligning the straight edge of the perforation with the straight edge of the half disc specimen, with the aid of a stereo-light microscope, it was possible to use the standard Tenupol unit to prepare foils within several micrometers of the cross-sectioned surface.(Figure 3.10.).

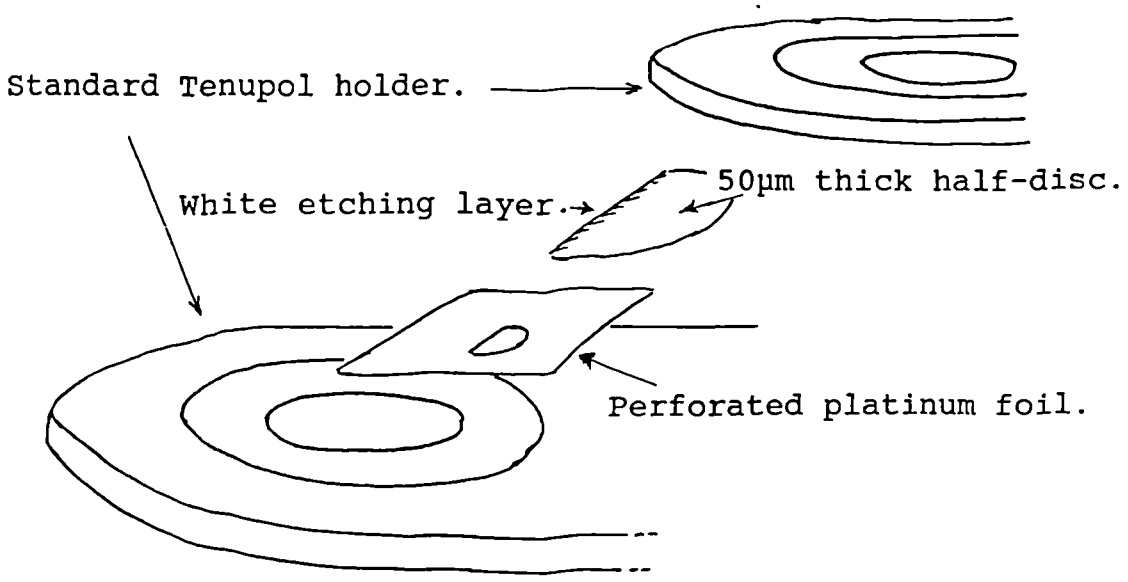

Figure 3.10. Schematic of technique for preparing thin foils at the edge of a polished cross-section.

An unforeseen but beneficial consequence of this necessary modification to the procedure, was that large flat areas of thinned material were produced, as a result of accelerated, but uniform thinning of the shielded side of the foil .

Ion-beam thinning has been recommended as a technique for the preparation of cross-sections of wear surfaces, following suitable protection of the surface, Ives, (1983), and this method was also used as a preparation technique for thin foils using an Ion-Tech instrument which allowed thinning from both sides of a pre-thinned 3mm disc of material. The rate of thinning was found to be considerably slower than electrochemical techniques, with a material removal rate of some 2μm per hour per side. Thus to thin a 50μm thick foil to electron transparency at some 0.1μm, required thinning times in excess of 12 hours. The technique has clear advantages where non-electrically conducting samples are to be thinned such as ceramics, but was not found to be particularly useful in this work where the slow etching rate and the generation of topographical artifacts after etching periods as short as 1 hour, were disadvantageous. Further details of the technique and its applications are described in Goodhew, (1985).

3.6.4. **Examination Techniques.**

Thin foils prepared in the form of 3mm discs by ion-beam or electrochemical thinning techniques were found to be easily mountable on the TEM stage without additional

support. Operation in the SEM mode was found to be a useful precursor to TEM operation, as this not only enabled rapid location of the small holes formed in the thinned areas of the foil during the electrochemical thinning process, but also enabled the cleanliness of the foil surface to be assessed both by appearance and by chemical composition, using the EDX facility.

A particular problem experienced during examination of thin foils, was that of variable astigmatism due to the interaction between the magnetic field of the highly excited objective lens and the ferromagnetic specimen. This problem was particularly severe on the 2000FX instrument and despite careful demagnetisation of the specimen following mounting in the microscope stage, the following alignment procedure was necessary, after every movement of the sample:

i) The area of interest was centred and the image focussed using the objective lens;

ii) The second condenser lens was focussed and the beam centred with the objective aperture removed;

iv) The current centre was aligned using the objective lens "wobble" control;

v) Stage two was repeated and the objective aperture replaced and centred;

vi) Finally the image was refocussed and the astigmatism corrected.

3.7. Electron Diffraction.

3.7.1. Introduction.

The TEM may be used as a selected area electron diffraction camera in which a specific region of the sample as small as 0.5μm in diameter is defined by the selected area aperture. The technique is well suited to the study of small volumes of material, allowing microstructural characterisation of phases and particulates. The combination of imaging at high resolution and in modern instruments , the ability to perform a localised chemical analysis by EDX for example, makes interpretation of the electron diffraction pattern less of a problem.

3.7.2. Experimental procedures.

Conventional selected area electron diffraction was carried out on thin foil samples prepared from cross-sections of surface layers, to establish the crystal structure of those layers in comparison to the underlying matrix. Diffraction patterns were collected using the JEOL 100CX at 100kV and the JEOL 2000FX at 200kV and indexed using the standard procedures described by Andrews et al (1971).

Calibration of the electron-optical column was achieved with reference to a thallous-chloride standard, from which the camera length could be measured. The accuracy of lattice parameter measurements derived from SAD patterns was estimated at ± 2% taking due account of

the reproducibility of diffraction data.

Where appropriate, the technique of micro-diffraction, in which the electron beam is focussed to a very small beam diameter on the sample surface, was applied to selected features. This technique which utilises the Scanning Transmission or STEM facility of the TEM, allows a diffraction pattern to be obtained from areas as small as 50nm in diameter and is applicable to the study of deformed and recrystallised samples. (Ralph and Ecob, 1984). The estimate of lattice parameter and hence c/a ratio is inherently more accurate using micro-diffraction but the size of the final pattern limits measurement accuracy, and results are quoted to an accuracy of ± 2%.

3.8. Surface Analysis by SIMS.

3.8.1. Introduction.

The technique of secondary ion mass spectrometry (SIMS), which is based on the process of sputtering atoms from the sample surface, with subsequent mass analysis, is a most powerful method of analysis with a wide range of application. The development of the technique and the principles of the sputtering and analytical processes are described in some detail by Sykes (1989).

The technique, which is basically destructive, as the surface layers are rapidly etched away during "dynamic" SIMS analysis, provides information from the surface at very high sensitivity, with detection limits quoted down to 100 ppb for many elements.

3.8.2. Experimental Procedures.

For comparison with data acquired by conventional and light element microprobe analysis, a number of samples exhibiting "white-layers" were analysed using a Cameca 4f ion microprobe, to provide a depth profile analysis for the elements; carbon, nitrogen, oxygen and hydrogen, through selected regions. The spatial resolution could be varied by selecting an area as small as 5μm in diameter, within the 120μm wide, approximately square crater, sputtered by the caesium primary ion beam.

Spectra were acquired as plots of ion yield versus etching time, and converted to semi-quantitative data with reference to the iron level of the relevant matrix composition. The depth of the craters were determined using an " Alphastep " surface profilometer allowing the results to be expressed as depth profiles where relevant.

CHAPTER 4

RESULTS SECTION.

4.1. Introduction.

The results of the various experiments performed on samples, representative of each of the white-layer forming processes studied, are presented in the following chapter; grouped in terms of the experimental or analytical technique employed to aid intercomparison of results.

White layers are first characterised by their high reflectivity, in comparison to conventional metallurgical structures when observed in the polished and etched condition by reflected light microscopy. High hardness is often associated with white-layer and may be considered to be an essential secondary characteristic of "white-layer" when that term is used in engineering (e.g. tribological) terminology. Accordingly, the results of the light microscopical examination and hardness test measurements are presented together, so that the white-layers examined may be first identified using well accepted criteria.

Scanning Electron Microscopy (SEM), was used to examine the surfaces of the various specimens to provide topographical information. The great depth of field and high resolution of the technique allowing examination of specimens at magnifications of up to 10,000 times. Metallographically prepared cross sections were also examined using SEM, both to identify areas suitable for electron probe microanalysis and to provide high resolution images of the metallographic structure.

The composition of the white-etching layers were determined by conventional microprobe analysis, light element microprobe analysis and secondary ion mass spectrometry. The results of these analyses are presented in separate sub-sections reflecting the different information obtained by each technique.

4.2. Light Microscopy and Hardness test measurements.

4.2.1. Laser treated 817M40 Steel.

The metallographically prepared cross section through the laser heat-treated tracks, produced at the surface of the 817M40 steel , allowed a comparison to be made between the structure of the underlying matrix and that of the laser heat-treated volume.

Figure 4.2.1. shows the cross section of a track produced by traversing the sample under the laser beam at a speed of some 25mms^{-1}, with an effective "on-line" laser power output of 1.5 kW focussed into a 6mm diameter spot at the sample surface. The resultant laser-treated zone is seen to be somewhat asymmetrical having a maximum depth of 600μm and a width at the surface of 3.16 mm. The transformed volume exhibited three distinguishable structural zones as shown in Figure 4.2.2, in differential interference contrast, (DIC). These vary from a dendritic grain structure close to the surface, a mid-region of coarse acicular product and a zone of fine-grained product with a clear boundary at the interface with the unmodified matrix.

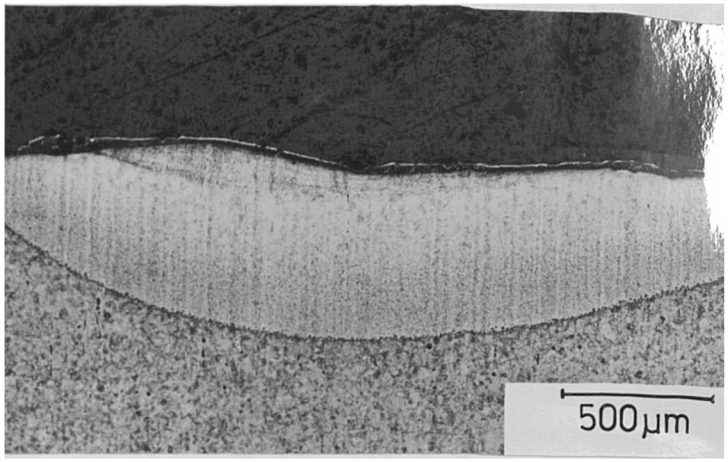

Figure 4.2.1. Laser treated 817M40. Track.1. 25mms^{-1} Cross-section through white-etching laser heat-treated zone.

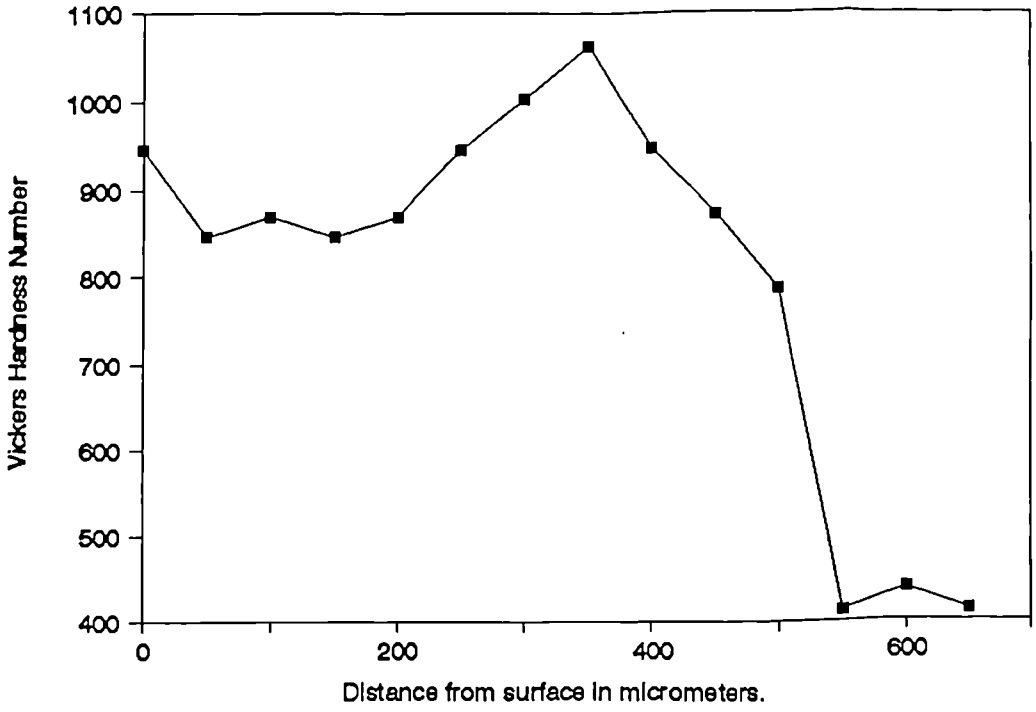

Figure 4.2.2. Laser treated 817M40. Track 1. 25mms^{-1} Hardness depth profile from the area shown in the above micrograph.

The hardness of the white-etching zone was measured as a function of depth from the sample surface; the results as shown in Figure 4.2.3, indicate that the maximum hardness within the heat-treated volume, of 1064 ± 30 HV.(25g), coincides with the region of fine structure observed at a depth of 350μm.

With a faster sample traverse of 50 mms^{-1}, the laser-modified zone was seen to diminish (Figure 4.2.4). Under these conditions, the maximum depth of the affected zone was 350μm, with a width of 2.8mm. At higher magnification (Figure 4.2.5), three different structural zones are visible, as in the more slowly traversed specimen. A manganese sulphide inclusion, apparently unaffected by transitory heating, is seen to extend into the dendritic region.

In a similar fashion, further laser-treated tracks generated at progressively faster traverse rates, show decreasing depths of laser-treatment. See Figures, 4.2.6, and 4.2.7, for a traverse rate of 75mms^{-1} and Figures 4.2.8, and 4.2.9, for a traverse rate of 100mms^{-1}. It can be seen that the laser-treated depth diminishes to 210μm at 75mms^{-1} and 100μm at 100mms^{-1}, whilst the width is reduced to 2.3mm and 1.3 mm respectively.

The structural details of the laser-treated zones are less complex at high traverse rates, exhibiting a fine grain structure at higher magnification, similar to the deepest affected zone shown in Figure 4.2.2.

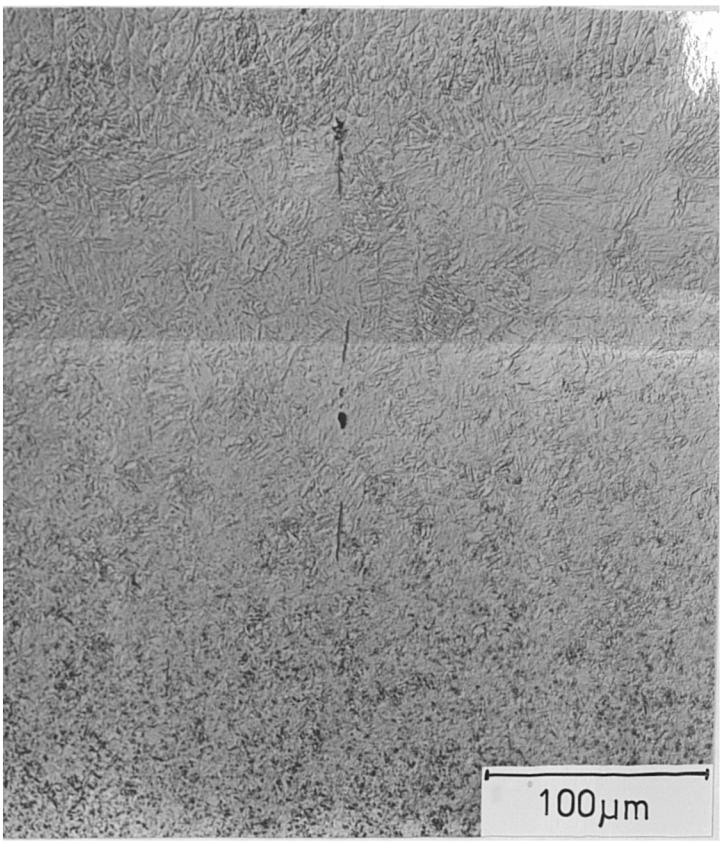

Figure 4.2.3. Laser treated 817M40. Track.1. 25mms^{-1} Structural variation through the laser heat-treated zone.

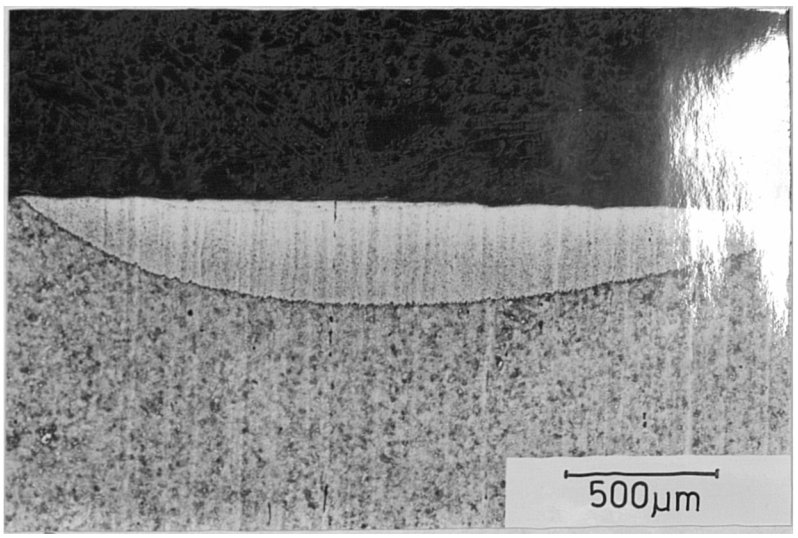

Figure 4.2.4. Laser treated 817M40. Track.2. 50mms^{-1}. Cross-section through white-etching laser heat-treated zone.

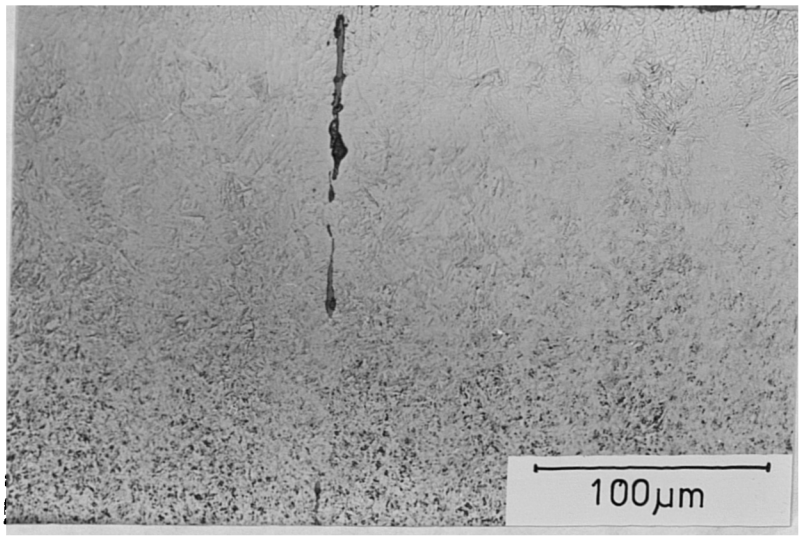

Figure 4.2.5. Laser treated 817M40. Track.2. 50mms^{-1}. Manganese sulphide 'stringer', unaffected by short duration heating.

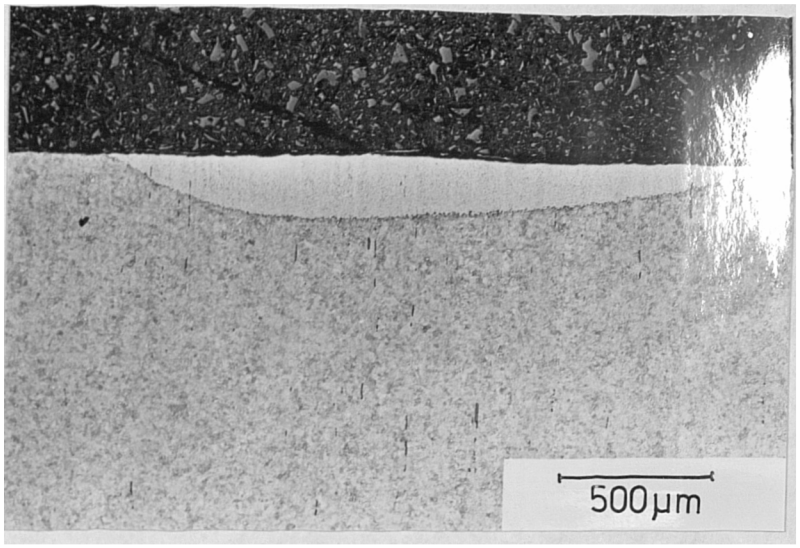

Figure 4.2.6. Laser treated 817M40. Track.3. 75mms^{-1}. White-etching zone 210µm in depth.

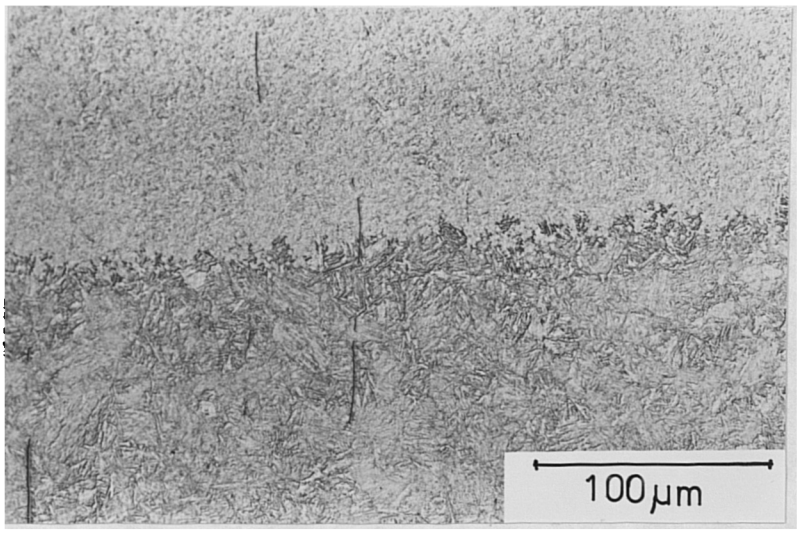

Figure 4.2.7. Laser treated 817M40. Track.3. 75mms^{-1}. Transition between fine grain product and the underlying matrix.

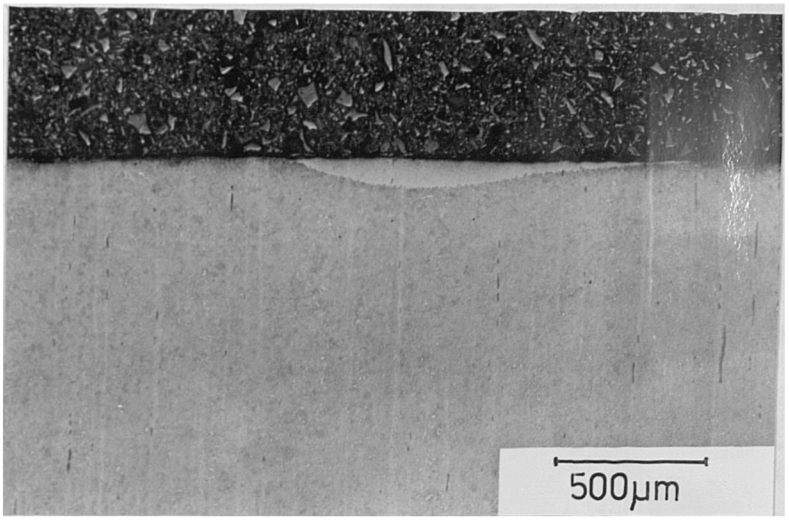

Figure 4.2.8. Laser treated 817M40. Track.4. 100mms^{-1}. Shallow single 'phase' white-etching zone.

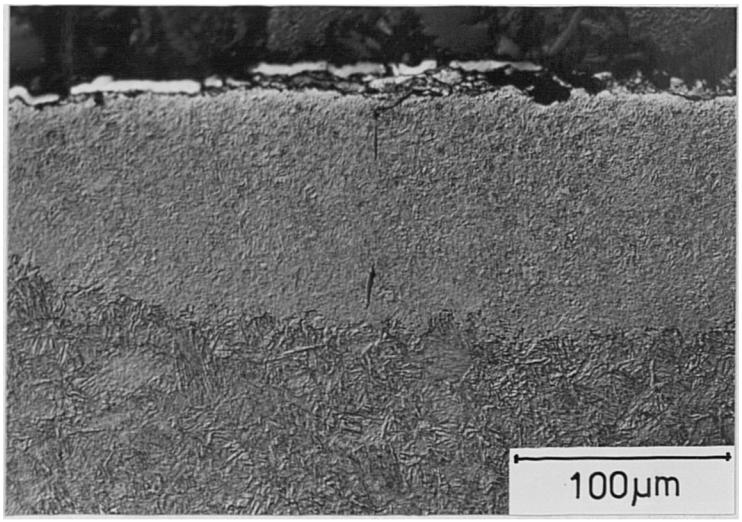

Figure 4.2.9. Laser treated 817M40. Track.4. 100mms^{-1}. Detail of above showing a fine grain structure containing manganese sulphides.

As the depth of the heat treated zone was reduced, the region of maximum hardness also moved closer to the surface. Figure 4.2.10, compares the hardness profile of the four tracks studied and demonstrates that hardness values of over 1000 HV(25g) may be attained at the surface, where exposure to the laser beam is limited.

4.2.2. Laser treated 080M40 steel.

The laser treated 080M40 steel, exhibited a transformed zone of material some 1.75mm wide by 230μm deep, as a result of a single traverse at a speed of 75mms^{-1}, using a laser beam focussed to a 6mm diameter spot on the sample surface and operated at an "on-line" power output of 1.5kW (Figure 4.2.11).

At higher magnification, (Figure 4.2.12), the region close to the surface exhibits an acicular structure and the pearlite colonies have become indistinct. Below this, the pearlitic phase within the laser-treated volume has been transformed to produce a featureless constituent which completely fills the volume previously occupied by pearlite. This phase is presumed to be a form of martensite, produced by the rapid heating and cooling of the local area. (Figure 4.2.13).

Hardness measurements through the heat affected zone and into the underlying matrix using a 100g load, revealed a gradual decrease in average hardness from 410 ± 20 HV to a matrix value of 230 ± 20 HV. (Figure 4.2.14).

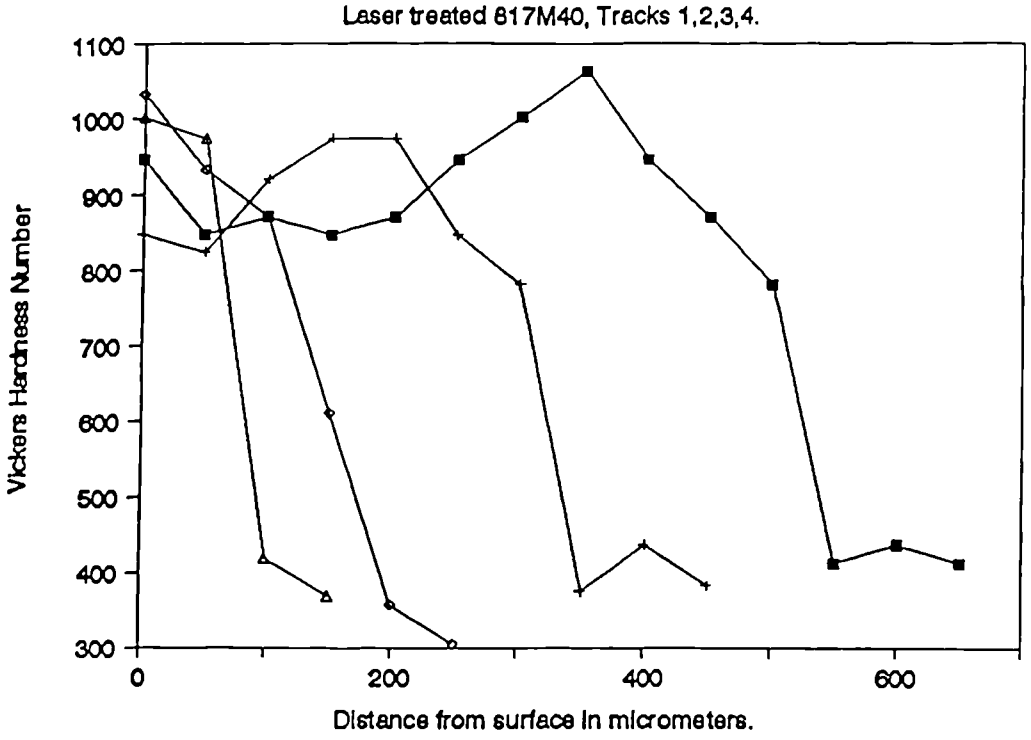

Figure 4.2.10. Laser treated 817M40. Showing the hardness depth profile from the laser heat-treated surface through to the underlying matrix for the varying depths of treatment shown in the micrographs, figures 4.2.2 to 4.2.9. The region of maximum hardness is shown to be situated closer to the surface as the exposure to the laser beam is reduced.

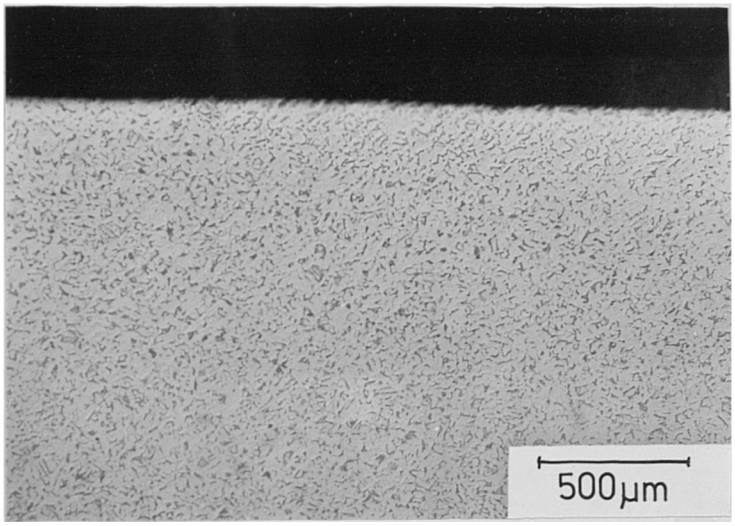

Figure 4.2.11. Laser treated 080M40. 75mms^{-1}.
Cross-section through the laser heat-treated track showing the depth profile of the modified zone.

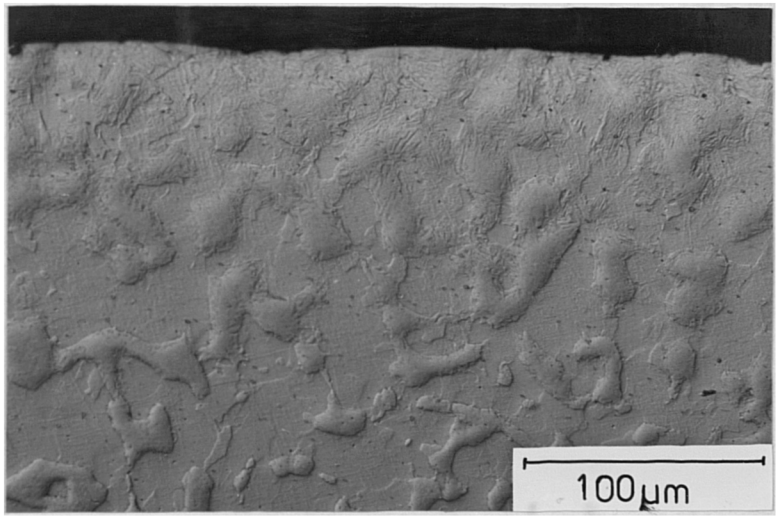

Figure 4.2.12. Laser treated 080M40. 75 mms^{-1}.
Detail of the modified HAZ showing an acicular product close to the surface, and partially spheroidised pearlite.

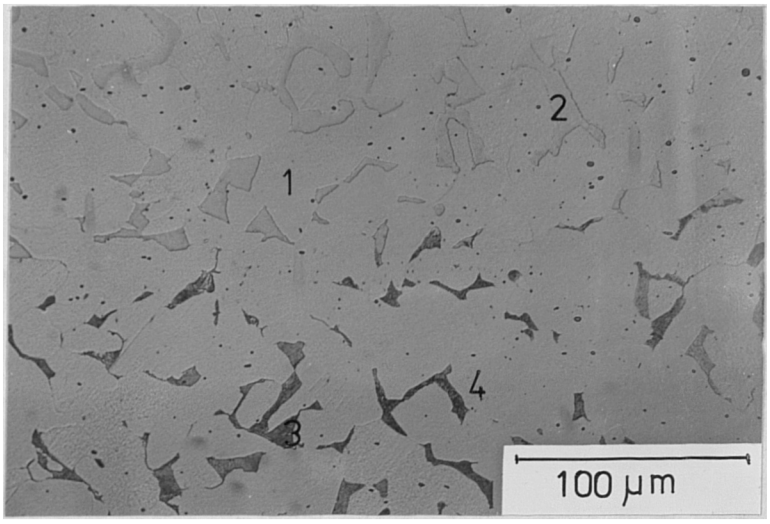

Figure 4.2.13. Laser treated 080M40. Transition region between 'modified' pearlite in the HAZ and conventional pearlite in the underlying matrix. Hardness values of selected features; 1) 210 HV, 2) 1132 HV, 3) 350 HV, 4) 212 HV.

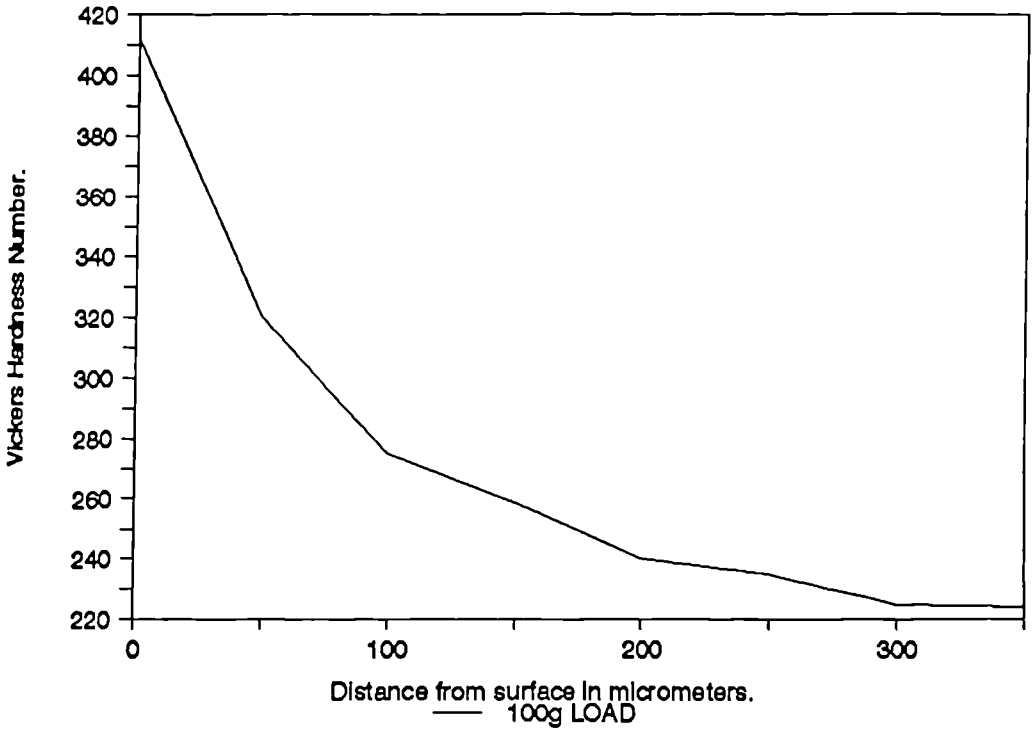

Figure 4.2.14. Laser treated 080M40. Hardness profile from the laser treated surface through to the underlying matrix in the region shown in figures 4.2.12 and 4.2.13.

Measurements of selected features using a 25g load showed that the islands of modified pearlite had hardness values in excess of 1100 ± 30 HV, in comparison to values of 210 ± 30 HV for ferrite in both the laser HAZ and the underlying matrix, and 350 ± 30 HV for pearlite.

4.2.3. Laser treated Armco iron.

A coupon of iron was laser-treated with a traverse speed of 25mms^{-1}, under a laser beam focussed to a beam diameter of 6mm and having an "on-line" power output of 1.5 kW. Figure 4.2.15, shows a cross section of this track in which a zone of fine grain structure extends some 300μm into the depth of the sample. Below this, a zone of larger grains extends to a depth of approximately 800μm. At higher magnification, the structure close to the surface is seen to contain an acicular form of ferrite, (Figure 4.2.16). The change in grain size between the laser treated zone with average values of 20μm and the underlying region of large grained material, with average values of 50μm, is illustrated at the boundary between the two areas (Figure 4.2.17). The average ferrite grain size in the underlying matrix was found to be 30μm.

A series of hardness measurements through the laser HAZ and into the underlying matrix, using a 25g load, showed a variation from a maximum of 240 ± 30 HV at the surface, through a minimum of 160 ± 30 HV in the large grained region, to an average value of 200 ± 30 HV in the matrix.(Figure 4.2.18).

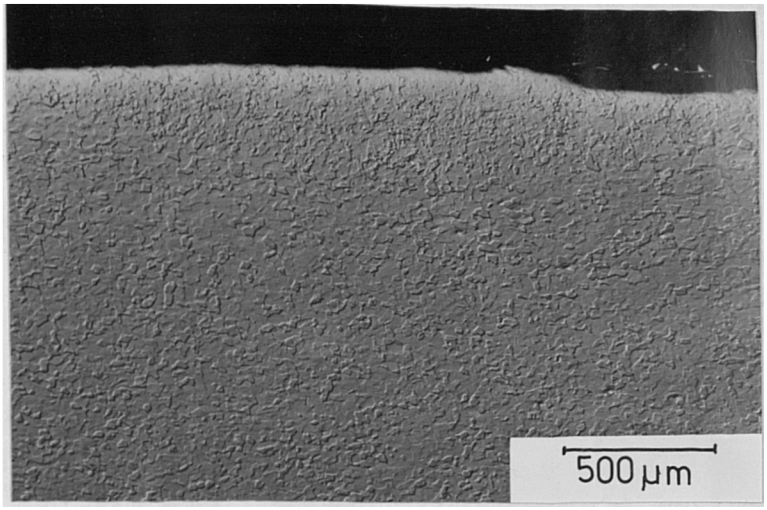

Figure 4.2.15. Laser treated Armco iron. Cross section through the HAZ showing a region of fine grain structure.

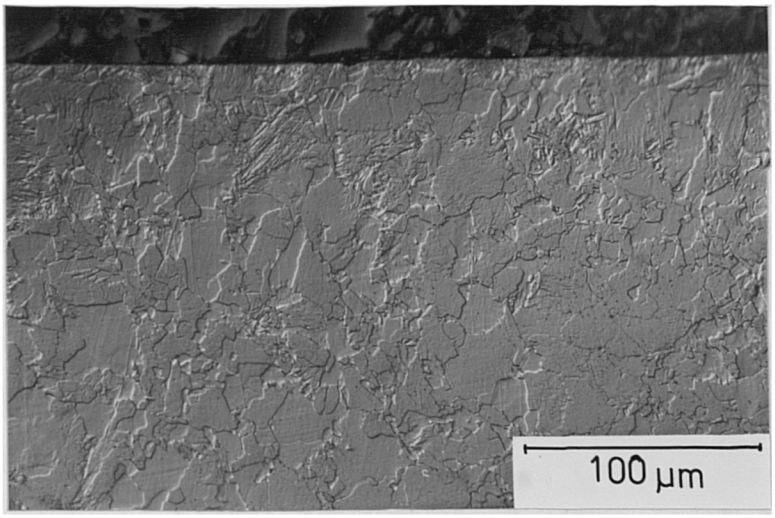

Figure 4.2.16. Laser treated Armco iron. Detail of the acicular product formed at the laser treated surface.

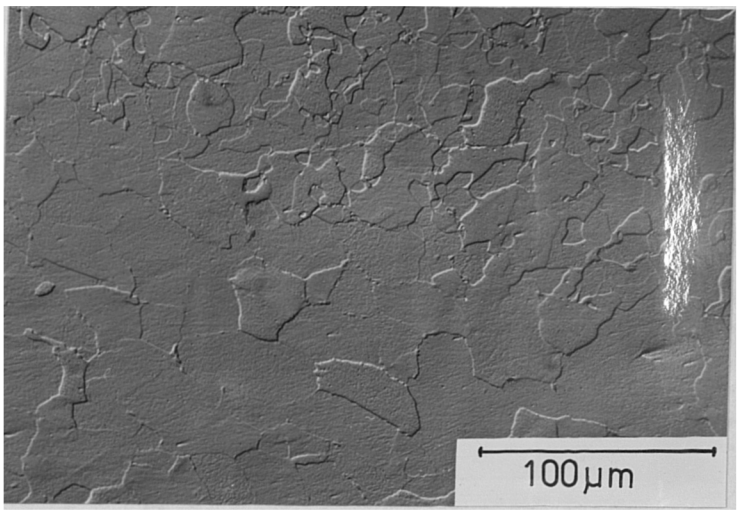

Figure 4.2.17. Laser treated Armco iron. Transition region between the fine grain and coarse grain material.

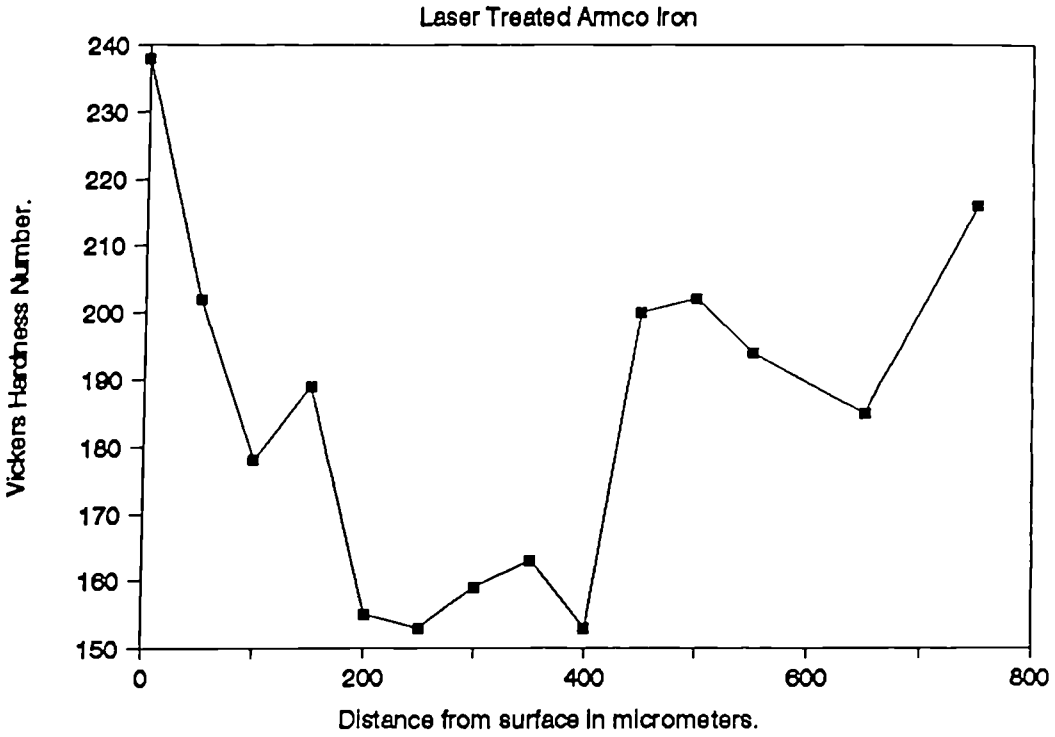

Figure 4.2.18. Laser treated Armco iron. Hardness values through the HAZ shown in figure 4.2.15.

4.2.4. Abusively Turned 817M40 Steel.

A section of a turned disc of 817M40 steel, machined under conditions conducive to the formation of a thin continuous white-layer, was prepared as an 11° taper section, following electroplating with nickel. The sample was then prepared using standard metallographic techniques and examined under incident reflected light.

Figure 4.2.19, shows the feed width step produced by one cutting revolution to be approximately 1mm. The depth of the thermo-mechanically modified layer, as indicated by the change in structure from that of the tempered martensite of the underlying matrix, has a maximum value of 200μm on the micrograph. This is equivalent to a depth of 40μm on the sample after correction for the *effect of* magnification in the "y" direction due to the taper-sectioning technique.

Hardness measurements taken from selected points within the surface white-layer, as indicated on Figure 4.2.20, show a maximum hardness of 894 ± 30 HV(25g). This may be compared with an average value for the underlying tempered martensite matrix of 370 ± 30 HV(25g), see Figure 4.2.21.

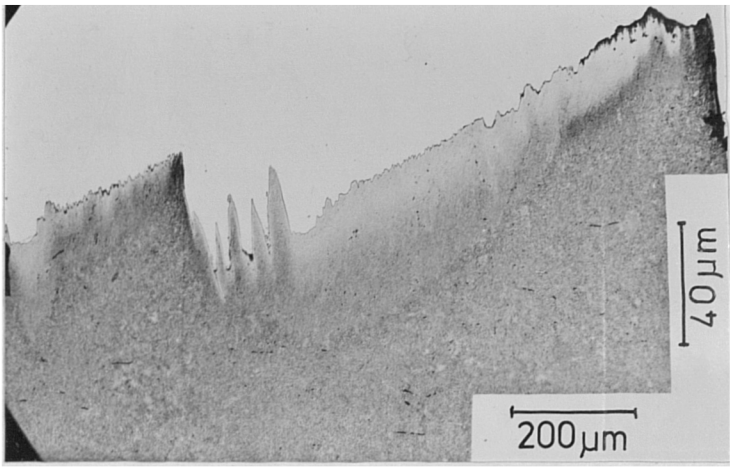

Figure 4.2.19. Abusively turned 817M40. Taper cross-section showing the white layer and feed step width.

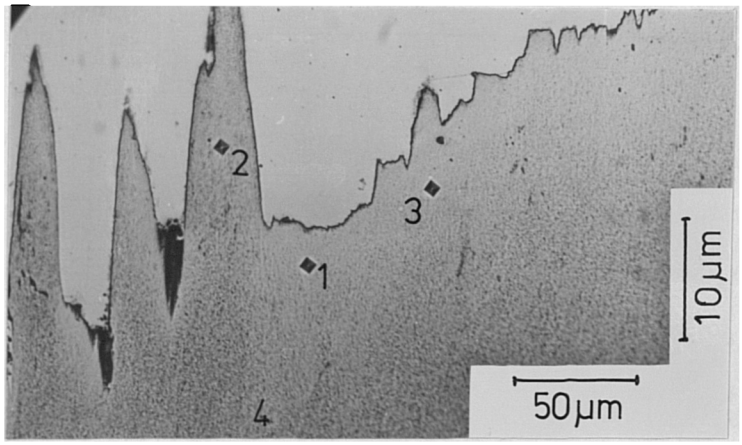

Figure 4.2.20. Abusively turned 817M40. Hardness values of selected features as indicated : 1) 762 HV, 2) 946 HV, 3) 894 HV, 4) 627 HV. 5) 370 HV (Matrix value).

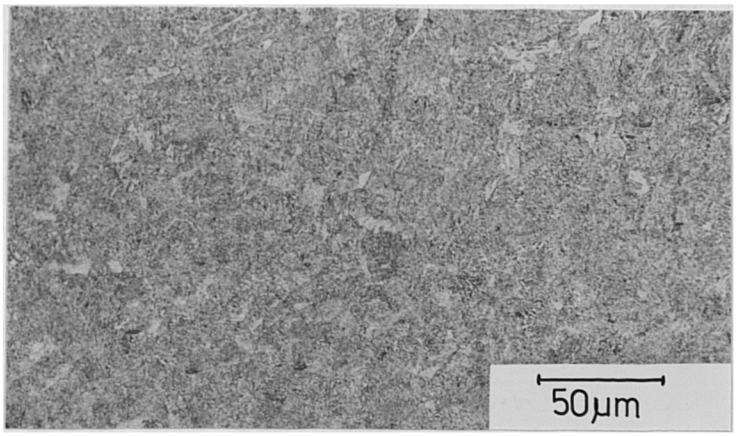

Figure 4.2.21. Abusively turned 817M40. Underlying matrix.

4.2.5. Wear Pin. 817M40 steel.

The composite micrograph, Figure 4.2.22, shows a taper cross section through the worn surface of an 817M40 steel "wear pin" subjected to severe wear on a pin-and-disc type wear machine. The near surface layers are shown to contain regions of deformed or transformed material, and isolated pools of darker material, presumed to be an oxide. With higher magnification, (Figures 4.2.23 and 4.2.24), the transition from the tempered martensite matrix structure to the tribologically-modified region becomes apparent, and well defined regions of white-etching material and darker " oxide " pools, may be readily distinguished from the plastically-deformed structure and the underlying matrix.

Hardness measurements of selected features obtained using a 25g load, as indicated in the micrograph, (Figure 4.2.25), show values of 890 ± 30 HV for the white-layer, over 1000 HV for the "oxide" pools and over 700 HV for the plastically-deformed material. The underlying matrix of this 817M40 steel had an average hardness of 610 ± 30 HV.

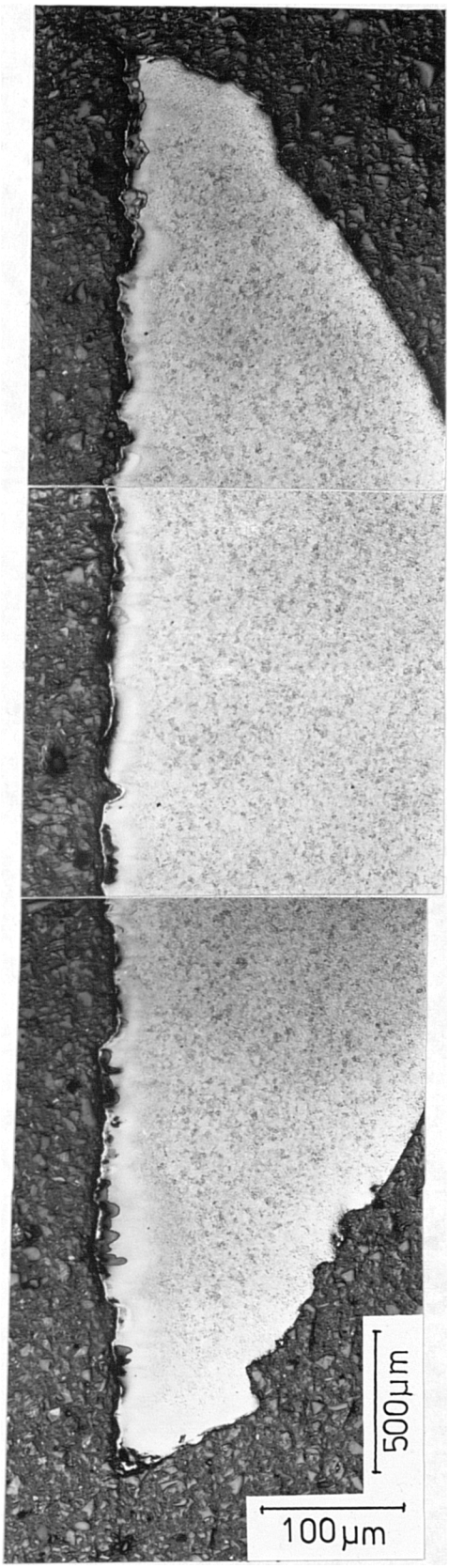

Figure 4.2.22. Wear pin 817M40. Composite micrograph showing the taper cross section through the wear surface.

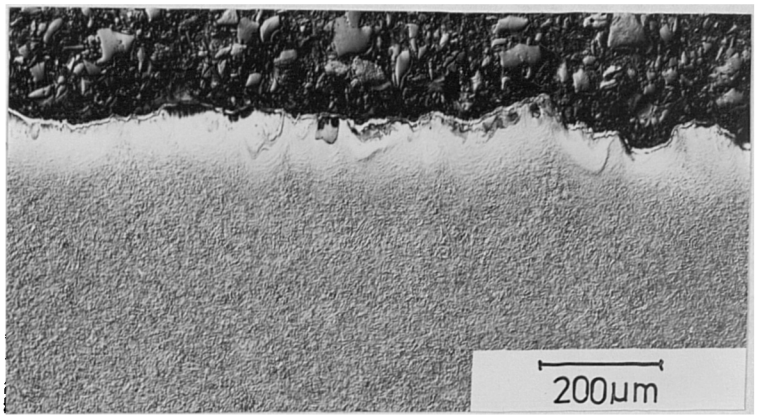

Figure 4.2.23. Wear pin 817M40. Cross section through the wear surface.

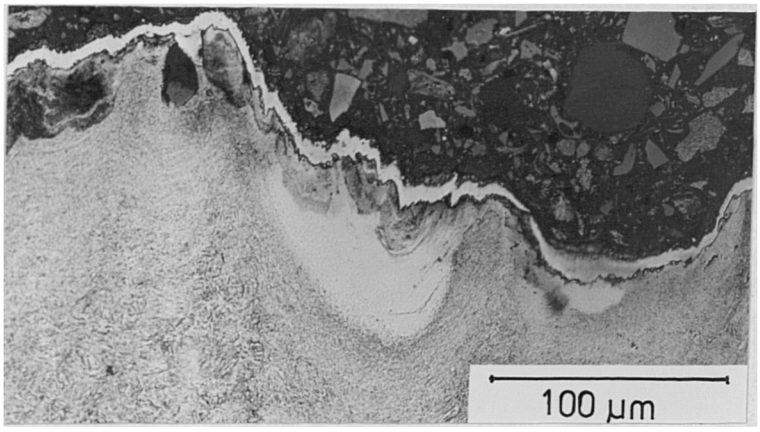

Figure 4.2.24. Wear pin 817M40. Detail of white-layer and "oxide" pools close to the wear surface.

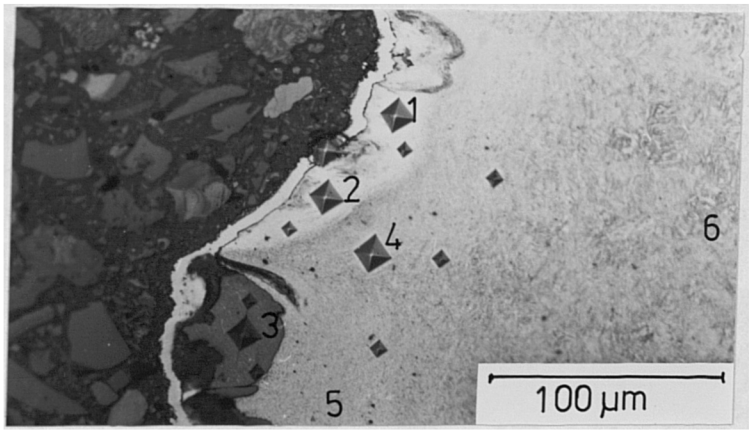

Figure 4.2.25. Wear pin 817M40.Hardness values of selected features. 1) 870 HV, 2) 894 HV, 3) 1018 HV, 4) 772 HV, 5) 734 HV, 6) 707 HV. (Matrix value).

4.2.6. Stone Abraded Digger Tooth.

The cross section through the working face of a used gravel extraction " digger tooth", exhibited regions of white-etching material, see Figure 4.2.26. The features appeared most frequently to be associated with grooves worn in the tool surface by hard rock fragments, and had a typical depth of some 30μm.

On closer examination using DIC contrast, the white-etching material was seen to show evidence of intense plastic deformation, with short cracks extending into the material from the surface. (Figure 4.2.27).

Underlying the white-etching, plastically-deformed layer, a band of dark-etching material separates the martensitic matrix from the transformed phase. This may be interpreted as being a region of tempered martensite. Microhardness measurements from isolated areas of white-layer identified in the Figures 4.2.28 and 4.2.29, are listed in the associated tables. Values for the white-layer in excess of 1200 ± 30 HV(25g) were measured in several areas, in contrast to the average matrix hardness of 670 ± 30 HV(25g).

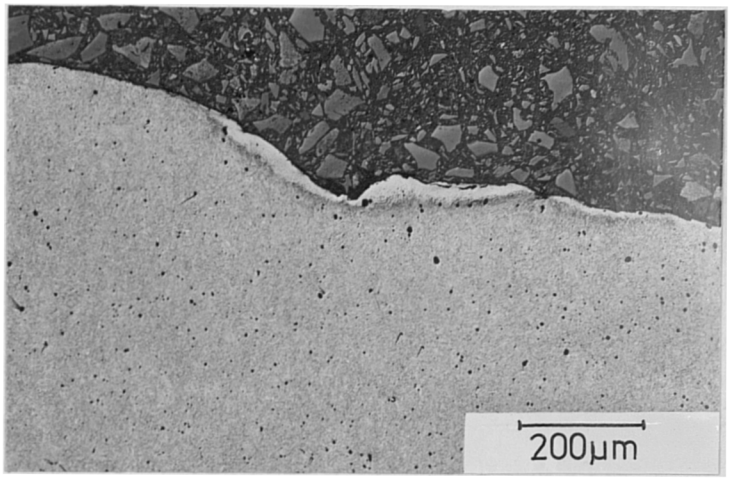

Figure 4.2.26. Digger tooth. Cross section through the worn surface showing an isolated region of white-layer.

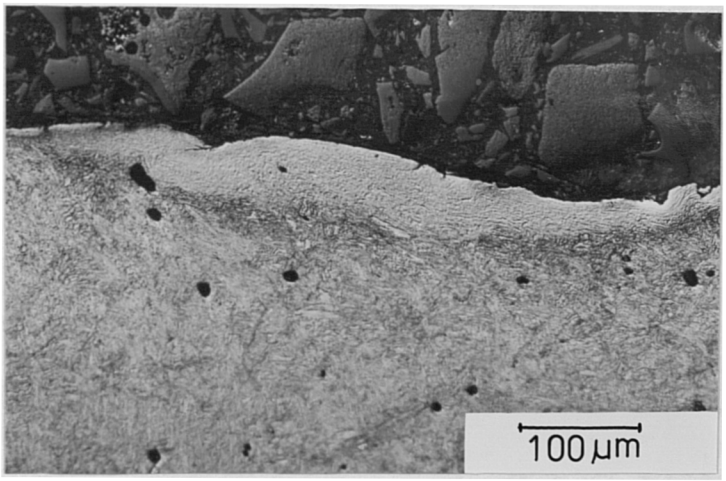

Figure 4.2.27. Digger tooth. Detail of a white-etching region showing evidence of plastic deformation.

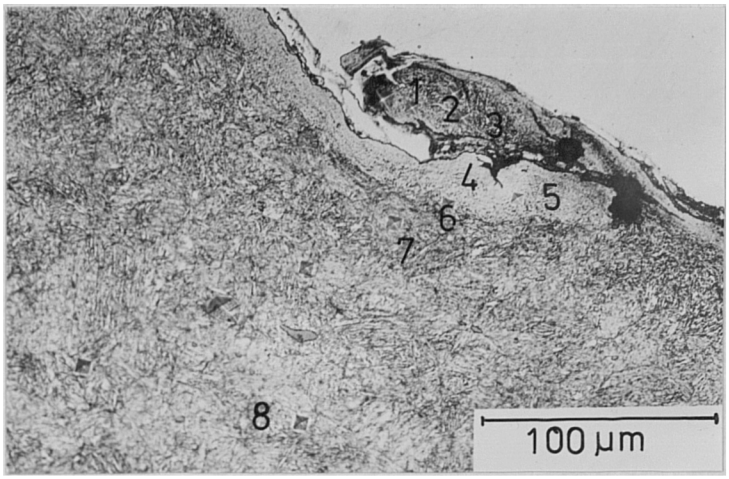

Figure 4.2.28. Digger tooth. Hardness values of selected features : 1) 847 HV, 2) 870 HV, 3) 803 HV, 4) 1288 HV, 5) 1206 HV, 6) 974 HV, 7) 847 HV, 8) 673 HV.

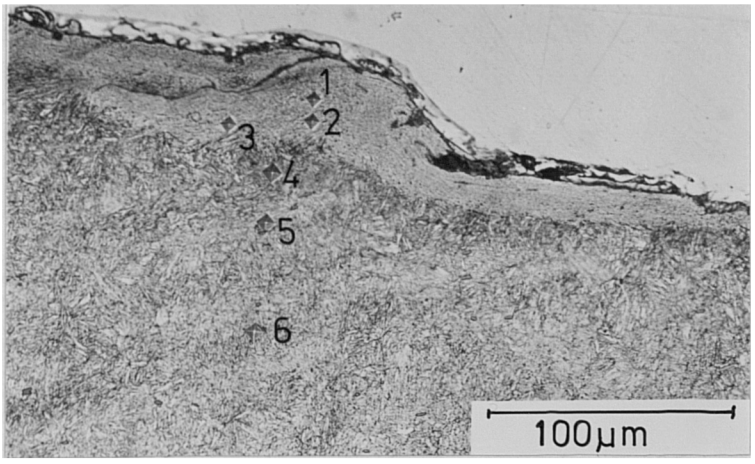

Figure 4.2.29. Digger tooth. Hardness values of selected features : 1) 1033 HV, 2) 1064 HV, 3) 974 HV, 4) 612 HV, 5) 673 HV, 6) 657 HV.

4.2.7. Chieftain Tank Gun Barrel Sections.

Metallographically prepared cross sections from the " commencement-of-rifling " region of Chieftain tank gun barrels, exhibit a layer of white-etching material at the bore surface. See for example Figure 4.2.30 in which such a layer, 110μm thick is shown. A number of cracks extend into this layer, some of these penetrating through to the underlying matrix material. (Figure 4.2.31).

At higher magnification, (Figures 4.2.32 and 4.2.33), the refinement of structure in the white-etching layer is shown and a thin, apparently structureless white-layer at the barrel surface is revealed. This material increases in thickness close to cracks, to exhibit a duplex form of white-etching material less than 10μm thick. (Figure 4.2.33). The hardness profile for this region, to a depth of 140μm, indicates that maximum values of hardness, in excess of 1000 ± 30 HV (25g), are attained at a depth of some 50μm from the bore surface. (Figure 4.2.34).

Due to the small dimensions of the thin surface white-layer, the hardness could not be measured in cross-section. A series of hardness indentations made directly on the bore surface gave an average value for the surface of 560 ± 30 HV (25g).

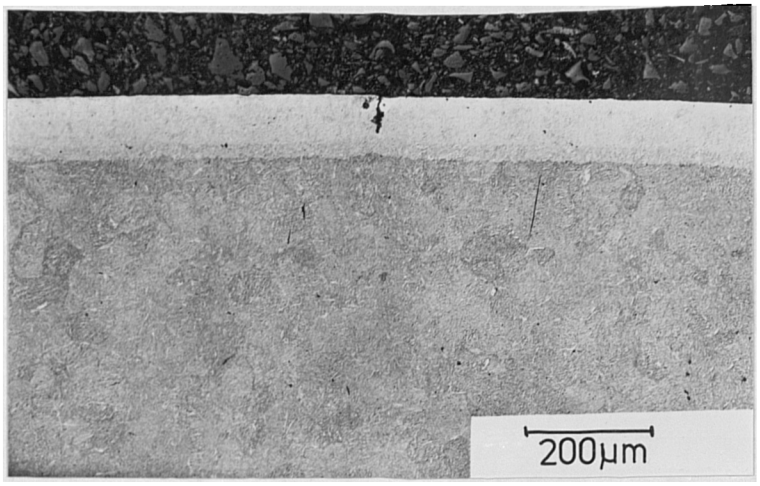

Figure 4.2.30. Chieftain gun barrel. Longitudinal cross-section close to the "commencement-of-rifling". Showing a continuous white-layer at the gun barrel surface.

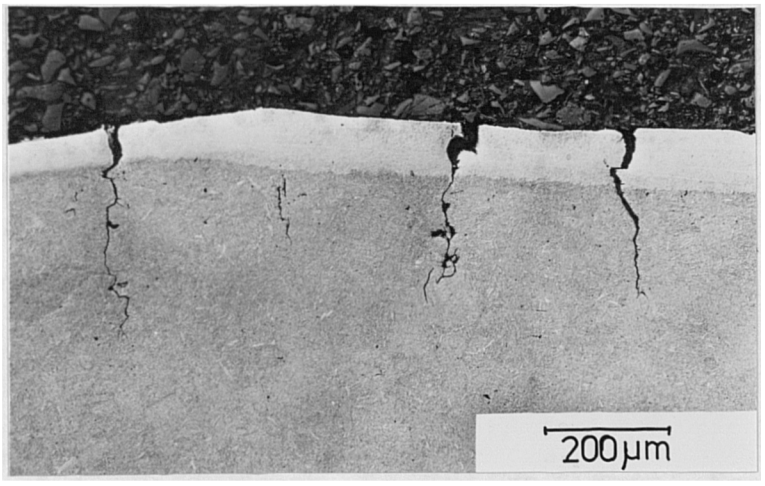

Figure 4.2.31. Chieftain gun barrel. Longitudinal cross-section at the "commencement-of-rifling", showing a region of white-layer exhibiting extensive cracking.

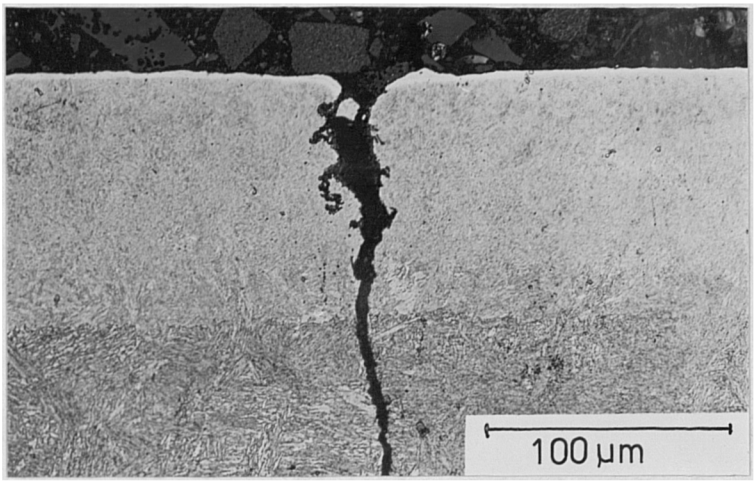

Figure 4.2.32. Chieftain gun barrel. Detail of the fine structure within the white-etching surface layer.

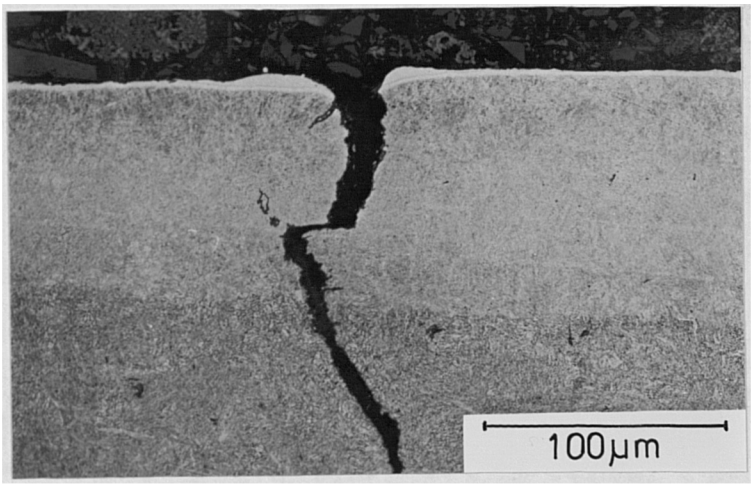

Figure 4.2.33. Chieftain gun barrel. Showing a region of duplex white-layer at the site of a crack.

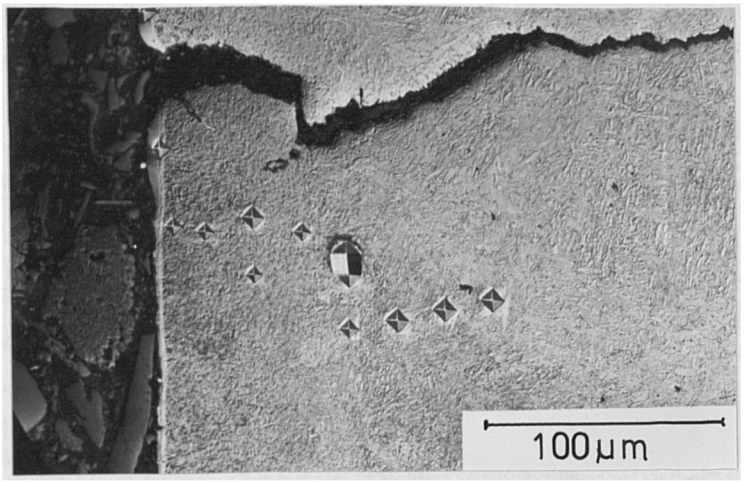

i) Micrograph showing indentations forming the hardness depth profile illustrated in the associated graph.

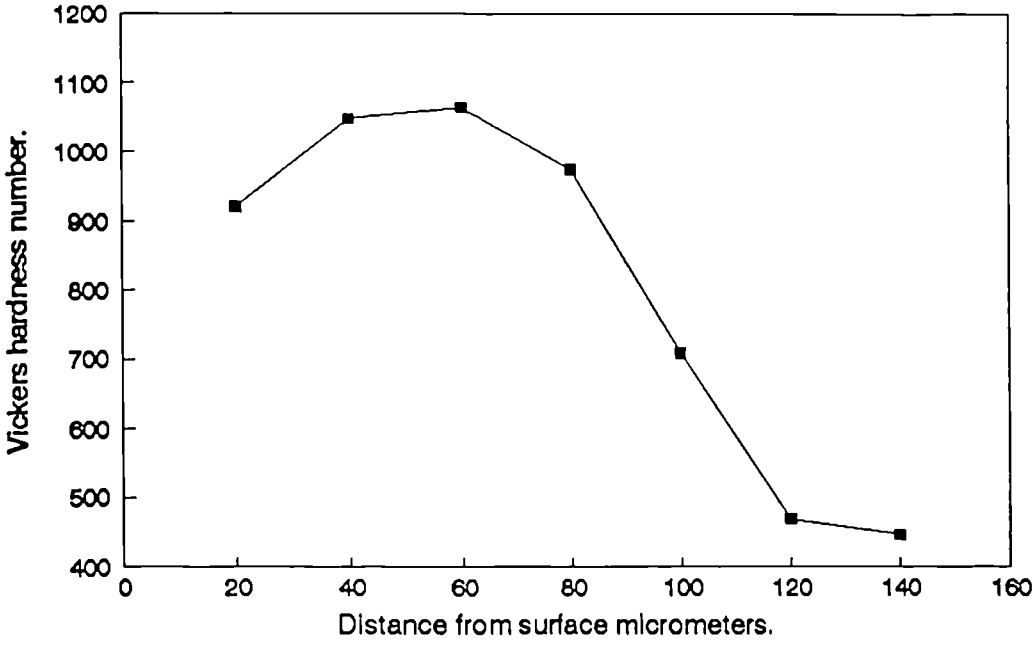

ii) Hardness depth profile through the white-etching surface layer.

Figure 4.2.34. Chieftain gun barrel.

4.2.8. RARDEN Gun Barrel Section.

Metallurgical cross sections prepared through the rifled inner bore of a RARDEN 30mm gun barrel, used in a test firing programme, showed that the bore surface had become severely damaged during testing.

The light micrograph Figure 4.2.35, illustrates the bottom of a rifling groove in which deep cracks have developed at regular intervals, perpendicular to the inner bore. Between these deep fissures, a number of shallow " V " shaped cracks are seen to have formed within the band of well defined white-etching layer at the barrel surface.

A series of microhardness indentations made through the white-etching layer and into the underlying material, showed a maximum value of over 1000HV (25g) at a depth of 30μm from the bore surface (Figure 4.2.36). The hardness of the very thin fragmented white-layer formed at the bore surface , see Figure 4.2.36, could not be measured in cross section. A series of measurements on the bore surface gave an average value of 460 ± 30HV (25g) for this material.

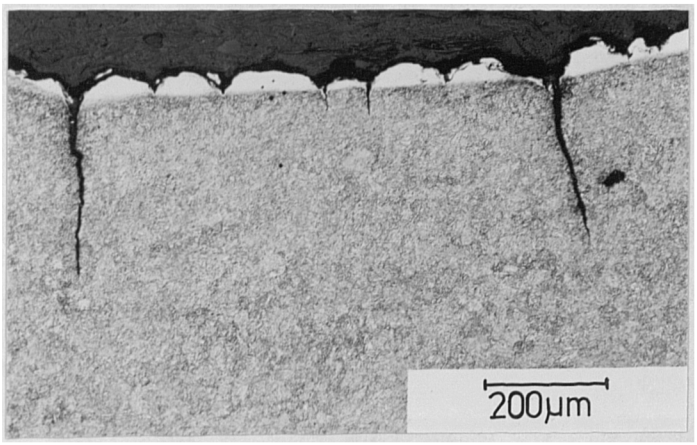

Figure 4.2.35. RARDEN gun barrel. Transverse cross-section at the base of a rifling groove.

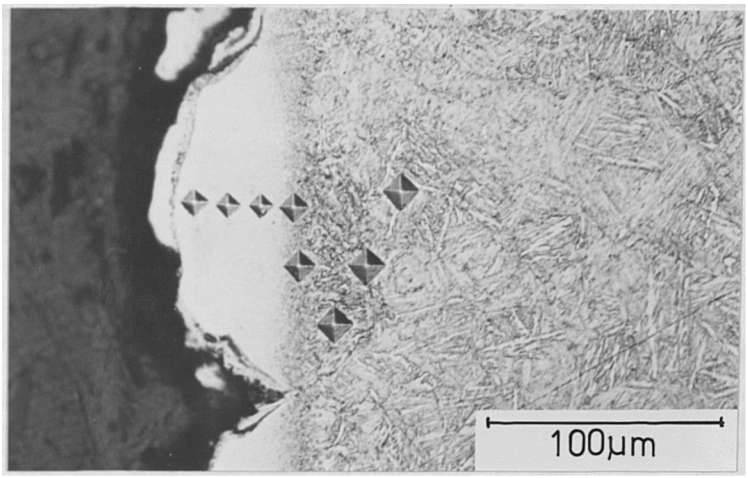

i) Detail of white-etching layer at the site of microhardness tests.

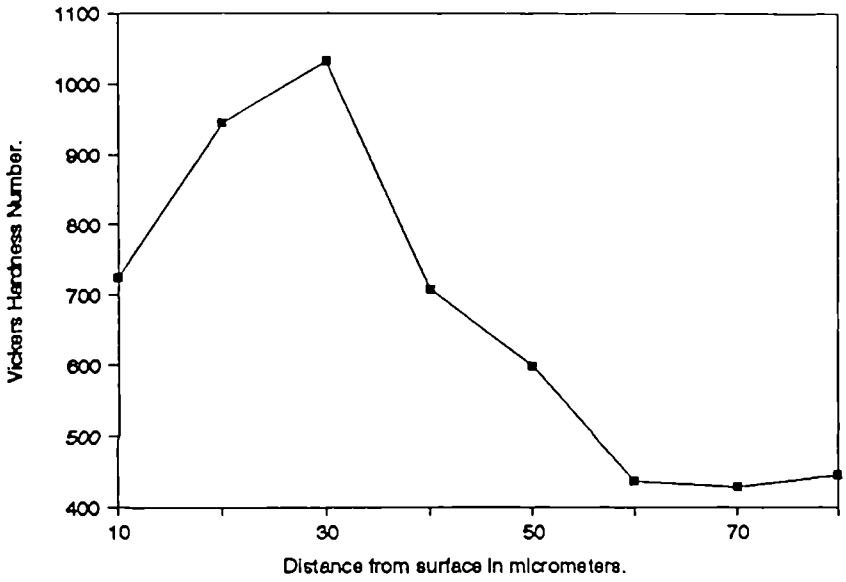

ii) Hardness depth profile of region shown above, from gun barrel surface through to the underlying matrix.

Figure 4.2.36. RARDEN gun barrel.

4.2.9. Adiabatic Shear Specimen.

Figure 4.2.37, shows the development of adiabatic shear banding and local cracking in a section of armour steel subjected to a high velocity impact. The original forming direction of the steel is clearly visible in the Figure 4.2.38, in which a shear band is shown as a horizontal light etching feature. At higher magnification, the contrast between the martensitic structure of the surrounding material and the relatively featureless shear band is revealed. (Figures, 4.2.39 and 4.2.40.)

The narrow width of the shear bands, generally less than 10μm in cross section, presented some difficulties in hardness measurement. To ensure that several values would be obtained from the feature, a series of indentations were made at an angle of 30° through the band as shown in Figure 4.2.41.

The results of these measurements indicate that the shear band has an average hardness of over 1200 ± 30 HV(25g) in contrast to the matrix value of 890 ± 30 HV(25g). The material either side of the band showed a decrease in hardness to less than 800 ± 30 HV (25g).

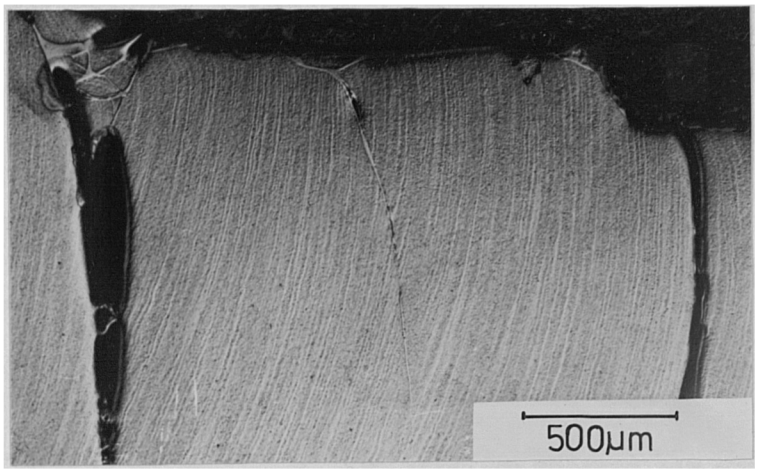

Figure 4.2.37. Adiabatic shear showing a network of white etching bands in a deformed matrix.

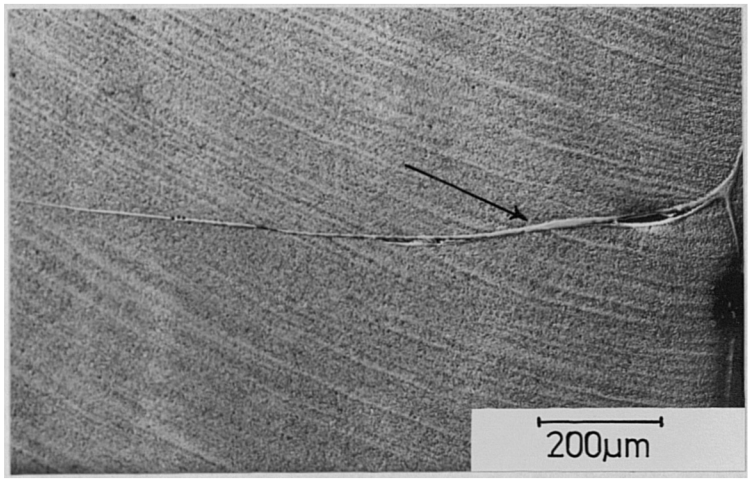

Figure 4.2.38. Adiabatic shear specimen exhibiting a white-etching shear band, arrowed.

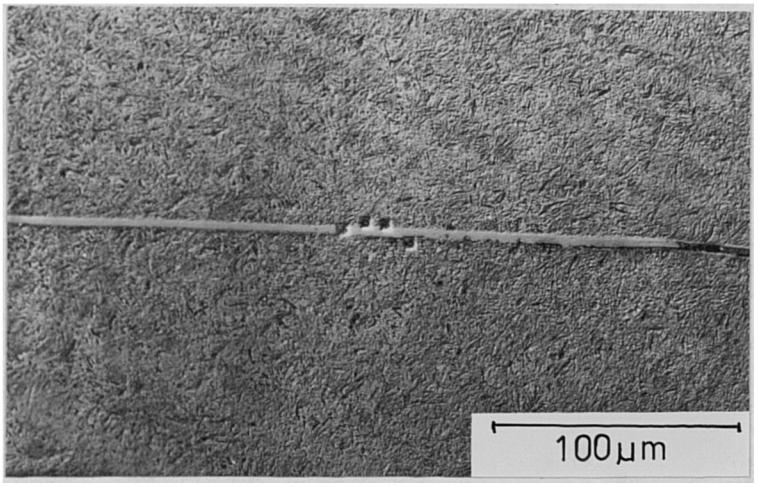

Figure 4.2.39. Detail of region showing an apparently structureless adiabatic shear band.

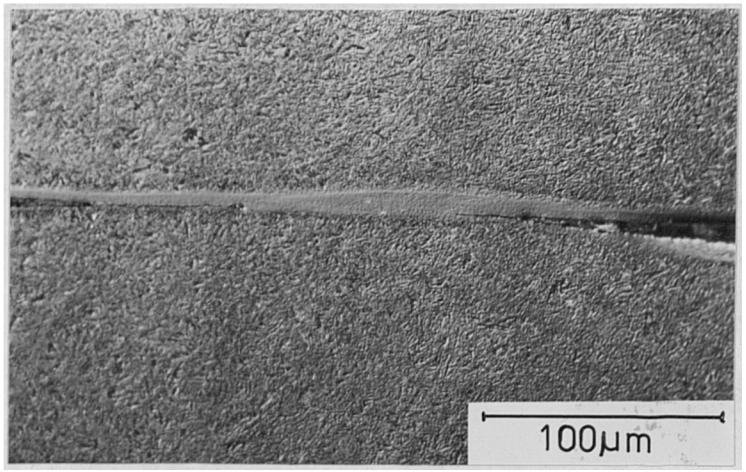

Figure 4.2.40. Adiabatic shear band exhibiting a fine structure revealed by DIC.

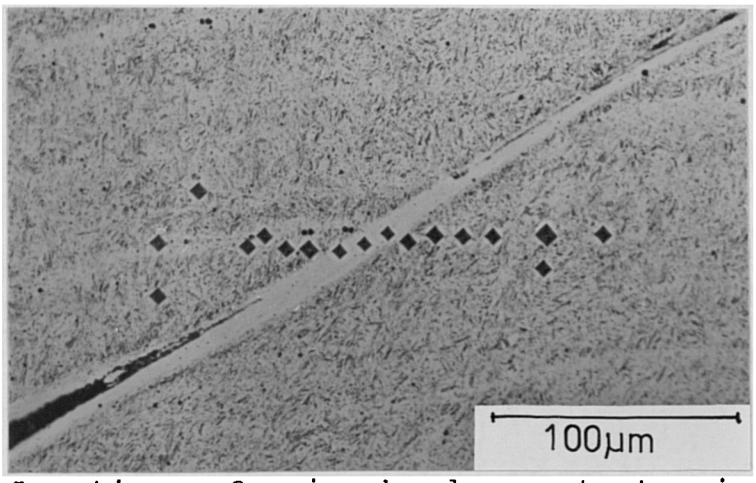

i) Location of microhardness test indentations across the region shown above.

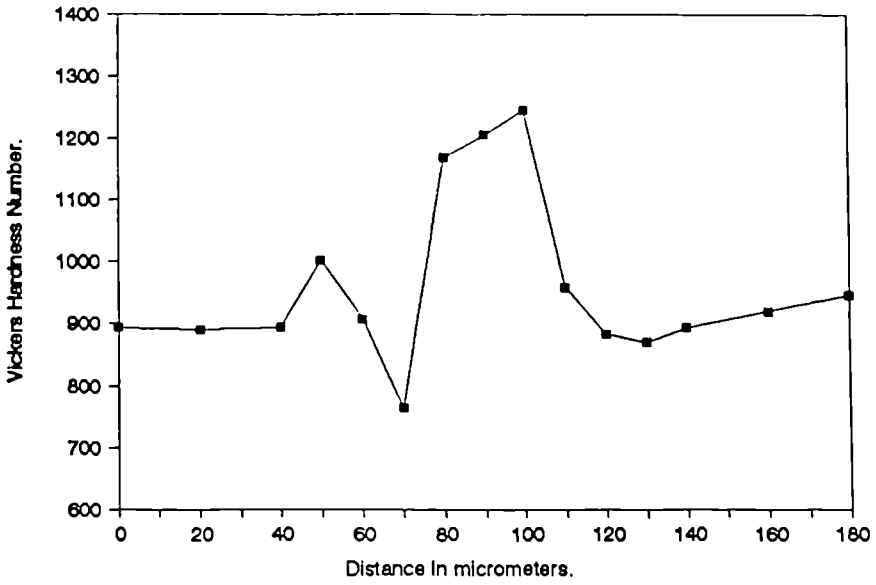

ii) Microhardness profile across the shear band illustrated in the associated micrograph.

Figure 4.2.41. Adiabatic shear specimen.

4.3. Scanning Electron Microscopy.

4.3.1. Laser Treated 817M40 Steel.

Prior to laser-treatment, the surfaces of the steel samples were grit blasted and coated with a thin layer of matte black paint to reduce reflectivity and hence improve the absorption of laser power. The surface so produced showed some evidence of previous machining operations, see Figure 4.3.1, but was uniformly roughened on a fine scale, as shown at higher magnification (Figure 4.3.2).

Following laser-treatment to produce a heat-affected-zone some 600μm in depth by traversing the sample at a speed of 25mms^{-1}, the surface showed signs of local melting, with the centre of the track exhibiting a smooth surface containing large open pores. The formation of these being attributed to the effect of entrapped gases escaping from the molten metal as shown in Figures 4.3.3 and 4.3.4.

In contrast, where a specimen traverse rate of 75mms^{-1} was employed and the depth of the heat-affected-zone accordingly reduced to some 200μm, the laser track does not exhibit surface porosity, see Figure 4.3.5, and at higher magnification still displays some of the surface roughness introduced by grit blasting (Figure 4.3.6).

Examination of the metallographically-prepared cross section through track 1, traversed at a speed of 25mms^{-1}, revealed a marked variation in structure from the surface to the bulk.

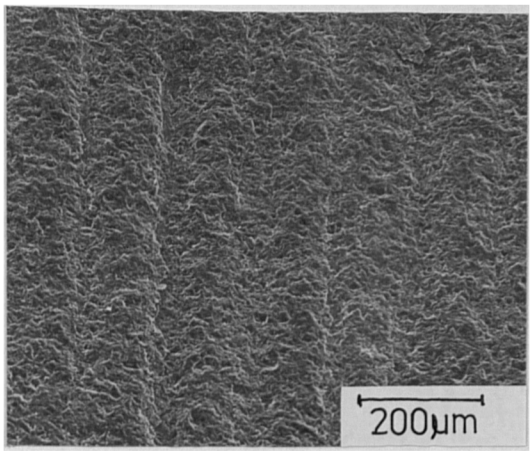

Figure 4.3.1.

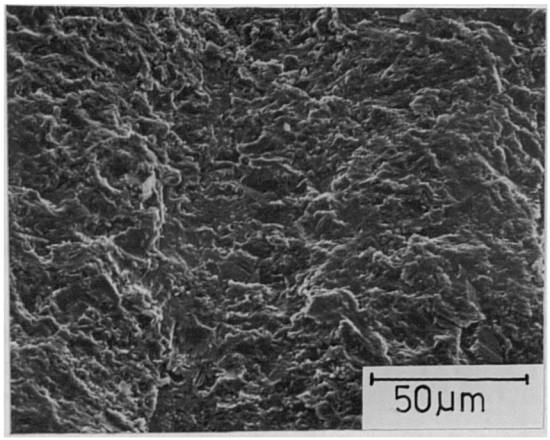

Figure 4.3.2.
817M40 steel. Surface prepared for laser treatment.

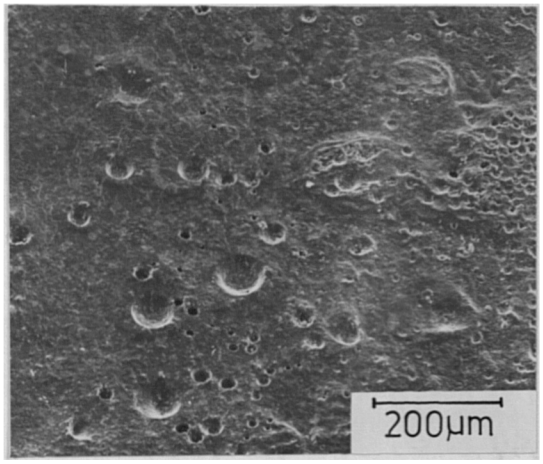

Figure 4.3.3.

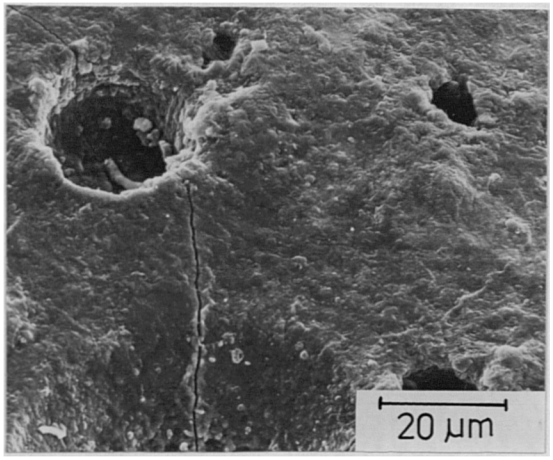

Figure 4.3.4.
Laser-treated 817M40. Track 1 surface following treatment at a traverse rate of 25mms^{-1}.

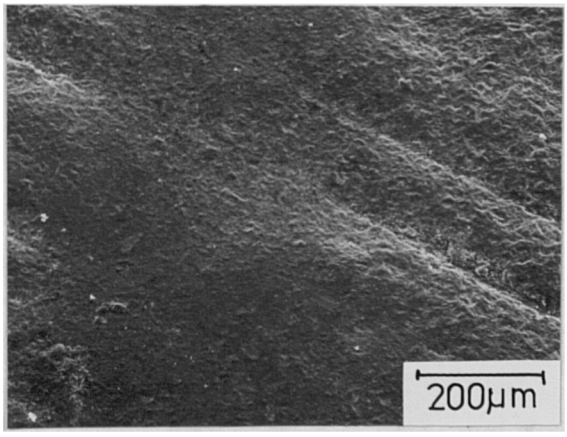

Figure 4.3.5.

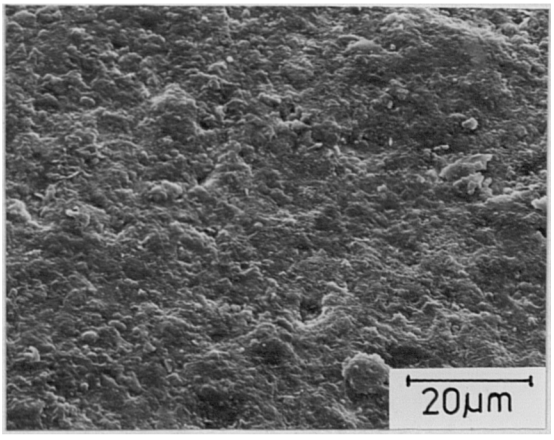

Figure 4.3.6.
Laser treated 817M40. Track 4 surface following treatment at a traverse rate of 100mm^{-1}.

In the near surface layer, see Figure 4.3.7, a coarse acicular structure extends to a depth of up to 50μm, gradually becoming more equiaxed in appearance. At a depth of 300μm from the surface, the structure changes to that of a small grained martensite, with fine carbides rendered visible following etching, (Figure 4.3.8). Below the laser treated zone the structure of the underlying matrix appears as a tempered, coarse grained, lath martensite containing a distribution of carbides, (Figure 4.3.9).

4.3.2. Laser treated 080M40 Steel.

Following laser heat-treatment, the grit-blasted surface of the 080M40 steel, shown in Figure 4.3.10, appeared smoother although exhibiting little evidence of surface melting (Figure 4.3.11).

Examination by SEM of the metallographically-prepared cross-section through the laser-treated tracks, showed the presence of a coarse acicular zone, close to the surface in the laser HAZ, see figure 4.3.12. Below this region, at a depth of 100μm from the surface, the structure consisted of ferrite grains and islands of an apparently structureless product, figure 4.3.13, generated by the transformation of the original pearlite phase and occupying the same volume as the parent material.

This structure may be compared with that of the pearlitic matrix, see figure 4.3.14, in which the characteristic lamellae of alternating ferrite and cementite are just visible in the pearlite grains.

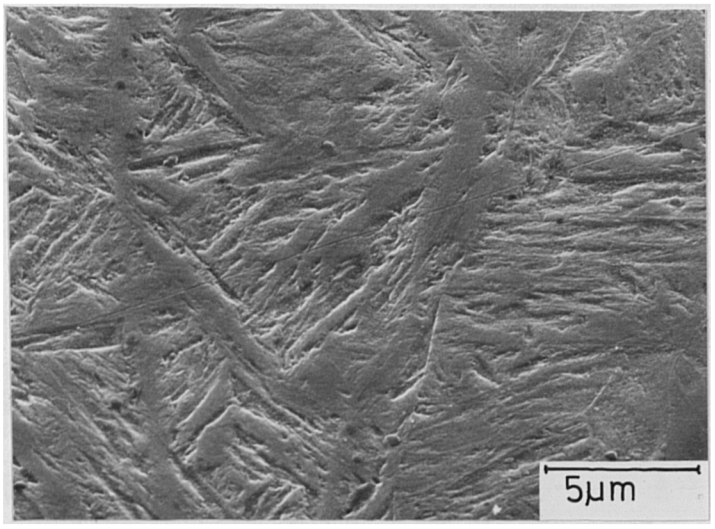

Figure 4.3.7. Laser-treated 817M40. Track 1. 25mms^{-1} traverse. Cross-section close to the surface showing an acicular structure.

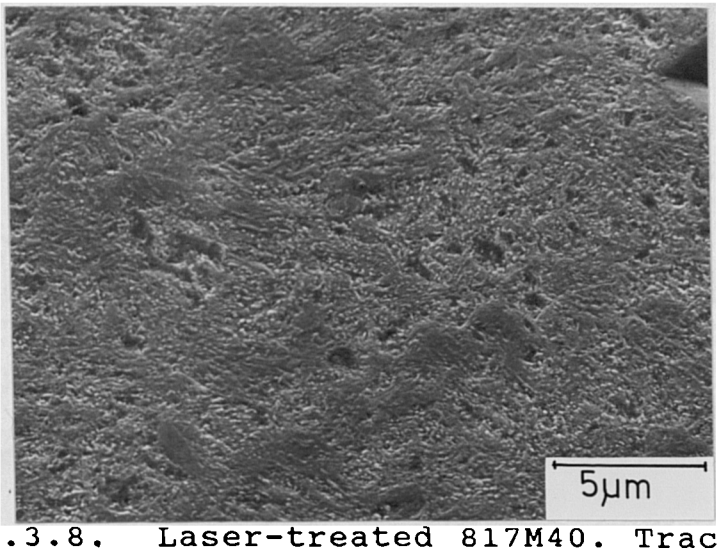

Figure 4.3.8. Laser-treated 817M40. Track 1. 25mm^{-1} traverse. Cross-section at a depth of 350µm, corresponding to the region of maximum hardness.

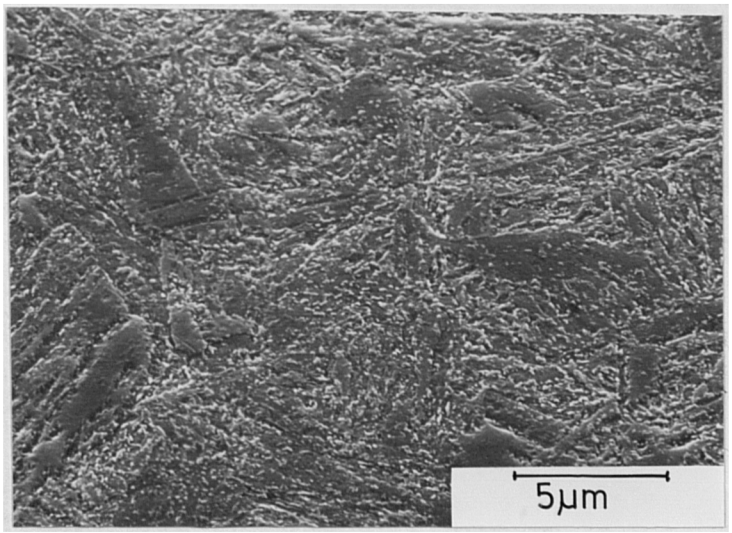

Figure 4.3.9. 817M40. Steel. Underlying matrix.

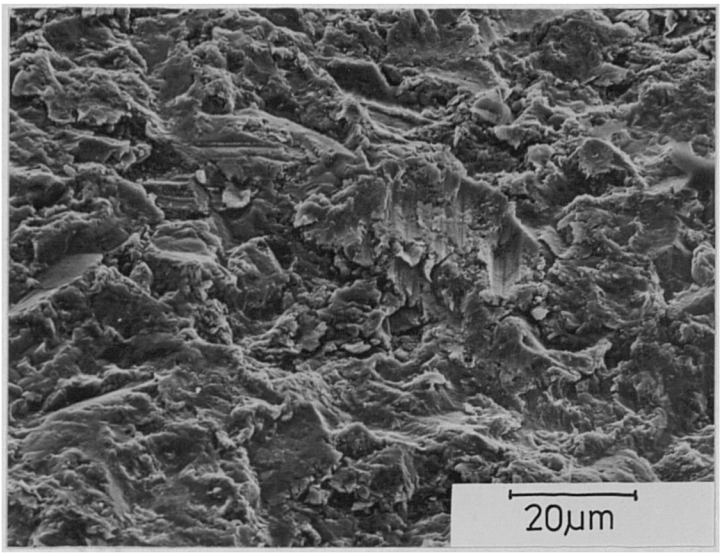

Figure 4.3.10. Surface of 080M40 Steel, prepared for laser heat-treatment by grit-blasting.

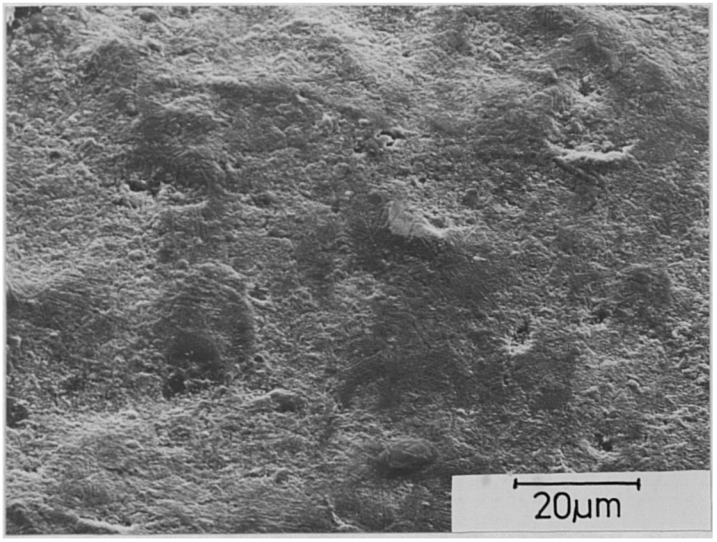

Figure 4.3.11. Surface of 080M40 steel, laser heat-treated at a traverse rate of 75mms^{-1}.

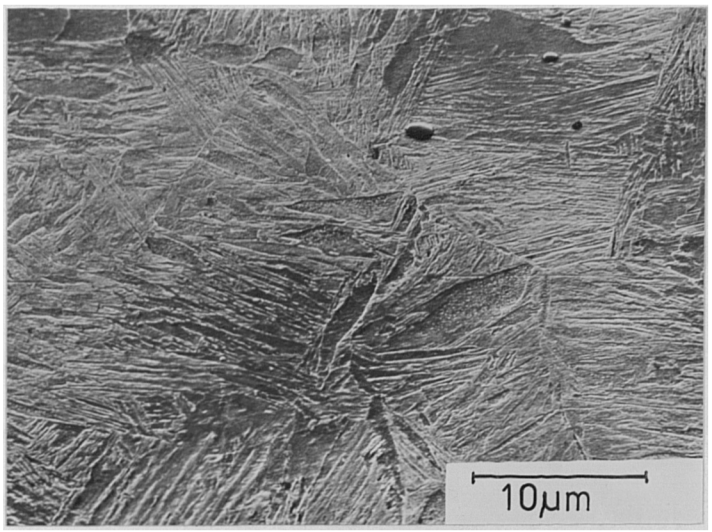

Figure 4.3.12. Cross-section of laser heat-treated 080M40, showing an acicular product at a depth of 20μm.

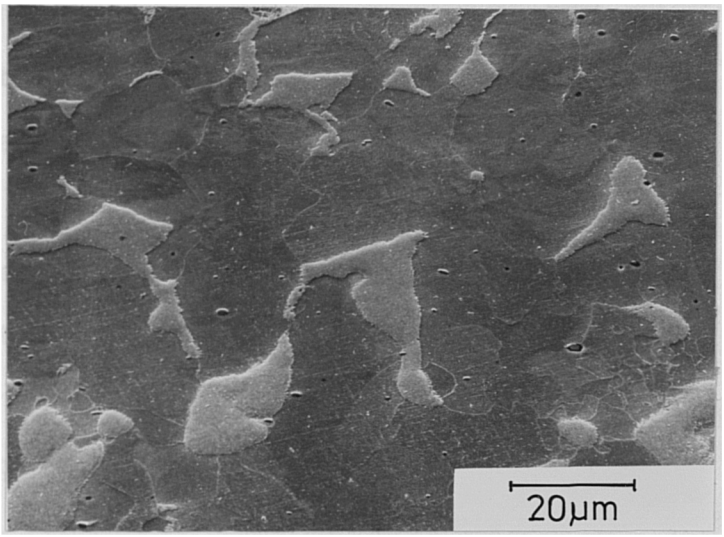

Figure 4.3.13. Cross-section of laser heat-treated 080M40, showing "modified" pearlite at a depth of 100μm.

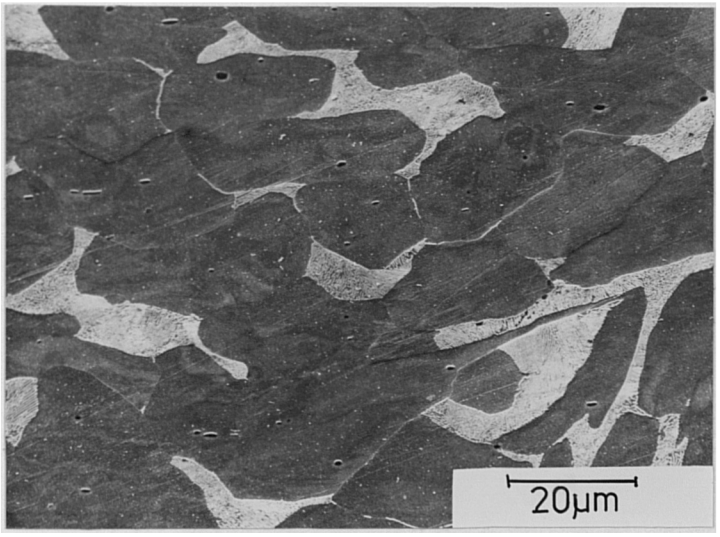

Figure 4.3.14. Underlying matrix of 080M40 steel showing the normal pearlite - ferrite matrix structure.

4.3.3. Laser treated Armco iron.

The fine surface structure produced by grit blasting, see Figure 4.3.15, has been locally smoothed by the effect of laser heat-treatment (Figure 4.3.16). The iron surface, revealed by the flaking away of the brittle film formed on the iron surface during laser treatment, exhibits an equiaxed grain structure at the site of laser interaction. Higher magnification of this region shows a needle like product within the grains. (Figure 4.3.17).

SEM examination of the metallographic cross-section of this sample showed a zone of acicular ferrite close to the surface in the laser-treated zone (Figure 4.3.18). The matrix of this material consisted of large equiaxed grains with several of the grain boundaries containing a second phase.(Figure 4.3.19).

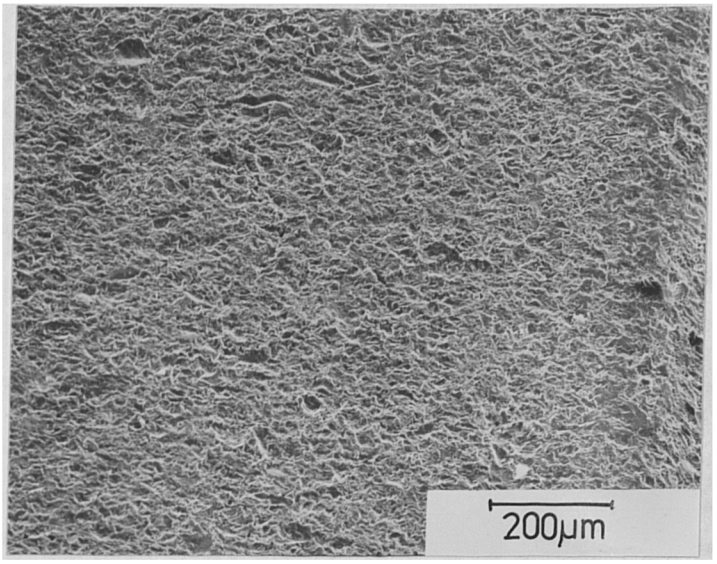

Figure 4.3.15. Surface of Armco iron, prepared for *laser* heat-treatment.

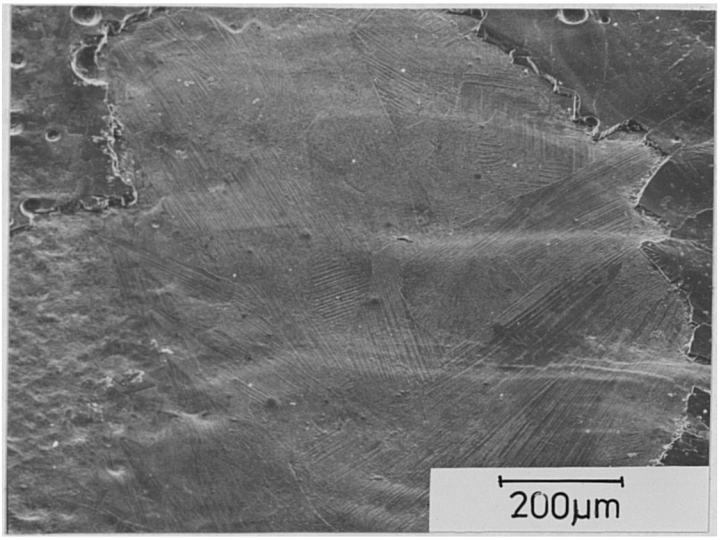

Figure 4.3.16. Surface of laser-treated Armco iron, showing a track of locally recrystallised material.

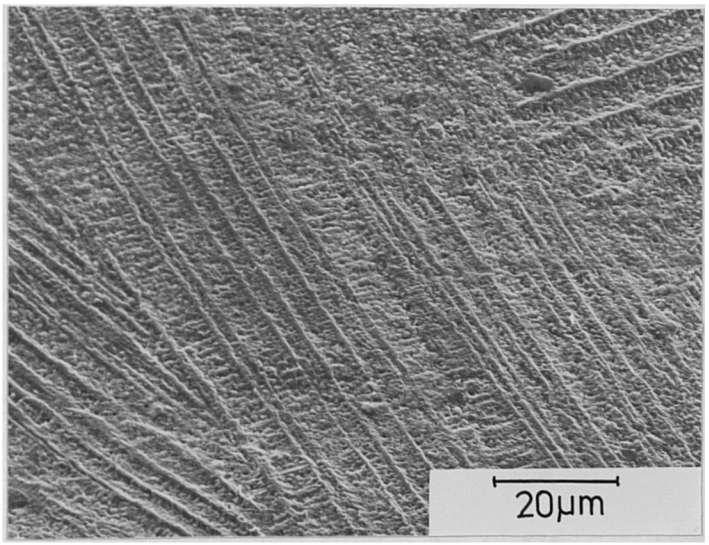

Figure 4.3.17. Laser-treated Armco iron surface, showing detail of the structure in the recrystallised zone.

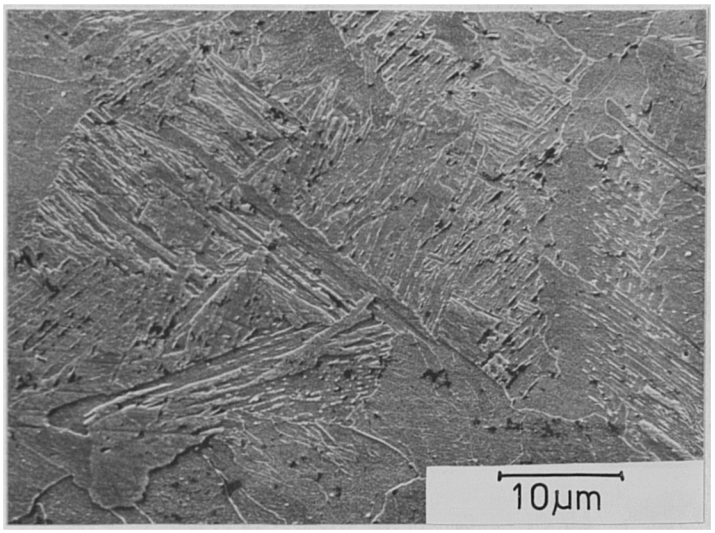

Figure 4.3.18. Cross-section of laser-treated Armco iron, close to the surface of the laser HAZ.

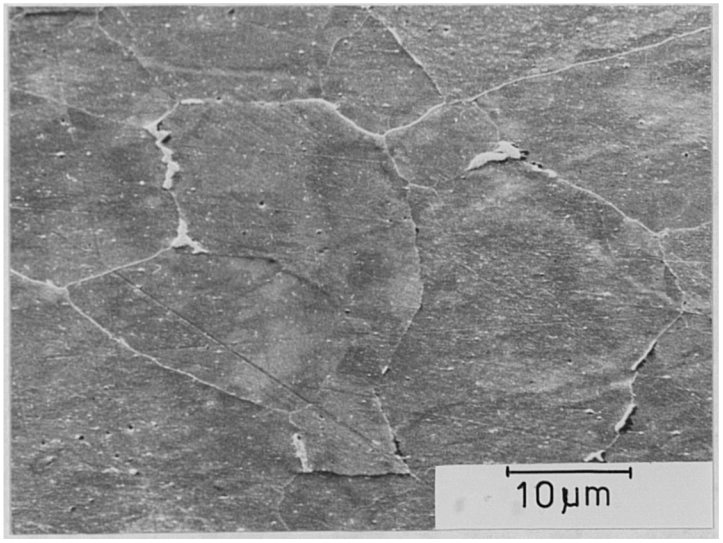

Figure 4.3.19. SEM image of the matrix underlying the laser-treated HAZ.

4.3.4. Abusively turned 817M40 steel.

The turned surface of 817M40 steel, shown in Figures 4.3.20 and 4.3.21, exhibits a series of parallel machining grooves with a separation determined by the feed rate employed during turning. Evidence of intense plastic deformation and tearing, with the formation of "tongues" of deformed material are an indicatiion of the abusive nature of the process.

SEM examination of a taper cross-section prepared through the surface shows a region of plastically-deformed material which appeared white-etching when viewed by light microscopy (Figure 4.3.22). At higher magnification, Figure 4.3.23 shows one of the plastically-deformed ridges of material extending from the surface. A fine disordered structure is visible, which when examined in detail, appears to consist of a dispersion of fine carbides in an extensively deformed matrix, (Figure 4.3.24). This region may be compared with the tempered martensite structure of the underlying matrix shown in Figure 4.3.25, in which carbides precipitated during tempering are seen to be distributed throughout the material.

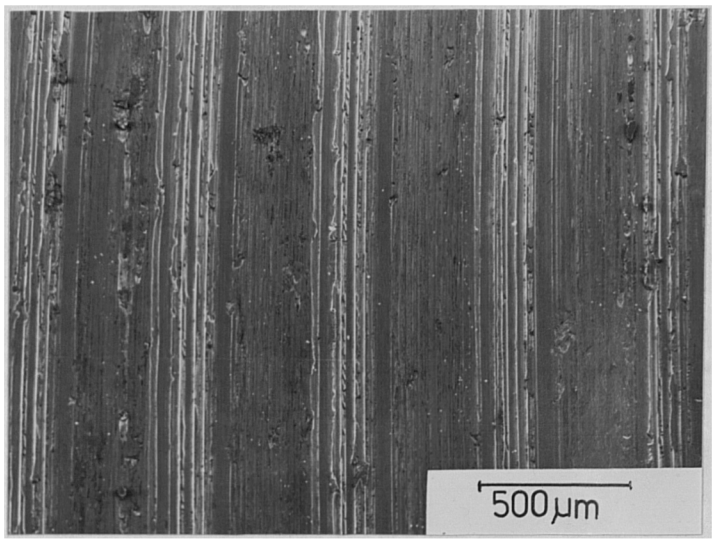

Figure 4.3.20. Abusively turned 817M40 showing parallel machining markings corresponding to the feed step width.

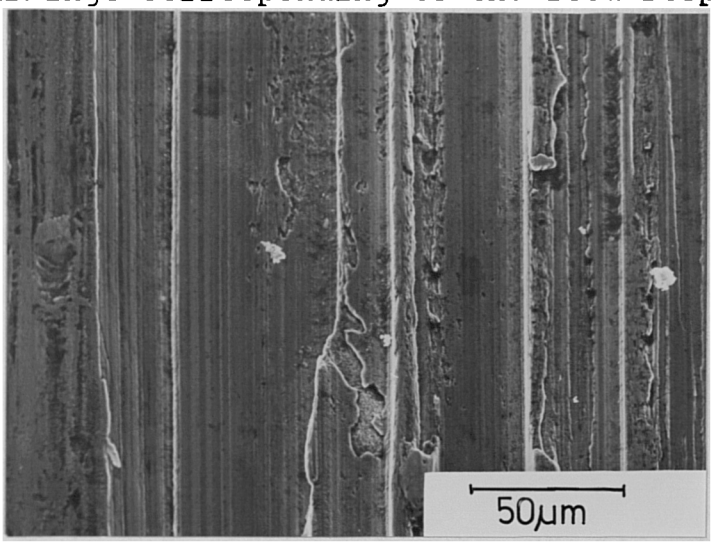

Figure 4.3.21. Detail of above showing ridges and extensive flat lands of plastically-deformed material.

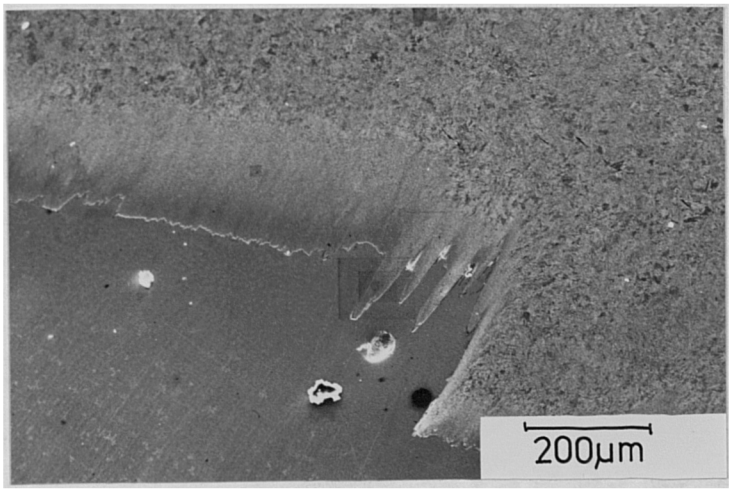

Figure 4.3.22. Abusively turned 817M40. Taper section of turned surface showing the white-etching layer.

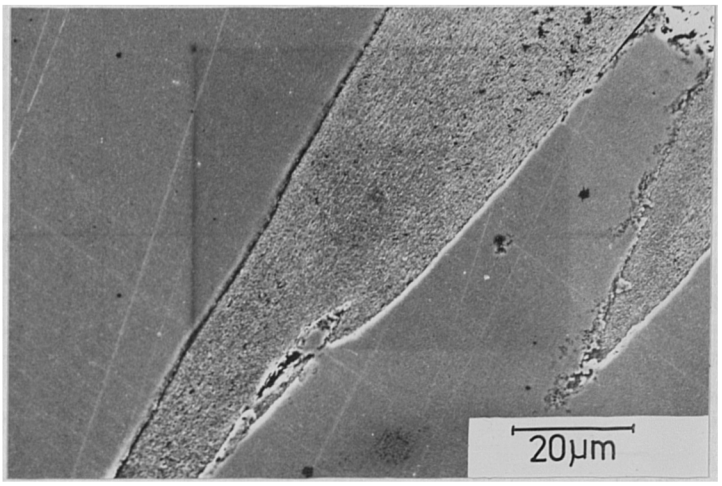

Figure 4.3.23. Abusively turned 817M40. Taper section of a ridge of plastically deformed material.

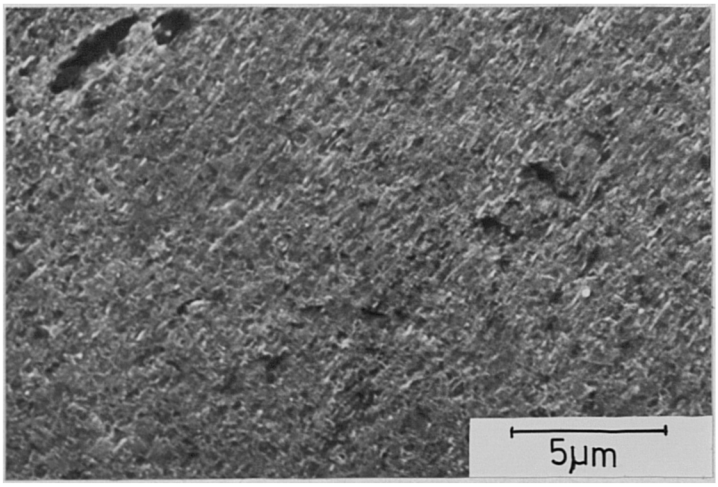

Figure 4.3.24. Detail of above showing a distribution of carbide particles in a heavily deformed matrix.

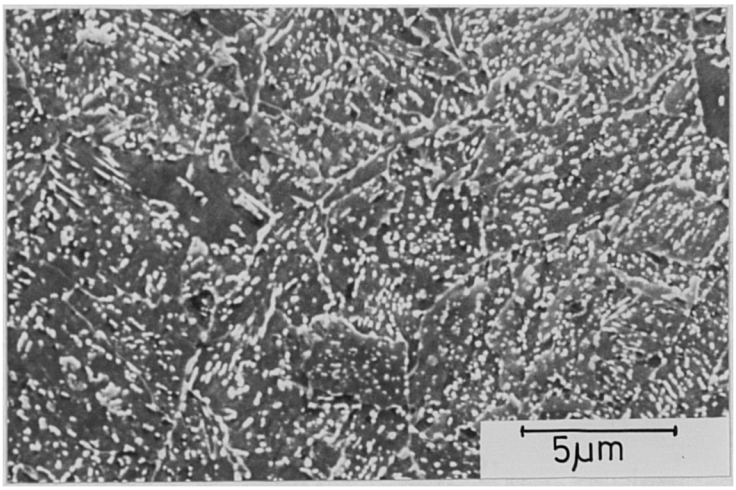

Figure 4.3.25. Underlying tempered martensite structure.

4.3.5. Wear Pin 817M40 steel.

At low magnification the surface of the wear pin exhibits the directional scoring associated with severe wear which has resulted in the formation of bands of plastically-deformed material (Figure 4.3.26). At higher magnification, fragments of oxide may be identified by their appearance under the electron beam (Figure 4.3.27).

Examination of the nickel-plated taper section prepared from this pin, shows regions of oxide extending into the matrix and a pool of a relatively structureless material, previously identified as white-layer by light microscopical examination and hardness testing of the same area. (Figure 4.3.28). The gradual transition between the underlying matrix and the white-layer, through a region of plastically-deformed material, may be compared with the abrupt transition between the matrix and the region of oxide in the same figure.

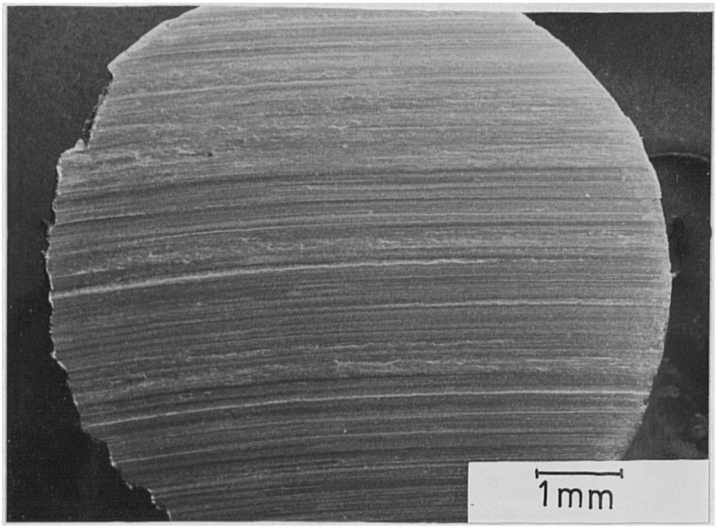

Figure 4.3.26. 817M40 Wear pin. Worn surface exhibiting heavy scoring due to severe wear.

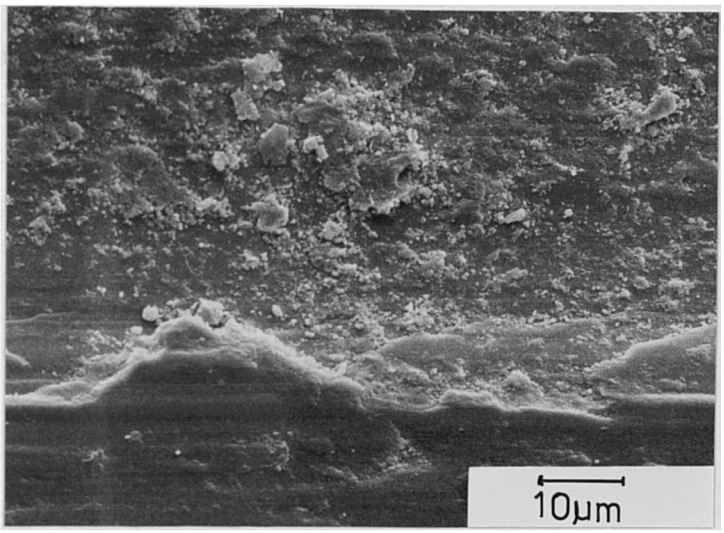

Figure 4.3.27. Detail of above exhibiting fragmented oxide particles and plastically deformed material.

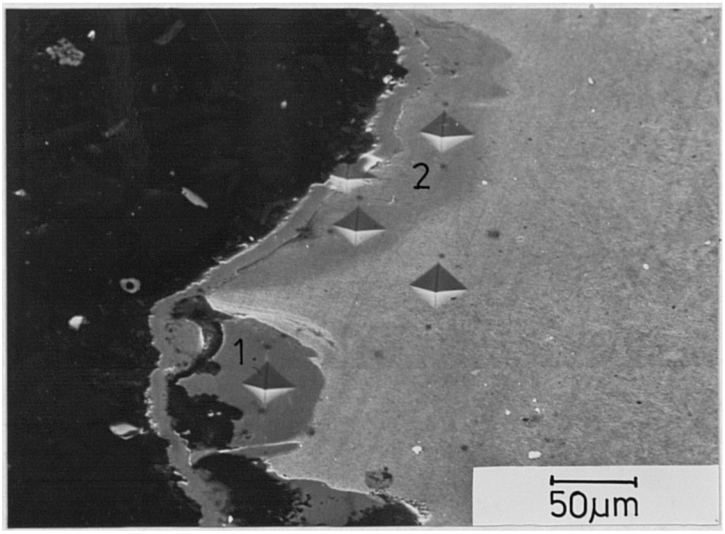

Figure 4.3.28. Wear pin. Metallographic cross-section showing: 1) a well defined area of oxide, 2) white-layer.

4.3.6. Stone Abraded Digger Tooth.

Figure 4.3.29, shows the surface of the stone-abraded steel to be relatively smooth, with several large score marks resulting from heavy localised wear. Detail of one of these score marks is shown at higher magnification in Figures 4.3.30 and 4.3.31, in which the extent of the surface deformation resulting from abrasion by hard rock fragments is visible.

A cross section prepared through one of the heavily deformed regions is shown in the SEM micrograph, (Figure 4.3.32). A partially detached fragment of plastically-deformed material is seen to overlay a region of white-layer. The structure of the white-layer formed in this region shows evidence of localised breakdown of the matrix to produce a fine uniform structure, see Figure 4.3.33, in contrast to the underlying material (Figure 4.3.34).

4.3.7. Chieftain Tank Gun Barrel Sections.

The low magnification micrograph,(Figure 4.3.35), shows the inner bore of a Chieftain tank gun barrel at a point close to the commencement-of-rifling position in the barrel. The surface shows the characteristic cracking associated with severe erosion, following extensive use. With increased magnification, see Figure 4.3.36, the cracks are seen to contain a deposit consisting of spheroidised combustion products, while the adjacent barrel surface appears smooth and glazed.

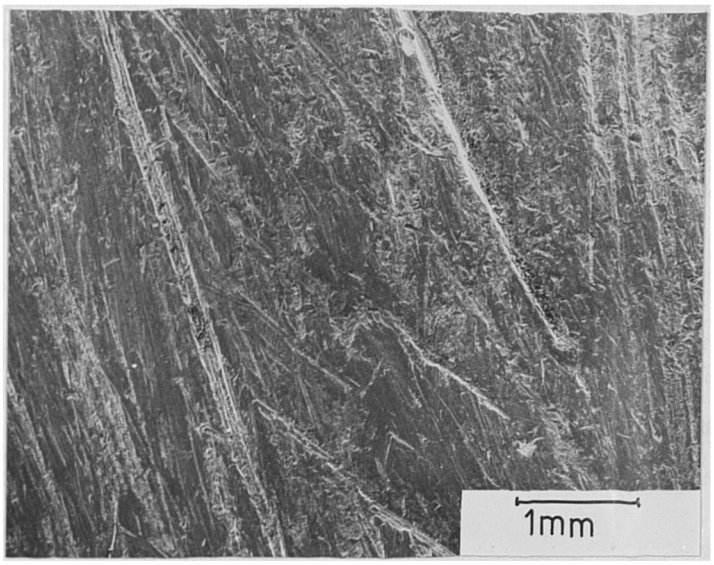

Figure 4.3.29. Digger tooth. Worn surface.

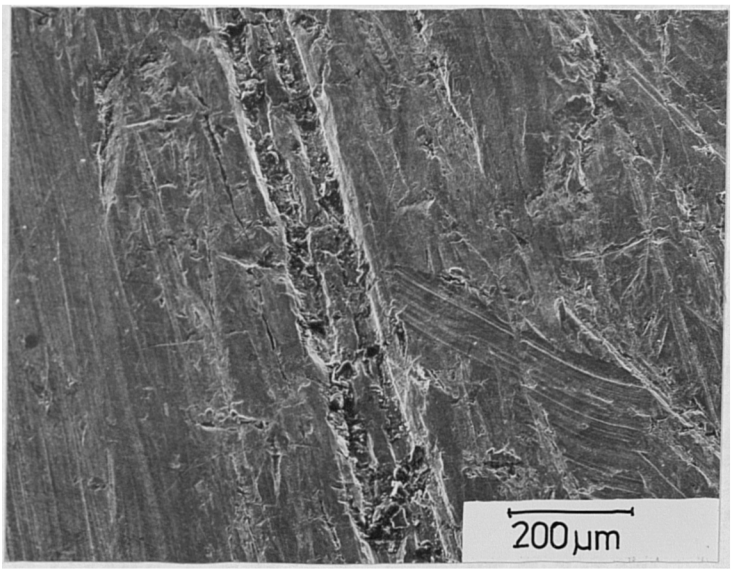

Figure 4.3.30. Digger tooth. Worn surface showing heavy scoring.

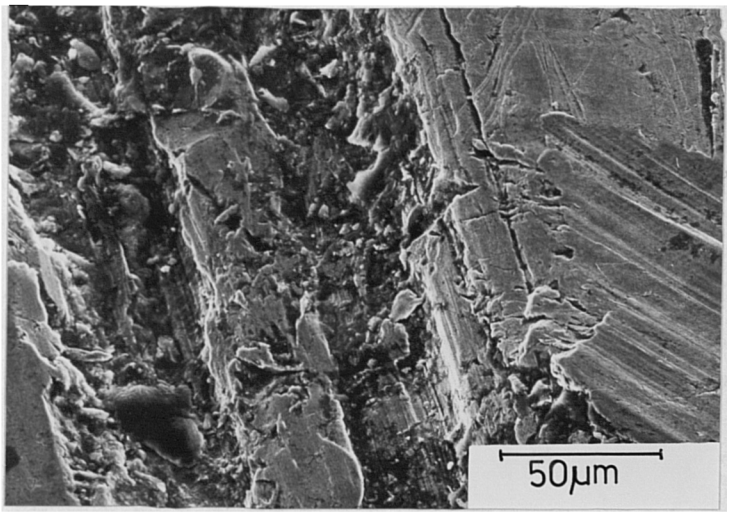

Figure 4.3.31. Digger tooth. Detail of scored region showing evidence of "ploughing" and plastic-deformation.

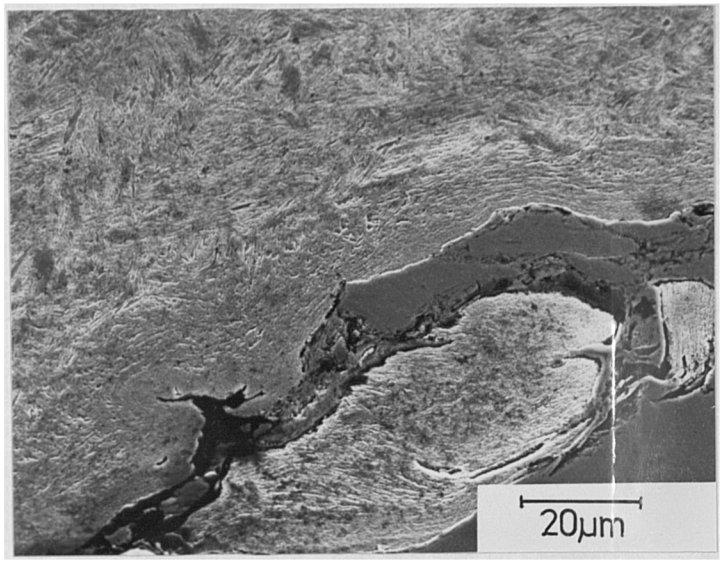

Figure 4.3.32. Digger tooth. Cross section through a heavily scored region showing the extent of the underlying plastic-deformation.

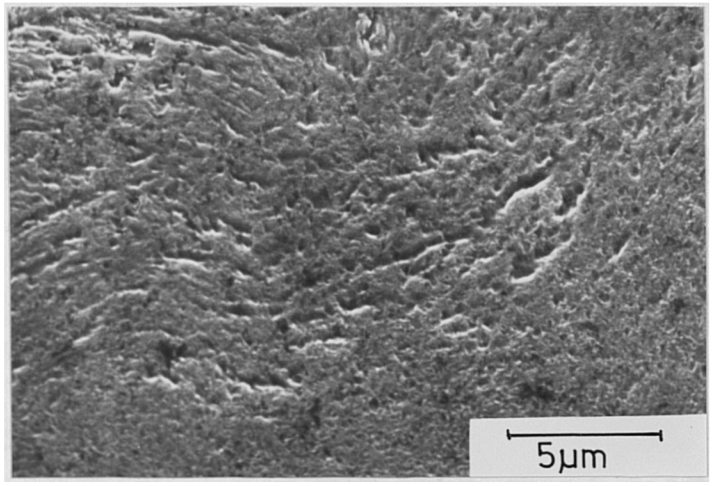

Figure 4.3.33. Detail of the region of white-etching plastically-deformed material, showing the development of a fine, uniform structure close to the surface.

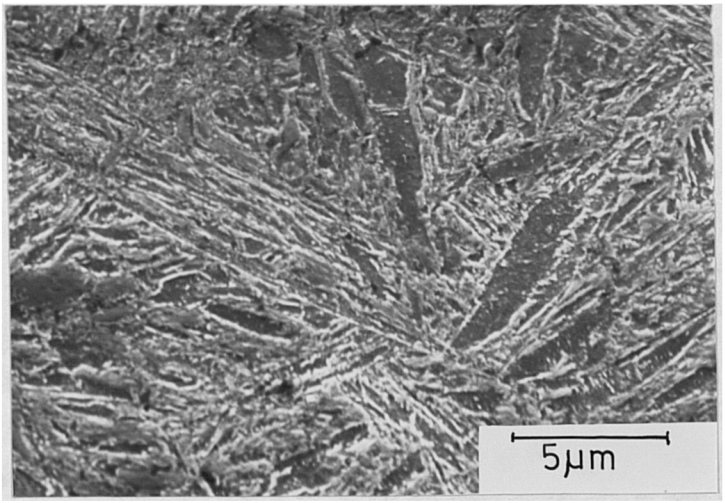

Figure 4.3.34. Digger tooth. Underlying tempered martensite structure.

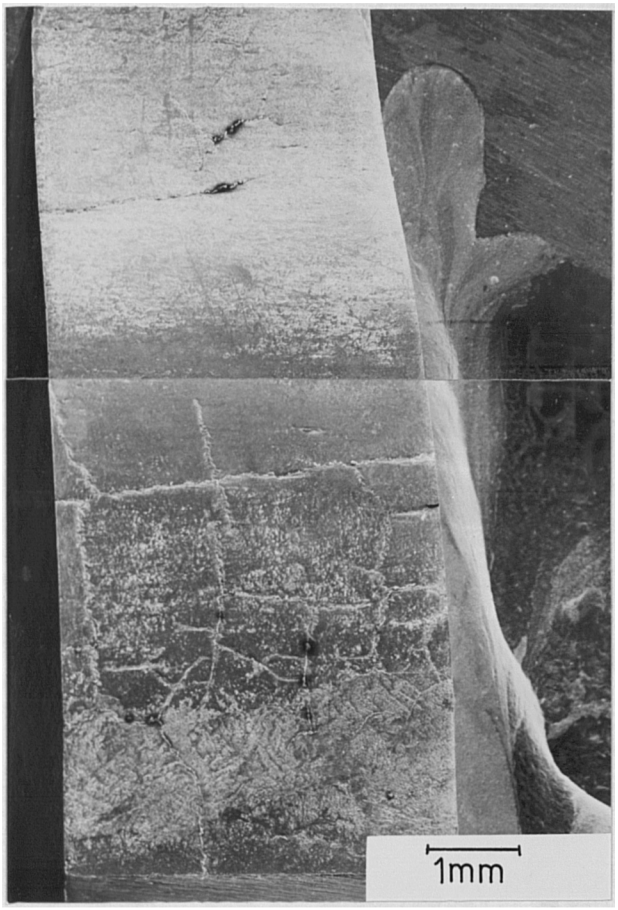

Figure 4.3.35. Chieftain gun barrel. Bore surface in the region of "commencement-of-rifling".

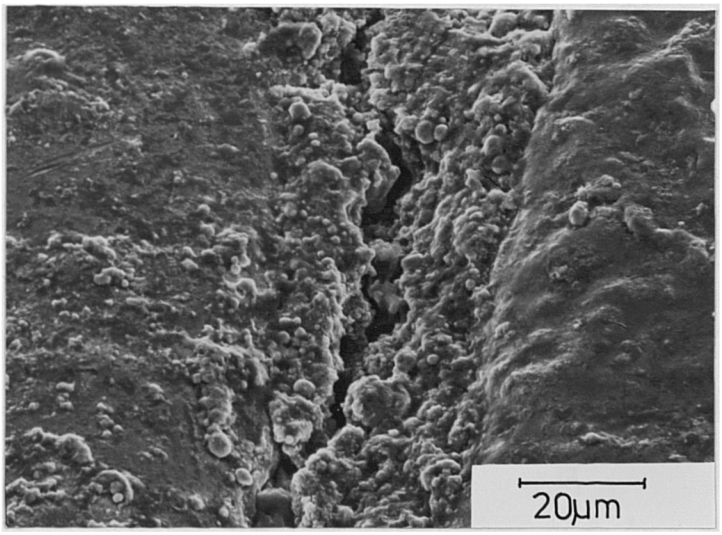

Figure 4.3.36. Chieftain gun barrel. Detail of a crack in the bore surface containing combustion products.

Examination of the microstructure following metallographic preparation, shows that to a depth of some 100μm, the material has experienced a structural change with a modification of the martensite to produce a more homogeneous structure with an apparently greater density of carbides. See for example Figure 4.3.37, close to the surface and Figure 4.3.38, within the underlying matrix.

4.3.8. RARDEN Gun Barrel Section.

The inner bore of the RARDEN barrel, shown in Figure 4.3.39, exhibits extensive surface cracking on both the raised lands and the valley areas of the rifling grooves.

Whilst the density of cracking is significantly greater in the valleys, the form of the cracks appears similar in both areas. Figures 4.3.40 and 4.3.41, show a typical region of crazing with a network of deep cracks and a secondary network of developing fissures.

The change in the microstructure of the steel from the surface through to the bulk is shown in Figure 4.3.42, in which the near surface layers, to a depth of some 40μm are seen to be relatively featureless in comparison to the martensitic structure of the underlying matrix. At high magnification the white-etching layer appears as an extremely homogeneous, finely textured material. (Figure 4.3.43).

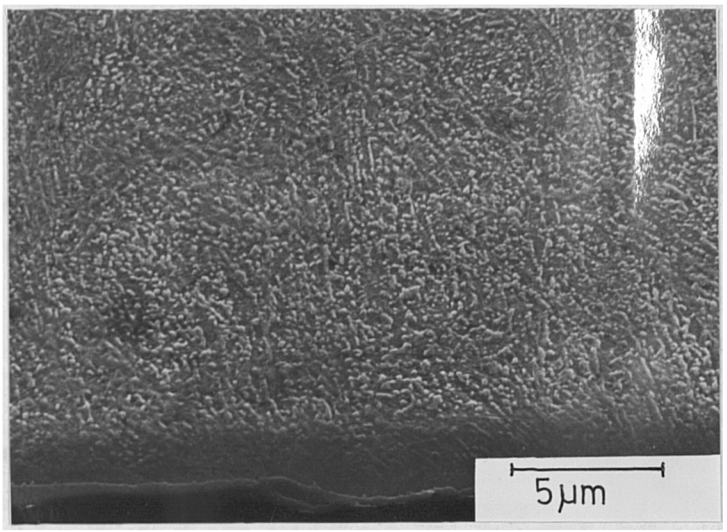

Figure 4.3.37. Chieftain gun barrel. Cross section of the barrel surface, showing a thin white-etching layer overlaying a zone of "modified" martensite.

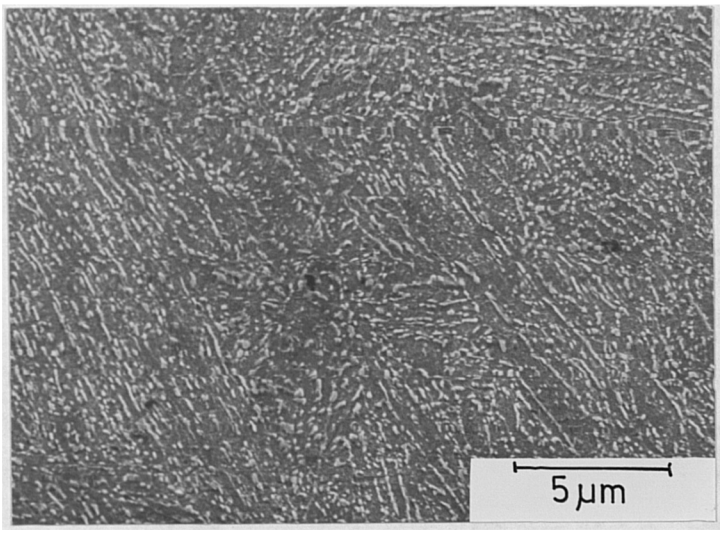

Figure 4.3.38. Chieftain gun barrel. Cross section of the underlying tempered martensite structure.

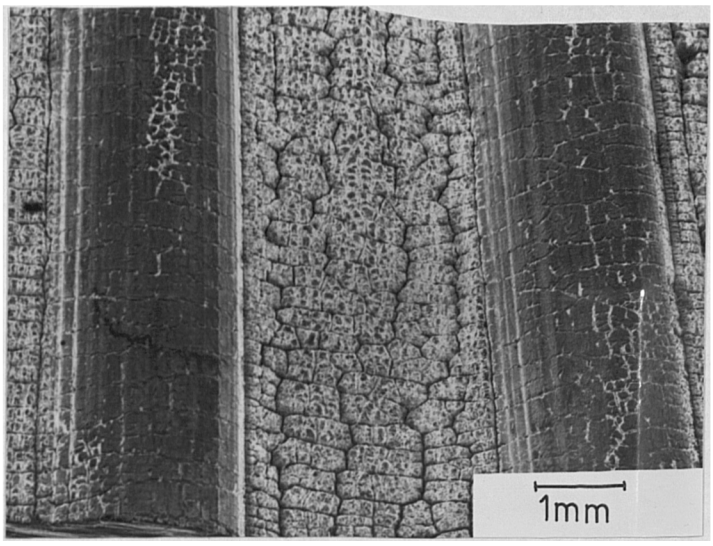

Figure 4.3.39. RARDEN gun barrel. Rifling grooves on the bore surface.

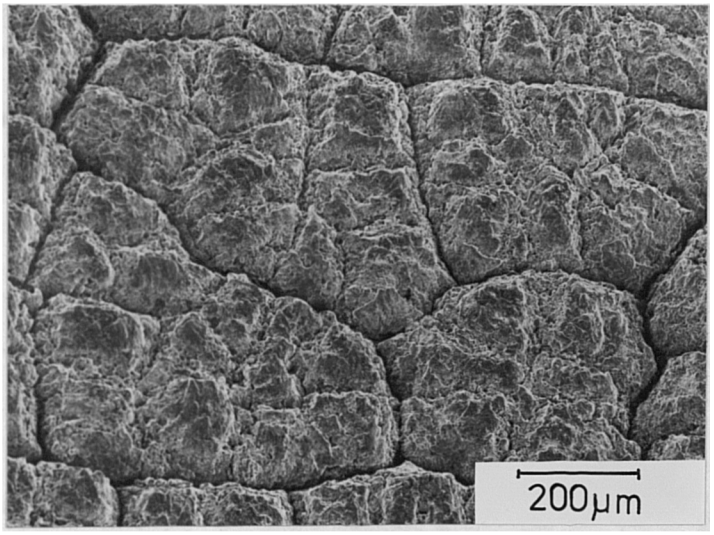

Figure 4.3.40. RARDEN gun barrel. Network of cracks developed in the valley area of rifling.

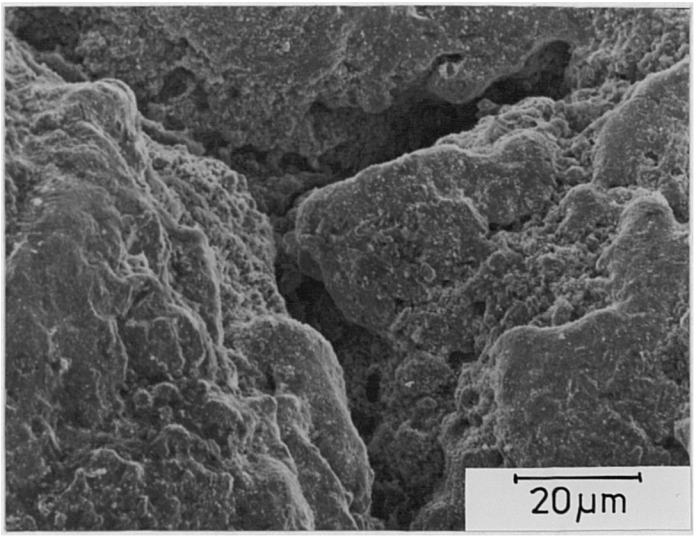

Figure 4.3.41. RARDEN gun barrel. Detail of cracking and firing residues within the rifling groove.

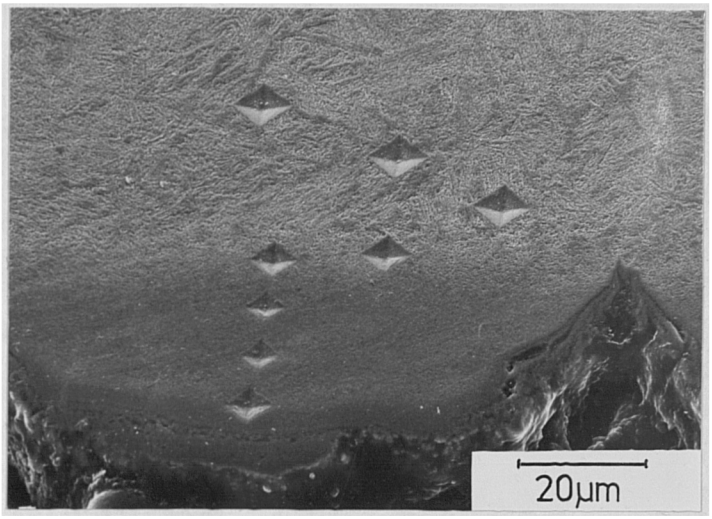

Figure 4.3.42. RARDEN gun barrel. Cross section through the bore surface showing a white-etching layer and a region of fine structure.

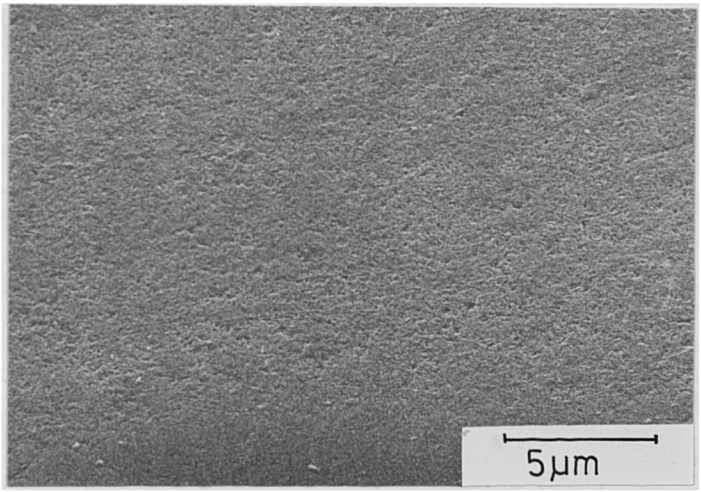

Figure 4.3.43. RARDEN gun barrel. Detail of the fine structured white-etching layer.

4.3.9. Adiabatic Shear Specimen.

Figure 4.3.44, shows at low magnification the cross-section of a portion of armour steel subjected to impact by a high velocity round. The cracks extending from the fracture surface are often associated with shear-bands as shown in Figure 4.3.45. At high magnification the shear band structure as shown in the micrograph, Figure 4.3.46, appears as a fine granular product with an abrupt and well defined transition from the adjacent material.

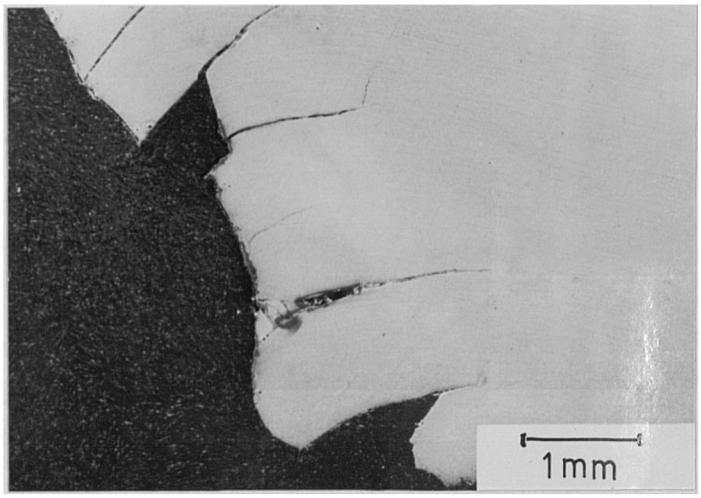

Figure 4.3.44. Adiabatic shear. Cross section of armour steel showing damage due to ballistic impact.

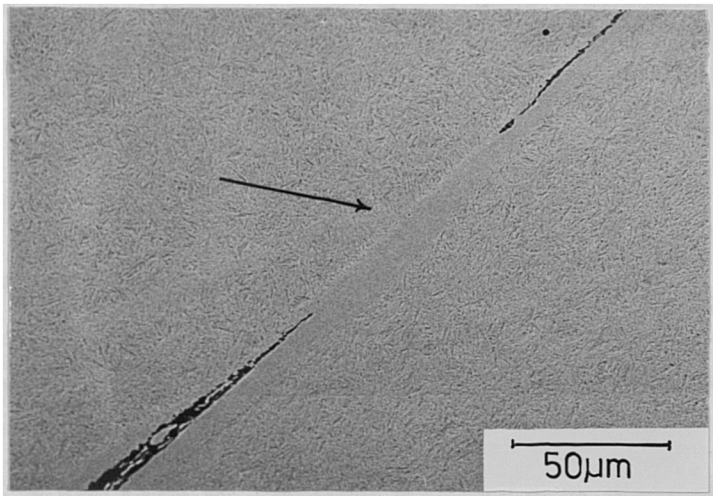

Figure 4.3.45. White-etching band and cracking associated with localised shear.

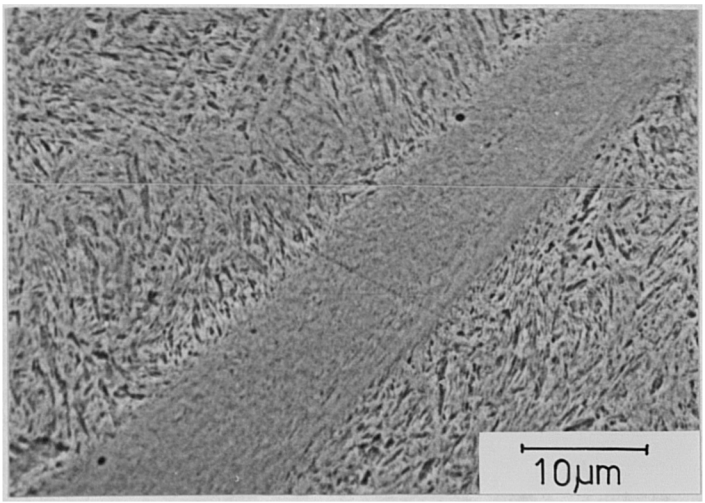

Figure 4.3.46. Detail of the shear band revealing a fine plastically-deformed structure,in contrast to the matrix.

4.4. Electron Probe Microanalysis

4.4.1. Laser Treated 817M40 Steel.

Figure 4.4.1, lists the results obtained for a series of conventional EPMA analyses (Analysed element Z > 11), performed on the metallographically prepared cross section through a laser heat-treated specimen of 817M40 steel. The analysis points were located close to the sites of microhardness indentations made at regular intervals from the surface through to the matrix in the laser heat-treated zone. With the exception of the first analysis point, acquired in the region of localised surface melting, the results, which represent the composition at steps of 50μm, do not appear to show any systematic variation and lie within the quoted composition for this material.

4.4.2. Laser treated 080M40 Steel.

The EPMA analyses shown in figure 4.4.2, were obtained from the polished cross section through a laser heat-treated track produced on 080M40 steel. The results represent analysis points at 50μm intervals from the surface to the underlying matrix . No significant variation in composition was observed.

Microprobe Analysis Results. Laser treated 817M40.					
Distance from edge µm	Element Wt%				
	Fe±0.5	Cr±0.1	Mn±0.1	Ni±0.1	Mo±0.1
50	97.6	0.8	0.4	1.3	0.0
100	96.7	1.1	0.4	1.4	0.4
150	96.4	1.1	0.9	1.2	0.4
200	96.3	1.0	0.9	1.3	0.4
250	96.5	1.0	0.9	1.4	0.3
300	96.3	1.2	0.8	1.4	0.3
350	96.2	1.1	0.7	1.5	0.4
400	96.4	1.3	0.6	1.4	0.4
450	96.6	1.2	0.9	1.2	0.2
500	96.6	1.2	0.8	1.4	0.0
550	96.4	1.1	0.6	1.4	0.4
600	96.5	1.1	0.8	1.4	0.2
650	96.2	1.2	0.6	1.6	0.4
900	96.5	1.1	0.8	1.3	0.4

Figure 4.4.1. Laser treated 817M40. Track 1. 25mms^{-1}. EPMA depth profile through the HAZ zone shown in figures 4.2.1. and 4.2.3.

Microprobe analysis results. Laser treated 080M40				
Distance from edge µm	Element Wt %.			
	Fe±0.5	Mn±0.1	Si±0.1	Phase
0	98.9	0.7	0.4	Acicular
50	98.9	0.7	0.4	Ferrite
100	99.0	0.7	0.3	Ferrite
150	99.1	0.6	0.3	Pearlite
200	99.1	0.4	0.4	Ferrite
250	99.1	0.6	0.3	Pearlite
300	99.1	0.5	0.4	Ferrite
350	99.0	0.7	0.3	Ferrite
400	99.3	0.6	0.1	Pearlite

Figure 4.4.2. Laser treated 080M40. EPMA depth profile through the laser HAZ shown in figure 4.2.11.

Microprobe analysis results.Laser treated ARMCO.			
Distance from edge µm	Element Wt %.		
	Fe±0.5	Mn±0.1	Si±0.1
0	99.5	0.2	0.1
200	99.4	0.3	0.2
450	99.3	0.2	0.3
700	99.5	0.3	0.3
950	99.6	0.2	0.2

Figure 4.4.3. Laser treated Armco iron. EPMA depth profile through the HAZ shown in figure 4.2.15.

4.4.3. Laser treated Armco Iron.

In a similar fashion to the analyses performed on the laser-treated 817M40 and 080M40 steels, a series of points were analysed close to the microhardness indentations made at 50μm intervals from the surface through to the matrix. The EPMA results, which are listed in Figure 4.4.3, indicate that the iron contained a low level of manganese and silicon.

4.4.4. Abusively turned 817M40 steel.

Examination of the metallographically prepared taper section through the turned surface of a disc of 817M40 steel, revealed a layer of plastically-deformed and white-etching material which differed in appearance to the underlying matrix. Figure 4.4.4, illustrates a typical field of view in which areas have been selected for micro-hardness testing and microprobe analysis. No significant variation in composition was noted.

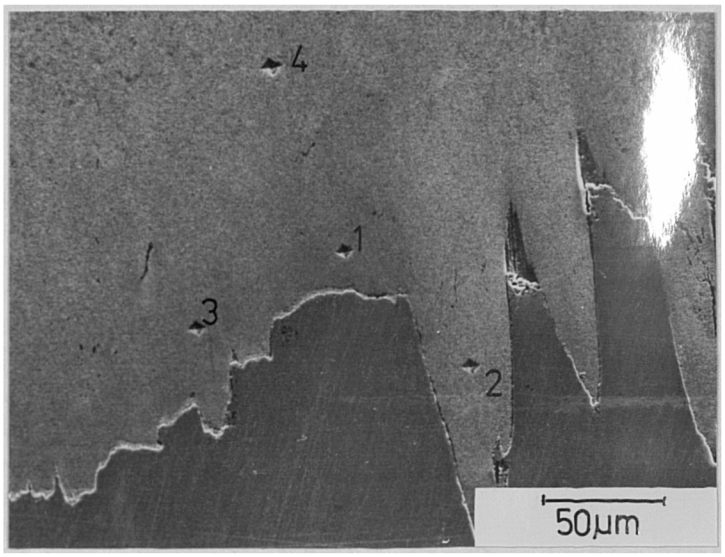

Microprobe analysis results. Abusively Turned 817M40.					
Analysis point.	Element Wt %				
	Fe±0.5	Cr±0.1	Mn±0.1	Ni±0.1	Mo±0.1
1	97.0	1.1	0.5	1.4	0.1
2	96.2	1.1	0.9	1.6	0.3
3	96.8	1.1	0.6	1.2	0.4
4	97.0	1.2	0.6	1.3	0.0

Figure 4.4.4. Abusively turned 817M40. EPMA of selected points close to the abusively machined surface, as shown in the associated micrograph.

4.4.5. Wear Pin. 817M40 Steel.

An 11° metallographically prepared taper section through the worn surface of a wear pin , was examined by light and scanning electron microscopy and areas representative of the various visually different regions shown in Figure 4.4.5, were selected for microhardness testing and electron probe microanalysis.

The analysis indicates that the levels of Cr, Mn, Ni, and Mo are similar in each of the areas examined and remain within the range of the quoted composition for this material. The Fe level is reduced in the regions of oxide where the average value for the oxygen content of 17wt%, derived by difference suggests that this constituent is a mixture of Fe and FeO.

4.4.6. Stone Abraded Digger Tooth.

The discontinuous areas of white-etching material observed on the metallographically-prepared cross-section of the digger tooth, were considerably smaller than similar features observed on other samples examined. To produce sufficient data for comparison, two areas were selected for analysis. See Figures 4.4.6 and 4.4.7. Points analysed by EPMA are identified on the micrographs and the corrected results listed in the associated tables.

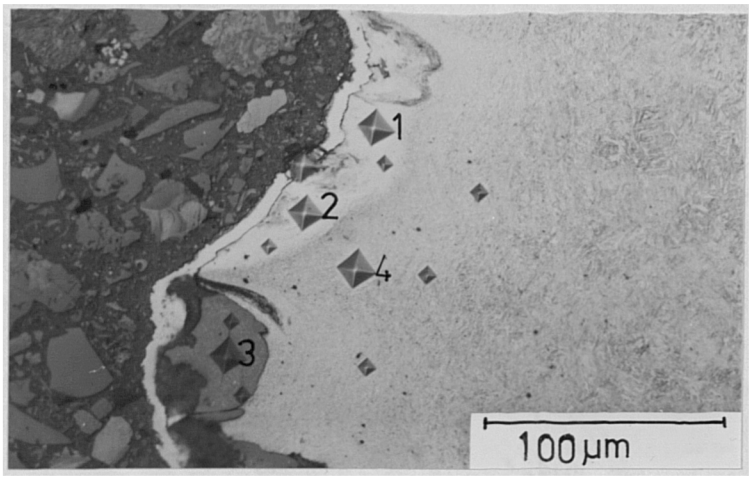

Microprobe analysis results. Wear Pin 817M40.						
Analysis point	Element Wt %					
	Fe±0.5	Cr±0.1	Mn±0.1	Ni±0.1	Mo±0.1	O±0.1
1	96.7	1.3	0.6	1.3	0.2	0.0
2	96.4	1.1	0.7	1.5	0.5	0.0
3	79.5	1.1	0.6	1.1	0.3	17.1
4	96.9	1.2	0.7	1.2	0.2	0.0
Matrix	96.4	1.2	0.8	1.1	0.5	0.0

Figure 4.4.5. Wear pin 817M40 steel. EPMA of white-etching features and oxide pools within the worn surface layers, as shown in the associated micrograph.

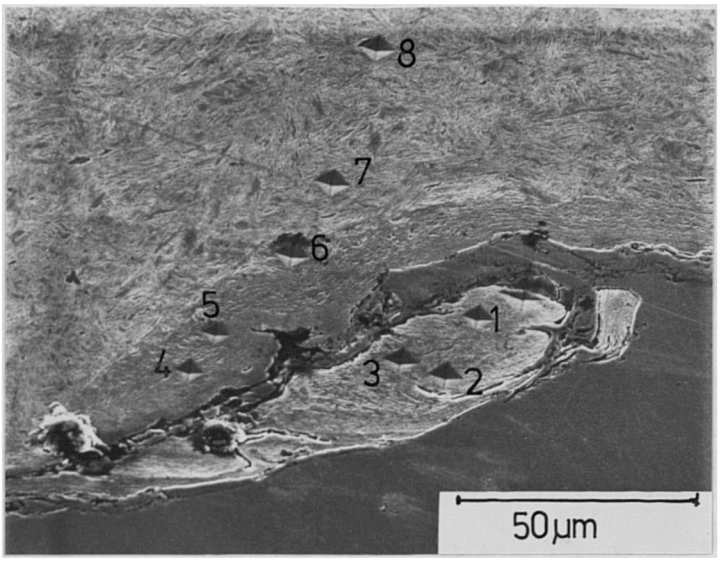

Microprobe analysis results. Digger Tooth						
Analysis point	Element Wt%					
	Fe±0.5	Cr±0.1	Mn±0.1	Ni±0.1	Mo±0.1	Si±0.1
1	95.4	2.0	0.7	0.6	0.2	1.1
2	95.6	2.1	0.7	0.4	0.2	1.1
3	95.6	2.1	0.8	0.4	0.0	1.2
4	96.4	1.9	0.5	0.1	0.0	1.1
5	96.0	1.9	0.7	0.3	0.0	1.1
6	95.8	2.1	0.6	0.4	0.0	1.1
7	95.5	2.1	0.7	0.2	0.4	1.1

Figure 4.4.6. Digger tooth. EPMA of white-etching and plastically-deformed material revealed in the cross section through the worn surface.

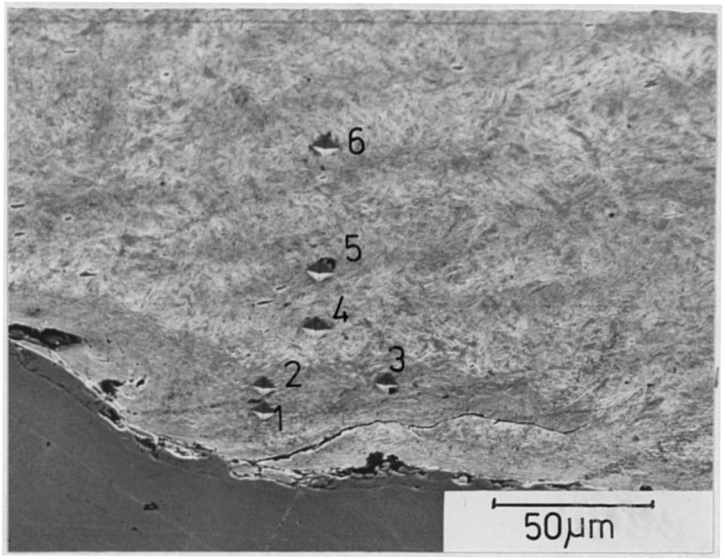

Microprobe analysis results Digger Tooth						
Analysis point	Element Wt%					
	Fe±0.5	Cr±0.1	Mn±0.1	Ni±0.1	Mo±0.1	Si±0.1
1	96.0	2.1	0.5	0.3	0.1	0.9
2	95.9	2.2	0.7	0.3	0.0	1.0
3	95.9	2.1	0.6	0.3	0.3	0.9
4	95.6	2.2	0.6	0.3	0.3	1.0
5	96.0	2.2	0.6	0.2	0.1	1.0
6	95.9	2.2	0.6	0.2	0.0	1.2

Figure 4.4.7. Digger tooth. EPMA of plastically-deformed and white-etching material within the metallurgically-prepared cross section of the worn surface.

4.4.7. Chieftain Tank Gun Barrel Sections.

Two metallographically-prepared cross sections through the bore of Chieftain Tank gun barrels, coded JW1 and JW4, were microprobe analysed at selected points adjacent to microhardness test indentations made at regular intervals from the surface to the bulk. Figure 4.4.8, shows a view of the sample JW1, following removal from the phenolic mounting material, in which a surface crack is seen to extend through the relatively structureless white-etching layer, into the martensitic matrix. Microprobe analysis of the white-etching layer close to the microhardness indentations shown in the field of view, and at two other sites of microhardness testing in the underlying matrix, are listed in the associated table. A further series of results were obtained from the sample JW4, from the area shown in the Figure 4.4.9, at intervals of 20μm from the sample surface, through the white-etching layer and into the underlying matrix. Also included in the table, and listed as point 1, is the average of three analyses acquired from the very thin, outer white-layer observed on this sample.

Conventional EPMA of the Chieftain barrel indicates that the outer white-layer contains a small amount of calcium, presumably originating from the propellant charge, and an increased level of nickel relative to the matrix. The chromium signal is significantly reduced in the outer white layer and together with molybdenum, appears depleted throughout the thick white-etching layer.

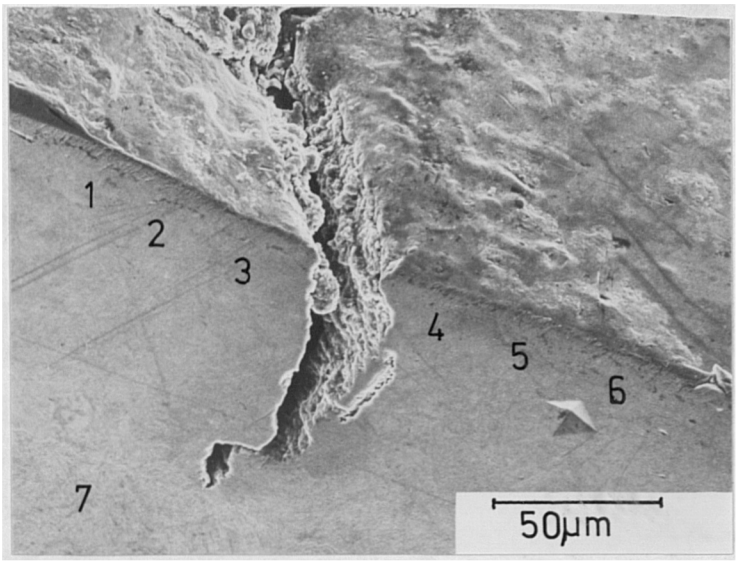

Chieftain Tank Gun. Sample JW1.					
Analysis point.	Element Wt%				
	Fe±0.5	Cr±0.1	Mn±0.1	Ni±0.1	Mo±0.1
1	95.0	0.9	0.7	2.7	0.7
2	94.7	1.1	0.6	2.8	0.8
3	94.1	1.1	0.8	3.2	0.8
4	94.2	1.2	0.9	2.8	0.9
5	94.9	1.1	0.6	2.6	0.9
6	94.2	1.1	0.8	2.7	1.2
7	94.6	1.3	0.7	2.7	0.8

Figure 4.4.8. Chieftain barrel. EPMA of selected points within the white-etching layer and the underlying matrix showing a slight depletion of chromium at the surface.

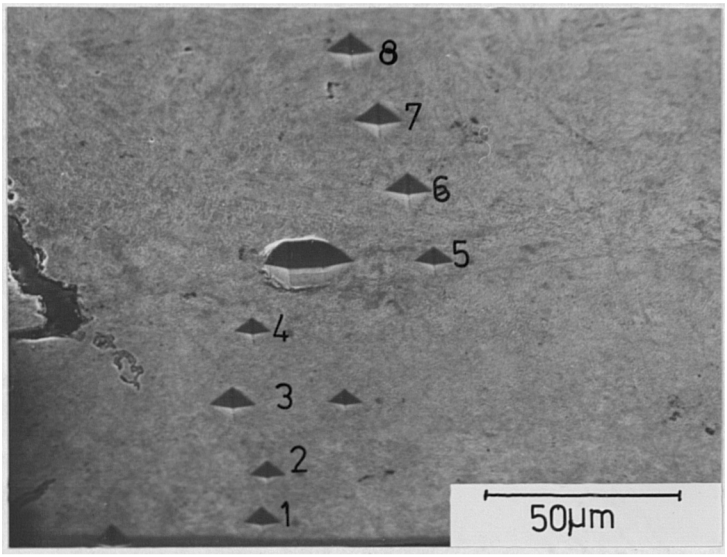

Chieftain Tank Gun. Sample JW4.					
Analysis point	Element Wt %				
	Fe±0.5	Cr±0.1	Mn±0.1	Ni±0.1	Mo±0.1
1	94.7	0.1	0.0	3.6	1.2
2	95.0	1.0	0.5	2.9	0.6
3	94.8	1.1	0.6	2.7	0.8
4	94.7	0.9	0.5	2.8	1.1
5	94.8	1.0	0.8	3.0	0.4
6	94.3	1.1	0.8	2.7	1.1
7	93.8	1.2	0.8	2.9	1.3

Figure 4.4.9. Chieftain barrel. EPMA depth profile of a cross section through the bore showing a depletion in chromium and manganese in the surface white-etching layer.

4.4.8. RARDEN gun barrel section.

The scanning electron micrograph Figure 4.4.10, shows the series of microhardness tests made at 10μm intervals from the surface of the rifled barrel section. The indentations were displaced laterally to avoid overlapping within the softer matrix material. Microprobe analyses obtained from points close to each of the indentations show no significant variation between the composition of the white-etching layer and the underlying matrix.

Analysis of the thin outer white-layer showed that this material had been chemically modified during firing and contained lower levels of Cr, Mn, and Ni, and an increased amount of Mo, when compared to the thick white-etching layer and the matrix.

4.4.9. Adiabatic shear specimen.

The small dimensions of the shear bands observed in the sample of armour steel subjected to ballistic impact, presented difficulties both for accurate hardness determination and for microprobe analysis.

The area selected for analysis exhibited an adiabatic shear band some 10μm wide, see Figure 4.4.11, in which a series of microhardness test indentations have been made across the shear band at an angle of some 45° to the direction of the shear band. Microprobe analysis from points adjacent to the indentations do not show any significant variation in composition between the shear band and the matrix.

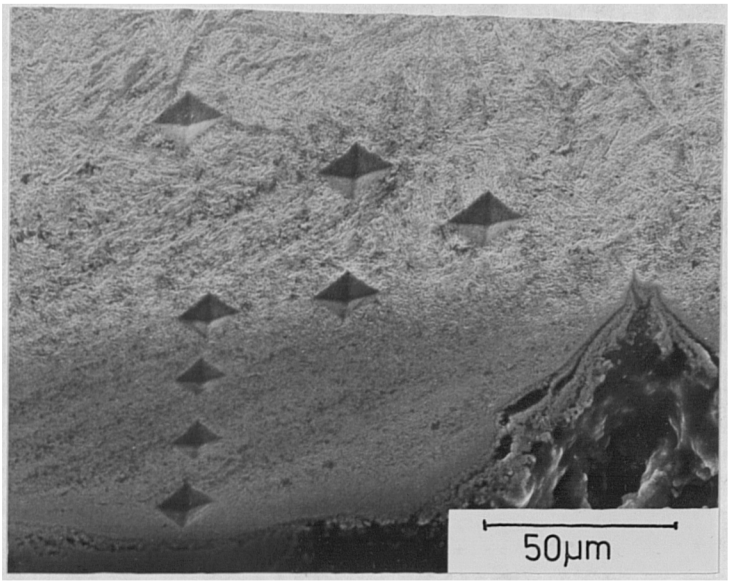

Microprobe analysis results. RARDEN Gun Barrel					
Distance from edge µm.	Element. Wt %				
	Fe±0.5	Cr±0.1	Mn±0.1	Ni±0.1	Mo±0.1
0	96.8	0.17	0.0	1.5	1.5
10	95.6	0.9	0.5	2.5	0.4
20	95.3	0.9	0.6	2.9	0.4
30	95.4	0.9	0.6	2.6	0.6
40	95.1	0.9	0.5	3.0	0.5
50	95.4	0.8	0.4	2.7	0.7
60	95.7	0.9	0.2	2.7	0.5
70	95.1	0.9	0.5	2.8	0.6
80	95.2	0.8	0.7	3.0	0.3

Figure 4.4.10. RARDEN barrel. EPMA depth profile through the cross section of the bore shown above. The analyses indicate a substantial depletion of chromium, manganese and nickel in the outer white-etching layer and a corresponding increase in molybdenum.

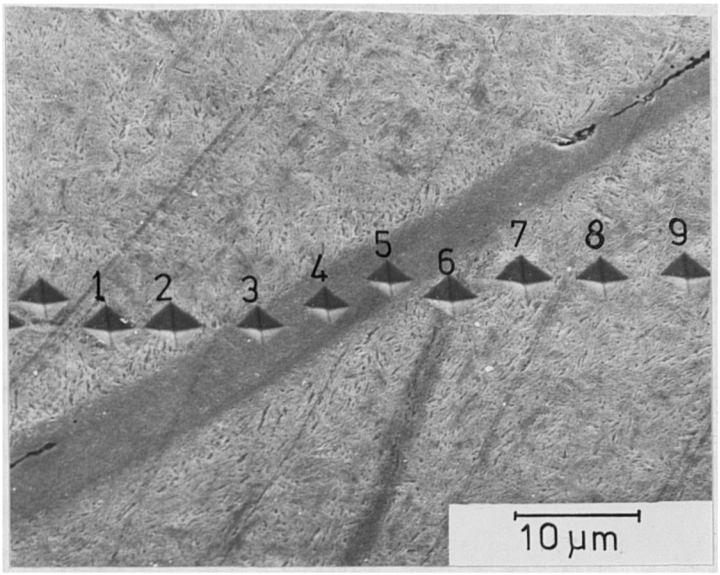

Microprobe analysis results. Adiabatic Shear Specimen.						
Analysis point	Element Wt%					
	Fe±0.5	Cr±0.1	Mn±0.1	Ni±0.1	Mo±0.1	Si±0.1
1	95.8	0.3	0.6	1.5	1.1	0.8
2	94.0	0.3	0.9	2.0	2.0	0.9
3	95.6	0.2	0.8	1.8	0.7	1.0
4	95.3	0.2	0.9	2.1	0.9	0.7
5	95.8	0.3	0.7	1.7	0.7	0.8
6	96.2	0.2	0.6	1.6	0.6	0.8
7	96.3	0.3	0.5	1.8	0.5	0.6
8	95.9	0.2	0.5	1.8	0.7	1.0
9	96.1	0.2	0.5	1.7	0.7	0.9

Figure 4.4.11. Adiabatic shear. EPMA profile through an adiabatic shear band at the points indicated. No variation in composition was observed.

4.5. EPMA Light element analysis

4.5.1. Laser Treated 817M40 Steel.

A series of analyses for carbon were obtained from points adjacent to the microhardness indentations used to locate sites for EDX-EPMA analysis on the laser heat-treated track 1. The results, presented in Figure 4.5.1, show a reducing carbon content from 0.53 (±.05) wt % at the surface, falling to 0.48 (±.05) wt% at a depth of 150μm , before becoming relatively constant. The initial variation is not thought to be significant and there is no correlation between the variation of hardness with depth and the measured carbon content.

Neither nitrogen or oxygen were detected by light element microprobe analysis at any point within the laser treated zone or the matrix of this material. The detection limits for these elements being estimated as 2000 ppm and 1200 ppm respectively, with reference to measurements made on standards, as described in chapter 3.

4.5.2. Laser Treated 080M40 Steel.

Analyses at selected sites within the laser heat-treated zone, corresponding to regions of transformed or modified pearlite, the surrounding ferrite and the acicular phase identified in the region of maximum heating, are compared with analyses obtained in the matrix, (Figure 4.5.2).

Laser treated 817M40 steel.		
Distance from edge µm	Track No. 1. 25mms^{-1}	
	HV 25g±30	C wt% ± 0.05
0	946	0.53
50	847	0.52
100	870	0.5
150	847	0.48
200	870	0.47
250	946	0.48
300	1003	0.46
350	1064	0.46
400	946	0.42
450	870	0.44
500	782	0.43
550	413	0.42
600	437	0.43
650	413	0.48

Figure 4.5.1. Laser treated 817M40. Carbon analysis and microhardness depth profile through the laser-treated zone illustrated in figure 4.2.1.

Laser treated 080M40 steel.		
AREA	HV(25g)±30	C WT % ±0.05
Matrix Pearlite	350	1.22
Matrix Ferrite	210	0.22
Modified Pearlite	1132	0.91
HAZ Ferrite	212	0.23
Acicular product	--------	0.42

Figure 4.5.2. Laser treated 080M40. Carbon analysis and microhardness values of selected phases within the laser heat-treated zone and the underlying pearlitic matrix.

The results show a higher than expected level of carbon in the unmodified pearlite, this is attributed to a selectively higher uptake of carbon contamination by the lightly etched pearlite structure. The measured carbon content of 0.9 (±.05)wt% in the modified pearlite area, is taken to indicate that carbon did not diffuse away from this phase during the short duration heating process. Some diffusion of carbon is however indicated in the region of acicular product close to the surface where carbon levels were found to average 0.4 (±.05)wt %. Neither nitrogen or oxygen were detected within the laser heat-treated zone or the matrix of this material.

4.5.3. Laser treated Armco Iron.

Analysis for carbon within the laser heat-treated zone and the underlying matrix, showed no regions with levels above that attributable to hydrocarbon contamination . Neither nitrogen or oxygen were detected within this specimen.

4.5.4. Abusively turned 817M40 steel.

Carbon analyses were obtained from the area shown in the micrograph at the points indicated. (Figure 4.5.3). These show that the variation in microhardness between the plastically-deformed surface layers, the white-layer and the matrix, is not related to any differences in the local carbon content. Light element analysis failed to detect nitrogen and oxygen in this specimen.

4.5.5. Wear pin. 817M40 Steel Pin.

Areas of white-layer, oxide and plastically-deformed material, identified on the taper cross-section of the wear surface shown in Figure 4.5.4, were selected for light element analysis . The highest level of carbon at 0.7 (±.05)wt%, was detected in areas of plastically-deformed material , whilst the measured carbon content of the white-layer, 0.5 (±.05)wt% was found to be lower than that of the matrix at 0.6 (±.05)wt%.

These results may be explained in part by the increased pick-up of hydrocarbon contaminants either during sample preparation or under analysis conditions. The presence of oxygen in the oxide pools and in regions of mixed oxide and plastic-deformation was confirmed, but nitrogen was not detected by light element EPMA.

4.5.6. Digger Tooth.

The two areas previously selected for conventional microprobe analysis were re-prepared before being analysed in the unetched condition for carbon, nitrogen and oxygen. Similar levels of carbon, averaging 0.45 (±.05)wt% were measured at each of the sites selected for analysis, in both the white-layer and underlying matrix. Oxygen and nitrogen were not detected.

Abusively turned 817M40 Steel.			
Point No. (ref fig.4.4.4)	Material	HV 25g ± 30	C wt% ± 0.05
1	White layer	762	0.40
2	White layer	946	0.48
3	White layer	894	0.52
4	Deformed	627	0.47
5	Matrix	370	0.48

Figure 4.5.3. Abusively turned 817M40. Carbon analyses of the white-layer, plastically-deformed region and underlying matrix.

Wear pin 817M40 steel.		
AREA	HV(25g)± 30	C Wt% ± 0.05
Oxide	1018	0.34
Deformed Oxide	-----	0.71
White Layer	894	0.51
Matrix	707	0.62

Figure 4.5.4. Wear pin 817M40. Carbon analysis of selected regions representing; white-layer, oxide pools and the underlying matrix. See for example figure 4.4.5.

4.5.7. Chieftain Tank Gun Barrel.

Light element analysis showed no significant variation in carbon content between the underlying matrix and the thick white-layer revealed by etching in Nital. The average value measured in these regions at 0.55 (±.05)wt%, was above the quoted carbon content of 0.45wt% for this steel. This increase is attributed to surface contamination by hydrocarbons. The very thin white-layer observed at the gun barrel surface was found to contain a much higher level of carbon than the matrix, averaging 2.8 (±.05)wt%. This layer was also found to contain a low level of nitrogen giving a peak to background ratio of 1.1 : 1 . This may be compared with similar analyses obtained from a section of nitrided steel in which the peak to background ratio for the outer layer hardened to 1288HV (25g), was found to be 5.9:1. (Figure 4.5.5).

4.5.8. Rarden Gun Barrel.

Light element microprobe analysis of this sample revealed no significant difference between the carbon content of the matrix and that of the thick white-etching layer. The very thin white-layer at the barrel surface however, exhibited a high level of carbon, estimated at 5.2 (±.05) wt%. Nitrogen and oxygen were not detected in any of the areas analysed on this sample.

4.5.9. Adiabatic shear specimen.

A series of analyses for carbon were carried out at the sites of the microhardness indentations made across a shear band. The results indicated that the shear band contained a slightly lower level of carbon than the surrounding matrix and that at the boundary between the shear band and matrix, the carbon content was increased. (Figure 4.5.6).

It is not clear to what extent the measured variation in carbon content may be attributed to a selective increase in hydrocarbon contaminants on those areas of the microstructure exhibiting surface structure following etching.

LIGHT ELEMENT ANALYSIS.			
Chieftain tank gun barrel.			
Area analysed.	C Wt% ± 0.05.	N Wt% ± 0.3	O Wt% ± 0.3
Surface white layer.	2.8	1.1	0.2
Thick white layer	0.57	----------	0.2
Matrix.	0.54	-------	--------

Figure 4.5.5. Chieftain gun barrel, light element EPMA showing the increased carbon content in the outer white-etching layer and estimates of nitrogen and oxygen content by comparison with nitrided steel and FeO standards.

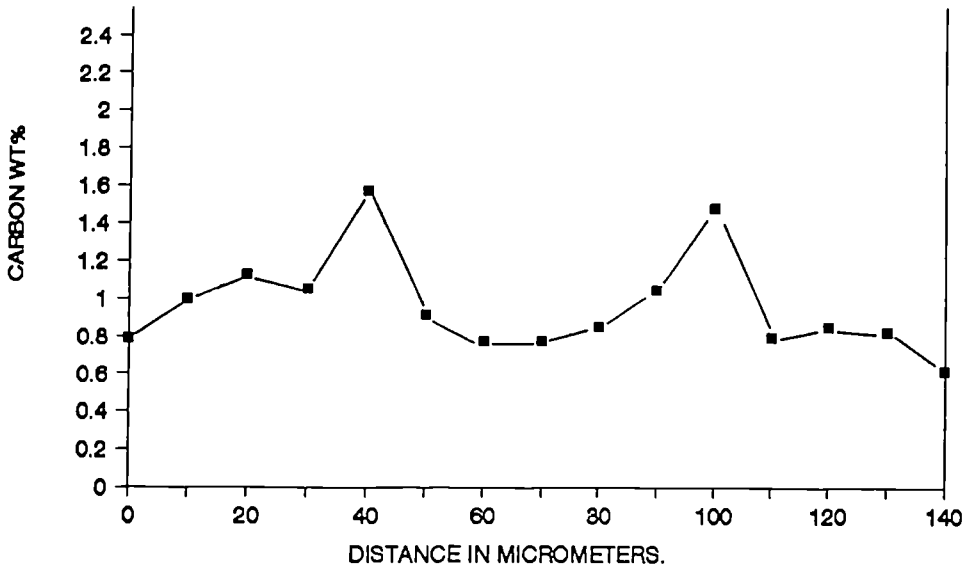

Figure 4.5.6. Adiabatic shear. Carbon distribution across the shear band illustrated in figure 4.4.11, determined by light element EPMA.

4.6. Secondary Ion Mass Spectrometry - SIMS.

4.6.1. Laser treated 817M40 Steel.

The large heat-affected zone produced by laser heat-treatment at a slow traverse rate, allowed SIMS analysis of the HAZ and the underlying matrix to be compared on a metallographically prepared cross section. Figures 4.6.1 and 4.6.2 show the spectra obtained from a 60μm deep crater formed in the white-etching zone and a 7μm crater formed in the matrix. No significant differences are observed between the levels of carbon, nitrogen, oxygen and hydrogen in these spectra.

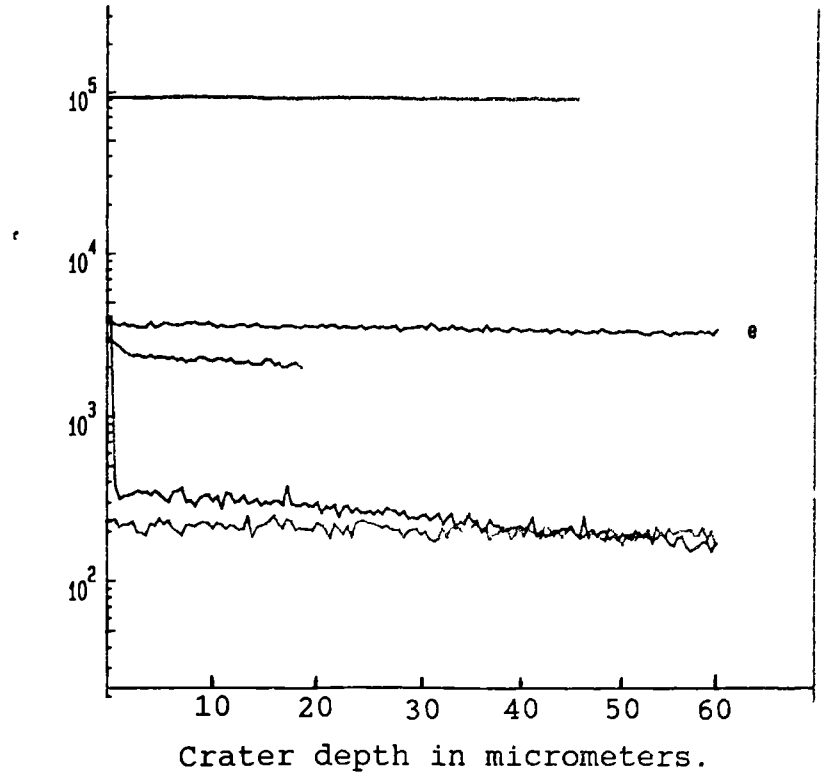

Figure 4.6.1. Laser treated 817M40. SIMS spectra acquired from a 60μm crater formed in the laser HAZ.

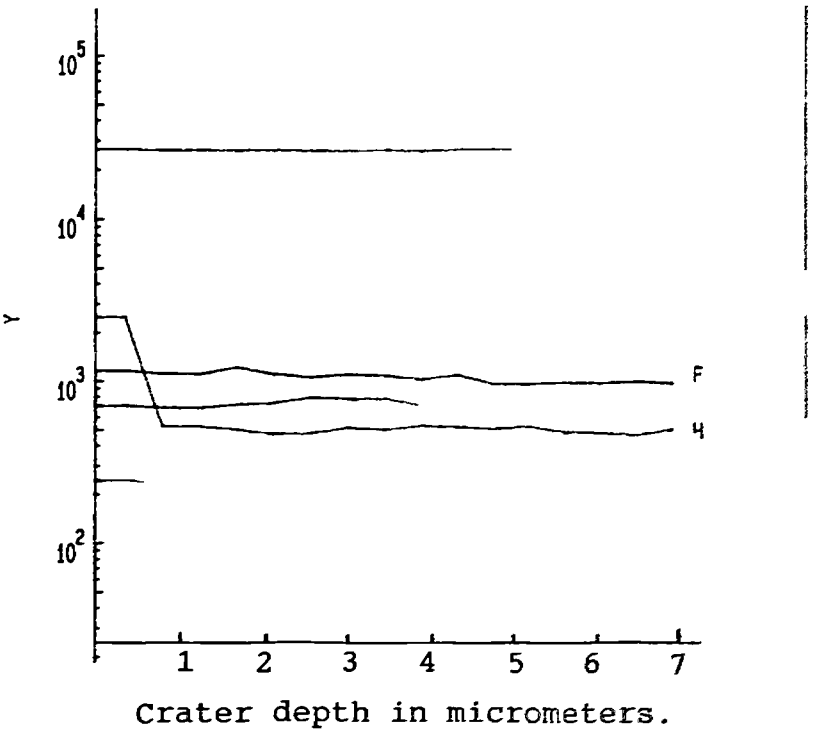

Figure 4.6.2. Laser treated 817M40, SIMS spectra acquired from a 7μm crater formed in the matrix material.

4.6.2. Abusively turned 817M40 steel.

A SIMS depth profile analysis through the surface layers and into the underlying matrix showed a rapidly changing light element content over the first 3μm, before the stable matrix composition was reached. The spectra shown in Figure 4.6.3, indicates that the surface layers contain increased levels of oxygen, hydrogen, carbon and nitrogen. The nitrogen signal in the form of the C-N group is noticeably higher than that of the Fe-N group to a depth of 4μm.

4.6.3. Wear pin 817M40 Steel.

Areas of oxide, white-layer and matrix identified on the metallographically-prepared taper section previously analysed by light element EPMA, were analysed by SIMS for comparison. Figure 4.6.4, illustrates the compositional profile to a depth of over 5μm for each area analysed. The matrix composition is similar to that obtained from other 817M40 samples analysed. The oxide and white-layer areas both exhibit increased levels of oxygen and nitrogen compared to the matrix, and the carbon level of the white-layer is reduced in comparison to the matrix.

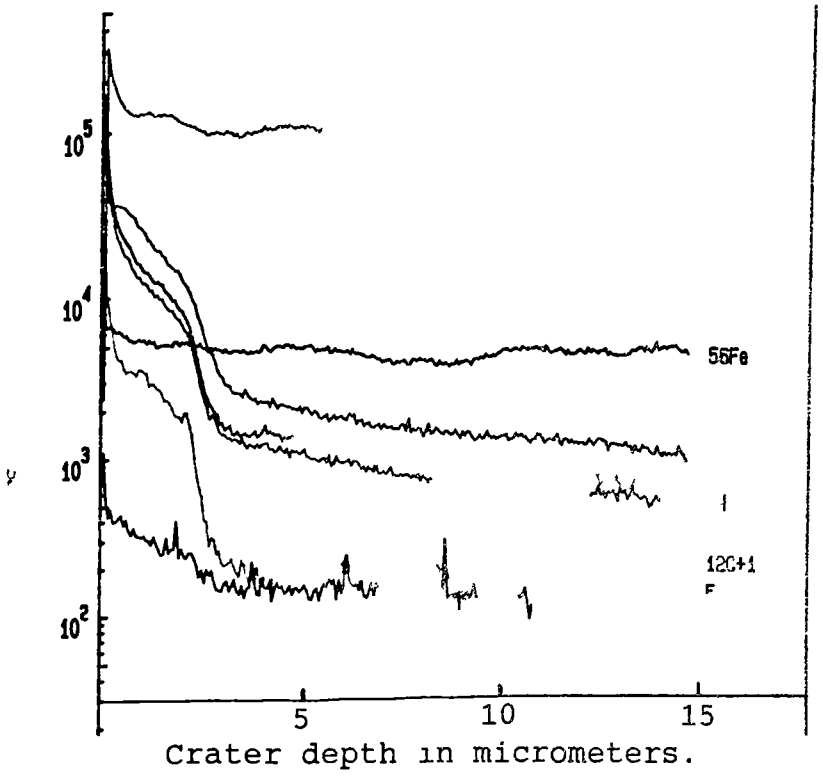

Figure 4.6.3. Abusively turned 817M40. SIMS depth profile through the white-layer, illustrating the relative increase in hydrogen, nitrogen and oxygen within the surface layers.

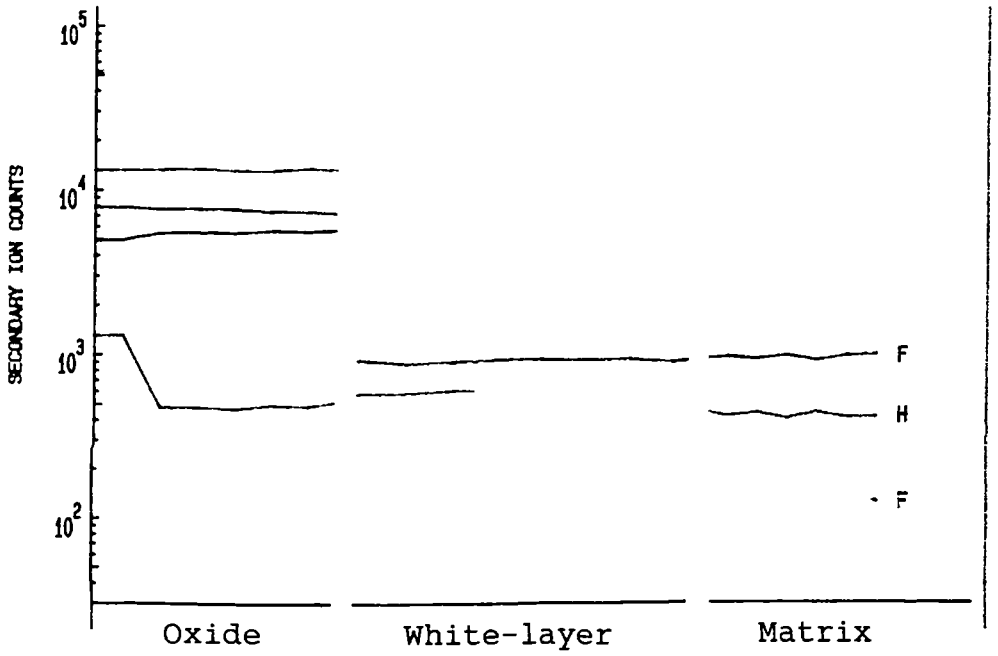

Figure 4.6.4. Wear pin 817M40. SIMS spectra from the white-layer, oxide phase and matrix showing the relative differences in oxygen and nitrogen content.

4.6.4. Chieftain tank gun barrel.

SIMS spectra acquired from a site on the internal bore close to a crack, indicates that the surface contained increased levels of oxygen, carbon, hydrogen and nitrogen to a depth of 10μm. (Figure 4.6.5). The enhanced signal for iron is attributed to the effect of the higher oxygen level on sputter rates. Below this outer layer, the high level of nitrogen persisted to a depth of 50μm.

4.6.5. Rarden gun barrel.

Increased levels of carbon, nitrogen, hydrogen and oxygen are shown to extend to a depth of 10μm in this specimen (Figure 4.6.6).

The relatively high yield for light elements over the first 1μm are attributed to surface contamination contained within the many small cracks and fissures which decorated the specimen surface. Below this region, the spectra show increased signals for oxygen, carbon, hydrogen and nitrogen to a depth of 10μm.

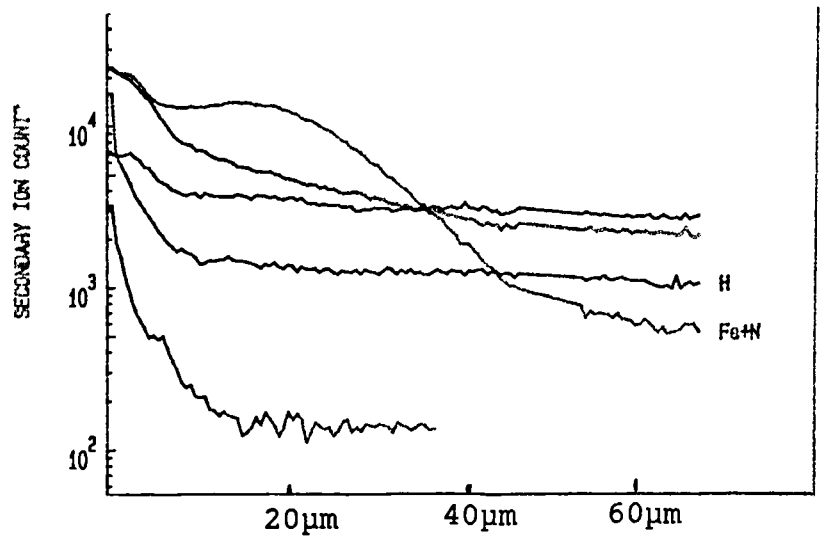

Figure 4.6.5. Chieftain gun barrel. SIMS depth profile showing increased levels of hydrogen, carbon, nitrogen and oxygen at the bore surface, to a depth of over 30μm.

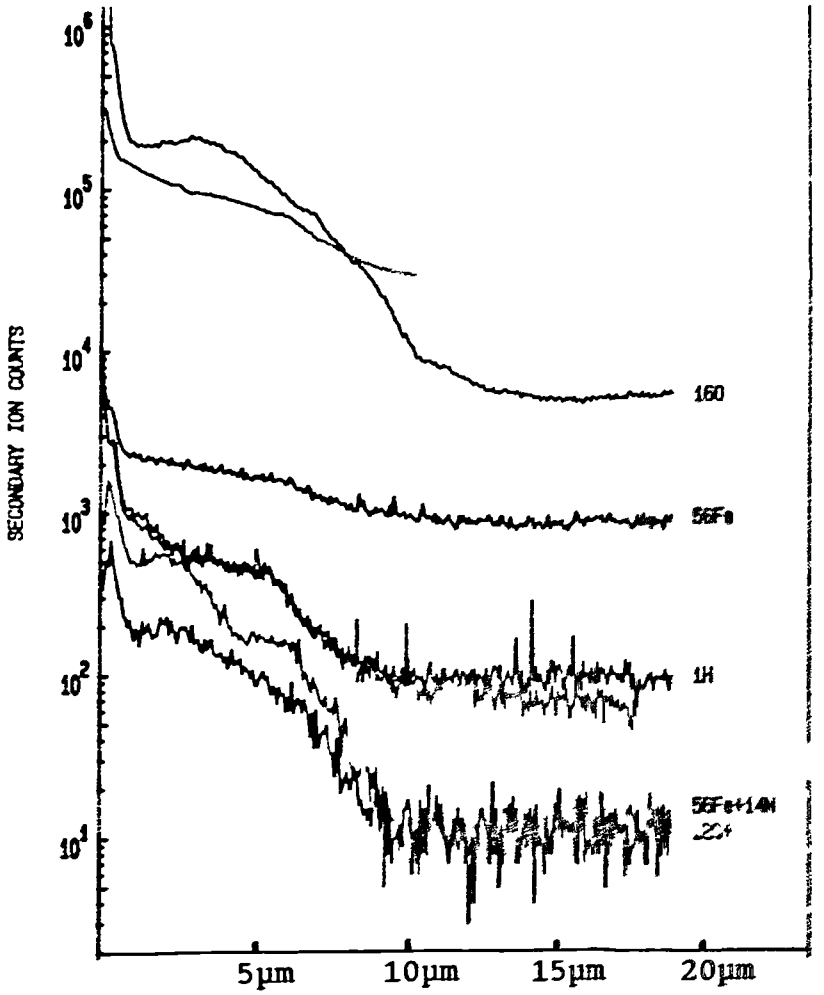

Figure 4.6.6. RARDEN gun barrel. SIMS depth profile through the bore surface showing increased levels of hydrogen, oxygen, carbon and nitrogen to a depth of 10μm.

4.7. Transmission Electron Microscopy.

4.7.1. Laser Treated 817M40 Steel.

The microstructure of the 817M40 steel used for the laser heat-treatment experiments, was found to be consistent with that of a tempered martensitic alloy steel. A typical area is shown in Figure 4.7.1, in which large elongated carbide particles have formed within the grains and along grain boundaries. Smaller carbides have precipitated as rod like features within the grains. Selected area diffraction from the centre of the field of view shown in Figure 4.7.1, identified the presence of M_3C carbides in an acicular ferrite matrix. The orientation relationship between the carbides and the matrix derived from the diffraction pattern is :

$$[413]\alpha \parallel [120]\ M_3C$$
$$(222)\alpha \parallel (212)\ M_3C$$

Deep within the laser-treatment transformation zone, the structure had been modified to a fine grain, heavily twinned martensite containing relatively few large carbide particles. Numerous fine particles of M_7C_3 carbide have precipitated out on dislocations and at twin boundaries on cooling (Figure 4.7.2). The diffraction pattern acquired from the large grain at the centre of the field of view, was indexed as a tetragonal crystal with a c/a ratio of 1.05 (± .03) . Grain sizes in this zone were found to range from 800nm to over 2000nm in diameter.

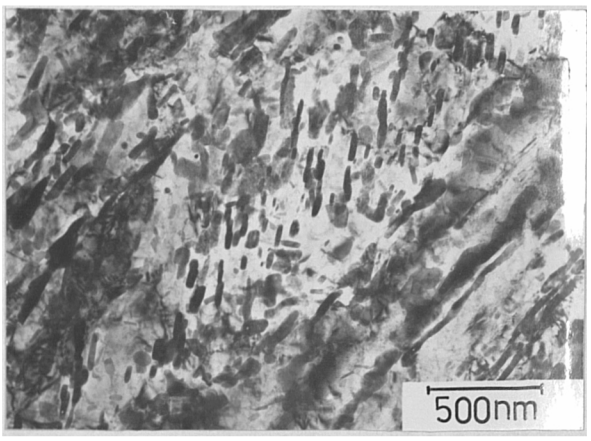

a)

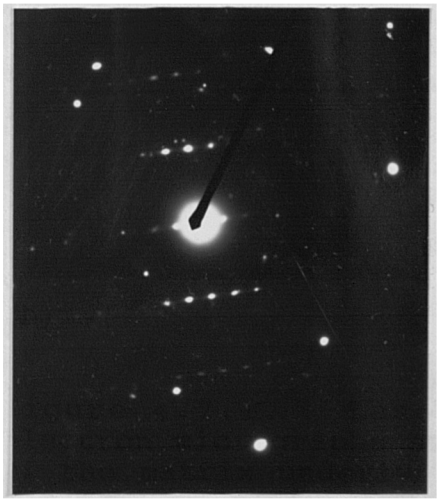

b)

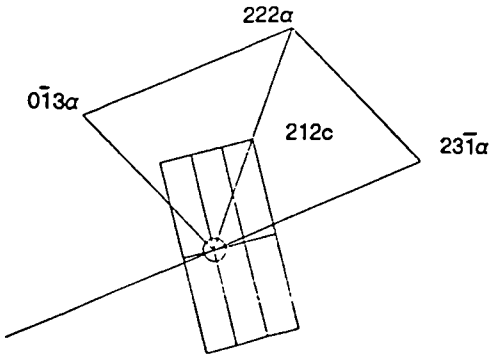

[4$\bar{1}$3]α ‖ [1$\bar{2}$0] M_3C

c)

Figure 4.7.1. Laser treated 817M40. Transmission electron micrographs showing; a) The tempered martensite of the matrix underlying the laser treated zone, b) The selected area electron diffraction pattern, c) The schematic solution of the diffraction pattern, from which was derived a value of c/a of 0.98 ± 0.03 for the matrix, and the orientation relationship:

[4$\bar{1}$3]α ‖ [1$\bar{2}$0] M_3C and (222)α ‖ (212) M_3C.

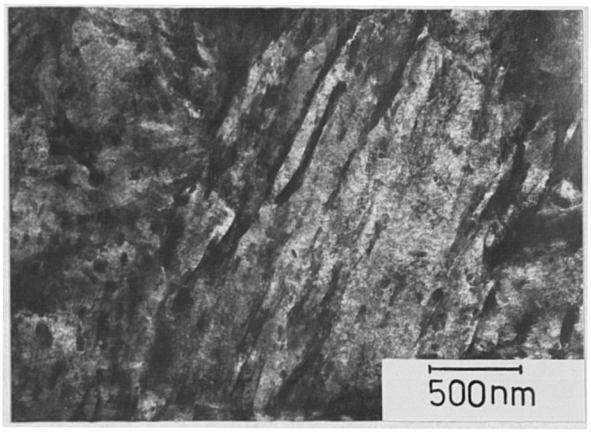

a)

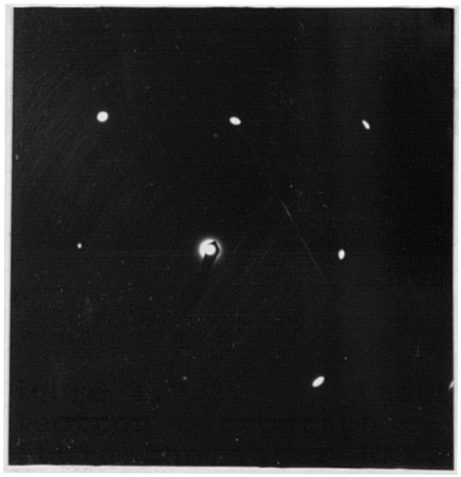

b)

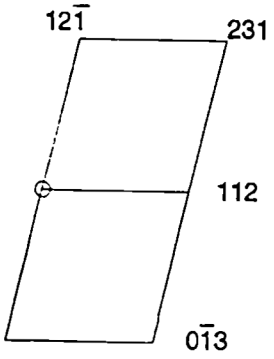

c) Martensite [5$\bar{3}\bar{1}$]

Figure 4.7.2. Laser treated 817M40. a) Transmission electron micrograph of the region of maximum hardness within the laser HAZ. b) Selected area diffraction pattern, c) Solution of the diffraction pattern giving c/a for the matrix of 1.05 ± 0.03.

Closer to the surface, where the thermal cycle was not so abrupt, the material had been tempered through a range of temperatures to produce fine acicular ferrite grains containing rod like precipitates and outlined by cementite (Figure 4.7.3). Where higher temperatures had been sustained for a longer period, the ferrite grains had become equiaxed and the carbide particles increased in size (Figure 4.7.4).

4.7.2. Laser treated 080M40 Steel.

The unmodified microstructure of this dual phase steel comprises a mixture of grains containing pearlite colonies and grains of ferrite. Figure 4.7.5 shows a typical region at a pearlite - ferrite boundary in bright field contrast.

Within the laser treated zone, several forms of modified pearlite are observed, representative of the different thermal conditions experienced. Close to the boundary with the underlying matrix, the pearlite appears fragmented and spheroidised (Figure 4.7.6). Adjacent ferrite grains exhibit a high density of tangled dislocations.

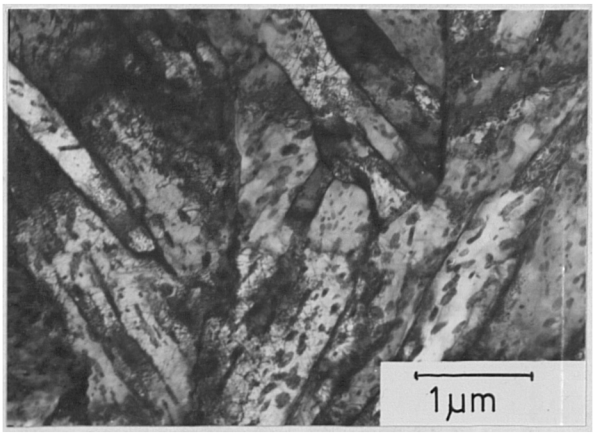

a)

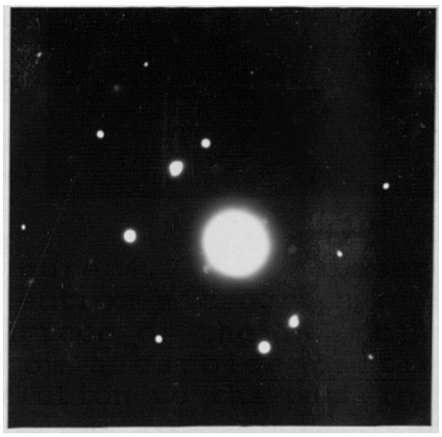

b)

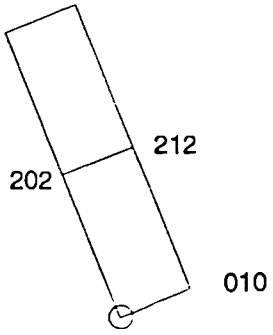

c) M_3C [$\bar{1}$01]

Figure 4.7.3. Laser treated 817M40. a) Transmission electron micrograph of the tempered region close to the surface of the HAZ. b) Selected area diffraction pattern from a carbide particle within a ferrite grain, c) Solution to the pattern, indexed as M_3C.

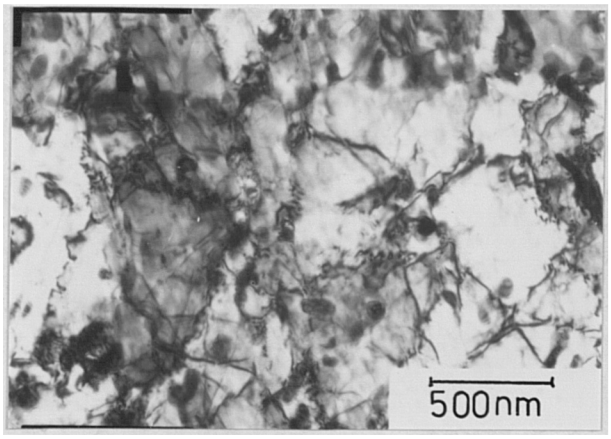

a)

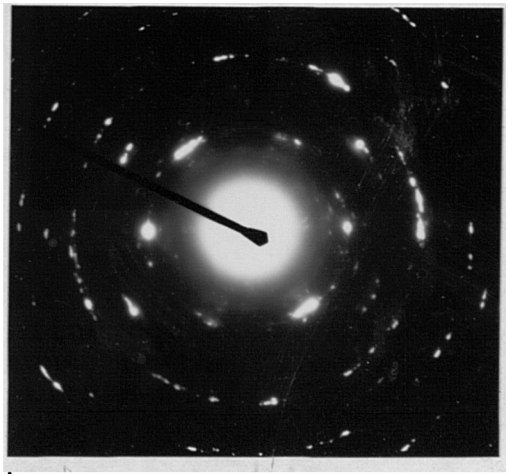

b)

Figure 4.7.4. Laser treated 817M40. Close to the surface of the HAZ showing a) a fine equiaxed structure containing a network of dislocations, b) the selected area ring pattern, indexed as ferrite with M_3C.

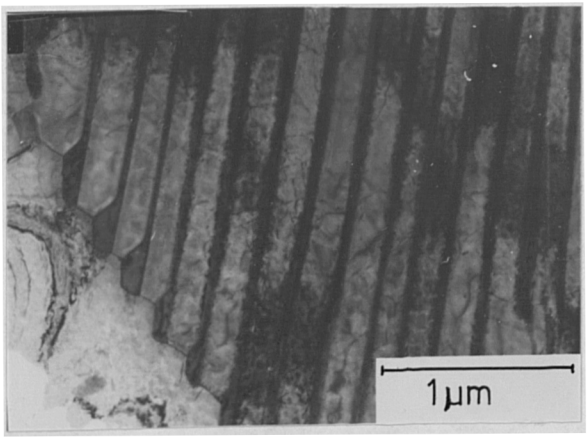

Figure 4.7.5. Laser treated 080M40. Transmission electron micrograph of the underlying matrix showing a ferrite - pearlite boundary .

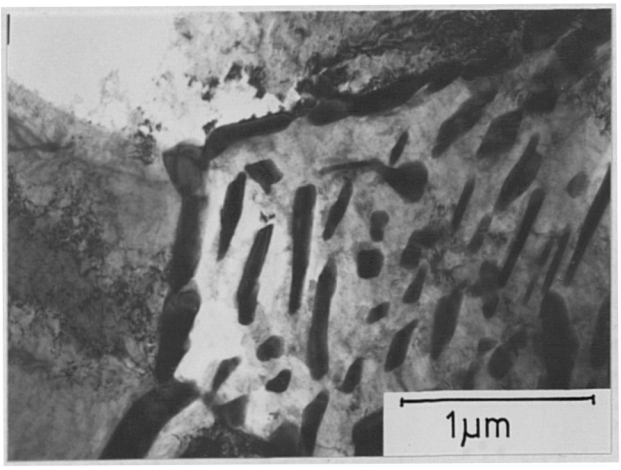

Figure 4.7.6. Laser treated 080M40. Transmission electron micrograph showing a region of partially spheroidised pearlite.

Where higher temperatures had been experienced, a lath structure had developed; based on the pearlite lamellae. Diffraction from one of the laths indicates the presence of Fe_3C and ferrite with an orientation relationship described by :

$$[001]\alpha \parallel [011]\ M_3C,$$
$$(110)\alpha \parallel (011)\ M_3C.$$

as shown in Figure 4.7.7. The ferrite grains in this region exhibit a "blocky" structure associated with a dislocation network (Figure 4.7.8).

Where the temperature cycle was more abrupt, the pearlite grains had transformed without change of shape to an electron dense phase containing a regular array of fine dislocations. (Figure 4.7.9). The associated diffraction pattern was indexed as a bcc structure with a lattice parameter of 0.284nm; slightly less than that quoted for ferrite (0.28664nm).

In the region close to the surface of the sample where the highest temperatures would have been attained, a martensitic structure had formed on cooling. This contained areas of large internally twinned grains,(Figure 4.7.10). and an acicular product containing precipitates of cementite (Figure 4.7.11).

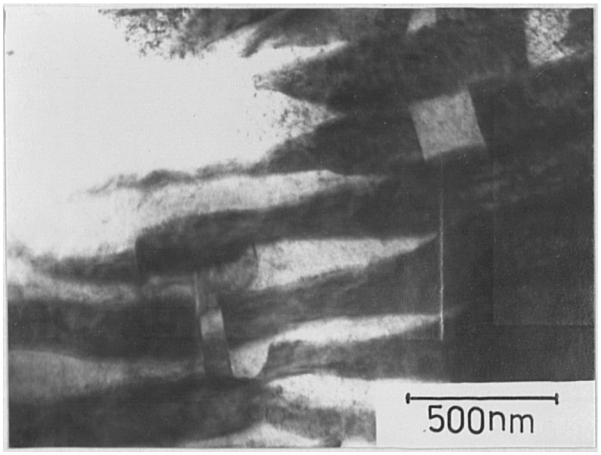

a)

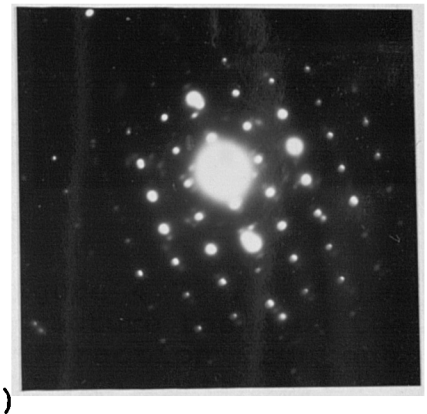

b)

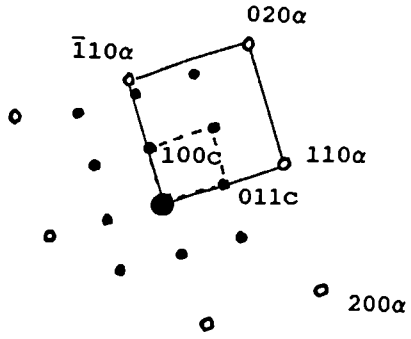

c) [001]α, [0$\bar{1}$1] M_3C

Figure 4.7.7. Laser treated 080M40. a) Ferrite lath structure based on the pearlite lamellae. b) Selected area diffraction from one of the laths, c) Solution of the pattern, with an orientation relationship of :

[001]α ∥ [0$\bar{1}$1] M_3C and (110)α ∥ (011) M_3C.

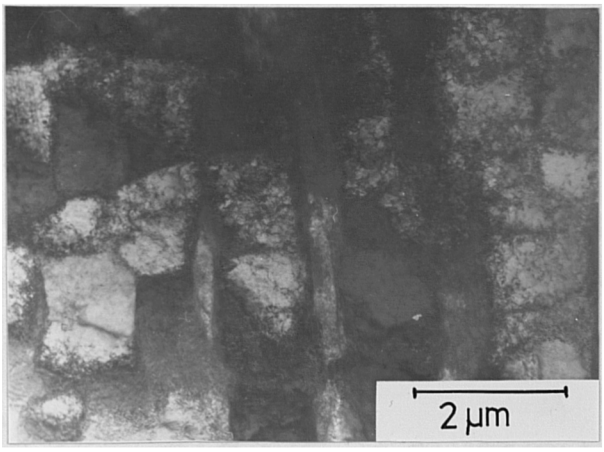

Figure 4.7.8. Laser treated 080M40. Dislocation networks observed in the ferrite grains.

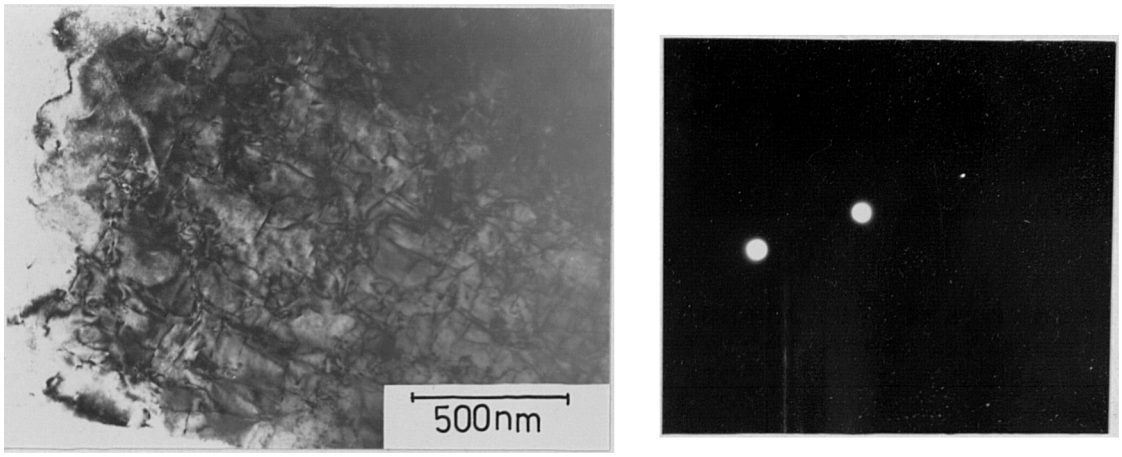

a) b)

Figure 4.7.9. Laser treated 080M40. a) Transformed pearlite in the laser HAZ. b) Selected area diffraction pattern indexed as martensite on [410] with a = 0.284 nm.

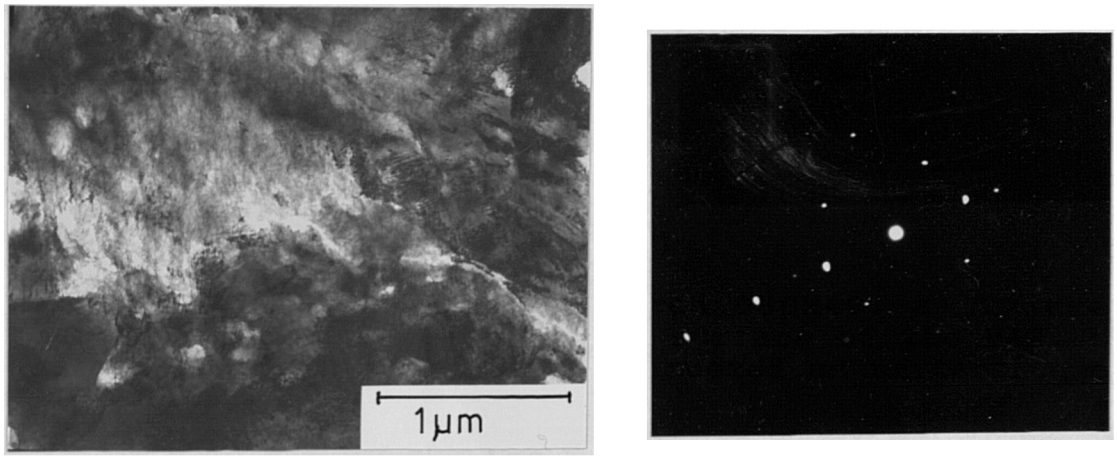

a) b)

Figure 4.7.10. Laser treated 080M40. a) Twinned martensite grains close to the surface of the HAZ. b) Associated diffraction pattern indexed as martensite on [101] with a c/a = 1.03 ± .03.

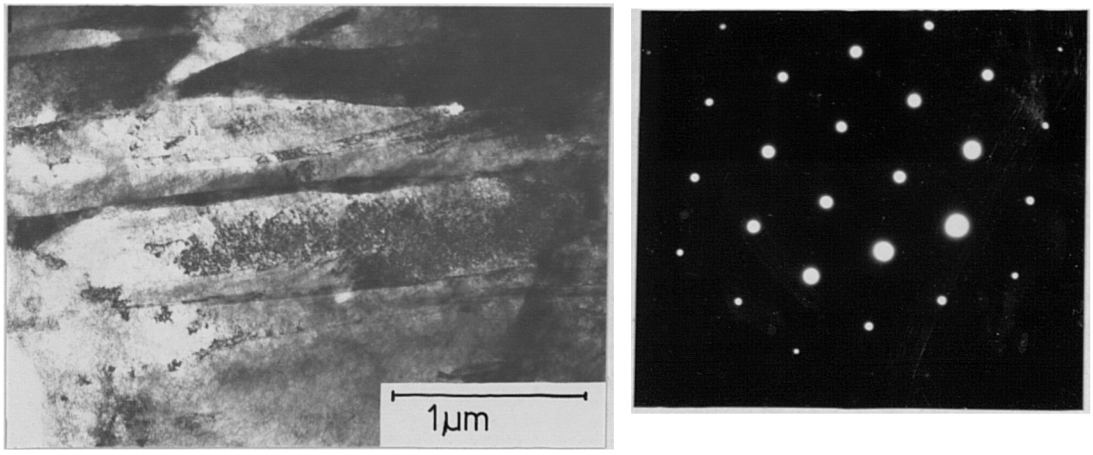

a) b)

Figure 4.7.11. Laser treated 080M40. a) Region showing lath - ferrite at the HAZ surface. b) Associated electron diffraction pattern indexed as ferrite on [111].

4.7.3. Abusively turned 817M40 Steel.

A typical area of untreated matrix of this material, shown in Figure 4.7.12, exhibits a distribution of mixed carbides in a matrix of ferrite which retains the morphology of the martensite produced on quenching. The centred dark field image (Figure 4.7.13) is formed from reflections indexed as M_3C and M_7C_3. With the orientation relationship :

$$[111]\alpha \parallel [120]\ M_3C,$$

$$(101)\alpha \parallel (411)\ M_3C.$$

The micrograph Figure 4.7.14, shows an area close to the turned surface where the carbides have become fragmented and the lath morphology of the matrix disrupted by plastic deformation. An area identified as white-layer, shown in Figure 4.7.15, exhibits a dispersion of spheroidised carbides in a heavily dislocated fine grain material. The associated ring diffraction pattern from this area was indexed as ferrite with dispersed M_3C and M_7C_3 carbides. At higher magnification, Figure 4.7.16 shows the white-layer to be comprised of fine equiaxed grains with an average diameter of less than 200 nm, containing dislocations and a fine twinned structure.

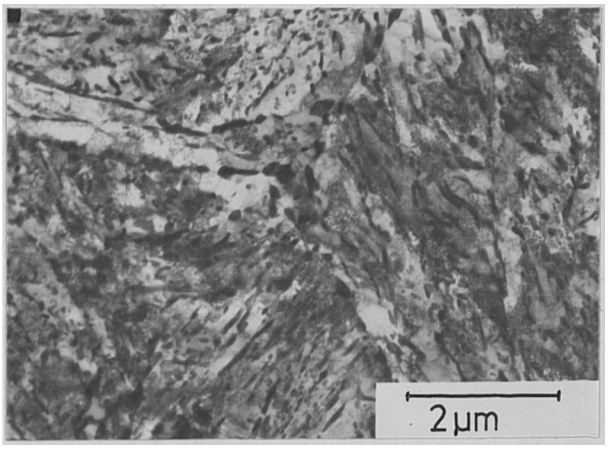

Figure 4.7.12. Abusively turned 817M40 . Underlying tempered martensite matrix.

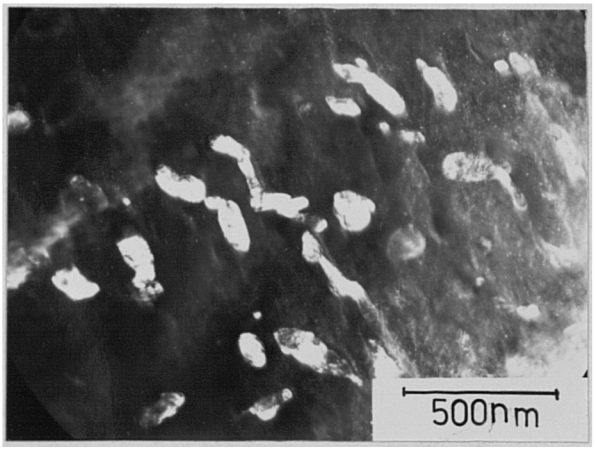

a)

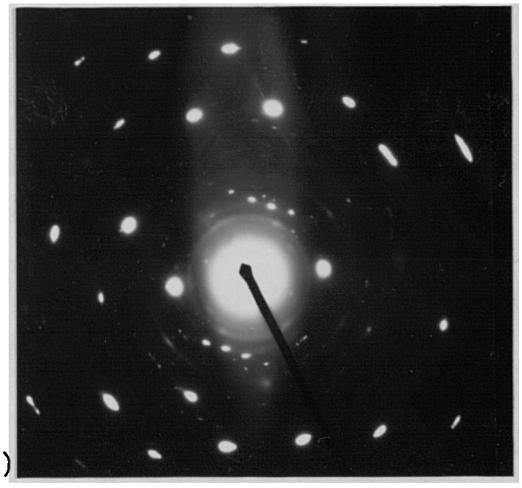

b)

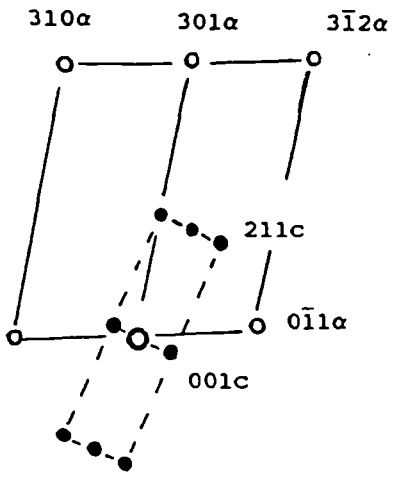

c)

Figure 4.7.13. Abusively turned 817M40. a) Centred dark field image from the (210) and (211) cementite reflections. b) Associated selected area diffraction pattern, c) solution to the pattern yielding the relationship:

$[1\bar{3}\bar{3}]\alpha \parallel [1\bar{2}0]\ M_3C$ and $(3\bar{1}2)\alpha \parallel (211)M_3C$.

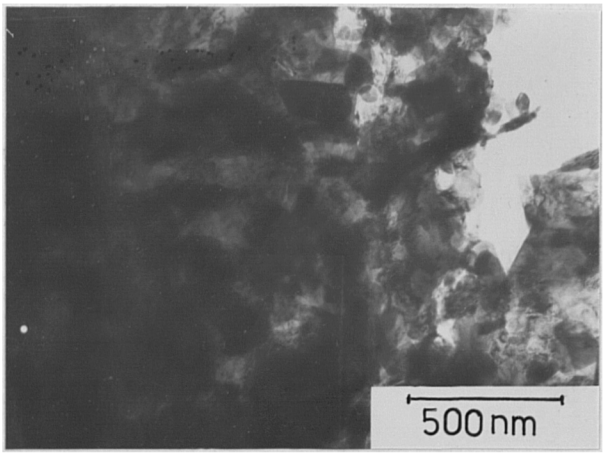

Figure 4.7.14. Abusively turned 817M40. Transmission electron micrograph of a plastically-deformed region.

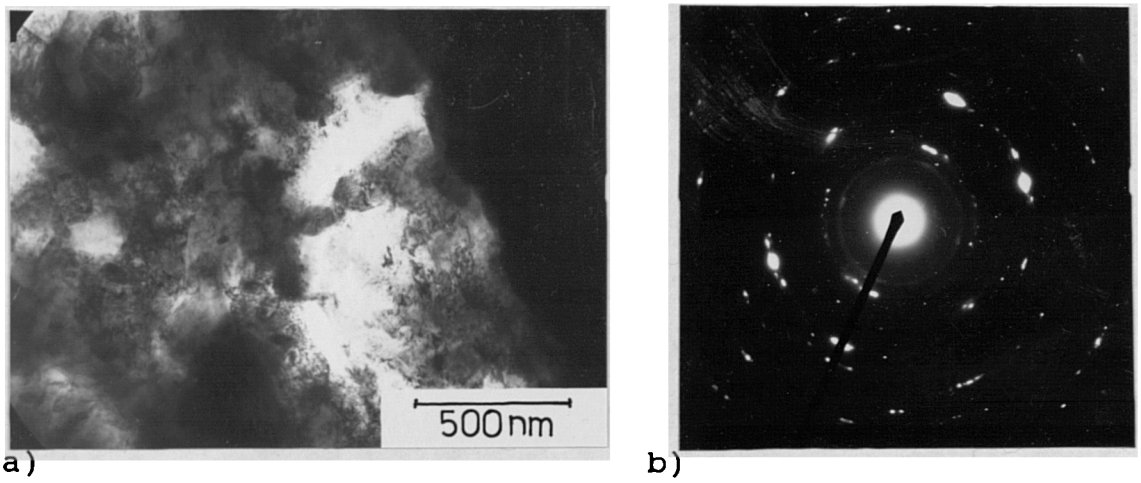

a) b)

Figure 4.7.15. Abusively turned 817M40. a) Micrograph of a thin foil prepared from the white-layer showing a dislocated fine grain product. b) Associated diffraction pattern, indexed as ferrite, containing M_3C and M_7C_3.

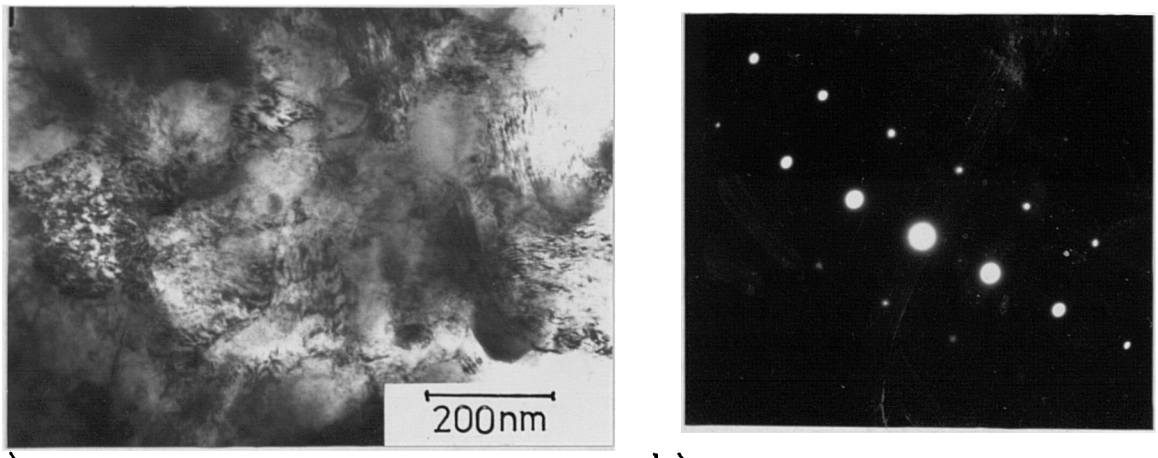

a) b)

Figure 4.7.16. Abusively turned 817M40. a) White-layer structure containing small equiaxed, twinned grains. b) Associated diffraction pattern indexed as α on [100].

4.7.4. Wear Pin 817M40 Steel.

The matrix of this specimen remote from the worn surface, appeared quite dissimilar from previous samples of 817M40 steel and exhibited a martensitic structure containing retained austenite at the interlath boundaries. (Figure 4.7.17). The centred dark field image from the $(11\bar{1})\gamma$ reflection also includes reflections for M_3C, giving rise to bright regions at the interlath boundary. The orientation relationship between the ferrite the austenite and the carbide is described by :

$$[\bar{1}2\bar{1}]\alpha \parallel [011]\gamma \parallel [01\bar{1}]\ M_3C,$$
$$(222)\alpha \parallel (200)\gamma \parallel (111)\ M_3C.$$

Close to the wear surface, the lath morphology of the matrix becomes less distinct and individual grains exhibit a greater density of dislocations (Figure 4.7.18). The interlath boundaries do not appear to contain austenite, which would be expected to transform to martensite as a consequence of the stresses associated with plastic-deformation.

The white-layer developed on the wear pin was of variable appearance with some areas exhibiting a dispersion of carbide and oxide particles within a disordered matrix (Figure 4.7.19); whilst adjacent areas appeared as a fine grained material containing a dispersion of M_3C and M_7C_3 carbide particles, (Figure 4.7.20).

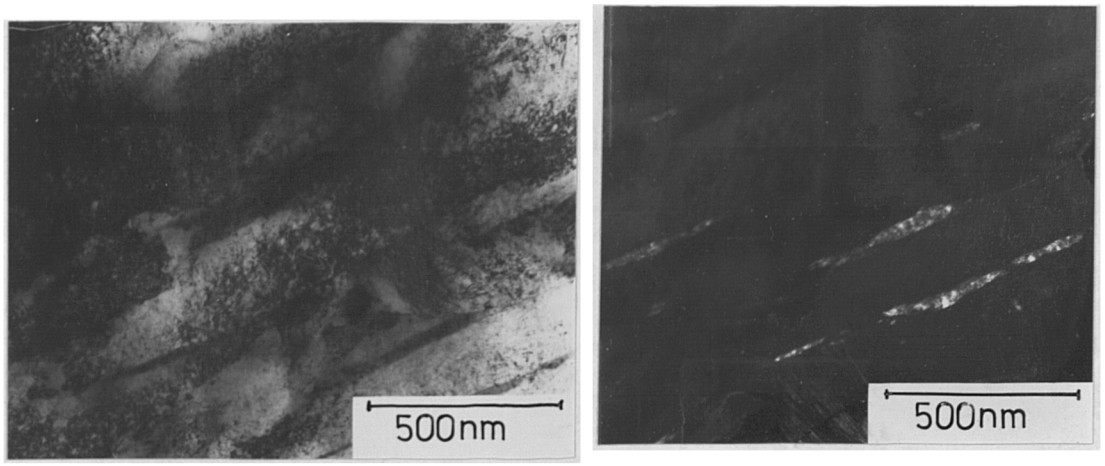

a) b)

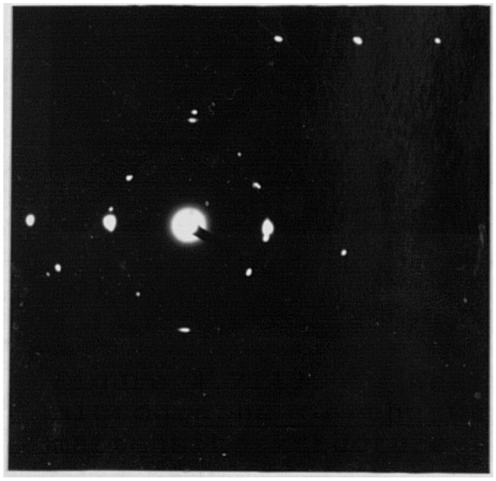

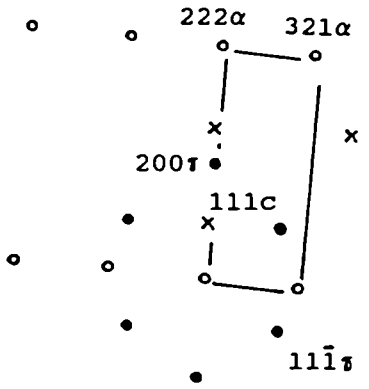

c) d)

Figure 4.7.17. Wear pin 817M40. Transmission electron micrographs of the wear pin matrix showing; a) A lath martensite structure with retained austenite and M_3C at the interlath boundaries. b) The centred dark field image from the (11$\bar{1}$) γ reflection, c) The selected area diffraction pattern from the area, d) The solution of the pattern showing :

$[\bar{1}2\bar{1}]\alpha \parallel [011]\gamma \parallel [01\bar{1}]c$ and $(222)\alpha \parallel (200)\gamma \parallel (111)c$.

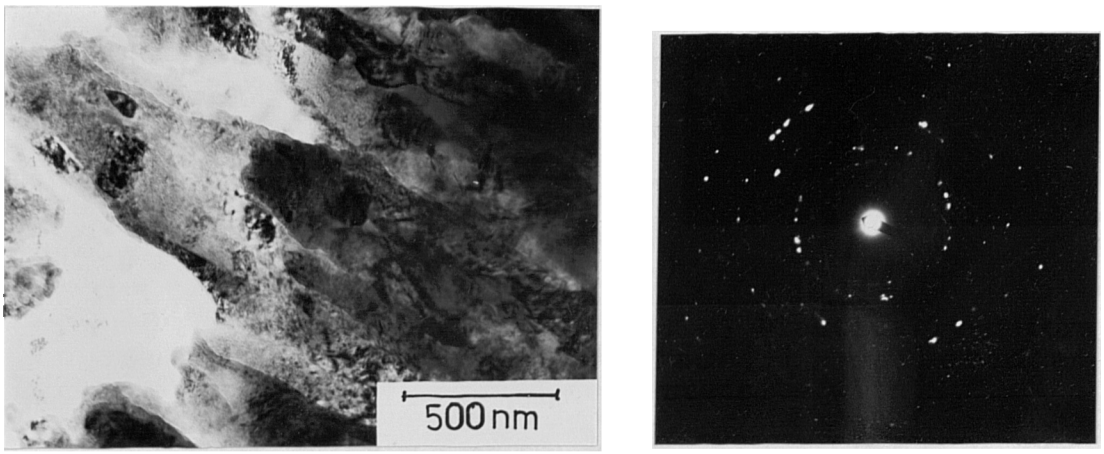

a) b)

Figure 4.7.18. Wear pin 817M40. a) Plastically-deformed region close to the wear surface, b) selected area diffraction pattern indexed as martensite with M_3C.

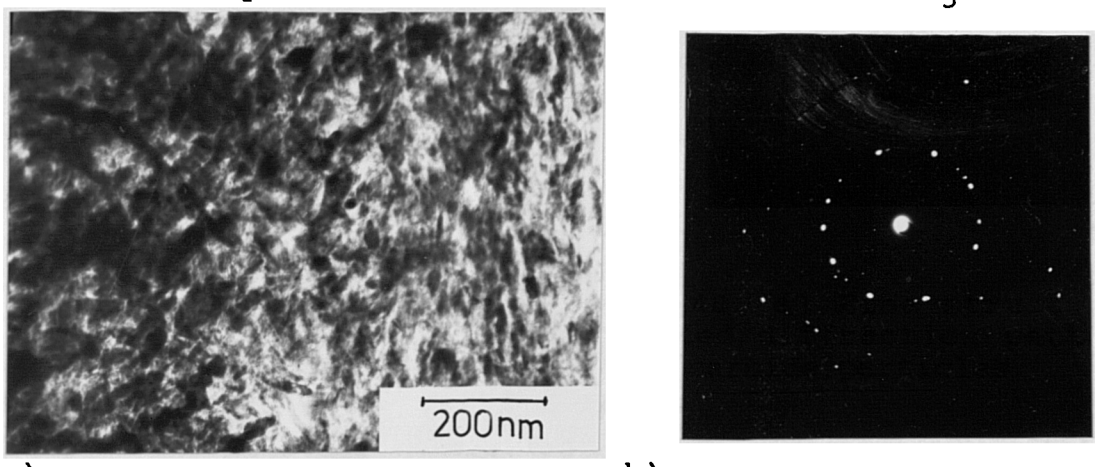

a) b)

Figure 4.7.19. Wear pin 817M40. a) Fine structured white-etching layer, b) associated diffraction pattern indexed as ferrite with oxide and carbide particles.

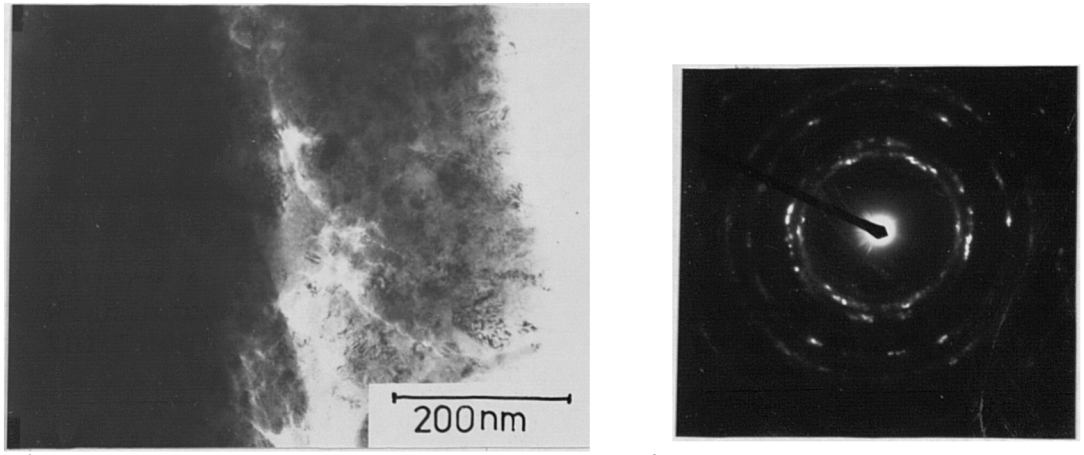

a) b)

Figure 4.7.20. Wear pin 817M40. a) White-layer at the wear surface , b) Selected area electron diffraction from this region, indexed as ferrite with M_3C and M_7C_3.

4.7.5. Digger Tooth.

The matrix of this steel consisted of tetragonal martensite laths containing a dispersion of M_3C and M_7C_3 carbide particles. Figure 4.7.21 shows a typical area in which bands of rod-shaped carbides have formed within the martensite grains and at interlath boundaries. Finer carbides have precipitated out within the grains on the internally twinned structure. The orientation relationship of these particles could not be determined from the patterns recorded.

At the worn surface, areas of plastically-deformed material exhibit a structure which has become aligned in the direction of wear. Figure 4.7.22 shows a region parallel to the wear direction with a layered appearance in which lines of fine carbides are distributed in a fine grain matrix, giving rise to a "spotty" ring pattern. Isolated areas of white-layer were identified in which the carbide distribution did not appear to be oriented in any preferred direction. The bright and dark field images shown in figure 4.7.23, illustrate such a region in which very fine M_3C and M_7C_3 carbides are distributed within a matrix of small equiaxed grains of martensite.

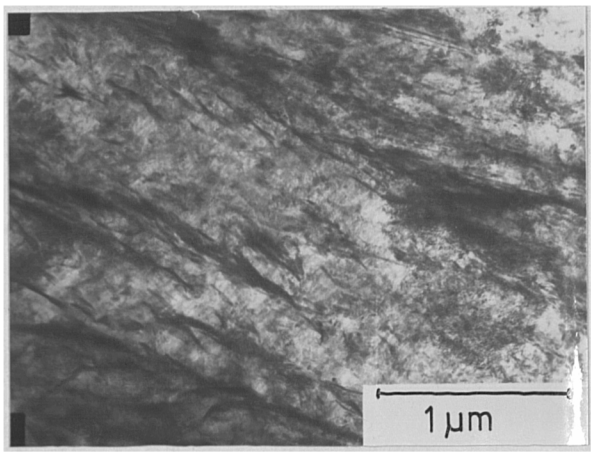

a)

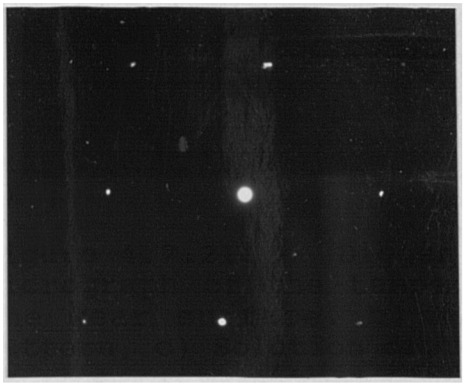

b)

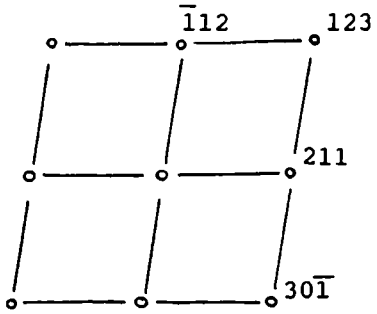

c) Martensite $[\bar{1}5\bar{3}]$

Figure 4.7.21. Digger tooth. a) Transmission electron micrograph of the tempered martensite matrix underlying the wear surface. b) Associated electron diffraction pattern, c) Solution of the pattern identifying the matrix as martensite with c/a of 1.07 ± .03.

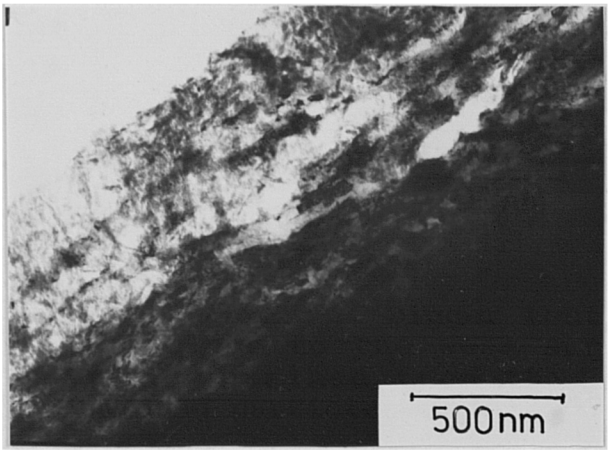

a)

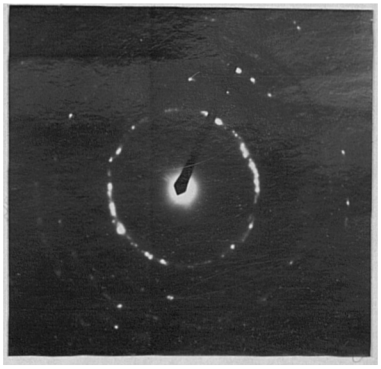

b)

Figure 4.7.22. Digger tooth. a) Plastically-deformed region close to the wear surface, b) Ring diffraction pattern obtained from this area indexed as ferrite containing particles of M_3C carbide.

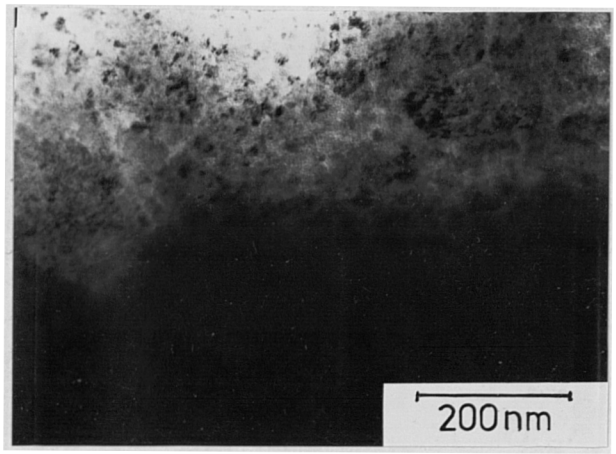

a)

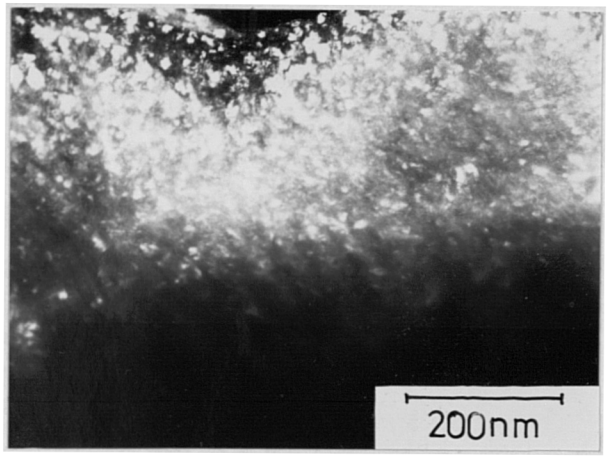

b)

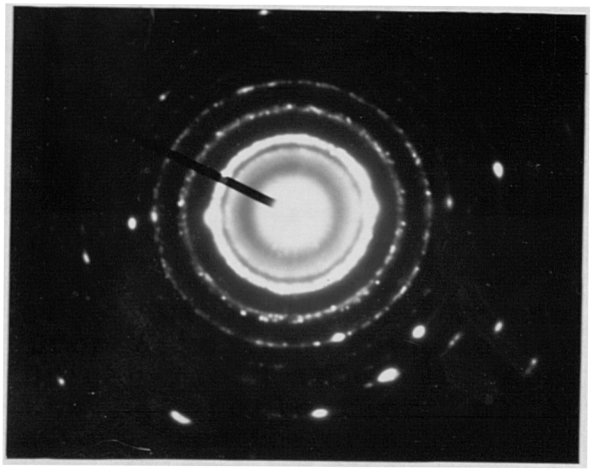

c)

Figure 4.7.23. Digger tooth. Transmission electron micrographs from a region of white-layer at the wear surface. a) Bright field image, b) Centred dark field image from the M_3C reflection. c) Associated ring diffraction pattern from the area.

4.7.6. Chieftain Tank Gun Barrel.

The change in structure resulting from conditions experienced during firing, is shown in Figure 4.7.24, recorded from the boundary between the underlying matrix and the HAZ . At higher magnification (Figure 4.7.25) the lath-like martensite grains of the matrix are seen to contain a regular network of dislocations. Large elongated M_3C particles have formed at the interlath boundaries on tempering and relatively few carbides have precipitated within the martensite grains. Diffraction analysis indicated that the c/a ratio for the tempered martensite was approximately 1.03 (± .03).

Within the heat affected zone, the martensite grains appear less elongated and contain a high density of dislocations and small M_3C and M_7C_3 carbide particles, (Figure 4.7.26). Selected area diffraction indicated that the c/a ratio for the martensite was approximately 1.05 (±.03). Closer to the bore surface, the structure is more complex, with large grains containing narrow lenticular twin features. A fine even distribution of carbide particles is visible within the grains. The associated diffraction pattern for the area was interpreted as showing M_3C and M_7C_3 carbide particles in martensite with a c/a ratio of 1.08(±.03). See figure 4.7.27. The orientation relationship determined from this pattern is described by :

$$[133]\alpha \parallel [121]\ M_3C,$$

$$(011)\alpha \parallel (210)\ M_3C.$$

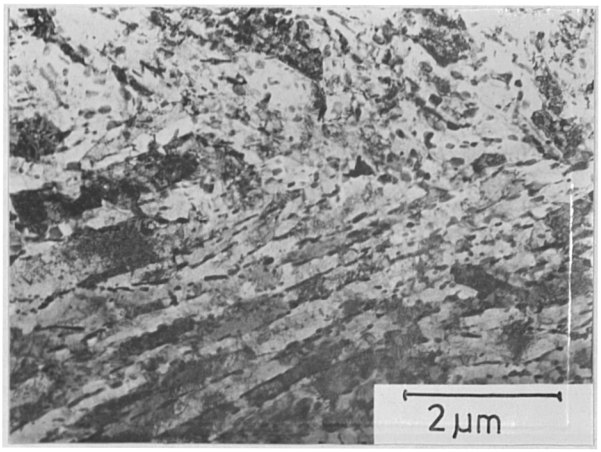

Figure 4.7.24. Chieftain gun barrel. Transmission electron micrograph showing the boundary between the thick white-etching layer and the underlying matrix.

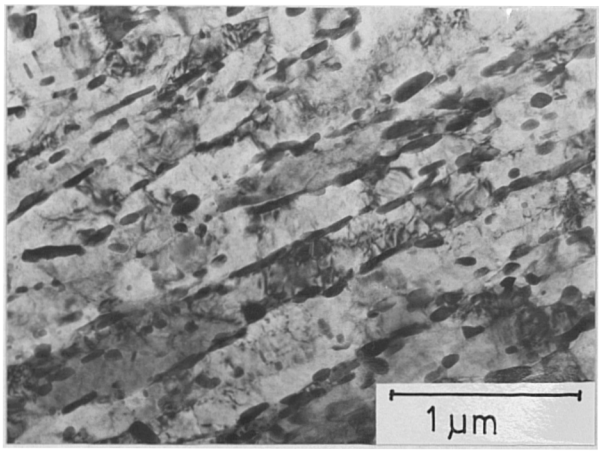

a)

c)

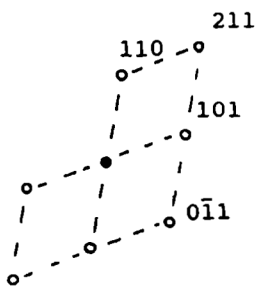

d) Martensite [1$\bar{1}\bar{1}$]

Figure 4.7.25. Chieftain gun barrel. a) Detail of underlying tempered martensite matrix, b) Selected area diffraction from the area, c) Solution of the pattern as martensite with a c/a ratio of 1.03 ± 0.03.

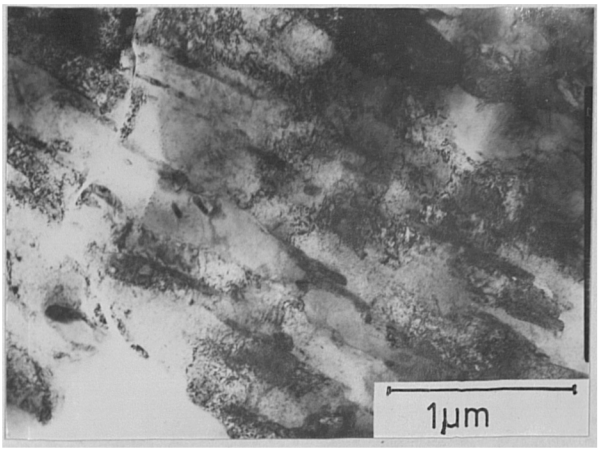

a)

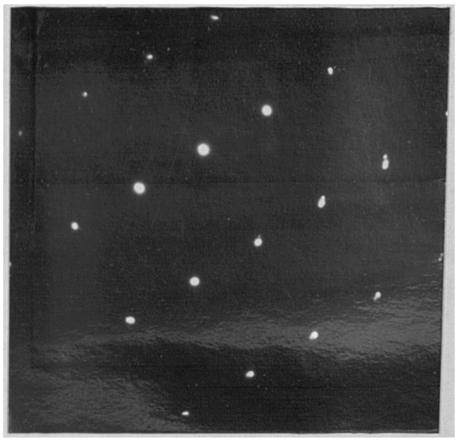

b)

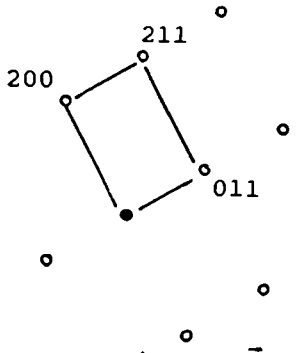

c) Martensite [0$\bar{2}$2]

Figure 4.7.26. Chieftain gun barrel. a) Transmission electron micrograph of the thick white-etching HAZ, showing a lath martensite structure, b) selected area diffraction pattern from one of the grains, c) solution of the pattern as martensite with a c/a ratio of 1.05 ± 0.03.

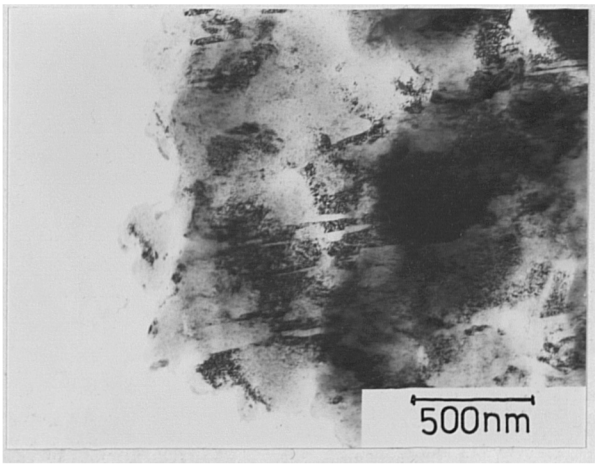

a)

b)

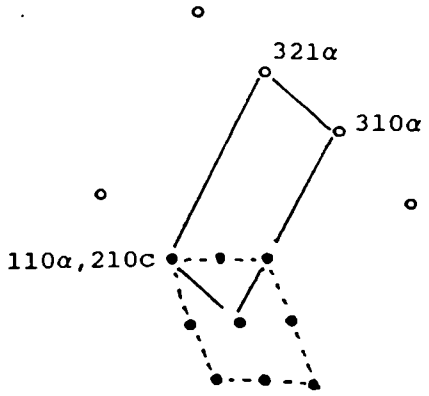

c) Martensite $[\bar{1}3\bar{3}]$, M_3C $[1\bar{2}1]$

Figure 4.7.27. Chieftain gun barrel. Transmission electron micrograph of the white-etching HAZ close to the bore surface. a) twinned martensite structure, b) associated selected area electron diffraction pattern, c) solution of the pattern as martensite with a c/a ratio of 1.08 ± 0.03 and M_3C with the orientation relationship:

$[\bar{1}3\bar{3}]\alpha \parallel [1\bar{2}1]$ M_3C and $(011)\alpha \parallel (210)$ M_3C.

4.7.7. RARDEN Gun Barrel.

The tempered martensite matrix of this steel, shown in Figure 4.7.28. consists of acicular ferrite grains with arrays of elongated M_3C carbides which have precipitated at preferred orientations within the grains and at inter-lath boundaries. The orientation relationship determined from the associated diffraction pattern shows :

$$[\bar{1}3\bar{2}]\alpha \parallel [\bar{1}20]\ M_3C,$$

$$(\bar{1}12)\alpha \parallel (001)\ M_3C.$$

Smaller carbide particles were observed in association with tangles of dislocations.

Figure 4.7.29, shows an ion beam etched foil taken from the thick white-etching layer close to the bore surface of the barrel. The structure in this zone had been modified by the thermal cycling experienced under test firing, to produce a fine grain material containing a distribution of small M_3C and M_7C_3 carbide particles.

The thin surface white-layer identified previously by SEM and light microscopy, appeared in the TEM as a distinct band of homogeneous material composed of small equiaxed grains with no visible internal structure. Diffraction from this area suggested that this layer was primarily composed of M_3C carbides in an austenitic matrix. See Figure 4.7.30 from which the following orientation relationship was derived :

$$[1\bar{1}0]\gamma \parallel [3\bar{2}\bar{2}]\ M_3C,$$

$$(11\bar{1})\gamma \parallel (01\bar{1})\ M_3C.$$

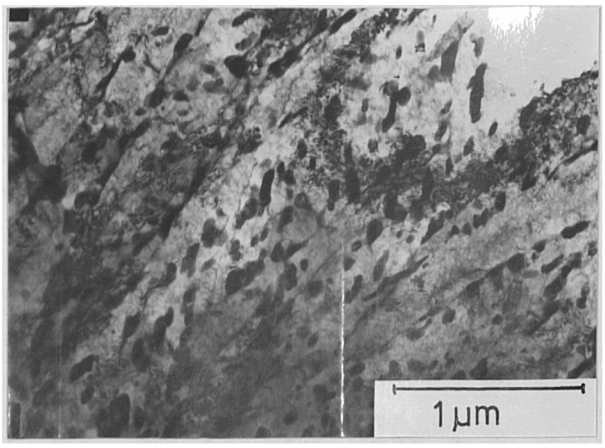

a)

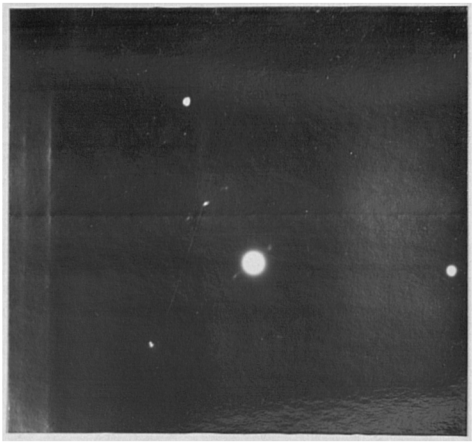

b)

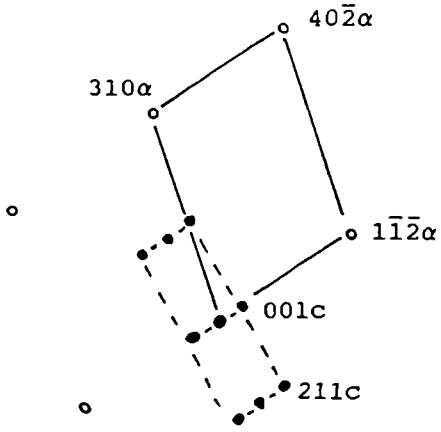

c) Ferrite [$\bar{1}3\bar{2}$]

Figure 4.7.28. RARDEN gun barrel. a) Transmission electron micrograph showing the tempered martensite structure of the matrix. b) the selected area electron diffraction pattern from one of the grains, c) the solution to the pattern identifying the material as lath ferrite containing M_3C carbides with the orientation relationship :

$$[\bar{1}3\bar{2}]\alpha \parallel [\bar{1}20]\ M_3C \text{ and } (\bar{1}12)\alpha \parallel (001)\ M_3C.$$

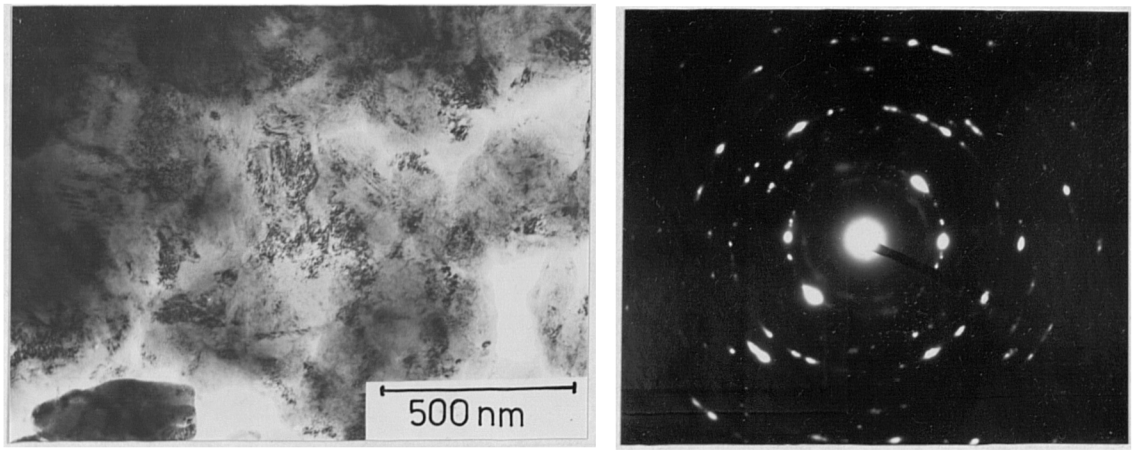

a) b)

Figure 4.7.29. RARDEN gun barrel. a) White-etching layer close to the bore surface. b) associated diffraction pattern indexed as ferrite with M_3C and M_3C_7.

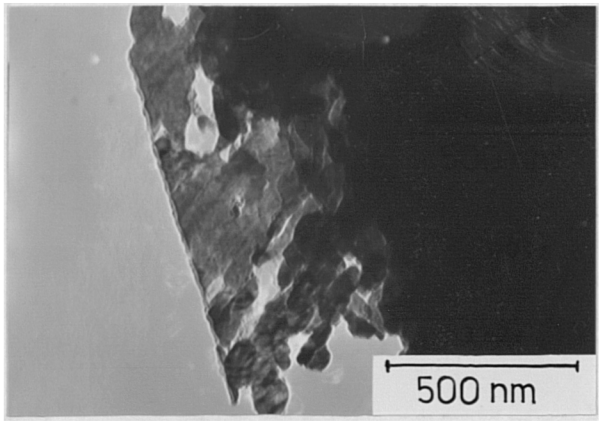

a)

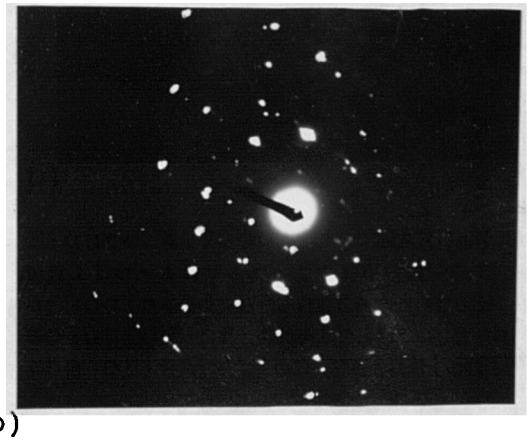

b)

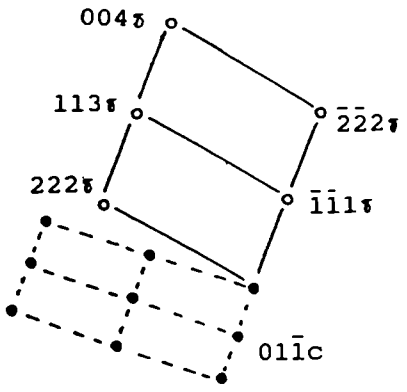

c) Austenite $[1\bar{1}0]$, M_3C $[3\bar{2}\bar{2}]$

Figure 4.7.30. RARDEN gun barrel. a) Fine grained thin white-layer formed at the surface of the bore, b) associated selected area electron diffraction pattern, c) solution of the pattern as austenite containing M_3C, with the orientation relationship:

$[1\bar{1}0]\ \gamma \parallel [3\bar{2}\bar{2}]\ M_3C$ and $(11\bar{1})\gamma \parallel (01\bar{1})\ M_3C$.

4.7.8. Adiabatically Sheared Armour Steel.

The bulk of this specimen exhibited a deformed martensitic structure containing small M_3C carbide particles (Figure 4.7.31). The associated diffraction pattern shows two martensite grains with the directions [111] and [173] respectively, parallel to the beam direction. The c/a ratio for both of these grains was calculated to be 1.05(±.03). The martensite grains contained a high density of dislocations and areas of internal twinning.

In contrast, the structure of the shear band as shown in Figure 4.7.32, appears as an extremely homogeneous distribution of small crystallites. The ring SAD pattern from the shear band was interpreted as a combination of martensite, M_3C and M_7C_3 carbides.

The shear band was studied in greater detail at high magnification and the Figure 4.7.33 shows an area at the centre of the band in which the structure is comprised of very small internally twinned martensite grains and carbide particles. Micro-diffraction techniques were used to analyse features approximately 50nm in diameter to illustrate the differing orientations of the martensite grains and to obtain an estimate of the c/a ratio of 1.07(±.03) for the shear band microstructure.

The microdiffraction pattern Figure 4.7.33 (c) indicates the presence of retained austenite within the shear band with the orientation relationship :

$$[011]_{\gamma} \parallel [111]_{\alpha}$$

$$(222)_{\gamma} \parallel (112)_{\alpha}$$

Precipitates of M_3C were also identified within the shear band and the orientation relationship derived from the microdiffraction pattern shown in Figure 4.7.33 (d) is described by:

$$[210]_{\alpha} \parallel [021]\ M_3C,$$

$$(002)_{\alpha} \parallel (012)\ M_3C.$$

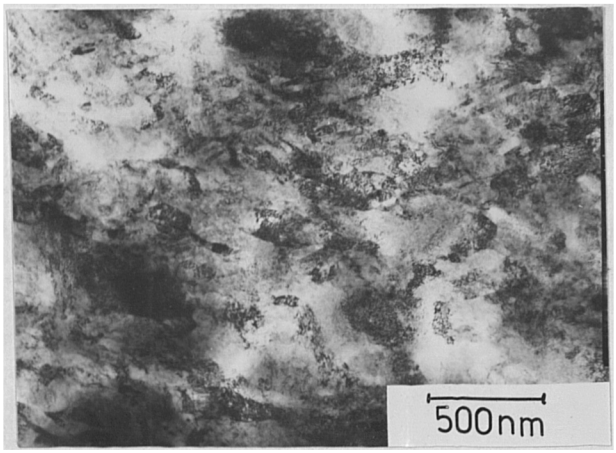

a)

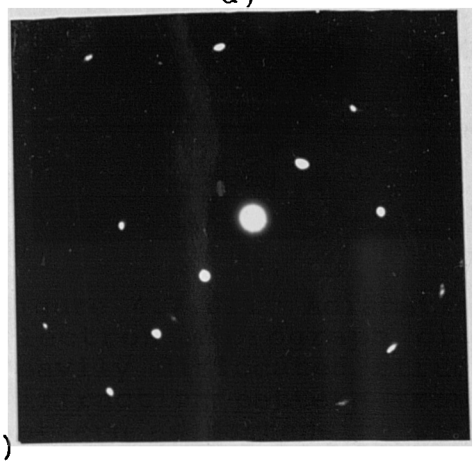

b)

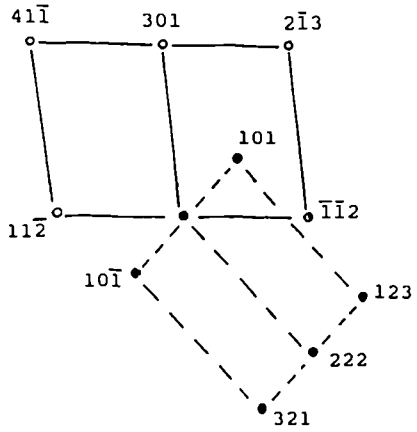

c) [173] [111]

Figure 4.7.31. Adiabatic shear specimen. a) Transmission electron micrograph of the matrix material showing a heavily dislocated structure, b) selected area electron diffraction pattern from the region, c) solution of the pattern as martensite with a c/a ratio of 1.05 ± 0.03.

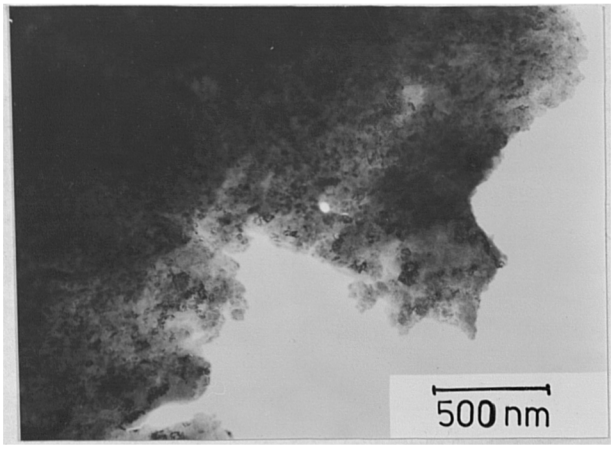

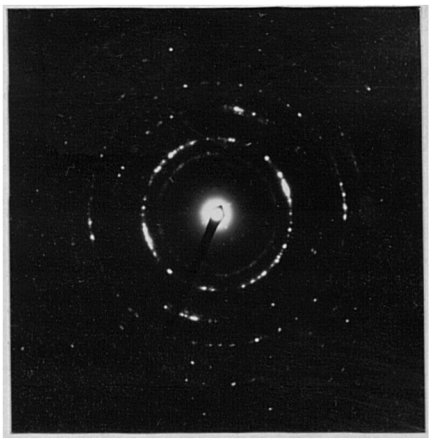

Figure 4.7.32. Adiabatic shear specimen. a) Transmission electron micrograph of the fine grained white-etching shear band. b) associated electron diffraction pattern indexed as martensite with M_3C carbides.

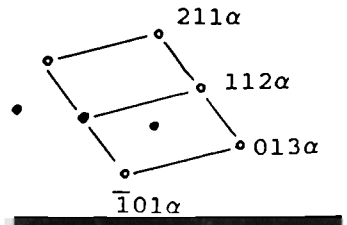

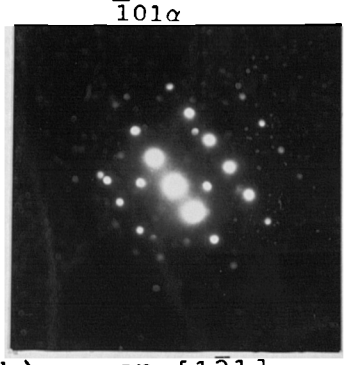

b) α on $[1\bar{3}1]$

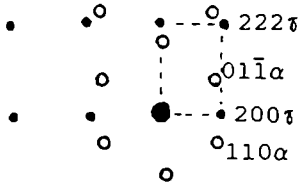

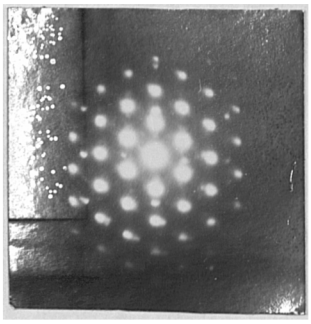

c) α on $[\bar{1}11]$, γ on$[01\bar{1}]$

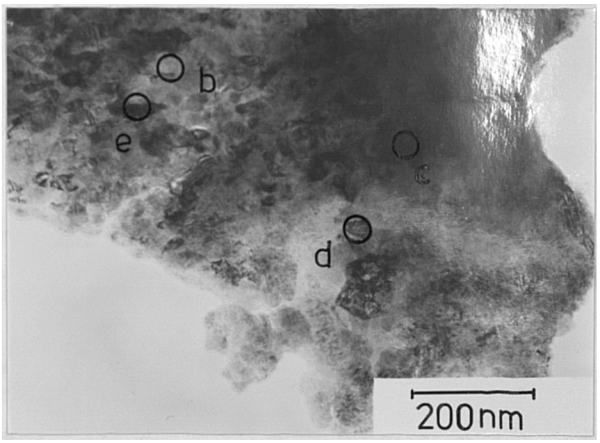

a)

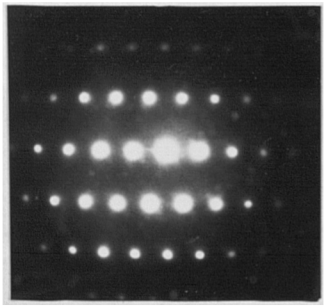

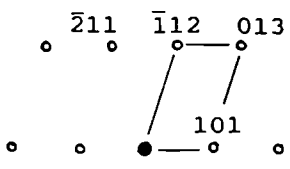

d) α on $[13\bar{1}]$

c/a = 1.07 ± 0.03.

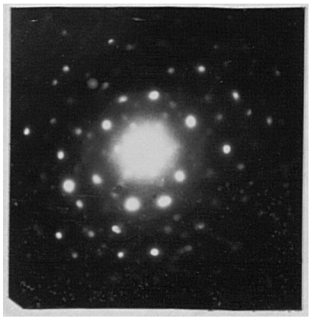

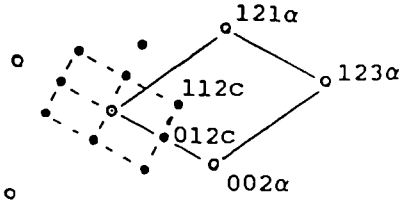

e) α on $[2\bar{1}0]$ ‖ $[0\bar{2}1]$ M_3C

with (002)α ‖ (012) M_3C

Figure 4.7.33. Adiabatic shear specimen.
a) Transmission electron micrograph of the centre of the white-etching shear band, b), c), d), e) micro-diffraction patterns from the areas indicated on the micrograph.

CHAPTER 5. DISCUSSION.

5.1. Introduction.

Discontinuous white-etching layers formed at the surface of worn or abusively-machined steel surfaces are known to reduce the resistance of components to fatigue and corrosion, and may dramatically increase rates of wear of contacting materials.

Conversely, it has been suggested that the deliberate formation of " white-layer " would provide an alternative method of surface hardening; with benefits in terms of increased wear resistance and improved surface integrity.

In this study, white-etching layers representative of several different formation mechanisms have been examined with a view to establishing their nature; an essential precursor to the generation of continuous " white-layer" under controlled conditions.

First, the significance of the various analytical and structural results acquired from each specimen are discussed in broad categories, based on the primary mechanism of white-etching layer generation. Secondly, the nature of "white-layer" is considered and the principal factors essential to the formation of this material are identified.

5.2. White-etching layer forming mechanisms.

White-etching layers are generated under a variety of conditions and in most cases a number of factors contribute to their formation. This is true of the samples studied in this work and whilst it is convenient to make a discrimination between groups of specimens , it must be recognised that a combination of the effects of temperature, stress, and chemical environment are present to a greater or lesser extent in each of the specimens examined . The properties of the white-etching layers formed on these materials are considered in detail in the following sub-sections :

1) Laser heat-treated specimens.
   - i) 817M40 Steel.
   - ii) 080M40 Steel.
   - iii) Armco iron.

2) Thermo-mechanically deformed metal surfaces.
   - i) Abusively-turned steel.
   - ii) Wear pin.
   - iii) Digger tooth.

3) Thermo-chemical interaction.
   - i) Rarden gun barrel.
   - ii) Chieftain tank gun barrel.

4) Bulk deformation by adiabatic shear.
   - i) Armour steel.

5.2.1 Laser heat-treated specimens.

The surface-hardening of steels by laser heat-treatment has been considered as a practical means of obtaining wear resistant surfaces on shafts, gears and other mechanical components. In practice, the increase in hardness attained and the resulting improvement in wear resistance, has been found to be minimal. As a consequence, only limited use has been made of this technique to date.

The samples of laser surface-hardened iron and steel studied in this work exhibited a range of metallographic structures; reflecting both the composition and structure of the parent material and the conditions of heat-treatment.

5.2.1.1 817M40 Steel.

Examination by light microscopy confirmed the white-etching nature of the laser heat-treated zone in this material, relative to the easily etched underlying tempered martensite. The heat-treated zone is clearly not however structureless; at higher magnification, conventional microstructures associated with rapid heating and cooling were identified.

Control of laser energy density at the specimen surface was achieved by varying the speed of specimen traverse under the focussed laser beam. The maximum useful energy density was found to be limited by the onset of undesirable surface melting, as revealed by surface

rumpling and the formation of a zone of resolidified dendritic material. Further evidence of the high temperatures reached within the recrystallised zone is evidenced by the local melting of manganese sulphide stringer inclusions (melting point 1610°C), indicating that transitory temperatures well in excess of the steel melting point (≈ 1500°C), were attained at the steel surface.

The distinct change in the microstructure at the boundary of the heat affected zone and the underlying matrix, marked the range of the austenite transformation isotherm which has a maximum depth determined by the duration of heating and the laser energy density. The hardness of the laser heat-treated zone, which is determined by the cooling velocity, and austenitising temperature, was found to be a maximum in the region of fine grained martensite where values of over 1000HV (25g) were measured.

This is well in excess of the hardness of 750HV quoted for conventionally heat treated steel of this carbon content. (Figure 2.2). The increase in attainable hardness is attributed to the effect of the small grain size achieved by short duration heating followed by rapid self-quenching.

A limitation of this hardening technique is indicated in Figure 4.2.10, which shows the variation of structure and hardness with depth, for tracks laser heat-treated at progressively lower total energy densities. This figure

demonstrates that, under simple short duration heating, the maximum depth of hardening is limited to 100μm. Increasing the period of laser-treatment in an attempt to harden the material to a greater depth, simply resulted in the formation of an overlayer of softer material, with the region of high hardness moving away from the surface.

TEM examination of thin foils prepared as a cross section through the laser-treated zone and underlying matrix, showed the distinct change in structure between the tempered matrix and the untempered martensite of the laser-transformed steel.

Analysis of diffraction patterns acquired from these areas showed that the tempered steel structure consisted of laths of ferrite containing a distribution of M_3C and M_7C_3 carbides. In contrast, the zone of maximum hardness, within the laser heat-treated volume, exhibited a structure consistent with untempered martensite containing a high density of fine precipitates.

The c/a ratio of 1.05 ($\pm$ 0.3) calculated for this phase, appears higher than would be expected for steel of this carbon content, but the measured value lies within the limit of experimental error of the value (1.02) indicated by the data presented by Honeycombe, (1981) citing Roberts (1962) (Figure 5.1.).

As might be anticipated, microprobe analysis and light element analysis showed no detectable differences between the chemical composition of the heat-treated zone and the underlying matrix.

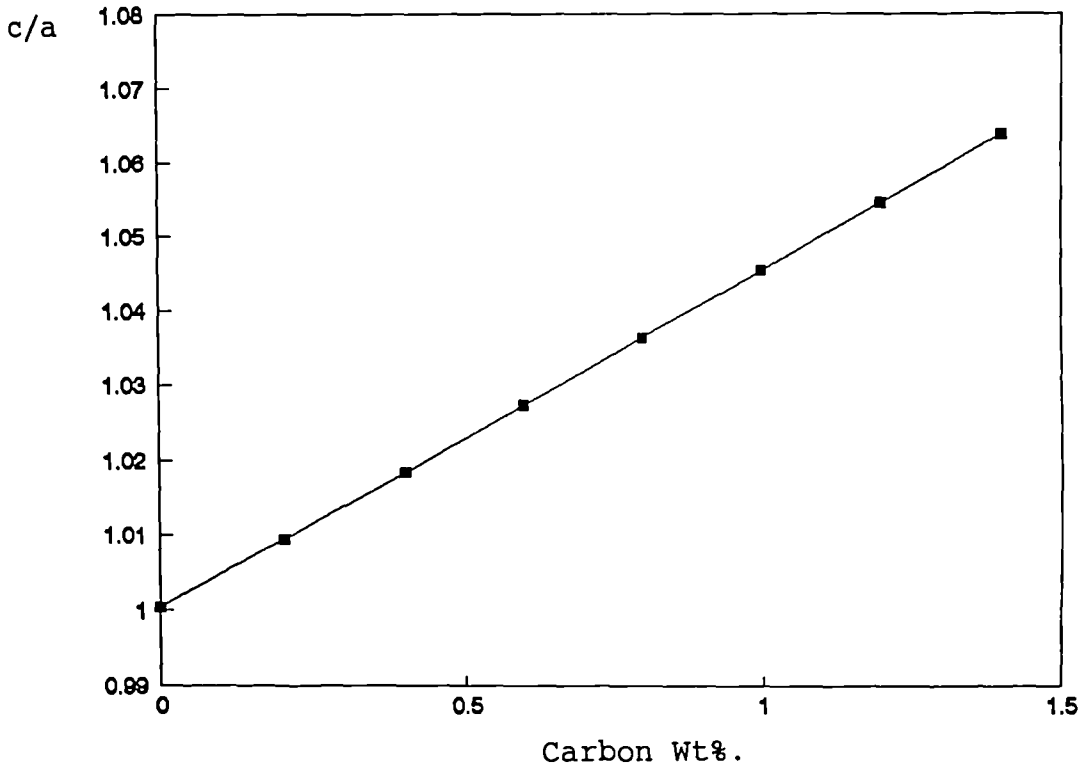

Figure 5.1. The variation of the martensite c/a ratio as a function of carbon content in Wt%. (After Roberts 1962).

5.2.1.2. 080M40 Steel.

Laser heat-treatment of this pearlitic steel, produced a white-etching layer with similar dimensions of width and depth, relative to the input energy density, as that produced in the martensitic, 817M40 steel.

Metallographic examination of a cross-section through the track showed that the outer zone, which was restricted to a depth of less than 30μm, contained a coarse acicular product identified by light and electron microscopy as martensite. No residue of pearlite colonies were visible, indicating that the region had been raised to a sufficient temperature, even under short duration heating, to permit the diffusion of carbon into the surrounding pro-eutectoid ferrite.

Underlying this layer, a zone of material had formed in which the pearlite phase had been transformed without change of shape, to produce islands of an apparently structureless material, shown by light element analysis to contain the same average carbon content as the pearlite phase. Examination by TEM identified this phase as a high carbon martensite containing a regular dislocation network and no obvious grain boundaries.

The development of this zone of dual phase structure under laser heat-treatment would have been facilitated by the large number of nucleating sites available for the $\alpha \rightarrow \gamma$ transformation at the ferrite - cementite interface within the pearlite lamellar structure. Thus under conditions of short duration heating, the pearlite colonies were austenitised to a depth of over 200μm, without diffusion of carbon into the surrounding pro-eutectoid ferrite, which itself may not have reached a sufficient temperature for transformation to austenite.

Following self-quenching, an inhomogeneous, hardened dual-phase structure comprising islands of 0.8% carbon martensite in a ferrite matrix was formed. The maximum hardness measured for the martensite islands was found to be in excess of 1000 HV(25g). This increased level of hardness over the value given for conventionally hardened 0.8% carbon steel (900 HV), may be attributed to the effect of the network of cells observed in the modified pearlite phase by TEM (Figure 4.7.9).

The formation of this network, which is similar in appearance to the low energy dislocation structures generated in ferrite by cyclic deformation (Yumen 1988), is attributed to internal stresses resulting from the physical constraint placed on the martensite product during transformation within the pro-eutectoid ferrite matrix. As a consequence of microhomogenisation resulting from the rapid thermal cycling of the former pearlite colonies on transformation to a high carbon martensite, the islands appeared structureless when etched in Nital. Thus the white-etching nature of the hard phase is attributed to the suppression of the conventional inhomogeneous martensitic structure.

5.2.1.3. Armco Iron.

The apparent depths of heat-treatment in this material were similar to those attained in both the 08M40 and 817M40 steels with zones representing; surface melting at high laser power density, a grain refined region and a region of grain growth.

Values of hardness varied from 240 HV(25g) at the surface where the structure was predominantly small grained with Widmanstatten ferrite, to 160 HV(25g) at a distance of between 200μm and 400μm from the surface coincident with the region of larger grain size. Laser heat-treatment of this material did not appear to produce any structures inconsistent with those which would be formed by conventional heat-treatment.

5.2.2. Thermo-mechanically deformed surfaces.

The factors associated with the formation of white-layers during sliding wear, have been categorised by several workers, as detailed in the preceding literature survey. The three factors which appear to be necessary either singly or in various combinations for the generation of white-layer are :

1) Rapid heating and quenching.
2) Deformation.
3) Surface chemical reaction.

White-layers examined in this study and considered under the general sub-heading of thermo-mechanical wear include; those formed intentionally as a result of abusive machining, those generated in laboratory wear tests and those formed adventitiously on a gravel extraction tool.

5.2.2.1. Abusively turned 817M40 steel.

The formation of white-layers during the manufacture or use of steel tools and components, is of prime economic importance due to the influence of this hard material on the wear characteristics of steel.

Whilst the formation of white-layer is generally regarded as undesirable, it has been proposed that the controlled formation of these layers under special machining conditions, could be used to selectively harden the surfaces of shafts and gears.

The perceived advantages of this method of surface hardening over other methods of surface or bulk hardening lie in the potential convenience of a hardening process which can simply be applied as an additional turning operation, to produce a hardened layer which is both continuous, and well bonded to the underlying matrix.

The mechanism of production of white-layers by abusive turning shows similarities to the mechanism of white-layer generation under conditions of scuffing wear, and could be considered as an example of controlled single pass wear. The microstructure of the white-layer formed by abusive turning, as determined by TEM examination, was found to be consistent with an extremely fine grain martensite in which the original carbides had become fragmented and dispersed. There was some evidence that carbide particles had begun to dissolve into the matrix, with many of the fragments becoming spheroidised.

Comparison could be made with other systems in which hardening is achieved as a result of the application of stress, to produce high local strains with resultant intense localised plastic deformation. This could include cold rolling operations, white-layer generation on railway lines, the wear mechanisms of ploughing, grinding, abusive machining, and the special case of adiabatic shear.

Light element EPMA of the turned surface showed no evidence of interaction with the atmosphere, in the form of oxidation for example, but SIMS depth profile analysis with detection limits at the ppb level, showed that

hydrogen, oxygen, carbon and nitrogen levels were increased by an order of magnitude over the matrix content to a depth of 3μm below the turned surface.(Figure 4.6.3). Whilst this phenomenon could have implications in terms of surface integrity following machining, due to the effect of localised strain-ageing and embrittlement, it is unlikely that the formation of white-layer would be promoted by such a low level of these elements.

5.2.2.2. 817M40 Wear Pin.

Extensive regions of adherent oxide deposits at the surface of the wear pin were evidence of interaction with the local atmosphere, facilitated by the high surface temperatures resulting from frictional heating.

Examination by electron microscopy of the white-layers identified on the wear pin, revealed a structure consistent with a deformed fine grain martensite, whilst electron micro-probe and SIMS depth-profile analysis, showed that this form of white-layer contained a low level of oxygen attributed to the incorporation of surface oxides during conditions of multiple-pass wear.

The gradual transition observed between the white-layer and the underlying matrix, is supportive of the view that this type of white-layer is not simply a transformation product formed under conditions of frictional heating.

5.2.2.3. Digger Tooth.

The digger tooth exhibited a surface formed under conditions of abrasive wear, with isolated regions of white-layer forming beneath ploughed grooves produced by hard fragments of rock. Light element micro-probe analysis showed no evidence of interaction with oxygen or nitrogen from the atmosphere and no indication that high surface temperatures had been attained during the wear process. Examination of the white-layer by thin foil electron microscopy revealed a structure similar to that of the abusively turned 817M40 steel, consisting of a fine grain martensite containing fragmented carbide particles. (Figure 4.7.23). In contrast to white-layers formed on the abusively turned 817M40 steel, those formed on the digger tooth were not intimately bonded to the underlying matrix. This is taken to indicate that white-layer formed under conditions of ploughing had been transported over the digger tooth surface during the wear process. Hardness tests of regions identified by light microscopy, indicated that higher hardness and greater etching resistance were associated with increased deformation.

5.3. Thermo - chemical surface interaction.

White-layers are formed at the bore surface of gun barrels as a result of thermo-chemical interaction, without the influence of plastic-deformation. This mode of white-layer generation may be contrasted to that of wear in atmosphere, where a combination of thermo-mechanical and thermo-chemical interactions operate.

5.3.1. Chieftain gun barrel.

The results obtained from sections of Chieftain tank gun barrel demonstrate that a thick layer of modified material some 60 μm in depth, is generated as a result of the heating effect of firing . Surface temperatures of up to 1000°C have been measured at the barrel surface during firing, and this transitory or short-duration heating effect may be directly compared to that produced by the laser heat-treatment experiments previously described.

The structure of the thick white-layer is similar to that of the very fine grain martensite produced in the martensitic 817M40 steel by laser heat-treatment. Whilst having a higher hardness than the matrix, reaching a maximum of over 1000HV 30μm from the surface, this material could not be described as a truly structureless white-layer. Examination by TEM showed the thick white-layer to be an untempered martensite containing a high density of dislocations (Figure 4.7.26).

Close to the bore surface in the region of maximum hardness, the martensite grains exhibited internal twinning and contained a uniform distribution of fine carbide particles. Analysis of diffraction patterns indicated that the c/a ratio of the martensite phase varied from 1.03(± 0.03) in the tempered matrix, to 1.08(± 0.03) close to the barrel surface, where increased levels of nitrogen were detected by SIMS depth profile analysis.

In contrast, the thin white-layers, some 5 to 10μm in depth observed at the surface of the gun barrel appeared completely structureless on etching. Hardness tests of these thin layers in cross section were not reliable and tests taken directly on the gun barrel surface using a 25g load suggested that these layers are less hard (560 ± 30 HV) than the underlying matrix (1000 ± 30 HV). Light element analysis by EPMA and SIMS showed that this layer contained high levels of carbon and nitrogen absorbed from the propellant gases.

5.3.2. **RARDEN gun barrel.**

Similarly to the Chieftain barrel, the RARDEN gun barrel surface exhibited a 60μm white-layer of untempered martensite formed by the short duration heating and cooling cycle, experienced on firing. The structure of this layer revealed by TEM consisted of equiaxed grains of martensite with an average diameter of 500 nm, containing a dispersion of fine carbide particles.

Overlaying the region of untempered martensite, a thin white-layer 10μm in depth had formed, containing an increased level of carbon and shown by electron diffraction to contain M_3C in association with austenite. The depth of this layer is indicative of the extent of the range of interaction between the steel and gaseous propellant products under the extreme conditions of temperature and pressure experienced during firing. The limited extent of this interaction suggests that a reaction with a standard atmosphere to form a high carbon or nitrogen martensite would be most unlikely under the physical conditions experienced during wear or abusive machining.

5.4. Adiabatic Shear.

There are clear similarities between the white-etching bands formed in the bulk of steel armour plate under conditions of adiabatic shear, and those formed at the surface of steel as a result of thermo-mechanical processes such as wear or abusive machining operations. The absence of any possible chemical interaction with the atmosphere during generation of the shear band, permits study of a white-etching layer produced solely by intense localised strain.

Examination by light microscopy showed that the bands had formed at boundaries between areas of relative movement of the bulk material. The band centre appeared entirely structureless following etching, when examined by

light microscopy, and exhibited hardness values of over 1200HV, thus conforming to the definition of a white-layer as applied in this work. High resolution SEM examination of an etched shear-band revealed a fine grain structure showing deformation in the direction of shear, with clear similarities to the white-layer produced by abusive machining. Transmission electron microscopy of thin foils prepared through a shear band, showed the band to consist of a well defined region of fine grained martensite containing very fine carbide precipitates. Analysis of microdiffraction patterns acquired from martensite grains within the shear band indicated a c/a ratio for the band of 1.07(± 0.03), in comparison to 1.05(±0.03) for the surrounding matrix. Analysis of microdiffraction patterns from the shear band also indicated the presence of austenite in this region, with an orientation relation to the matrix similar to the Kurdjemov-Sachs relationship.

The area immediately adjoining the shear band showed evidence of plastic deformation, and contained carbide particles somewhat larger than those observed in the matrix. This suggests that this region experienced a limited degree of tempering as a result of the localised heating effect induced by high localised levels of strain. Hardness measurements of this tempered band showed a reduction from the average matrix value of 900 (± 30)HV to less than 800 (±30)HV.

5.5. The Nature of White Layer.

5.5.1. Introduction.

The term "white-layer" is generally taken to refer to hard layers formed on steel surfaces during a wear or abusive machining process. It is clear that many metallic and non-metallic phases formed in steel during conventional heat-treatment could be described as white-layers; in the sense that they are etch resistant in certain commonly used etching solutions, and can therefore be made to appear white against the matrix background.

A second criteria which must be applied in order to distinguish white-layer formed by wear or abusive machining, is that of unusually high hardness, generally in excess of that which can be attained by conventional heat-treatment of the same steel.

The three factors which are variously considered to influence the formation of white-layer include :

1) Chemical change.
2) Metallurgical transformation.
3) Thermomechanical deformation.

5.5.2. Chemical change.

In this work it has been demonstrated that the increase in hardness of white-layers formed by wear or abusive machining of steels, cannot be attributed to a local increase in carbon which could perhaps assist in the formation of a higher carbon martensite, or the pickup of sufficient nitrogen to allow formation of a nitrided

layer or a high nitrogen martensite.

Indeed, the results of the analysis of gun barrel sections, the only surfaces found to exhibit significant chemical interaction with the local environment, showed that the thin, high carbon and nitrogen containing layers at the gun barrel surfaces had a lower hardness than the underlying thermally refined martensite. Thus despite their being white-layers in terms of etching resistance, and hence appearance when viewed under a light microscope, these layers should properly be identified as "white-etching" layers and not "white-layer".

Comparison with a nitrided steel , showed that very much higher levels of nitrogen were associated with the very hard white-etching layer formed at the surface of components by this hardening process.

SIMS analysis showed that the thick white-etching layer formed on both the Chieftain and RARDEN barrels contained increased levels of hydrogen, nitrogen, oxygen and carbon to a depth of 30μm and 10μm respectively, when compared to the underlying matrix. It is not clear whether the absorption of these elements has an influence on the formation of the thick white-etching layer observed on these gun barrels, which extends to a greater depth and which is comparable to the white-etching heat-affected zone produced by laser heat-treatment.

SIMS depth profile analysis also showed that low levels of oxygen, nitrogen, carbon and hydrogen are absorbed into the surface layers of steel during abusive

machining. The depth of penetration of these elements was somewhat less than the depth of the white-layer formed on this sample, but may nonetheless be significant in terms of the hardening effect. For example, the nitrogen content of abusively turned 817M40 steel was increased by more than an order of magnitude within the 3μm close to the surface, when compared to the nitrogen content of the underlying steel. This would imply a nitrogen content of between 0.04wt% and 0.1wt% depending upon the initial steel composition.

From the foregoing it is apparent that whilst chemical changes may be induced in the surface layers of steels as a result of interaction with the local environment, that such an interaction, whilst perhaps contributing to increased hardness or etching resistance, is neither a prerequisite or guarantee of white-layer formation and should be regarded as a secondary or contributory mechanism.

5.5.3. Metallurgical transformation

White-etching layers formed by laser heat-treatment of martensitic steel, exhibit greater structural homogeneity and smaller grain size than the tempered martensite of the underlying matrix. This refinement of the structure results from the rapid heating and self-quenching cycle achieved under conditions of laser heat-treatment.

The high hardness of the untempered martensite, when compared to that obtained by conventional heat-treatment,

is attributed to a combination of factors, including the distribution of small carbide particles, the high density of dislocations, the extent of internal twinning and the small grain size.

It is quite clear that the hard phase produced by laser heat treatment of 817M40 steel, is not white-layer in the tribological sense, although possessing some of the characteristics of that material. Similarly, the thick white-etching layer produced on the internal bore surface of gun barrels is also identified as a region where localised heating above the austenite transformation temperature and subsequent self-quenching, has resulted in the formation of a layer of refined, untempered martensite.

Laser heat-treatment of the dual phase 080M40 pearlitic steel, produced a distinctive modification of the structure, with the transformation of the pearlite colonies to a high carbon martensite. The short duration of the heat-treatment cycle, confined austenitisation to the pearlite phase, with the result that the final structure consisted of well defined martensite islands contained within a matrix of proeutectoid ferrite.

Whilst short cycle heat-treatment enables the production of novel microstructures, with potential advantages in terms of improved wear characteristics and corrosion resistance, these layers have a well defined structure and are clearly distinguishable from "tribological" white-layer.

5.5.4. Thermomechanical deformation.

White-layers formed by wear or abusive machining processes do not appear to require any change in their local chemical composition to achieve substantially higher values of hardness than the parent material. In this respect, white-layer departs from the established relationship for steel which shows that the maximum hardness attainable by heat-treatment, is proportional to the carbon content and has a limit of approximately 850HV.

The white-layers formed by wear and abusive machining are similar in structure as revealed by TEM, both to one another, and to the white-etching bands produced by adiabatic shear. The process of thermo-mechanical deformation, which underlies the formation of these white-layers, has resulted in the generation of an extremely fine grain structure, identified by TEM as a form of martensite containing an apparently uniform distribution of small precipitates. Measurement of grain sizes by TEM examination of thin foils, showed the average grain size of white-layer within the adiabatic shear band to be 80nm, whilst those of surface white-layers formed on the digger tooth and abusively turned steel, averaged 200nm in diameter. By fitting these values to a linear extension of the Petch-type plot presented by Grange (1966) and based on experimental results for a 0.4wt%C, low alloy steel, the yield strength and thus an estimate of the expected hardness of the white-layers may be obtained. (Figure 5.2).

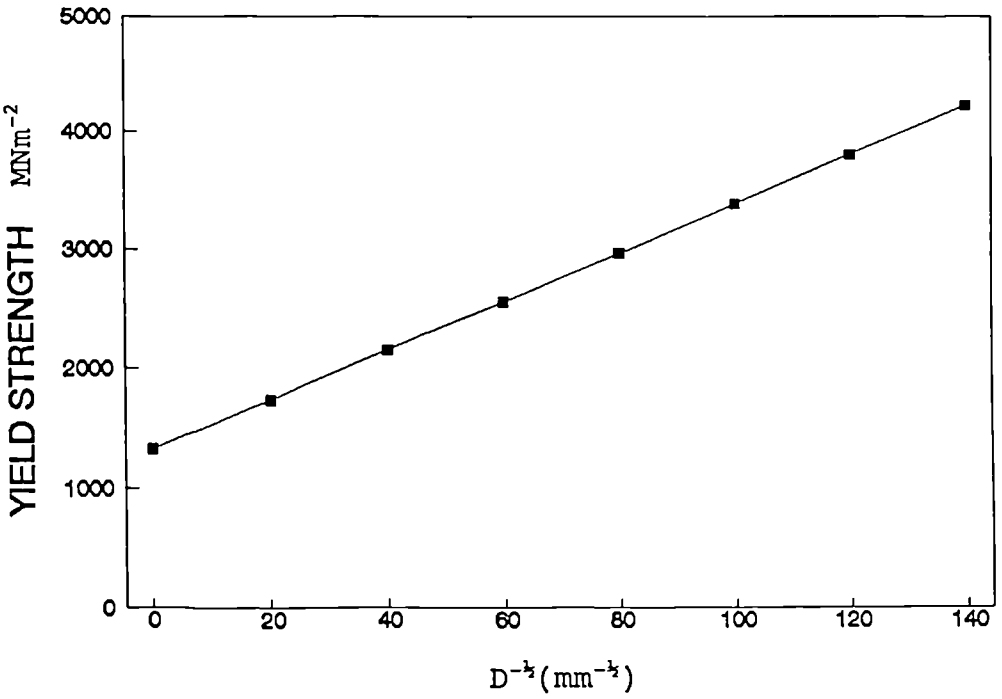

Figure 5.2. The variation of yield strength with grain size (after Grange 1966), extended linearly to grain diameters of 50nm.

A comparison of measured white-layer hardness values with those predicted by application of the Hall-Petch relationship:

$$\sigma_y = \sigma_i + k_y\, d^{-\frac{1}{2}}$$

where; σ_y = the yield stress,

σ_i = the lattice friction stress,

k_y = the locking parameter,

d = grain diameter.

assuming that the values of lattice friction stress and locking parameter are similar for the materials examined, is in very close agreement. (Figure 5.3). This suggests that the primary hardening mechanism of white-layer formed by a thermo-mechanical process, such as wear or adiabatic shear, is that of grain refinement.

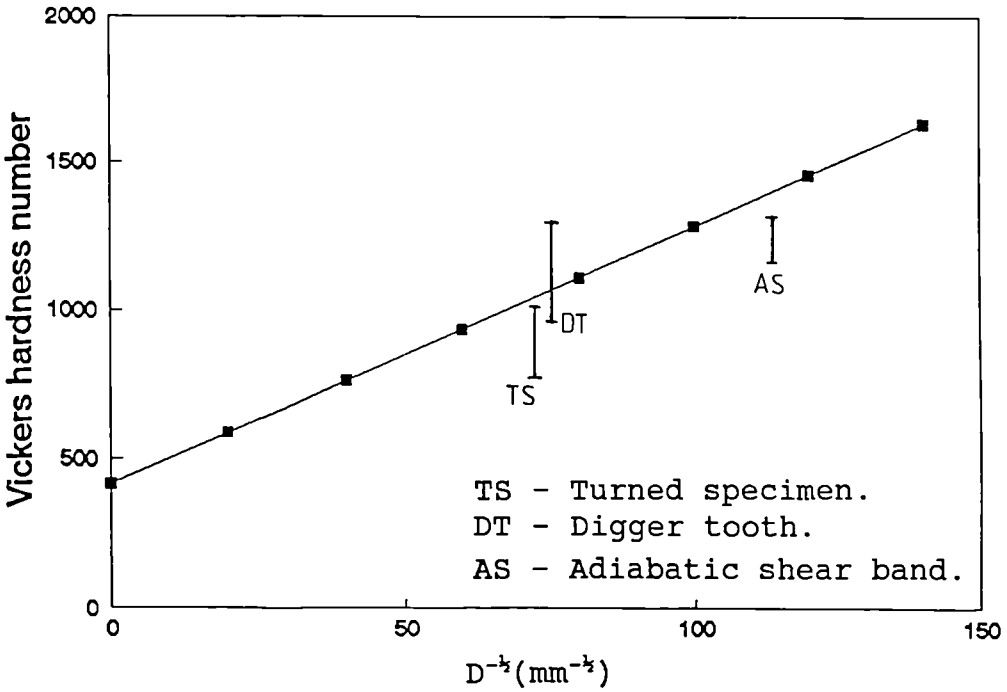

Figure 5.3. A comparison of measured hardness values with those predicted by an extension of the Hall-Petch relationship between hardness and grain size.

5.6. The mechanism of white-layer formation.

This study has demonstrated that there are clear distinctions to be made between white-etching layers formed by surface chemical modification, those produced by localised short cycle heat-treatment and those formed primarily by thermo-mechanical processes.

Thermo-mechanical treatment is a general term which embraces hot-rolling, controlled rolling, ausforming, and isoforming, all of which processes can improve the properties of steels by grain refinement. Substantial increases in yield strength are attainable with careful control of ausforming, where steel is deformed at low temperature with the material quenched from the austenite

phase to a metastable condition, with transformation delayed until deformation is completed. Isoforming involves allowing transformation during deformation, which is continued until transformation is complete. Grain sizes of less than 0.5μm are attainable by this process.

There are obvious parallels to be drawn between the above controlled processes and the mechanism of adventitious generation of white-layer by thermo-mechanical deformation.

Adiabatic shear is a special case of thermo-mechanical deformation and studies on ballistically-deformed materials by Rogers and Shastry (1980), have demonstrated that there is a well defined transition between deformation band formation and the production of a white-etching band. This is taken to imply that the level of localised strain may exceed a threshold value where the associated temperature increase is sufficient to allow austenitisation of the shear band. The resultant structure, as demonstrated in this work, consists of a fine grain martensite, transformed by rapid self-quenching at the instant that deformation ceases, to produce a white-etching "transformation band ". The width of these bands appears to be determined by the strain rate, the value of local strain and the thermal conductivity of the material.

In this study, white-etching layers formed by wear and abusive machining were found to have a similar structure to that of the adiabatic shear band, differing in the related properties of grain size and hardness. A

reasonable argument for their description as a surface form of adiabatic shear transformation product may be advanced by considering the model of a plastically-deformed structure developed by Olsen (1980). This demonstrates that at high deformation velocities, the resultant shear is localised at the surface, leading to shear instability with effective strain rates above 10^6. These conditions are analogous to those experienced in bulk adiabatic shear; and where conditions of temperature and pressure allow, austenitisation and subsequent transformation to martensite would be expected. These model studies may be compared with experimental measurements on turned surfaces by Dao and Shockey (1979), and of deep drilled steel by Griffiths (1982), in which strain rates in excess of $2.4 \times 10^2 s^{-1}$ and 10^5 respectively, were recorded under conditions where white-layers were generated.

CHAPTER 6. CONCLUSIONS.

6.1. Summary of conclusions

The observations made of the various white-etching layers examined, provide a most satisfactory explanation for the characteristic properties of etch-resistance and high hardness, associated with "white-layer".

Taking the first criteria used to identify white-layer, that of the "white" appearance of this material when viewed by light microscopy following standard metallographic preparation and chemical etching , this characteristic is entirely attributable to the structural and chemical micro-homogeneity of the material, howsoever formed. Secondly, the characteristic high hardness, with values in excess of those normally attainable for a particular steel composition, and making due allowance for any local chemical modification, are primarily ascribed to the extremely fine grain size of the white-layer. The Hall-Petch relationship between grain size and yield strength, is relevant to the micro-homogeneous white-layer structure, and linear plots are obtained for yield stress against $d^{-1/2}$ for grain sizes as small as 80nm in diameter.

The phenomenon of white-layer formation in steels, either in the bulk as a well defined shear band, or at the surface as a white-etching layer; is attributed to the formation of a fine grain, chemically and structurally micro-homogeneous equiaxed form of martensite.

The primary mechanism of white-layer formation on worn or abusively machined surfaces is attributed to localised austenitisation, as a result of the temperature rise associated with strain-localisation and shear-instability at high strain-rates, followed by rapid transformation on self-quenching.

The contribution made by frictional heating in either the single or multiple pass wear or machining operation, would be to reduce the level of strain-localisation required for transformation, and also to temper any martensite produced on cooling.

It is proposed that a distinction should now be made between " white-etching" layers (a generally descriptive term based on the property of etch-resistance), which may be produced under a variety of conditions, and which may or may not have a high hardness, and "thermo-mechanically transformed white-layer". As demonstrated in this work, this is a structurally and chemically homogeneous phase which comprises of an extremely fine-grain martensite, produced exclusively by a thermo-mechanical mechanism incorporating transformation at high strain rates .

6.2. Recommendations for Further Work.

It is recommended that a series of further investigations be initiated to establish the precise conditions necessary for the onset of "thermo-mechanical transformation white-layer" generation at the surface of

worn and abusively machined 817M40 steel. These would include;

1) A two phase research programme combining computer modelling of strain-localisation effects during wear and abusive-machining, with a transmission electron microscopy micro-diffraction, micro-structural analysis of parent material and plastically-deformed surface layers.

It is anticipated that a model would be developed which would permit the conditions necessary for controlled white-layer generation to be predicted. Plastically-deformed layers and white-layer would then be produced by controlled abusive machining and pin-on-disc wear tests, over a range of effective pressures and strain velocities, to establish the practical onset of strain localisation.

The starting material should be tempered to provide a lath ferrite structure with a c/a ratio of unity which could be readily compared with the c/a ratio of any transformation product generated during the mechanical tests, using microdiffraction techniques.

2) It is proposed that a study be undertaken to evaluate the significance of the increased levels of light elements; hydrogen, nitrogen, carbon and oxygen, observed within the surface layers of abusively turned 817M40 steel. Mechanical test data and SIMS analyses of steels machined under "normal" and "abusive" conditions would be correlated to indicate whether the strength or fatigue resistance of a machined component could, under certain conditions, be compromised by localised strain-ageing or hydrogen embrittlement for example.

REFERENCES.

Amos, L.J. and Sheward, J.A. (1983). Ministry of Defence. RARDE. Fort Halstead. Report 10/83. Unclassified.

Andrews, K.W., Dyson, D.J. and Keown, S.R. (1971). " Electron diffraction patterns." Adam Hilger, London.

Archard, J.F. (1959). The temperature of rubbing surfaces. Wear.2. pp 438-455.

Argawala, R.P. and Wilman, H. (1955). J.I.S.I. 179. pp 124-131.

Babei,Yu.I., Golubets, V.M., Vygovskii,I.P., Ryabov,B.F. and Gnatyshak,N.N. (1971). Sov.Mat.Sci. Vol 7. No 5. pp 511-514.

Bain, E.C. and Paxton, H.W. (1966) In: Alloying Elements in Steel. 2cnd Ed. 3rd Rev. A.S.M.

Bell, T. (1970). Martensitic and Massive transformations in Ferrous Alloys. In: Martensite, Fundamentals and Technology. Ed. Petty, E.R. p 65. Longman. London.

Bibby, J. and Parr, J.G. (1964).The Martensitic Transformation in Pure Iron. J.I.S.I. February. 1964. pp. 100-104.

Black, J.T. (1979). Journal of Engineering for Industry. A.S.M.E. 101. pp 403-415.

Blunt, L.A. (1989). The Metallurgy of Centreless Ground Surfaces. PhD Thesis. Coventry (Lanchester) Polytechnic.

Bowles, J.S. and Barrett, C.S. (1953). Progress in Metal Physics. Vol 3, p 1.

Brammar, I.S. (1965). In: "Techniques for electron microscopy. " Ch 12. Ed. Kay, D., Blackwell Scientific Publications. Oxford.

Burwell, J.T. and Strang, C.D. (1952).
Proc. (A). Roy. Soc. 212. p 470.

Castaing, R. Thesis. (1951). University of Paris.
ONERA Publ. No. 55.

Clayton, P. (1976). British Rail Technical Note. TN FM 55.

Dao, K.C. and Shockey, D.A. (1979). J. Appl. Phys. 50 (12). pp 824-8246.

De Sveschnikoff, W.W. (1925). Army Ordnance 5, pp 794-797.: Cited by Rowntree, R.A. PhD Thesis. University of Leicester. 1982.

Derep, J.P. (1987). Acta Met. Vol 5. No 6. pp 1245- 1249.

El Heliaby, S.O.A. and Rowe, G.W. (1981). Metals. Tech. Vol.8. pp 58-66.

Eyre, T.S. and Baxter, A. (1972). Tribology. Dec. 1972. pp 256-261.

Farrell, R.M. (1969). The Friction and Wear Characteristics of Chromium Containing Steels. PhD Thesis. Brunel University.

Fay, H. (1917). Trans. Am. Inst. Min. Eng. Vol. 56. pp 468-495.

Field, M., Koster, W.P., Kohls, J.B., Snider, R.E. and Maranchik, J. (1970). "Machining of high strength steels with emphasis on surface integrity." American Air Force Machinability Data Center, AFMDC 70-1.

Fisher, G.L. and Farningham, G.D. (1972). Quantitative carbon analysis of nickel steels with the electron probe microanalyser. ASM Materials Eng. Congress. Cleveland, Ohio, Oct 1972.

Furuichi, H. and Nakamura, S. (1984). Formation and structure of unusually hard, thick damaged layer of copper, 18-8 stainless steel and iron. J. Mat. Science Letters. 3. pp 917-920.

Garwood, R.D. (1970). Martensitic and Massive Transformations in Non-Ferrous Alloys. In: Martensite. Ed. Petty, E.R. Longman. London.

Gentile, A.J.,Jordan, E.F, and Martin, A.D. (1965). " Phase transformations in high carbon, high hardness steels under contact loads." Trans. Met. Soc. A.I.M.E. Vol. 233. pp 1085-1093.

Glenn, R.C. and Leslie, W.C. (1971). "The nature of white streaks in impacted steel armor plate." Met. Trans. Vol 2. pp 2945-2947.

Goddard, J., Harker, H.J. and Wilman, H.J. (1962). Proc. Phys. Soc. 80. p 771.

Goldstein, J.I. (1975). In; Practical scanning electron microscopy. Ed. Goldstein, J.I. and Yakowitz, H. Plenum Press. New York and London.

Golubets, V.M., Dyadchenko, B.T. and Babei, Yu.I. (1972). " The influence of the white layer on the resistance of 40Kh steel to abrasive wear." Sov. Mat. Sci. 8 (3). pp 359-361.

Goodhew, P.J. (1985). " Thin foil preparation for electron microscopy." Vol 11. Practical Methods in Electron Microscopy. Ed. Glauert, A.M. Elsevier, Amsterdam.

Grange, R.A. (1966). Trans. A.S.M. 59. p26.

Griffiths, B.J. (1986). " Mechanisms of white layer generation with reference to machining and deformation processes." Paper No 86-Trib-30. ASME/ASLE Joint Lubrication Conf. Pittsburgh. 1986.

Griffiths, B.J. (1985). "White layer formations at machined surfaces and their relationship to white layer formations at worn surfaces." Trans. ASME. Journal of Tribology. Vol 107. p 165.

Griffiths, B.J. and Furze, D.C. (1986). " Tribological advantages of white layers produced by machining." Paper No 86-Trib-31.ASME/ASLE Joint Lubrication Conf. Pittsburgh. 1986.

Grozin, B.D. and Iankovich, V.F. (1962). " The structure of white layers." In: " Friction and wear in machines symposium." Moscow, USSR, Vol 15. p 143.

Hansen, M. (1958) "The Constitution of Binary Alloys." Materials Science and Engineering Series. McGraw Hill.

Harrison, D. (1979). " The corrugation of railway rails." PhD, Thesis, Cambridge University.

Honeycombe, R.W.K. (1981). "Steels, Microstructure and Properties." Metallurgy and Materials Series. Edward Arnold. London.

Howe, H.M. (1918). Trans. Am. Inst. Min. Engrs. 58. pp 513-568.

Hume-Rothery, W. (1966). " The structures of alloys of iron." Pergamon Press. Oxford.

Jain, J.C., Kumar, A.N., Mittal, R.N. and Juneja, B.L. (1986). " Surface integrity of a hardened and ground low alloy steel- study based on surface and subsurface damage." Materials Science and Technology. Vol 2. pp 856-864.

Karpenko, G.V., Babei, Yu.I., Karpenko, I.V. and Gutman, E.M. (1965). " Hardening steel by mechanical working." Izd. Naukova Dumka. Cited by Golubets et al, (1972).

Kawamoto, M. and Okabayashi, K. (1971). "Wear of cast iron in vacuum and the frictional hardened layer." Wear. Vol 17. pp 123-138.

Kay, D. (1965). " Techniques for electron microscopy." Blackwell, Oxford.

Kuritsyna, A.D. (1956). " On the origin of the white phase on rubbing surfaces." Trenie.Iznos. 11. pp 182-203.

Kuznetsov, V.D., Savitskiy, K.V. and Sukharna, N.N. (1963). " Some features of the structure of white layers." Physics of metals and metallography. Vol 15. No 1. pp 145-147.

Leng, J.A. and Davies, J.E. (1989). "Examination of wear debris produced using a four-ball machine." Tribology Int. Vol 22. No.2 pp 137-142.

Lester, H.H. (1929). " The white layer in gun tubes and its relation to the case of nitrided chromium aluminium steel." Trans. Am. Soc. Steel Treatment. Vol 16. pp 1-17.

Manion, S.A. and Stock, T.A.C. (1970)." Adiabatic shear bands in steel." Int. Journal of Fracture Mech. Vol 6. pp 106-107.

McIntire, H.O. and Manning, G.K. (1958). " Producing martensite by impact." Metal progress. Vol. 74, pp 94-95.

Modin, H. and Modin, S. (1973). In "Metallurgical Microscopy." Butterworths. London.

Murdock, C.J. (1932). " Hardening by grinding." Am. M/Cist. 76. p7. Cited by Furze, D.C. PhD Thesis, Brunel University. 1988.

Newcombe, S.B. and Stobbs, W.M. (1984). " Transmission electron microscopy study of the white etching layer on a rail head." Mat. Science Eng, Vol 66, pp 195-204.

Olsen, G.B. (1981). "Adiabatic deformation and strain localisation." pp 221-247 In : " Shock waves and high-strain-rate phenomena in metals". Ed. Meyers, M.A. and Murr, L.E. Plenum Press. New York.

Paranjpe, V.G., Cohen, M., Bever, M.B. and Floe, C.F. (1950). Trans. AIME. 188. p 261.

Perry, J. (1976). Unpublished work. Brunel University.

Perry, J. and Eyre, T.S. (1977). " The effect of phosphating on the friction and wear properties of grey cast iron." Wear, 43. pp 185-197.

Petch, N.J. (1953). " The cleavage strength of polycrystals." J.I.S.I. 173. pp 25-28.

Petty, E.R. (1970). In: "Martensite, fundamentals and technology." Ed. Petty, E.R. Longman, London. 1970.

Quirke, S.J. (1987). " Abrasive wear testing of steels in soils." M.Sc. Thesis. University of Cape Town.

Ralph, B. and Ecob, R.C. (1984). "The application of electron diffraction techniques to studies of the microstructure of deformed and of recrystallised samples." In: Proc. Risø Int. Symp., Microstructural Characterisation. N. Hessel Anderson et al., Eds. Risø Press, Roskilde, pp109-130.

Reed, S.J.B. (1975). " Electron probe microanalysis." University Press. Cambridge.

Roberts, C.S. (1962). Cited by Cohen, M. In " The strengthening of steel". 1962 Howe Memorial Lecture. Trans. AIME, 224. p638.

Rogers, M.D. (1969). "Metallographic characterisation of transformation phases on scuffed cast-iron diesel engine components." Tribology. 2. pp 123-127.

Rogers, M.D. (1970). "The mechanism of scuffing in diesel engines." Wear. 15. pp 105-116.

Rogers, M.D. (1979). "Adiabatic plastic deformation." Ann. Rev. Mater. Sci. 9. pp 283-311.

Rogers, M.D. and Shastry, C.V. (1980). " Material factors in adiabatic shearing in steels." In: " Shock waves and high strain rate phenomena in metals." Ed. Meyers, M.A. and Murr, L.E. Plenum Press. New York. pp 285-298.

Ross, R.B. (1968). Metallic Materials. Chapman and Hall. London.

Rowntree, R.A. (1982). " Metallurgical phase transformations in the rubbing of steels." Ph.D. Thesis. University of Leicester.

Samuels, L.E. (1967). " Metallographic polishing by mechanical methods." Sir Isaac Pitman & Sons. Melbourne.

Schlicht, H. (1973). " On the formation of white etching areas in rolling elements." Hart. Tech. Mitt. 29 (3) pp 125-131.

Schottky, H. and Hiltenkamp, H. (1936). " The part played by atmospheric nitrogen in the wear and fatigue failure of rubbing steel surfaces." Stahl und Eisen, 56. pp 444-446. Cited by Rowntree, R.A. Ph.D Thesis. University of Leicester. (1982).

Scott, D., Loy, B., and Mills, G.H. (1967). " Metallurgical aspects of rolling contact fatigue." 5th Conv. Lub.& Wear. 181. (30), pp 94-103. London. I. Mech E.

Scott, D., Smith, A.I., Tait, J. and Tremain. (1975). " Materials and metallurgical aspects of piston ring scuffing- a literature survey." Wear, 33. pp 293- 315.

Scott, V.D. and Wilman, H. (1958) Proc. Roy. Soc. 247A. p 353.

Snair, W.H. and Wood, W.P. (1939). " The white layer structure in the erosion of machine gun barrels." Trans. A.S.M. 27, pp 608-624.

Stahli, G. (1981). " Physical and materials related problems in short time surface hardening of steel using high frequency laser and electron beams." Tribology. Int. April 1981. pp 101-106.

Stead, J.W. (1912). J.West. Scot. Iron & Steel Inst. Vol 19. pp 169-204.

Steen, W.M. and Courtney,C. (1979). " Surface heat treatment of En 8 steel using a 2kW continuous-wave CO2 laser." Metals Tech. 6,(12). pp 456-462.

Steen, W.M. (1985). "Surface engineering with a laser." Metals and materials. Dec 1985. pp 730-736.

Steininger, Z. and Krzeminski, A. (1962). "Alterations in the structure of steel wires as a cause of premature wear in wire ropes." Wire Ind. 340. pp 351-357.

Steininger, Z. and Krzeminski, A. (1965). " Some common defects in pre-stressed concrete wire, Wire Ind. 382. pp 963-968.

Stroud, M.F. and Wilman H. (1965). Acta Cryst. 15. p 443.

Styri, M. (1951). " Fatigue strength of ball bearing races and heat treated 52100 steel specimens."Proc. Am. Soc. Test Mat. 51. pp 682-700.

Sykes, D.E. (1989). " Dynamic secondary ion mass spectrometry.", In: Methods of Surface Analysis. Ed. Walls, J.M. Cambridge University Press. Cambridge.

Tarasov, L.P. (1946). " Detection causes and prevention of injury in ground surfaces." Trans. A.S.M. 36. pp 389-441.

Tarasov, L.P. and Lundberg, C.O. (1949). "Nature and detection of grinding burn in steel." Trans. A.S.M. Vol 41. pp 893-933.

Thornton, P.A. and Heiser, F.A. (1971)." Observations on adiabatic shear zones in thick wall cylinders." Met. Trans. Vol 2. pp 1496-1499.

Timothy, S.P. (1987). "The structure of adiabatic shear bands in metals : A critical review." Acta Met. Vol 35. No 2. pp 301-306.

Tomlinson, W.J., Blunt, L.A. and Spraggett, S. (1988). " Running in wear of white layers formed on En 24 steel by centreless grinding." Wear.

Torrance. A.A. (1978). " The metallography of worn surfaces and some theories of wear." Wear.50. pp 169-182.

Torrance, A.A. (1978). " Metallurgical effects associated with grinding." Proc. 19th. Int. Conf. MTDR. pp 637-644.

Torrance, A.A. and Cameron, A. (1974). " Surface transformations in scuffing." Wear. 28. pp 299-311.

Trent, E.M. (1941). " The formation and properties of martensite on the surface of rope wire." J.I.S.I. 143. pp 401-417.

Turley, D.M. (1971). J.Inst. Metals, 99 p 271.

Turley, D.M. (1975). " The nature of the white etching layers produced during reaming ultra high strength steel." Mat. Science & Eng. 19. pp 79-86.

Turley, D.M., and Samuels, L.E. (1972). J. Australian. Inst. Metals. 17. p 114.

Turley, D.M., Doyle, E.D. and Samuels, L.E. (1974). " The structure of damaged layers on metals." Proc. Int. Conf. Prod. Eng. Pt2. Tokyo, 1974. pp 142-147.

Watson, D.W. and Murphy, M.C. (1979). " The effect of machining on surface integrity." The Metallurgist and Materials Technologist. April 1979. pp 199-204.

Welsh, N.C. (1957). J. Appl Phys. 28. (9). p 960.

Welsh, N.C. (1964). " The dry wear of steels. II Interpretation and special features. Phil Trans. Proc. Roy. Soc. 257. (A). pp 51-70.

Wheeler, H.E. (1922). " Nitrogen in steel and the erosion of guns." Trans. Am. Inst. Min,. & Met. Engrs. 68. pp 257-316.

Wilson, F.and Eyre, T.S. (1969). " Metallographic aspects of wear." Metals and materials. Vol 3. pp 86-91.

Wingrove, A.L. (1971). " A note on the structure of adiabatic shear bands." J. Aust. Inst. Met. Vol 16. No 1. pp 67-70.

Wrazej, W.J. (1945). " Local heating in plain carbon steels." J.I.S.I. Vol 152. No2. pp 189-193.

Yumen, L. (1989). "Low energy dislocation structures in cyclically deformed quench tempered steel." Mat.Sci and Eng. A113. pp 237-244.

Zener, C. and Holloman, J.H. (1944). " Effect of strain rate upon plastic flow of steel." J. Appl. Phys. Vol 15, pp 22-32.

APPENDIX.

Nickel plating for thin foil preparation.

Introduction.

The preparation and subsequent examination of cross-sectional thin foils at the surface of steel samples, is facilitated by the application of a thick > 1mm layer of ductile nickel prior to sectioning, mechanical pre-thinning and ion-beam or electrochemical thinning. The layer acts both to protect the surface of the specimen during thinning and also provides a most useful indication of the surface during microscopical examination.

Several plating techniques were attempted including; electroless nickel deposition and various electrochemical formulations, with varying success. The major difficulties being; poor adherence of the nickel layer, and delamination and fracture of the plated layer during mechanical preparation, due to the brittle nature of the deposit and residual internal stresses. The following technique based on the method described by Goodhew (1985) was found to be most satisfactory.

Plating Technique.

The sample to be plated was first prepared as a metallographic cross-section and examined under a light microscope, following etching to confirm the presence of the surface features to be examined (white-etching layers in this instance). All traces of mounting material, where

used, were then removed and the specimen cleaned and plated as follows :

1) The specimen was ultrasonically cleaned in acetone to remove adherent mounting medium.

2) The specimen was gripped in a pair of nickel tweezers and all surfaces other than that to be plated were protected by a layer of "Lacomit" varnish.

3) When the varnish had dried, the specimen was cleaned by reverse plating at a current density of 0.2 mA mm^{-2}, with the specimen as the anode, for a period of 10s in a solution of "Wood's" nickel; 60g nickel chloride in 31ml HCl and 250ml distilled water, using a circular nickel electrode. The solution was ultrasonically agitated during cleaning and the current reversed at the end of this period without removing the specimen from the bath.

4) A "flash" coat of nickel was then applied to the specimen by plating for a period of 6 minutes at a current density of 0.2 mA mm^{-1} whilst still ultrasonically agitating the plating solution.

5) At the end of this period, the sample was transferred rapidly, without rinsing, into a plating solution based on the nickel-sulphide bath (Critchley, 1989) consisting of 330gl^{-1} $NiSO_4.6H_2O$, 45gl^{-1} $NiCl_2.6H_2O$, 38gl^{-1} of Boric acid and 1 ml of Na-lauryl sulphate, made up with distilled water and adjusted to a pH of between 3-4. To this was added 0.5 ml H_2O_2 each time the solution was used. The solution was maintained at a temperature of 50°C and the voltage adjusted to provide a current density of 0.3 mA mm^{-2} throughout the plating

process which continued for up to 72 hours to produce a plated layer of up to 2mm thick.

6) During plating, the solution was continuously agitated with a magnetic stirrer to prevent the gas evolved at the sample surface during electroplating from forming a porous plated layer. It was also found helpful to periodically tap the specimen cathode assembly to release adherent gas bubbles.

The resultant thick nickel plated layer was found to be strongly adherent to wear surfaces containing oxides, as well as to clean metal surfaces, and permitted mechanical thinning using standard metallographic grinding and polishing to thicknesses of less than 50μm in preparation for ion-beam or electrochemical thin-foil preparation.